THE USE OF ISOTOPIC OXYGEN EXCHANGE TO INVESTIGATE CARBON MONOXIDE OXIDATION OVER SUPPORTED GOLD CATALYSTS

MICHAEL J. DUGGAN

A thesis submitted in partial fulfilment of the requirements of The Nottingham Trent University for the degree of Doctor of Philosophy

March 2003

Abstract

Until recently, gold was viewed as catalytically inert, due in large part to the noble character of bulk gold. However, when gold is finely dispersed on a suitable support, the material is often endowed with high catalytic ability for a number of reactions, most notably, CO oxidation at ambient conditions.

In this thesis, isotopic oxygen exchange is used to probe the reactivity of surface oxygen, with a view to correlate these results with the CO oxidation results and better understand the surface processes governing CO oxidation. In this study, both MgO and Fe_2O_3 have been chosen as supports for gold. The first one is known to exchange oxygen well and Fe_2O_3 as a support is associated with high activity for CO oxidation at room temperature. Both sets of catalysts have been prepared by either co-precipitation or impregnation and pre-treated by calcining in air at 435°C, 800°C or left uncalcined, in addition they have both been tested for their ability to exchange oxygen and oxidize CO.

Results suggest a strong influence of preparation technique and support type on isotopic oxygen exchange and CO oxidation. Comparison of exchange and oxidation data suggest oxidation occurs by a non-lattice pathway. Several experiments indicate this is augmented by oxidation from the lattice in some cases. All samples have been characterised by a range of techniques aimed at elucidating the nature of their surfaces, with the aim of correlating these data with sample isotopic exchange and CO oxidation performance. These techniques include; BET surface area determination, XPS, TPR, SEM and XRD.

Acknowledgments

There are many individuals who have been generous in their support and assistance during my studies. I would especially like to thank my supervisors, Professor Richard Joyner, for his continual support and guidance throughout my time at NTU, and Dr Michael Stockenhuber, for his superb practical guidance. I would also like to thank Dr Justin Hargreaves, who supervised my first year, for easing me into the world of full time research.

I am also indebted to Dr Fran Karpowitz for instructing me on the use of quantachrome surface area measurements, Steve Furzeland for running SEM analyses on some of my samples, Dr Olga Tkachenko for showing me how to perform XPS analyses and running some of my samples, and all the members, past and present, of the Catalysis Research Laboratory for providing me with a most enjoyable three years.

Lastly, I would like to thank my parents, family and friends for their constant support on all levels throughout my time at NTU.

List of Abbreviations

BET	Brunauer, Emmet and Teller
DRIFTS	Diffuse Reflectance Fourier Transform Infrared
E_a	Activation Energy
EDX	Energy Dispersive Analysis of X-rays
EPR	Electron Paramagnetic Resonance
EXAFS	Extended X-ray Absorption Fine Structure
FWHM	Full Width Half Maximum
GC	Gas Chromatography
GHSV	Gas Hourly Space Velocity
JCPDS	Joint Committee on Powder Diffraction Standards.
RDS	Rate Determining Step
SEM	Scanning Electron Microscopy
TAP	Temporal Analysis of Products
TCD	Thermal Conductivity Detector
TEM	Transmission Electron Microscopy
TPR	Temperature Programmed Reduction
XPS	X-Ray Photoelectron Spectroscopy
XRD	X-Ray Diffraction

Sample Nomenclature used in this thesis:

All samples are referred to according to their gold loading, method of preparation, temperature of calcination and support type, following the system: **WW% XY (Z)** or **WW_{at}% XY (Z)** where: WW% = percentage gold loading, WW_{at}% = percentage gold loading for co-precipitated iron oxide, in which weight of gold to iron, not weight of gold to weight of precursor material was used. (WW_{at} refers to atomic weight of gold to iron).

X = method of preparation, i.e., impregnation or co-precipitation

Y = temperature of calcination, i.e., 435°C, 800°C or uncalcined

(Z) = support type, either MgO or Fe_2O_3

Thus 10%CP800 (MgO) is a co-precipitated magnesia sample that is 10% gold loaded and has been calcined at 800°C.

Contents

Chapter one

The aim of science is not to open the door to infinite wisdom, but to set a limit to infinite error.

Bertolt Brecht

General Introduction

1.0 Range of introduction

Supported gold catalysts have recently found utility [1,2] in CO oxidation and other reactions where they have been found to be very successful, especially at low temperatures where previous catalysts were less effective. In particular, metal oxide supported gold catalysts are particularly effective for low temperature CO oxidation.[2] In relation to metal oxide catalysis is the Mars-van Krevelen mechanism in which the support is reduced by carbon monoxide and replenished (oxidized) by gas-phase oxygen. Metal oxides have a range of reactivities regarding lattice oxygen and this reactivity can be probed using isotopic oxygen exchange.

Isotopic oxygen exchange is a robust technique for following the reactivity of surface oxygens in metal oxides. Understanding this reactivity is of importance because it could give information regarding oxygen activation, which may be the rate determining step for some catalytic reactions, most notably carbon monoxide oxidation.

In the research described, isotopic exchange data from eight different types of material covering two different supports, magnesium oxide and iron oxide, are compared to carbon monoxide oxidation data in the hope of elucidating the mechanism for CO oxidation.

This introduction gives information regarding the structure and reactivity of MgO and an account of related exchange studies that have been performed together with information on the nature of exchange itself. Isotopic exchange studies using iron oxide will also be discussed together with research on pre-treatment of exchange samples and the kinetics of exchange. Also the kinetics of oxidation will be discussed together with an appreciation of the possible rate determining steps that could be involved.

Next will be an examination of CO oxidation studies over Au / MgO and Au / Fe_2O_3 catalysts as well as other supports. Here, complex factors that are relevant

to CO oxidation will be presented. These include the effect of: pre-treatment, preparation, role of gold, of small gold particles, moisture, calcination, and deactivation. Attention will also be paid to issues surrounding selectivity and the use of manipulating CO and O_2 partial pressures on activity. Later on, special focus is paid to MgO supported gold and iron oxide supported gold catalysts for CO oxidation, and O_2 other supported gold catalysts.

Finally, there will be discussion of the several theories that have been advanced to account for catalysed CO oxidation and the importance of isotopic oxygen exchange in understanding the CO oxidation process.

1.1 Magnesium Oxide Bulk Structure

Magnesium oxide is an alkaline earth metal oxide possessing a rock salt type structure. It possesses a lattice parameter of 4.2 Å. The equilibrium state exhibits the cubic structure with few defects. In the figure below, Mg and O ions occupy equivalent positions so the co-ordination environment applies equally to both types.

Figure 1.1.1: the face centred cubic structure of MgO

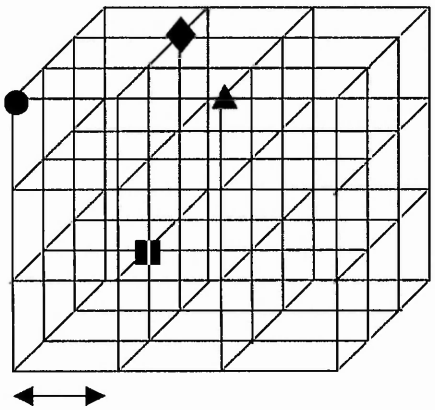

3 co-ordinated ● 4 co-ordinated ▲ 5 co-ordinated ◆ 6 co-ordinated ■

As can be seen there is a difference in co-ordination environment depending on position in the crystallite. From electron microscopy studies, the main, stable termination plane of MgO is the (100) plane.[3] This is shown in figure 1.1.2.

Figure 1.1.2: The 100 plane for magnesium oxide

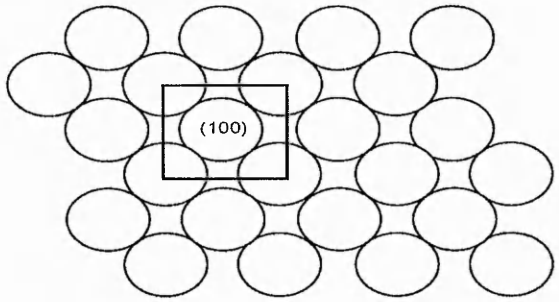

1.2 Magnesium Oxide Surface Features.

Because isotopic oxygen exchange is primarily a surface phenomenon at the temperatures in this research, it is important to discuss the surface environment of Magnesium oxide.

On the surface there are several different structural features that might be relevant to isotopic oxygen exchange: Steps, Kinks and Terraces.

1.2.1 Steps.

Steps provide a range of co-ordination environments from 3 co-ordination to 6 co-ordination as figure 1.2.1 indicates.

Figure 1.2.1. A typical step on the MgO surface

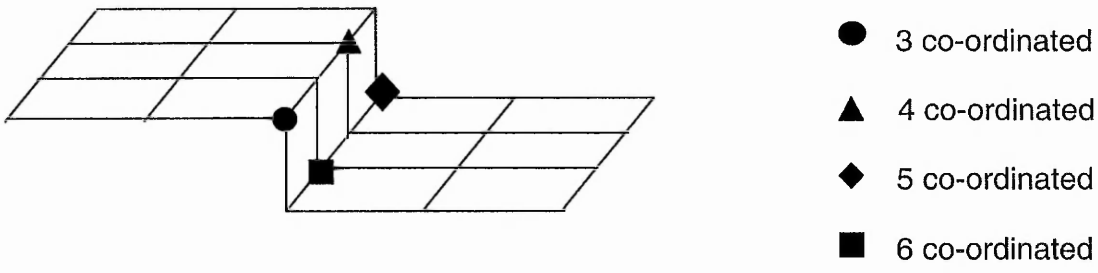

1.2.2 Kinks.

Other features responsible for differences in co-ordination environments are kinks. These are usually produced during agglomeration of small crystallites during sintering. Chemical attack by carbon dioxide or water can also cause such features to occur.[4]

A typical kink is shown in figure 1.2.2

Figure 1.2.2 using the same key as figure 1.2.1

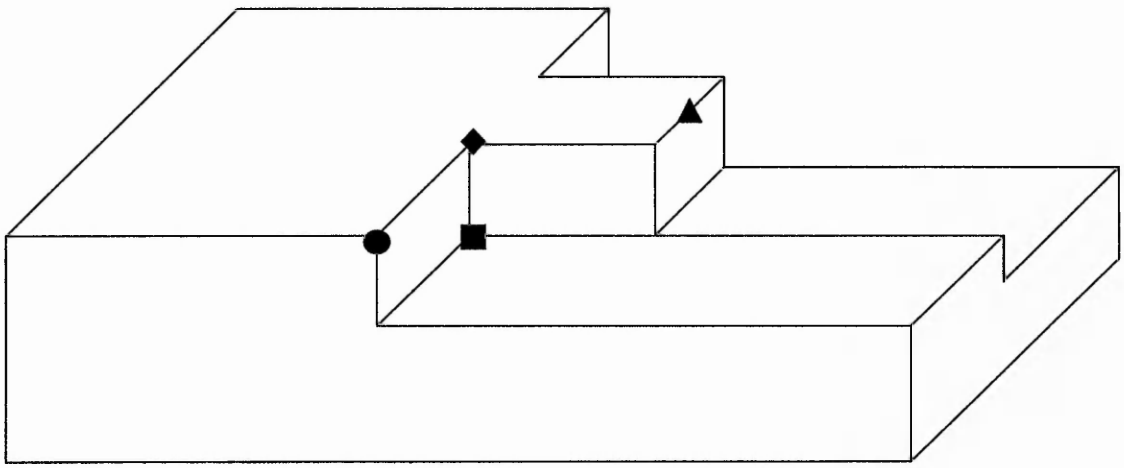

1.3 Isotopic oxygen exchange

Isotopic oxygen exchange is a very useful tool for investigating the surface reactivity of oxygen species on the surface of a metal oxide. In the research to be described, isotopic oxygen exchange across the surface of magnesium oxide / iron oxide supported gold materials is followed.

One type of isotopic oxygen exchange can be represented by equation 1.3.1. This is referred to as the R1 mechanism.[7]

Equation 1.3.1: $^{18}O^{18}O_{(g)} + {}^{16}O_{(s)} \longrightarrow {}^{18}O^{16}O_{(g)} + {}^{18}O_{(s)}$. R1

Here a single molecule of $^{18}O^{18}O$ undergoes exchange with a surface oxide, which results in the production of $^{18}O^{16}O$ and replacement of a surface oxide ion by ^{18}O. Some researchers have also reported the R2 exchange mechanism where two surface oxygen atoms undergo exchange[3], such as over Cr_2O_3 or WO_3.

Equation 1.3.2: $^{18}O^{18}O_{(g)} + 2^{16}O_{(s)} \longrightarrow {}^{16}O^{16}O_{(g)} + 2^{18}O_{(s)}$. R2

Because oxidation of CO (as discussed later) might involve participation of lattice oxygen, it is important to illustrate the Mars van Krevelen mechanism that is thought to occur during oxidation. As can be seen, both isotopic oxygen exchange and this model of CO oxidation involve participation of lattice oxygen. This is revisited later on.

1.3.3 The Mars-van Krevelen mechanism.

Here the reactant molecule denoted R adsorbs on the metal oxide surface. Desorption then occurs with loss of the lattice oxygen leaving essentially a hole containing two electrons.

$R_{(ads)} + O^{2-} \longrightarrow$ Products $+ 2e^-$

Gas phase oxygen then reacts with the vacancy as follows:

$O_{2(g)} + 2e^- \longrightarrow 2O_{(lattice)}$

This process can be represented schematically:

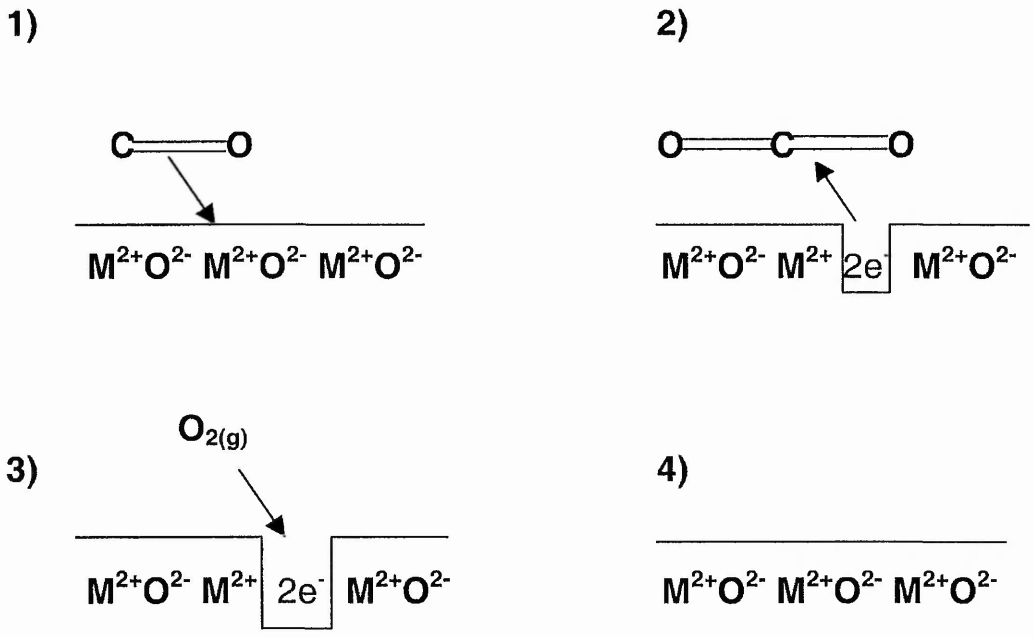

1.4 Previous studies of Isotopic exchange on magnesium oxide

Isotopic oxygen exchange has been studied over a wide range of oxides. Winter[7] and Boreskov[8] have both been very active, and have shown that exchange occurs at as low a temperature as 25°C for ZnO and as high as 880°C for SiO_2. Exchange with MgO typically occurred at 370°C to 510°C while exchange over FeO_3 was found to occur at 260°C to 400°C.

There has been a significant amount of research conducted on MgO using isotopic exchange as a probe. This is not surprising as magnesium oxide forms a highly ordered structure whose defect chemistry is well understood.

Among the first to investigate the isotopic exchange with MgO was Winter[7] who found that the activation energy of exchange changed around 693°C. Winter attributed this change to a transition from surface exchange to migration across the surface and/or into the bulk.

Next, Winter lowered the temperature of reaction from 420°C to 25-250°C and found that in the temperature range 25-250°C exchange of gas phase oxygen with the lattice was not observed but the equilibration reaction between $^{16}O^{16}O$ and $^{18}O^{18}O$ was still catalysed. This indicated that exchange of surface oxides is less favourable than simple gas phase equilibration.

However, Winter's finding of a change in activation energy at 420°C was not reproduced by Boreskov[8] who found no change in activation energy at 420°C for heterophase exchange.

Boreskov suggested that Winters work could be invalidated by diffusion limitations at the higher temperature of exchange.

It was Klier[5] who made a detailed study of the mechanism of isotopic oxygen exchange over MgO and formulated the concept of R1 and R2 exchange, in which one or both of the oxygens undergo exchange, respectively. This designation (R1 and R2) is adopted in the current research, which extends earlier studies of Mellor et al,[9] who examined the structure sensitivity of magnesium oxide for exchange. By changing the magnesium oxide precursor, materials with different surface areas, exposing variations in the relative numbers of co-ordinatively unsaturated ions, were prepared. Analysis of Arrhenius plots of four samples revealed that they all showed similar specific rates of reaction and activation energies, despite wide variations in surface area, leading to the conclusion that isotopic oxygen exchange is *structure insensitive*. Specifically, changes in surface area and hence particle size will expose different populations of 3 and 4 co-ordinated oxygen atoms while the majority 5 fold co-ordinated oxygen atoms will remain relatively unchanged in number. The research demonstrated that co-ordinately unsaturated species do not appear to undergo preferential isotopic exchange as previously suspected.

It was also observed that switching experiments in which after exchange with $^{18}O^{18}O$ the gas phase was evacuated and then replaced with $^{16}O^{16}O$, lead to a continuation of $^{16}O^{18}O$, meaning that exchange of gas phase $^{16}O^{16}O$ with lattice ^{18}O was occurring. This unexpected result leads to the assumption that there are specific sites that are responsible for exchange and that are not randomised or destroyed during exchange.

1.5 Previous studies of Isotopic exchange on iron oxide and other supports

Most studies examining isotopic oxygen exchange on iron oxide supported gold have usually done so in conjunction with carbon monoxide oxidation in order to provide information regarding the mechanism of CO oxidation. Compared to the volume of literature on supported gold CO oxidation (approx 200 papers, summer 2002) there is a paucity of publications that include isotopic oxygen exchange. This is unfortunate as combining both approaches is a productive way of gaining mechanistic insight into CO oxidation.

One of the most comprehensive investigations into the mechanism of CO oxidation over supported gold catalysts by Kozlov et al[1] using gold triphenylphosphine nitrate to load gold onto an iron oxide support. Here the catalyst was exposed to CO and oxygen 32 and oxygen 36. The main finding was an absence of isotopic exchange as evidenced by a failure to observe the expected product of exchange, $^{18}O^{16}O$. This ruled out both heterophase exchange with the lattice and homophase surface equilibration. (Exchange at this sample was performed only at 25°C. This is much lower than that employed by others[5,7,8] and is not surprising in the context of other results.) Next, in the same experiment, CO was exposed to the surface *without* any gas phase oxygen present. There was no oxidation or production of labelled CO. These two observations ruled out isotopic exchange with CO or oxidation by the lattice of CO. Finally, when the catalyst was exposed to CO and oxygen 36 there was oxidation and the CO_2 produced contained $C^{16}O^{16}O$, $C^{18}O^{16}O$, $C^{18}O^{18}O$, in a 1:2:1 ratio. These findings strongly indicate that oxygen is adsorbed molecularly not dissociatively, and suggests that CO oxidation occurs via a carbonate intermediate as this provides the opportunity for the production of doubly labelled CO_2. However not all researchers have found evidence for molecular oxygen adsorption. Schubert et al[10] working with Au / Fe_2O_3 at 80°C found no support for this model as attested by an absence of doubly labeled CO_2. However in other work[11] they did find DRIFTS evidence for Au-O, supporting a dissociation model.

Bocuzzi et al[12] using FTIR did find evidence for molecularly adsorbed oxygen at –183°C on gold / titania but no evidence for dissociation or involvement of lattice oxides was forthcoming. Interestingly there was evidence to suggest that oxygen pre-adsorption inhibits oxidation unless there is sufficient moisture on the support. Here it is speculated that a superoxide species attacks an incoming water molecule, producing the required oxygen and hydroxyl groups (which can oxidize CO via a formate intermediate). This is similar to model 6, that is detailed later on. For CO pre-adsorption, this is thought to activate any subsequent oxygen that adsorbs.

In another FTIR study by Bocuzzi et al,[13] gold on titania and gold on zinc oxide was investigated. By following the absorption bands for adsorbed CO on titania (carbonate species, 2186 cm^{-1}) and CO on gold (molecular carbon dioxide, 2105 cm^{-1}) it was shown that there was a difference in the co-adsorption frequencies (both CO and O_2) between oxygen 32 and oxygen 36 regarding CO on gold (2105 cm^{-1}) but not CO on titania (2186 cm^{-1}). This was hypothesized to be an effect of lattice oxide participation for CO oxidation on titania and gas phase oxygen participation for CO on gold (hence the invariance with either gas phase oxygen 32 or 36 co-adsorption for CO on titania but not for CO on gold particles). From these results two separate pathways were envisaged; a fast direct oxidation of CO on gold by gas phase oxygen and a much slower lattice involved pathway for CO oxidation on titania.

Further evidence against the dissociative adsorption of oxygen and participation of the lattice oxide was reported by Naito,[14] who found an absence of oxygen exchange over silica supported gold at 150°C. Collectively these studies provide equivocal evidence concerning the nature of the oxygen species. It is still not clear if molecular adsorption or dissociative adsorption of oxygen occurs. Contradictory evidence also surrounds the adsorption site for CO and O_2, (support, gold particle surface, gold / support interface?) and also the nature of the adsorbed O_2 species, (peroxy, superoxide, uncharged).

1.6 Isotopic exchange testing of samples

Pre-treatment

Because it is desired to investigate the exchange of lattice oxygen species at the surface of the oxide it is important to remove as many surface species (i.e., hydroxyl groups) as possible before exchange commences. This is usually done by others through high temperature treatment for a certain amount of time. Winter[5], who was the first to investigate exchange, heat-treated samples under vacuum before exchange, unfortunately exchange appeared to be far too rapid initially. This was hypothesized to be an effect of defect formation on the surface (most likely Frenckel defects, i.e., an oxygen vacancy containing 2 electrons) that were rapidly filled before exchange proper. Subsequent exchange investigations have omitted the use of vacuum pre-treatment and instead opted to pre-treat under atmosphere or enriched oxygen 16. This modification had the effect of reducing the very rapid initial exchange in favour of exchange that obeyed kinetic predictions.

1.7 Kinetics of exchange

The earliest investigator to try to quantify exchange was Winter[7] (previous attempts only recorded a qualitative decline in gas phase labeled oxygen) who found the decrease in oxygen 36 followed first order kinetics according to the expression:

Equation 1.7.1: $-dp/dt = kPO_2 (P_t - P_f)$

where: $-dp/dt$ = the fall in gas phase oxygen 36 over the course of the experiment

k = the rate constant for the reaction

PO_2 = the partial pressure of oxygen

P_t = the pressure of gas phase oxygen at time t

P_f = the final pressure of gas phase oxygen

Winter assumed an R1 mechanism was operating in which each $^{18}O^{18}O$ lost was replaced by $^{18}O^{16}O$. Later researchers confirmed the production of $^{18}O^{16}O$ but controversy still remained concerning the production of $^{16}O^{16}O$, i.e., R2 exchange.

1.8 Kinetics of oxidation

Unlike in exchange in which the rate is measured as a drop in the pressure of oxygen 36 that is related to the fraction of unexchanged sites, CO oxidation, which is a bimolecular reaction follows Langmuir-Hinshelwood kinetics in which one species (oxygen) is adsorbed more strongly than the other species (CO), this is commonly seen in supported gold catalysts. Ideally it is preferable to have both species in a 50:50 surface ratio in order to maximize the reaction rate (although gas-phase composition doesn't necessarily equal surface concentration), but in CO oxidation the flammability limits (12.5% - 78%) prevent such a scenario. In fact the ideal ratio would be 1:2, O_2 :CO, as oxygen can oxidize two CO molecules.

The rate expression for CO oxidation is:

Equation 1.8.1: $R = k[CO(a)][O(a)]$

Where:

R = rate of reaction

k = rate constant

CO(a) = amount of CO adsorbed

O(a) = amount of O adsorbed (dissociatively)

According to the above expression, a 50:50 surface coverage of both species is preferred as this produces the greatest rate of reaction. Langmuir-Hinshelwood reactions occur either competitively or non-competitively. Species in competitive

reactions compete for the same adsorption sites whilst in non-competitive reactions distinct adsorption sites exist for both (or more) species.

1.9 Determination of the rate-determining step in CO oxidation

In CO oxidation it is of interest to investigate the rate-determining step for the reaction as this allows development of more effective catalysts.

The sequence of events for CO oxidation can be summarized:

1) Transportation of O_2 and CO to the reactive sites
2) Adsorption of O_2 and CO
3) Dissociation of O_2 (speculative)
4) Migration of oxygen or CO to the place of reaction
5) Reaction between CO and O_2 (or O)
6) Desorption of CO_2
7) Transportation of CO_2 away from the site of reaction

The activation energies[15,16,17] for CO oxidation usually fall within 20 ± 10 kJ mol^{-1}. Diffusion limitation for most of these results can be ruled out as this usually causes a fall in activation energy to less than 10 kJ mol^{-1}.
At the present time the most suspected rate determining step is sequence 3: dissociation of oxygen. In fact oxygen activation is also required in isotopic oxygen exchange (prior to exchange with the lattice) and this is the reason the two sets of data are examined for correlations.

1.10 Catalytic investigations over supported gold materials with emphasis on CO oxidation: (An overview, 1.10-1.22)

In order to investigate the catalytic performance of gold catalysts employing either magnesium oxide or iron oxide as a support, the oxidation of carbon monoxide was chosen.

There are several reasons for this choice, the principal reason being the correlation of these data with isotopic exchange studies performed concurrently. This will be enlarged upon later.

Apart from gaining a theoretical understanding of the basis behind carbon monoxide oxidation, the reaction is of immense practical importance.

One application is to develop catalysts that are effective at removing CO at ambient and low temperatures from car exhausts. Usually rhodium, platinum and palladium supported on alumina that has been washcoated on a monolith is used, unfortunately this catalyst is only active at temperature above 300°C and some of the unoxidised CO has already been released during 'cold start-up'. Therefore a catalyst that removes CO at ambient temperature would be much welcomed, perhaps in conjunction with already existing catalysts that work at high temperatures. This is important because gold sinters and becomes ineffective at relatively low temperature (800°C).

There are other practical applications that include; the removal of CO from CO_2 lasers, where a build up of CO results in inefficient operation. Also in enclosed environments such as in submarines or space exploration were the air can't readily be replenished, there is a need to remove any build up of CO. As well as removing CO, there may be applications in terms of increased sensitivity of CO for CO detection purposes.

1.11 The role of the support in gold catalysis.

The observation that choice of support has marked influence on catalytic function has been reported by many investigators in the field.[18] Often, one support encourages high catalytic performance whilst another is quite inert for CO oxidation, but also for other reactions. This disparity is of intense interest and some clues have been forthcoming.

A common feature of the most successful supports is that of reducibility at low temperatures. This is particularly true of oxides of some of the first row transition metals; vanadium, iron, nickel, titanium and cobalt, while those supports that are ineffective at catalysis are not generally reducible at low temperatures. Most notably alumina and silica.[10,19]

This suggests it is oxygen supply that is important in CO oxidation catalysis. A support that can release lattice oxygen with ease and form anion vacancies is more active than a support that can't.

Another mechanism that seeks to explain CO oxidation does not require the participation of lattice oxygen and so lattice oxygen supply becomes less important. Here, the dissociative adsorption of oxygen occurs at the interface of the gold particle and support. Reaction with carbon monoxide that has molecularly adsorbed and migrated across a gold particle thus ensues. However, the situation regarding oxygen supply might not be so simple because vacancies (which are created through lattice oxygen loss) provide good sites for oxygen adsorption and subsequent dissociation. Therefore the fact that highly reducible supports are also good carbon monoxide oxidizers should not count as evidence for a mechanism that employs lattice oxygen.

1.12 The effect of preparation on supported gold catalysis

The choice of support is not the only crucial factor to consider in supported gold catalysis. Of equal importance is the preparation method.

Seker et al,[20] found that the impregnation method was the most susceptible to a decrease in activity under the presence of water for NO_2 reduction over Au / Al_2O_3 and also gave the lowest activities. They also found that co-doping with silver did not improve performance.

Haruta[21] found that co-precipitated materials gave far superior activities for CO oxidation over a range of 3d transition metal oxide supports than impregnated materials. This disparity was explained by the much larger gold particle size conferred by impregnation than co-precipitation as calculated from XRD reflection sizes.

In fact, the majority of workers have found that co-precipitation offers superior catalytic activity than impregnation,[22,23] most probably due to smaller gold particles being obtained by the co-precipitation route. However, not all investigators have found that impregnation produces the largest gold particles. Schimpf et al,[2] found that gold particle size increased from around 1 nm for the sol-gel process through to 3 nm for impregnation and 6 nm for deposition-precipitation. They found that for the hydrogenation of unsaturated aldehydes, there was a *positive* correlation between particle size and catalytic activity. This was explained by the assumption that the reaction occurs on the surface of gold particles and hence will not be affected by interface considerations in the same way that CO oxidation is. It is therefore important to regard the stereochemistry of the catalysed reaction as well as support / gold factors. Also noted was a steady increase in the size variation of gold particles going from sol-gel through impregnation to deposition-precipitation. The particle size distribution can have ***a*** marked influence on catalysis.[24] It is now generally agreed that co-precipitation[25] confers the greatest benefit to catalytic performance whilst impregnation[26] offers mediocre performance at best.

The chief reason for this difference is often an effect of much smaller gold particle sizes of 2-5 nm in diameter for co-precipitated materials whilst impregnation frequently results in much larger particles in excess of 20 nm in diameter.[25,27,28]

1.13 The effect of preparation: (pre-treatment conditions)

One of the most important areas in gold catalysis is that of pre-treatment. Researchers have found that a variation of pre-treatment conditions can have very marked influences on catalysis. Not surprisingly there is a large amount of conflicting debate concerning the effect of pre-treatment on catalysis. Pre-treatment includes drying conditions, and oxidative / reductive treatments.

Cunningham et al,[29] investigating CO oxidation over Au / Co_3O_4 found that drying the reactant and pre-treatment gases increased the oxidation rate as opposed to the highly retardant effect of not drying the gases. It was postulated that water and other groups occupy sites on the surface and that removing these groups by using dried pre-treatment gases would result in available sites for catalysis.

Su[30] et al found that drying conditions (i.e., either vacuum or oven dried) impacted on the morphology and oxidation state of the gold particles. It was found that high temperature reduction and high temperature calcination followed by low temperature reduction produced the most active catalyst. It was hypothesized that these treatments increased the amount of metallic gold on the support. Following on from this, Choudhary[17] et al repeated the earlier result and found an association between a particular pre-treatment regime and gold particle dispersion, with high temperature reduction followed by low temperature calcination (HTR/LTC) producing much smaller particles than high temperature calcination followed by low temperature reduction (HTC/LTR). However not all investigators have found benefits from reductive treatments.

Gupta[31] found that reductive treatment of Au / Fe_2O_3 lead to reduction of haematite to magnetite support, which is known to be a less catalytically active support than haematite.[31] and which indeed produced a reduction in catalytic performance. Lee et al,[32] investigating CO oxidation over Au-Mn co-precipitates found that catalysts dried in air demonstrated higher CO conversion than those treated in H_2 or dried in vacuum. Subsequent heat treatment at 400°C (i.e., after the initial flash-off test) increased activity. This was thought to originate from an increased interaction between gold supported on manganese.

Investigations by Su et al,[30] might shed light on the effect of pre-treatment. They found XPS evidence to suggest that drying under vacuum produced highly dispersed non-metallic gold species whereas drying in air caused reduction of gold and agglomeration of gold particles to occur.

Grunwaldt[33] cast doubt on the benefit on calcination. It was found that for CO oxidation, dried catalysts (Au / TiO_2) outperformed their calcined counterparts and that a mixture of O_2 and CO fully activated these materials. The enhancement of catalytic performance was ascribed to an increasing number of co-ordinatively unsaturated gold sites-a product of increased gold-support interaction.

Schubert et al[34] investigating the preferential oxidation of CO, found that reductive pre-treatment lead to an increase in the preferential oxidation rate. This was hypothesized to be a function of increased hydroxyl moieties on the surface. Unfortunately the effect was not long lasting and catalytic activity quickly diminished on stream.

The other prevailing form of pre-treatment is oxidative. Grisel[35] found that oxidation of supported gold catalysts bestowed inferior CO oxidation ability than reductive pre-treatments, a result repeated elsewhere.[36] However Hao et al[37] found that oxidative pre-treatment gave complete low temperature oxidation of CO over iron oxide supported gold catalysts as low as –23°C, whereas reductive pre-treatment only gave comparable activity at 87°C. Others have also found significant benefit from oxygen pre-treatment.[38] The situation is probably more complex than one particular pre-treatment is superior to the other one, as work by Uphade et al[39] suggests. Investigating epoxidation over Au / Ti-MCM-41, it was found that the best approach was calcination followed by reductive pre-treatment

and finally oxidative pre-treatment using oxygen mixed in argon. It can be argued that reductive pretreatment with H_2 is sometimes successful as it promotes hydroxyl group formation on the surface of a catalyst; OH groups have been implicated in CO oxidation. However in some circumstances, oxidative pre-treatment would be advantageous, for instance, in replenishing oxygen vacancies or just enriching a surface with oxygen. Ultimately the benefits of pre-treatment selection depend on the type of support and the mechanism of catalysis that is occurring as well as other factors.

1.14 The role of the gold: why is gold so special for catalysis?

It is highly evident that when gold is carefully supported on a metal oxide (especially a first row transition metal oxide) then high catalytic performance can be observed although the support alone is often ineffective. This remarkable catalytic ability of gold has only recently been discovered, what can explain it?

Gold, which is found in group 11 of the periodic table, does exhibit a number of anomalous effects that make it stand out from comparable elements. These include a very high electronegativity for the gold III ion, second to copper in electrical conductivity, high resistance to corrosion, a very high electron affinity, and a high electrode potential with mercury.

Conversely gold's electronic configuration gives no clues to its catalytic potential. The configuration [Xe] $4f^{14}$ $5d^{10}$ $6s^1$ reveals the presence of a lone outer s electron. Because of the high proton number of gold (79) there is a strong attraction of the inner s electrons to the nucleus. This causes the inner s electrons to increase speed up to velocities approaching the speed of light. Consequently there is a *relativistic* contraction that causes the inner s electron orbitals to contract.

The outer 6s orbital contracts also and this causes gold to be *more* stable than otherwise suspected. This relativistic effect accounts for much of the anomalous properties just mentioned such as high resistance to corrosion. However there must be another reason why gold is so active catalytically.....

1.15 The effect of small particles

The principle reason why gold is so effective at catalysis can be traced to the development of small gold particles on the surface of a support. As the particle becomes smaller there is a concomitant increase in the periphery (as contributed by *all* gold particles) of the particles. Most catalysis is thought to occur at the periphery and so smaller particles are more catalytically active from a statistical perspective. Also, as the size of the particles decreases there is an increase in the proportion of *surface* atoms that are more mobile and have higher free energy. These mobile atoms behave less like a metal and more individually. These factors conspire to create a catalyst that is active especially if the other conditions are right such as support, etc.[40]

1.16 The influence of gold loading on catalysis

It is of interest to compare catalysts containing different gold loadings as this is of commercial interest (what is the lowest gold loading that will give appreciable catalytic activity?) and theoretical importance in understanding the role of gold in catalysis.

Bailie et al[24] investigating the hydrogenation of but-2-enal over supported Au / ZnO found a general increasing trend of catalyst activity with gold loading, peaking at 5% loading. Interestingly, selectivity towards the alcohol reached a maximum for 1% gold loaded sample, however, under steady-state conditions there was an over-all positive trend with gold loading for selectivity towards the alcohol. Others have found general positive trends with gold loading as well.[39]

Hayashi et al[41] investigating the epoxidation of propene over Au / TiO_2 in the presence of oxygen and hydrogen found that the reaction pathway switches from oxidation to hydrogenation at a specific gold loading. It was found that catalysts with a gold loading from 0.39% to 0.98% favoured propylene oxide while those catalysts with less than 0.1% gold loading gave the hydrogenation product propane. At 0.20% gold loading there was equal production of PO and propane. TEM revealed that the gold particles produced had diameters in the expected range (2-4 nm) but that at 0.1% gold loading there were very few particles observed. The observation that a *specific* gold loading is associated with a particular change in selectivity has been seen elsewhere.[42]

Haruta,[21] investigating CO oxidation over a variety of gold catalysts, found that the optimum gold loading was 5%. Others have found that there is not necessarily a positive relationship between gold loading and catalyst activity with often intermediate gold loadings (around 2%) producing the most active catalysts.[20,25] This suggests that there are changes that occur at very high gold loadings that do not favour catalysis such as morphological changes[42] or high chloride content.[43] It has been observed that chlorine itself encourages larger gold particle formation[44] and therefore is associated with both poisoning effects and negative morphological influences. To give an indication of how small changes in gold loading can affect catalyst activity it is of interest to recall a study by Hodge[27] et al, who found that a small decrease in gold loading from 2.1% to 1.44% reduced CO conversion by half. A further reduction in gold loading from 1.44% to 1.15% lead to a near collapse in CO conversion to 3%.

1.17 Further factors related to gold

Some researchers have speculated as to the active form of gold. The catalytic community appears to divided as to this question, with investigators gaining evidence that the oxidized form of gold is the most active (Au^{3+}) and others that metallic gold is the favoured form. These observations are complicated by the fact

that changes in preparation technique such as higher calcination temperature or the absence of moisture can lead to reduction of any oxidized gold present. Therefore researchers have to be explicit in detailing their preparation conditions if any legitimate comparisons are to be made and hence confidence in what species of gold are most likely to be present on the support.

Figure 1.17: (taken from Bond.G.C, Thompson.D.T, Gold Bulletin 2000, 33 (2))

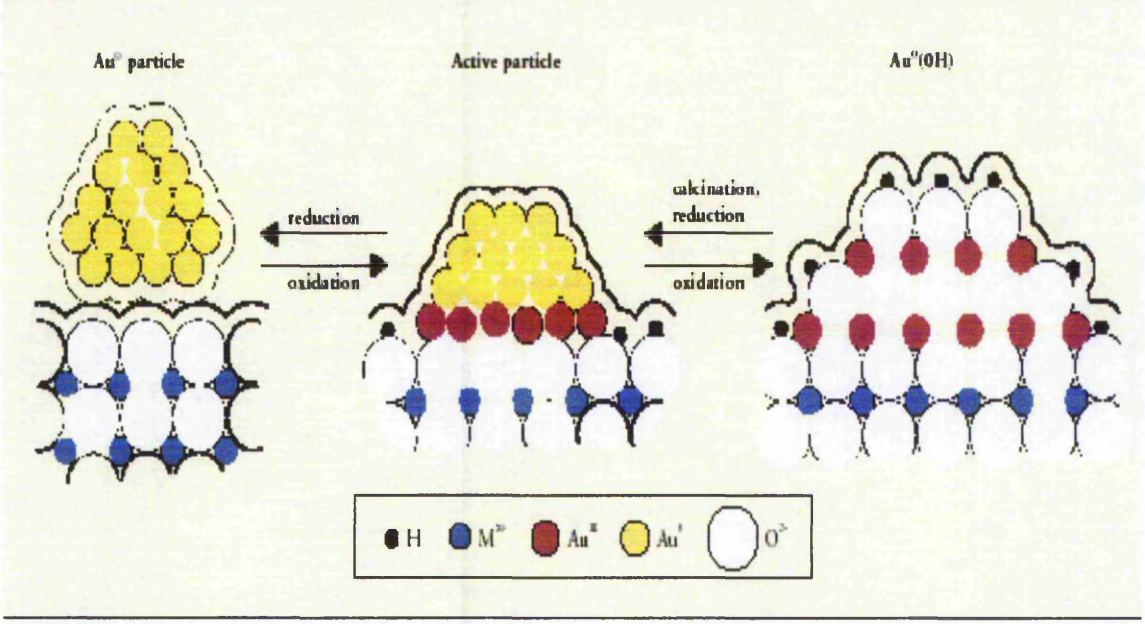

Figure 1.17 is a tentative model for the effect of oxidation and reduction[45] on a supported gold catalyst. It can be seen that reduction encourages the formation of a discrete gold cluster on the support surface whilst oxidation of gold leads to greater interaction of gold with the support. Oxidation under calcination conditions is thought to lead to greater mixing of gold ions and oxygen ions on the surface therefore providing an active calcined catalyst.

1.18 The role of moisture in CO oxidation and general catalysis

Because so many supported gold catalytic applications involve the presence / generation of water, it is of importance to understand the influence of water on catalytic performance. So far the role of moisture in CO oxidation catalysis is not completely understood and any attempt at a theoretical analysis is undermined by the often contradictory findings from researchers. Also some investigators have found varying results within the same experiment. Ueda and Haruta[46] investigating NO reduction of Au / Al_2O_3 and Al_2O_3 found increasing water content inhibited conversion to N_2 over Al_2O_3 but increased conversion over Au / Al_2O_3, suggesting gold catalysis offers advantages for reactions that are not completely moisture free. Interestingly, the preponderance of studies investigating CO oxidation over simple metal oxides or mixed oxides (supporting no gold) reveal a poisoning effect of water on CO oxidation. Hopcalite, for instance, shows a significant decline in CO oxidation with increasing water content.[90] For Mn / Ag catalysts[47] CO conversion deceases from 98% to 81% with 11% moisture levels. However for supported gold catalysts some researchers have reported reactive stability in the presence of water.[48,49] Park and Lee[19] also reported a significant enhancing effect of moisture on CO oxidation, this time over Au / Fe_2O_3. This effect occurred regardless of whether calcination was employed and therefore appears to be quite robust.

Hayashi, Tanaka and Haruta[41] investigating the epoxidation of propene over Au / TiO_2 found TPD evidence to suggest that pre-treatment in water reduced the rate of propene desorption therefore enhancing catalysis. Analysis of the TPD integration areas suggested that propene adsorbs preferentially to gold particles under the influence of moisture.

Intriguingly, CO oxidation over supports other than Fe_2O_3 such as TiO_2[50] and Al_2O_3[35,20] reveal a significant retardant effect of water on CO oxidation for reasons that are not completely understood, but could be related to the supply of support oxygen or the blocking action of water on oxygen vacancies necessary for the Mars Van Krevelen mechanism (as discussed later) in which lattice oxygen is

used as an oxidant. Indeed not all investigators have found enhancing effects of water on CO oxidation over Au / Fe_2O_3. Some have found slight negative influences.[1] Bocuzzi et al,[12] investigating CO oxidation over Au / TiO_2, formulated a hypothesis in which the hydrogens of water react with oxygen to form the reactive and unstable intermediate OOH^- which degenerates to a surface hydroxyl group and oxygen on the support. The reactive oxygen species oxidizes CO to CO_2. The hydroxyl group can also undergo reaction with either CO or O_2 and therefore participate in several different oxidation pathways.

Daté and Haruta[51] undertook a detailed quantitative investigation of CO oxidation over Au / TiO_2. Here they found that oxidation was indeed enhanced by moisture levels up to 200 ppm, thereafter there was a significant fall in activity. Suggestively, they found that the activation energy was not affected by the amount of moisture in the passing gas (unlike the rate of oxidation), this indicated that CO oxidation involves surface derived water species (such as hydroxyl groups) and not gas phase water itself.

1.19 The role of calcination in CO oxidation and general catalysis

Calcination is an important aspect of catalyst manufacture. However investigators often provide contradictory evidence in support of its catalytic efficacy, with most researchers concluding that calcination of catalyst does actually lead to a significant loss of activity, especially for carbon monoxide oxidation. Unfortunately, uncalcined materials may lose their activity after a very short time on stream even though they do tend to be more active initially.

The reason for this change on calcination is not clear, but it is more than an effect of surface area (as measured by BET[52] method) reduction and is possibly due to a loss of surface defects and general ordering of the support as the initially non-crystalline structure is converted to a crystalline (and hence more ordered) form.[27] This is not surprising as areas of surface disorder (such as defects) are high in free energy and so are favourable to catalysis. Also with calcination there is a

reduction in the number of co-ordinatively unsaturated sites. These sites are particularly active for catalysis.

Not all investigators find a deleterious effect of calcination on activity. Kozlova[53] et al found calcination of $Fe(OH)_3$ improved CO activity from 200°C to 300°C and higher calcination temperatures than this had only insignificantly negative effects on CO oxidation performance. Interestingly, calcination of Au / Fe_2O_3 did have a negative effect on CO oxidation activity. Several characterization techniques (TEM, XRD, EXAFS, XPS) confirmed the presence of smaller gold particles (2.5 nm in diameter) for Au / $Fe(OH)_3$ and much larger gold particle diameters for Au / Fe_2O_3 (12 nm). This shows that $Fe(OH)_3$ is much better at stabilizing gold than Fe_2O_3 under calcination conditions. Haruta,[26] investigating CO oxidation over Au / Fe_2O_3, found superior catalytic activity for materials calcined at 300°C as opposed to 200°C. In fact Haruta has been the strongest advocate of calcination, which is brought out by the fact that most of his groups research (Osaka National Research Institute, ONRI)[54] does show benefits of calcination. Park and Lee[19] found a significant negative effect from calcination on Au / Fe_2O_3 for CO oxidation. XPS revealed the formation of Au metal from $Au(OH)_3$ via Au_2O_3 and haematite from ferrihydrite. Both of these forms are catalytically inactive compared to their precursors.

Some hints as to effects of calcination are forthcoming from a study done by Tripathi, Kamble and Gupta.[50] They found that CO oxidation activity over Au / Fe_2O_3 was increased for calcined catalysts up to 487°C and then decreased at higher calcined temperatures. Most intriguingly however, they found that at higher calcination temperatures the amount of O_2 and CO adsorbed actually decreased but the conversion to CO_2 *increased.* This suggests that calcined materials are not very effective at retaining adsorbed species, possibly due to changes in gold / support configuration.

An answer might be forthcoming from research done by Hodges et al.[27] In this multi-lab effort the microstructures of calcined and uncalcined Au / Fe_2O_3 catalysts were compared. Although there was a sharp decrease in CO oxidation performance with calcination, characterization (XRD, HREM, STEM-EDX) revealed highly disordered micro crystallites of $Fe_5HO_8{\cdot}4H_2O$ (Ferrihydrite, 4-8 nm

in diameter) supporting uniform gold oxy-hydroxide (the most active form: AuOOH·xH2O) for uncalcined materials. Conversely, calcination produced large well-ordered haematite crystallites (20 nm in diameter) supporting cuboctrahedral gold particles (3-5 nm in diameter). This observation again reinforces a recurrent theme, that of disordered support particles being catalytically active and the support ordering effect of calcination endowing low activity on catalysts.

1.20 Catalyst Deactivation

The investigation of catalyst deactivation is of obvious practical importance as a premature loss of catalytic activity during an industrial process or in an important application could have expensive consequences.

Mul et al,[55] found epoxidation over Au / TiO_2 to be deactivated over the course of several hours. By comparing relevant infra-red data it was suggested that propylene oxide undergoes Brønsted catalysed ring opening by reaction with hydroxyl groups. The adsorbed glycol compounds produced blocked subsequent epoxidation of propene on the surface. Stangland et al,[56] also found for the same reaction and catalyst that deactivation decreased at higher temperatures, indicating the presence of strongly adsorbed species as above.

Schubert et al,[34] investigating preferential oxidation of CO over Au / MnO_2 found a deactivation response that was associated with carbonate formation on the catalyst surface as evidenced by DRIFTS and weight gain during reaction. Investigation of CO oxidation over Au/$Mg(OH)_2$ found no XRD evidence for carbonate formation but DRIFTS evidence for surface carbonate formation. This suggests the formation of a thin layer of carbonate across the catalyst surface, as XRD investigations would only detect bulk crystallite changes and not surface changes. The fact that MgO alone is inert for CO oxidation suggests that the carbonate formed over the gold particles themselves. Preferential oxidation investigation over Au / Fe_2O_3 also found deactivating carbonate species, this time in the form of $Fe(CO_3)$, siderite, and surface carbonate species. Most deactivation

was associated with these surface carbonate species. It was found that reactivation of catalyst could occur on flushing with nitrogen gas at 80°C, as a result of which most carbonate species were removed. Knell et al,[57] also observed deactivation over Au / ZrO_2 during CO oxidation. By manipulating the composition of the gas phase it was found that deactivation was not influenced by molecular adsorption of gases but by the ratio of O_2 to CO in the gas stream. At 0.5:0.5 stoichiometry there was constant activity for 20 hours, however, excess oxygen in the mixture led to rapid deactivation. This and other observations lead to a hypothesis in which CO reacts with hydroxyl groups to produce formates. Formate is oxidized by surface oxygen to yield carbonate, (this is similar to scenario 4 that is found later on), desorption of CO_2 gives a complete cycle. If this proposal is correct it means that some models of CO oxidation (which follow a similar route) inevitably lead to carbonate production and subsequent deactivation. This is extremely important and will be visited later on.

Hutchings et al [58,59,60,61] investigating hydrochlorination of acetylene over carbon supported gold found that this catalyst gave higher activity than the established $HgCl_2$ catalyst. Also the rate of deactivation was much reduced if gold loadings greater than 1% were employed. However, even these catalysts deactivated eventually, often producing a characteristic U shaped reaction profile of deactivation against temperature. The deactivation rate would start high at relatively low temperatures due to coke formation, at intermediate temperatures this would oxidize away causing a fall in deactivation rate, until at high temperatures deactivation occurred again, this time due to sintering of gold particles. Hutchings found that the catalyst could be reactivated in a stream of HCl. In practical terms this was achieved by removing acetylene from the gas source for a certain time leaving the catalyst exposed only to HCl. It was assumed that HCl acts to restore the oxidized state of gold that is associated with high catalytic activity.

1.21 Orders of reaction.

Because investigating the effect of altering the partial pressure of gases in the reactant feed and measuring the subsequent influence on reaction rate can give important hints as to an underlying reaction mechanism, it is surprising that this approach has not been more widely employed. Daniel et al,[62] investigating CO oxidation on Rh(100) crystals at 177°C found that at CO partial pressures equal to or greater than O_2 there was a hypothesized accumulation of CO therefore making O_2 adsorption rate limiting. At low CO partial pressures, CO adsorption became rate determining.

Others have found that modeling the data for rhodium based materials supports a Langmuir-Hinshelwood type reaction between CO and atomic oxygen, unlike some investigations on supported gold[17] that suggest molecular oxygen.

Kahlich et al,[15] investigated the preferential oxidation of hydrogen at 80°C over Au/Fe_2O_3, in which the amount of either CO or O_2 was kept constant while the other reactant concentration was varied. By following the influence of magnitude changes in CO and O_2 (i.e., CO partial pressure ranged from 0.025 - 1.5 kPa) it was established that the order of reaction for CO was 0.55 and for O_2 at 0.27. The authors are cautious about speculating on a mechanism from the data, however, it does appear from the lower O_2 order of reaction that oxygen is rapidly associated with the surface and hence is not needed as much as CO in the gas phase (i.e., the lower reaction order).

Lin et al,[43] investigating the effect of temperature on reaction orders for Au / TiO_2 catalysed CO oxidation found that at 40°C the reaction order with respect to oxygen was 0.4 and CO at 0.24 which is a reversal of the findings of Kahlich et al.[15] (A reason for this difference, other than different supports, could include the higher reaction temperature used in Kahlich et al investigations. In particular these conditions favour greater CO desorption and facilitate the dissociative adsorption of oxygen. Both of these observations conspire to inflate CO reaction orders with respect to oxygen at higher temperatures.) Next, Lin et al, followed

the reaction at 60°C and 80°C and found that the CO reaction order increased from 0.24 to 0.6, similar to Kahlich et al and supporting the above argument.

In order to probe this effect more deeply several hypotheses which could account for the data including: Eley-Rideal mechanism (Langmuir adsorption for CO or O_2 followed by first order impulsive collision and reaction on these pre-adsorbed species), adsorption as RDS, Langmuir-Hinshelwood (reaction between adsorbed CO and dissociatively adsorbed O_2 as RDS) both competitive and non-competitive adsorption and finally Langmuir-Hinshelwood (reaction between CO and $\mathbf{O_2}$) both competitive and non-competitive adsorption. The absence of first order kinetics ruled out an Eley-Rideal and adsorption as RDS mechanism. Entropic considerations removed the reaction between CO and O as a possibility. This left a Langmuir-Hinshelwood mechanism between CO and O_2, both competitive and non-competitive adsorption. By plotting the activity data against partial O_2 and CO pressures it was found that the non-competitive model fitted the data best. This finding was confirmed in a replication study by the same authors.[63] This suggests that O_2 is the reacting form of oxygen and that there are distinct sites for adsorption of O_2 and CO. This is in keeping with the general consensus that CO adsorbs on gold particles and O_2 at the particle / support interface or support. In fact an increasing proportion of TAP (temporal analysis of products) and isotopically labeled studies[10,64,65,66] suggest that O_2 adsorbs in molecular form (in particular O_2^-, as witnessed by EPR investigations[67,68]) and not dissociatively.

Choudhary et al,[17] also investigating a Au / TiO_2 system found reaction orders of 0.2 for CO and 0.46 for O_2 at constant pressure (27.5 Torr) and 20°C thus confirming the previously mentioned research. A result very closely repeated by others.[65]

Lizuka et al,[64] investigating CO oxidation over Au / TiO_2, found that the rate of oxidation was independent of the partial pressure of O_2 suggesting that initial oxygen adsorption was rapid. Also the rate was found to be independent of CO partial pressure at high CO partial pressures (>1850 Pa), suggesting that CO is adsorbed in relatively small quantities on specific sites at the catalyst surface. It is clear that comparing different investigations in order to arrive at generalizations

regarding reaction mechanisms for CO oxidation is replete with difficulties.
In principle this is due to different catalyst reaction conditions such as differences in temperature, pressure and experimental set-up.

1.22 Selectivity

Supported gold catalysts have been used for a number of reactions with the observation that selectivity for the desired product is often enhanced compared to previously employed materials. For CO oxidation, selectivity is only an issue for preferential oxidation reactions in which both CO and H_2 are present. Here it is the oxidation of CO that is highly desired as a build up of CO is associated with sub-optimum performance in fuel cell technology, which employs preferential oxidation catalysis.
Other catalyst systems have been used for the preferential oxidation of CO, notably Rh/Al_2O_3[69] and Pt supported on zeolite[25] however supported gold catalysts possess superior ability to oxidize CO relative to H_2 oxidation than rhodium or platinum based materials. It is therefore not surprising that supported gold has been used in the preferential oxidation of CO.
Sanchez et al,[70] investigating the preferential oxidation of CO over Au / MnO_2 found that 100% CO conversion occurred at temperatures below 0°C while H_2 oxidation occurred at temperatures above 0°C. A high temperature difference between CO and H_2 oxidation is important in maximizing the selectivity of the preferential oxidation reaction. Crucially it was found that that lower Au / Mn ratios (i.e., lower gold loading) favoured a greater temperature difference between CO and H_2 oxidation. Previous observations by the group found that low gold loading was associated with smaller gold particles than higher gold loadings, hence the observed temperature difference was ascribed to the higher intrinsic activity towards CO oxidation resulting from a greater number of surface gold atoms (and also a greater number of support / particle interface species, this author's note). This implies different mechanisms for CO and H_2 oxidation.

Grisel et al,[35] investigating preferential oxidation of CO over Au/Al_2O_3 and $Au/MO_xAl_2O_3$ (where M = Mg, Mn), found that the addition of MgO improved the CO activity and selectivity towards CO oxidation. This was hypothesized to be an effect of gold particle stabilization from MgO. In general it was found that selectivity towards CO oxidation decreased with increasing temperature (similar to Sanchez[70] et al). In particular the influence of three temperature regimes was identified. From 25°C to 50°C CO oxidation occurred exclusively with no detectable H_2 oxidation. This can be explained by resorting to site blocking by adsorbed CO. As the temperature is increased above 50°C, significant desorption of CO occurs therefore releasing sites for H_2 dissociation. This transition is followed by a concomitant decrease in the activation energy for H_2 dissociation. At higher temperatures above 300°C there is a resumption in selectivity towards CO, possibly due to limited H_2 residence time as a consequence of rapid recombination of dissociatively adsorbed hydrogen.

Schubert et al,[34] found that choice of support for the materials under investigation impacted significantly on selectivity for the preferential oxidation of CO, with Co_3O_4 giving the highest selectivity and Au / CeO_2 (doped with Vanadia which can readily change its oxidation state) giving the lowest selectivity towards CO oxidation. Given these results it was speculated that hydrogen oxidation was occurring via a redox mechanism and therefore lowering the selectivity towards CO oxidation.

Milone[71] et al, investigated the oxidation of ortho-hydroxy benzyl alcohol (salicylic alcohol) over Au / Fe_2O_3 and found that selectivity towards salicylic aldehyde was the main product at low gold loadings (<1%) and for higher gold loadings conversion to the aldehyde decreased while conversion to the salicylic acid remained constant. The impact of gold loading on selectivity has been mentioned before (section 1.16) and is most likely a result of particle size differences.[24] However, in this research a build up of heavy products with increasing gold loading (which increased overall conversion of salicylic alcohol) leading to site blocking is responsible for the decrease in salicylic aldehyde production. Another area of intense investigation is the selective oxidation of hydrocarbons. This is industrially important as the oxidation of hydrocarbons is an important chemical

technology for the production of oxygenates, epoxides, and alkanols. Generally these studies[41,72] reveal an increase in the desired product selectivity relative to non-gold catalysts but with the caveat that changing gold loading can have a marked influence on the product selectivities.

It addition to gold loading, reaction conditions are also important in establishing selectivity for the desired product as Biella et al,[73] demonstrated following the oxidation of D-glucose over Au / C. It was found that the pH used influenced selectivity by avoiding unwanted isomerisation of glucose. At higher pH it was found that selectivity towards conversion of the aldehyde over the alcohol group was apparent. In other research by the same group[74] it was found that oxidation of primary alcohols in diols was favoured at higher operating pH.

1.23 Au/MgO supported catalysts.

Although there are now many studies on gold catalysts on a range of supports,[19,33,43,76] there has been almost no work using magnesium oxide. Most researchers have concentrated on other supports such as iron oxide[21] that appear to be effective for carbon monoxide oxidation at room temperature. Why this is so is not clear as the reports that do exist suggest some catalytic ability for magnesium oxide supported gold and for magnesium oxide doped with lithium.[77,90] Magnesium oxide supported gold is reported to be effective for methane oxidation[42] with yields comparable to other support based catalysts. In research by Blick et al,[42] two distinct morphologies were present depending on initial gold doping levels. Two-dimensional rafts at low gold loadings and three-dimensional discrete hemispheres at higher gold loadings. Methane coupling was seen to be poisoned by the rafts, but enhanced by discrete gold particles. Cunningham[78] et al, also found that gold particles supported on magnesium oxide that were less than 1nm in diameter were highly active for low temperature carbon monoxide oxidation whilst those greater than 1 nm had little activity. The main preparation factor controlling gold particle size was calcination temperature, with lower

temperatures giving smaller particles. The observation of particle sintering at higher temperature has strong experimental support and is predicted by a thermodynamic appreciation that large particles are more stable than smaller ones. In this experiment samples were prepared by deposition precipitation, whilst Blick et al, employed the impregnation method and yet particle size / morphology was relevant to both preparation methods.

Cunningham et al,[79] also found that CO oxidation over Au / $Mg(OH)_2$ occurred with an apparent negative activation energy. This is a common finding with MgO and $Mg(OH)_2$ supported gold research in which higher reaction temperatures lead to a decrease in rate. The reason is not entirely clear but is assumed to be related to either the strong bonding of OH groups with gold particles and the associated loss of rotational and vibrational degrees of freedom, or desorption of weakly bonded CO at higher temperatures.

In order to probe the CO oxidation effect more deeply, Sanchez et al[70] used labelled ^{13}CO in a TPR (temperature programmed reaction) experiment. Only $^{13}C^{16}O^{18}O$ was detected, suggesting the absence of lattice oxide participation in Au / MgO catalysis and the participation of gas phase oxygen (which was labeled). It was also found that the smallest active form of gold was the octamer, Au_8 species. All other forms up to this were inactive for CO oxidation. Extensive ab initio calculations based on these data suggested that both CO and O_2 adsorb on the gold particles themselves but that O_2 could also adsorb on the perimeter interface, a finding supported by most investigators.[1, 10, 13]

Galvagno and Parravano [80] investigating NO reduction over Au/MgO and Au/SiO_2 found that choice of support gave very different products, with MgO giving complete reduction to H_2O and N_2, silica as support gave only partial reduction. It was hypothesized that back π donation of electrons from the catalyst to the adsorbed NO weakened the NO bond, thus facilitating dissociation. In a detailed replication study, Lee and Schwank[49] repeated this earlier study but with the finding that NO adsorption (dissociative or molecular) was not influenced by support type, in disagreement with the observations of Galvagno and Parravano.

Margitfalvi, et al,[81] found that ascorbic acid modifcation of Au / MgO increases the activity of this catalyst for low temperature CO oxidation by shifting the ratio of metallic gold / oxidized gold in favour of oxidized gold (which is associated with high catalytic activity). It is hypothesized that ascorbic acid prevents the reduction of oxidized gold during manufacture and the stabilization of both gold nano clusters and oxidized gold sites. It was also found that modification by ascorbic acid had a suppressive effect on carbonate formation that is introduced by spillover of CO onto the support.

It should also be noted that the negative activation effect of Cunningham, et al,[13] was again repeated, however the authors disagreed with the conclusions of Cunningham and suggested the effect was a result of aging of the catalyst. An effect reversed at much higher temperatures.

1.24 Au/Fe_2O_3 supported catalysts.

Unlike magnesium oxide supported gold, iron oxide supported gold catalysts have received considerable attention over the past twenty years and have found utility in catalysing a whole range of reactions from carbon monoxide oxidation,[45] oxidation of benzoyl alcohol,[71] oxidation of volatile organics,[82] ozone decomposition[83] and the water gas shift reaction.[84]

It is not surprising that iron oxide supported gold should be one of the supports most investigated as this material provides a good oxidizing environment for many reactions at low to intermediate temperatures.

Some interesting findings have emerged from iron oxide investigations, notably the absence of isotopic oxygen exchange at room temperature even between carbon monoxide and support oxygens.[1]

Also, as mentioned above, due to the reducibility of iron oxide which is related to its oxygen 'reservoir', the availability of gas phase oxygen is less important and consequently particle size effects become correspondingly inconsequential. However, the gold particle support interface becomes more important if the support is providing oxygen for oxidation,[10] as does the crystallite nature of the

support, which is why pre-treatment and preparation effects are important for reducible metal oxide supports.

Other researchers have found that increasing gold content causes a drop in 'light-off' temperature,[82] it was also found that calcination temperature had marked differential influence on partial oxidation compared to complete oxidation of volatile organics, with higher calcination temperature causing a loss in conversion to carbon dioxide. It was postulated that the transition from ferrihydrite to haematite with the concomitant reduction of oxidized gold to metallic gold was responsible for these performance changes. These observations are supported elsewhere[85] with haematite and metallic gold being the optimium system for CO oxidation. Also, reduction of support resulted in significant loss in activity even though the gold particles were unaffected. This lends extra credence to the importance of the support in catalysis in general and carbon monoxide oxidation in particular.

As mentioned before, It was Haruta,[25] the first to popularize the use of supported gold catalysts, who initially established that the best catalysts have relatively mono-dispersed gold particles in the range of 2-5 nm in diameter. Other researchers have generally confirmed these observations, especially for iron oxide supported gold, but with the additional findings as mentioned above. An especially recurring theme is preparation technique, with co-precipitated iron oxide supported gold performing considerably better than impregnated materials. This will be touched on in greater detail later in the report.

1.25 Other supported gold catalysts for carbon monoxide oxidation.

So far only magnesium oxide and iron oxide supported gold catalysts have been discussed in detail but there exists an abundance of literature on other supported gold materials for many reactions, but in particular, the oxidation of carbon monoxide. Many researchers have investigated the catalytic effects of supported

gold on carbon monoxide oxidation employing a variety of different supports including titania,[63] copper oxide[86] and zinc oxide.[86]
A variety of different preparation methods have been utilised ranging from co-precipitation[21] to deposition/precipitation[75] with a range of different gold loadings.[33] From the published material It appears that the activity of the gold catalysts studied depend strongly on the support chosen,[18,33,43] for reasons that have been discussed before. Apart from the choice of the support, the preparation method is seen to be crucial. Some Investigators suggest gold/support interaction effects are important for any level of catalytic ability.[49,75,76] In particular the gold particle-support interface is claimed to be an essential feature for carbon monoxide oxidation.[25]

1.26 Theories of the mechanism of carbon monoxide oxidation.

From the literature there appear to be two classes of theory for the action of supported gold materials in carbon monoxide oxidation, one that involves oxidation by the lattice oxide and the other theory that doesn't require lattice oxide oxidation. These two theories can be broken down into models according to different reactions that can occur on the catalyst surface.

Model 1 (no lattice involvement, dissociation of oxygen)

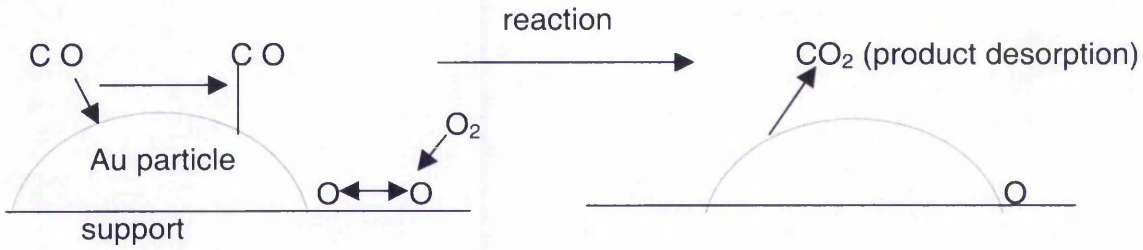

For this model there is no involvement of lattice oxygen, only surface species are involved.[26] Carbon monoxide adsorbs on the surface of a gold particle and migrates to the particle / support interface, where it reacts with oxygen provided by the dissociative adsorption of gas phase oxygen. Carbon dioxide then desorbs and another CO molecule reacts with the remaining oxygen species.

Model 2 (lattice oxygen involvement)

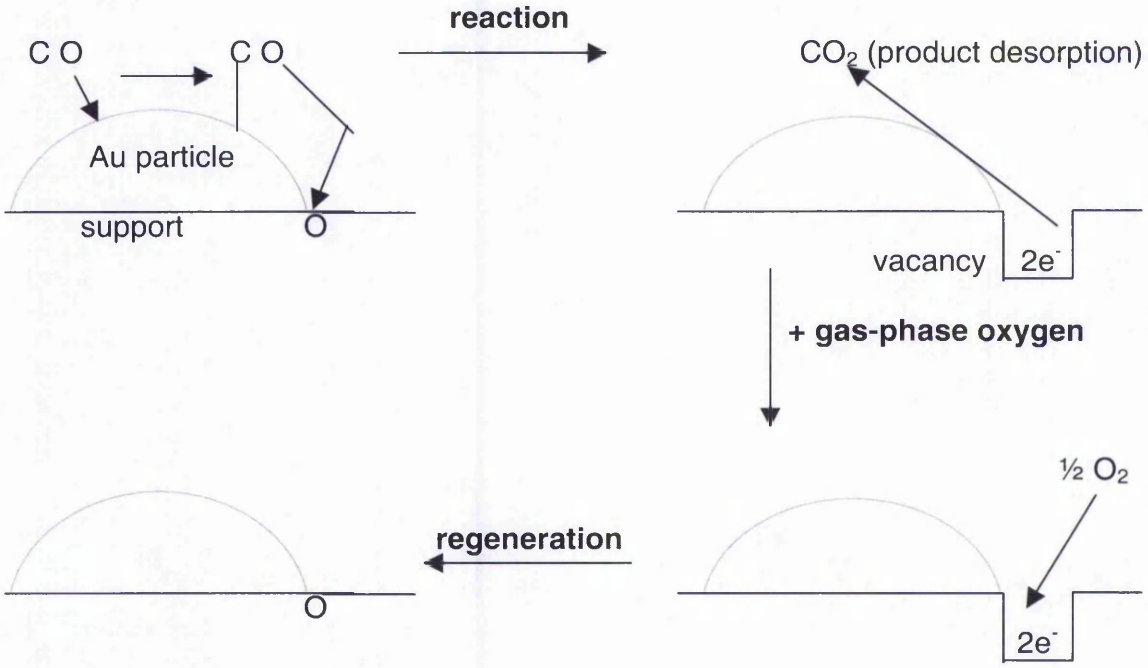

This model requires the use of lattice oxygen in the reaction. In the diagram the impression is given that particles are required for lattice oxide participation but others have observed this reaction on metal oxide alone.[87]

Initially carbon monoxide adsorbs on the gold particle and migrates to the interface where it reacts with lattice oxygen. This leaves a vacancy that is regenerated by gas phase oxygen. It is here that isotopic oxygen exchange studies should be useful. Analysis and comparison of carbon monoxide oxidation and exchange data should give a clue as to which theory (no lattice, lattice) is more likely to be correct, for magnesium oxide supported gold.

Model 3 (lattice oxygen involvement with gold / support induced vacancy formation)

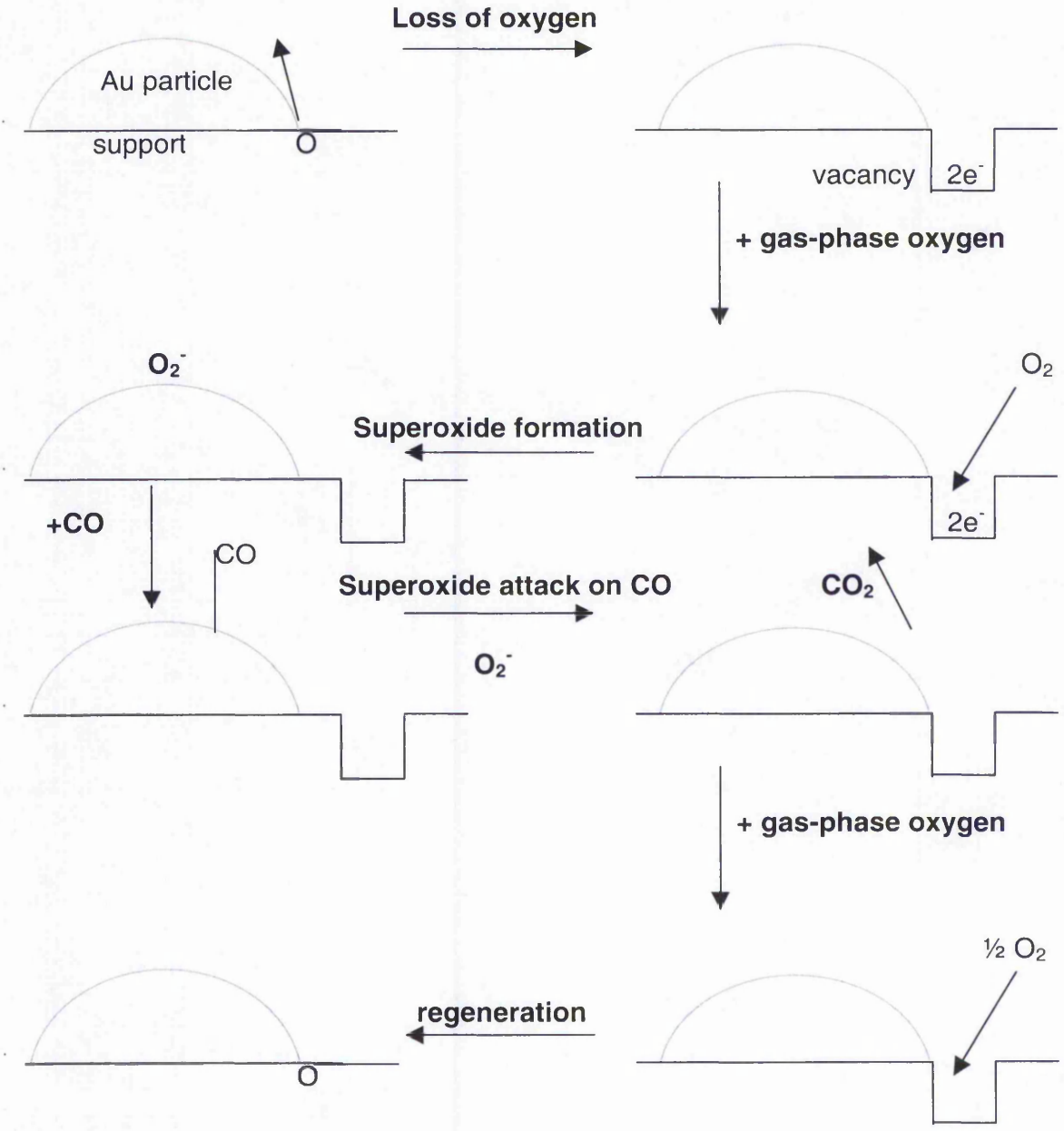

Model 3 also requires the participation of lattice oxygen but here the vacancy is induced by the support / gold system not initiated by carbon monoxide. Obviously, highly reducible supports such as iron oxide will more likely undergo the above scenario than magnesium oxide. However, because lattice oxygen is involved a correlation with exchange is still predicted.

Model 4 (lattice oxygen involvement with hydroxyl group participation)

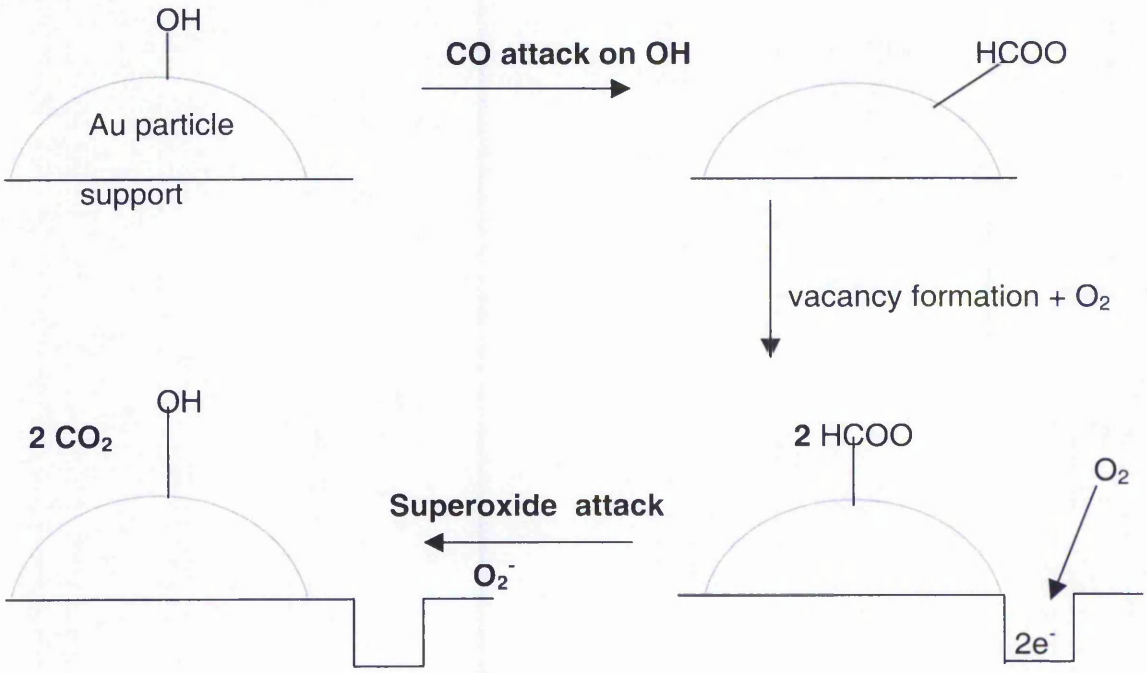

In the fourth model there is again involvement of the lattice oxide but with the participation of hydroxyl groups. These are attacked by an incoming CO molecule. Consequently a formate group is produced which undergoes attack by a superoxide species (which is formed the same way as in model 3, ie, through vacancy formation). This second attack replenishes the hydroxyl group and releases CO_2.

Model 5 (attack on CO by molecularly adsorbed O_2, no lattice involvement)

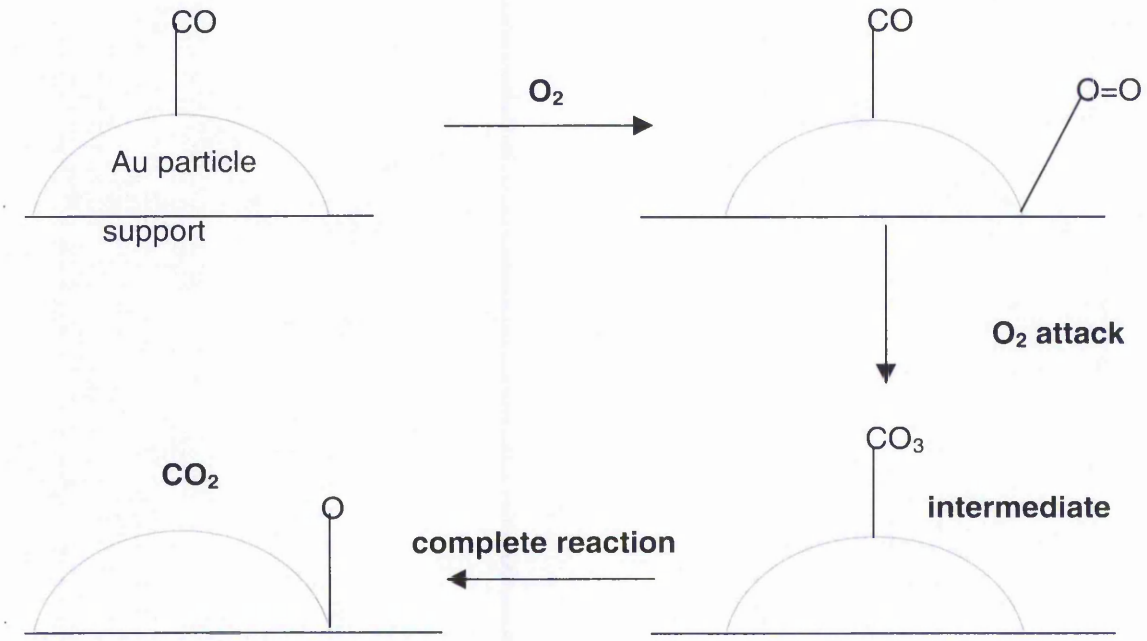

In model 5, CO undergoes attack by molecularly adsorbed oxygen. A carbonate intermediate is hypothesized to occur which breaks down to CO_2. A remaining oxygen adatom can react with a CO molecule as in model 1.

As with all these scenarios there are additional pathways that can occur, the eventual number of variations is large. In model 4, for instance, dissociatively adsorbed oxygen can act to replenish the vacancy that is produced in the last step and also oxidize carbon monoxide as in the first model.

Model 6 (attack on water by molecularly adsorbed O_2, no lattice involvement)

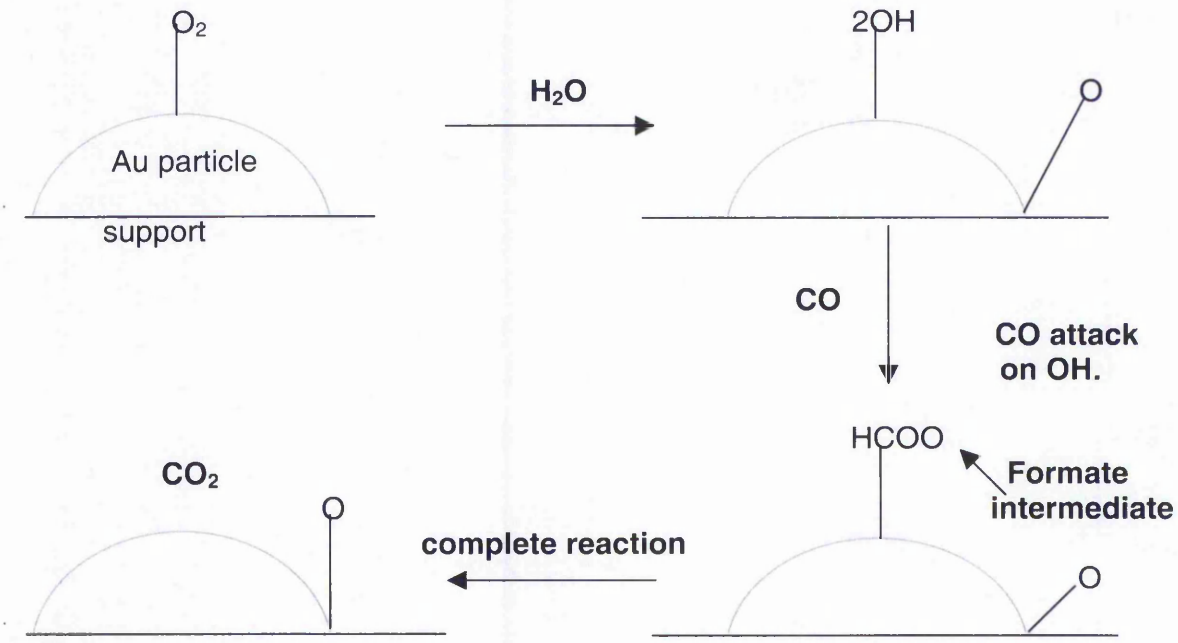

In model 6, pre-adsorbed oxygen (perhaps as a superoxide) attacks an incoming water molecule resulting in the formation of hydroxyl groups. These then attack an adsorbed CO molecule resulting in a formate intermediate. This can undergo a reaction with a dissociated oxygen species to produce the desired CO_2, leaving behind a dissociated oxygen that can take part in another CO oxidation.

1.27 Putting it all together: The relationship between carbon monoxide oxidation data and isotopic exchange data.

The exchange of oxygen with the lattice that occurs during isotopic oxygen exchange is thought to involve weakening or activation of the oxygen bond prior to exchange. This is also thought to occur during the Mars van-Krevelen (section 1.3.3) mechanism that is hypothesized to occur for some scenarios that try and explain carbon monoxide oxidation. As can be appreciated, the third step in the Mars van Krevelen mechanism is highly pertinent to isotopic oxygen exchange where lattice species are involved in both processes. If oxygen activation is the rate-determining step then it can be understood why a relationship should exist between isotopic oxygen exchange and carbon monoxide oxidation data,[88] as both processes require the weakening of the oxygen-oxygen bond. Combining reactor and exchange data with characterisation information could give clues as to why supported gold materials are effective for many reactions in general and carbon monoxide oxidation in particular.

Others have also investigated this relationship. Winter,[7] by following the oxidation of carbon monoxide on an earlier $^{36}O_2$ enriched support surface detected labeled carbon dioxide, suggesting a Mars van Krevelen mechanism.

Boreskov[8] demonstrated a correlation in carbon monoxide activity with exchange activity across first row transition metals, indicating the involvement of lattice oxides and hence the Mars van Krevelen mechanism in carbon monoxide oxidation.

It is entirely possible that both exchange and oxidation involve lattice oxygen, but differences in mechanism could result in very different kinetics. Oxygen exchange could be a pre-dominantly support based effect whereas carbon monoxide oxidation could be dependent on particle/support interactions. It is important to note, however, that some researchers have found evidence that supports the existence of two mechanistic pathways operating in synergy, a fast non-lattice pathway with a co-existing slow lattice involved pathway.[13]

References for introduction:

1. Liu.H, Kozlov.K.I, Kozlova.A.P, Shido.T, Iwasawa.Y
Phys.Chem.Chem.Phys, **1**, 2851-2860, (1999)

2. Schimpf.S, Lucas.M, Mohr.C, Rodemerck.U, Bruckner.A, Radnik.J, Hofmeister.H, Claus.P
Catalysis Today, **72**, 63-78, (2002)

3. Coluccia, S., Tench, A.J., and Segall, R.L.,
J. Chem.Soc, Faraday Trans, **1**, 75, 1769-1779, (1979)

4. Moodie, A. F and Warble, C. E.,
J. Cryst. Growth, **10**, 26-38, (1971)

5. Klier, K., Novakova,J.,and Jiru,P.
Journal of Catalysis, **2**, 479-484, (1963)

6. Muzykantov. V.S, Jìru. P, Klier. K, and Novakova. J,
J. Collection Czech. Chem. Commun, **33**, 829-835, (1968)

7. Winter. E.R.S
Adv Catal, **10**, 196-241, (1958)

8. Boreskov, G.K.,
Adv. Catal. **15**, 285-339, (1964)

9. Hargreaves J.S.J, Joyner.R.W, Mellor.I.M
Journal of Molecular Catalysis A: Chemical, **141**, 171-176, (1999)

10. Schubert.M.M, Plzak.V, Andre.C.V.V, Behm.J.R, Muhler.M, Hackenburg.S
Journal of Catalysis, **197**, 113-122 (2001)

11. Schubert, M.M., Kahlich, M.J., Gasteiger, H.A, Behm, R.J.,
J.Power Sources, **84**, 175-182, (1999)

12. Boccuzzi.F, Chiorino.A, Manzoli.M, Lu.P, Akita.T, Ichikawa.S, Haruta.M
Journal of Catalysis, **202**, 256-267 (2001)

13. Boccuzzi.F, Chiorino.A, Tsubota.S, Haruta.M
J. Phys. Chem, **100**, 3625-3631, (1996)

14. Naito. S, Tanimoto.M
J. Chem. Soc., Chem. Commun,**12**, 832-834, (1988)

15.Kahlich.M.J, Gasteiger.H.A, Behm.R.J
Journal of Catalysis, **182**, 430-440, (1999)

16. Xia.G.G, Yin.Y.G, Willis.W.S, Wang.J.Y, Siub.S.L
Journal of Catalysis, **185**, 91-105 (1999)

17. Choudhary.T.V, Sivadinarayana.C, Chusuie.C.C, Datye.A.K, Fackler.J.P, Goodman.D.W
Journal of Catalysis, **207**, 247-255 (2002)

18. Haruta.M, Genet.M.J, Delmon.B
Journal of Catalysis, **144**, 175-192. (1993)

19. Park.E.D, Lee.S.J
Journal of Catalysis, **186**, 1-11, (1999)

20. Seker.E, Cavataio.J, Gulari.E, Lorpongpaiboon.P, Osuwan.S
Applied Catalysis A: General, **183**, 121-134, (1999)

21. Haruta.M, Kobayashi.T, Sano.H, Yamada.N
Chemistry Letters,**17**, 405-408, (1987)

22. Visco.A.M, Neri.F, Donato.A, Milone.C, Galvagno.S
Phys.Chem.Chem.Phys, **1**, 2691-2873, (1999)

23. Bond.G.C, Thompson.D.T
Catalysis Reviews-SCI.ENG. **41**,(3&4), 319-388, (1999)

24.Bailie.J.E, Abdullah.H.A, Anderson.J.A, Rochester.C.H, Richardson.N.V, Hodge.N, Zhang.J.G, Burrows.A, Kiely.C.J, Hutchings.G.J
Phys. Chem. Chem. Phys, **3**, 1-9, (2001)

25. Haruta.M, Yamada.N, Kobayashi.T, Ijima.S
Journal of Catalysis, **115**, 301-309, (1989)

26. Haruta.M, Tsubota.S, Kobayashi.T, Kageyama.H, Genet.M, Delmon.B
Journal of Catalysis, **144**, 175-192, (1993)

27. Hodge.N.A, Kiely.C.J, Whyman.R, Siddiqui.M.R.H, Hutchings.G.J, Pankhurst.Q.A, Wagner.F.E, Rajaram.R.R, Golunski.S.E
Catalysis Today, **72**, 133-144, (2002)

28: Kozlova.A.P, Sugiyama.S, Kozlov.A.I, Asakura.K, Iwasawa.Y
Journal of Catalysis, **176**, 426-438, (1998)

29. Cunningham.D.A.H, Kobayashi.T, Kamijo.N, Haruta.M
Catalysis Letters, **25**, 257-264, (1994)

30. Su.Y-S, Mei.Y.L, Lin.S.D
Catalysis Letters, **57**, 49-53, (1999)

31. Gupta.N.M, Tripathi.A.K
Journal of Catalysis, **187**, 343-347, (1999)

32. Lee.S.L, Gavriilidis.A, Pankhurst.Q.A, Kyek.A, Wagner.F.E, Wong.P.C.L, Yeung.K.L
Journal of Catalysis, **200**, 298-308, (1984)

33. Grunwaldt.J.D, Kiener.C, Wögerbauer.C, Baiker.A
Journal of Catalysis, **181**, 223-232, (1999)

34. Schubert.M.M, Plzak.V, Garche.J, Behm.J.R
Catalysis Letters, Vol **76**, No.3-4, 143-150, (2001)

35. Grisel.R.J.H, Nieuwenhuys
Journal of Catalysis, **199**, 48-59, (2001)

36. Dekkers.M.A.P, Lippets.M.J, Nieuwenhuys.B.E
Catalysis Letters, **56**, 195-206, (1998)

37. Hao. Zhengping, An.Lidun, Wang.H, Tiandou.H
React.Kinet.Catal.Lett, Vol. **70**. No. 1, 153-160, (2000)

38. Yuan.Y, Asakura.K, Wan.H, Tsai.K, Iwasawa.Y
Chemistry Letters, **9**, 755-768, (1996)

39. Uphade .B.S, Yamada.Y, Akita.T, Nakamura.T, Haruta.M
Applied Catalysis A: General, **215**, 137-148, (2001)

40. Bond. G. C
Catalysis Today. **72**, 5-9, (2002)

41. Hayashi.T, Tanaka.K, Haruta.M
Journal of Catalysis, **178**, 566-575, (1998)

42. Blick. K, Mitrelias.T.D, Hargreaves.J.S.J, Hutchings.G.J, Joyner. R.W, .Kiely.C.J, Wagner.F.E.
Catalysis letters, **50**, 211-218, (1998)

43. Lin.S, Bollinger.M, Vannice.M.A
Catalysis letters, **17**, 245-262, (1993)

44. Yuan.Y, Kozlova.A.P, Asakura.K, Wan.H, Tsai.K, Iwasawa.Y\
Journal of Catalysis, **170**, 191-199, (1997)

45. Bond.G.C, Thompson.D.T
Gold Bulletin, **33**(2), (2000)

46. Ueda.A, Haruta.M
Gold Bulletin, **32**, 3-11, (1999)

47. Inamura.S, Sawada.H.R, Uemura.K, Ishida.S
Journal of Catalysis. **109**, 198-212, (1988)

48. Hoflund.G.B, Gardner.S.D, Schrer.D.R, Upchurch.B.T, Kielin.E.
J. Chem. Soc. Faraday Trans. **93**, 187-195, (1997)

49. Lee.J.Y, Schwank.J
Journal of Catalysis, **102**, 207-215, (1986)

50. Tripathi.A.K, Kamble.V.S, Gupta.N.M
Journal of Catalysis, **187**, 332-342, (1999)

51. Daté.M, Haruta.M
Journal of Catalysis, **201**, 221-224, (2001)

52. Gregg.S.S, Sing.K.W.S, Adsorption Surface Area and Porosity. Academic Press, 2nd Edition, (1982).

53. Kozlova.A.P, Kozlov.A.I, Sugiyama.S, Matsui.Y, Asakura.K, Iwasawa.Y
Journal of Catalysis, **181**, 37-48, (1999)

54. Report of the Research Achievements of Interdisciplinary Basic Research Section (April 1994-March 1999) Osaka National Research Institute (ONRI)

55.Mul. G, Zwijnenburg.A, Liden. B.V.D, Makkee.M, Moulijn.J.A
Journal of Catalysis, **201**, 128-137, (2001)

56. Stangland.E.E, Stavens.K.B, Andres.R.P, Delgass.W.N
Journal of Catalysis, **191**, 332-347, (2000)

57. Knell.A, Barnickel.P, Baiker.A, Wokaun.A
Journal of Catalysis **137**, 306-321, (1992)

58. Hutchings.G.J
Catalysis Today, **72**, 11-17, (2002)

59. Nkosi.B, Coville.N.J, Hutchings.G.J
J.Chem.Soc.,Chem.Commun, 71-73, (1988)

60. Nkosi.B, Coville.N.J, Hutchings.G.J, Adams.M.D
Journal of Catalysis, **128**, 378-386, (1991)

61. Nkosi. B, Coville.N.J, Hutchings.G.J, Adams.M.D, Friedl.J, Wagner.F.E
Journal of Catalysis, **128,** 366-377, (1991)

62. Daniel.W.M, White.J.M,
Int. J. Chem. Kinet, **17**, 413-422, (1985)

63. Bollinger.M.A, Vannice.M.A,
Appl. Catal.B, Environ. B, **4**, 417-443 (1996)

64. Lizuka.Y, Tode.T, Takao.T, Yatsu.K, Takeuchi.T, Tsubota.S, Haruta.M
Journal of Catalysis, **187**, 50-58, (1999)

65. Liu.H, Kozlov.A.I, Kozlova.A.P, Shido.T, Asakura.K, Iwasawa.Y
Journal of Catalysis, **185**, 252-264, (1999)

66. Olea.M, Kinitake.M, Shido.T, Iwasawa.Y
Phys. Chem. Chem. Phys. **3**, 627-631, (2001)

67. Hao. Z, Fen.L, Lu.G.Q, Liu.J, An.L, Wang.H
Applied Catalysis A: General **213**, 173-177, (2001)

68. Okumura.M, Coronado.J.M, Soria.J, Haruta.M, Conesa.J.C
Journal of Catalysis, **203**, 168-174, (2001)

69. Oh.S.H, Sinkevitch.R.M
Journal of Catalysis, **142**, 254-266, (1993)

70. Sanchez.R.M.T, Ueda.A, Tanaka.K, Haruta.M
Journal of Catalysis, **168**, 125-127, (1997) (research note)

71. Milone.C, Ingoglia.R, Neri.G, Pistone.A, Galvagno.S.
Applied Catalysis A: General, **211**,251-257, (2001)

72. Zwijnenburg.A, Saleh.M, Makkee.M, Moulijn.J.A
Catalysis Today, **72**, 59-62, (2002)

73. Biella.S, Prati.L, Rossi.M
Journal of Catalysis **206**, 242-247, (2002)

74. Prati.L, Rossi.M
Stud. Surf. Sci. Catal. **110**, 509-518 (1997)

75. Sakurai.H, Ueda.A, Kobayashi.T, Haruta.H
Chem Comm, **3**, 271-272, (1997)

76. Stangland. E.E, Stavens. K. B, Andres. R.P, Delgass. W. N.
Journal of Catalysis, **191**, 332-347, (2000)

77. Hargreaves, J.S.J, Hutchings, G.J, Joyner, R.W, and Kiely C.J.
Journal of Catalysis, **135**, 576-589, (1992)

78. Cunningham, D.A.H, Vogel. W, Kageyama, H. Tsubota, S. Haruta. M,
Journal of Catalysis, **177**, 1-10, (1998)

79. Cunningham.D.A.H, Vogel.W, Haruta.M
Catalysis Letters, **63**, 43-47, (1999)

80. Galvagno.S, Parravano.G.J
Journal of Catalysis, **55**, 178-190, (1978)

81. Margitfalvi.J.L, Fási.A, Hegedüs.M, Lónyi.F, Gõbölös.S, Bogdanchikova.N
Catalysis Today, **72**, 157-169, (2002)

82. Minico.S, Sciré.S, Crisafulli.C, Galvagno.S
Applied Catalysis B: Environmental, **34**, 277-285, (2001)

83. Hao.Z, Cheng.D, Guo.Y, Liang.Y
Applied Catalysis B: Environmental, **33**, 217-222, (2001)

84. Andreeva.D, Idakiev.V, Tabakova.T, Andreev.A
Journal of Catalysis, **158**, 354-355, (1996)

85. Horvath. D, Toth.L, Guczi.L
Catalysis Letters, **67**,117-128, (2002)

86. Hutchings.G.J, Rafiq.M, Siddiiqui. M, Whyman. R, Burrows.A, Kiely C.J
J.Chem.Soc., Faraday Transactions, **93(1)**, 187-188, (1997)

87. Jansson.J
Journal of Catalysis, **194**, 55-60, (2000)

88. Ramesh. S, Hegde. MS.
J. Phys. Chem, **100**, 8443-8447, (1996)

89. Puckhaber.L.S, Cheung.H.R, Cocke.D.L, Clearfield.A
Solid State Ionics, **32/33**, 206-215, (1989)

90. Peil, K. P., Goodwin Jr, J. G., and Marcelin, G.,
Journal of Catalysis, **131**, 143-155, (1991)

Chapter two

The most beautiful thing we can experience is the mysterious. It is the source of all true art and science.

Albert Einstein

Chapter 2: Experimental

2.1 BET surface area measurement

Physisorption of nitrogen at –196°C onto a surface and measurement of the uptake as a function of equilibrium pressure allows the construction of an isotherm. This isotherm is then linearised mathematically. The approach most often used was devised by Brunauer, Emmett and Teller, [1] who derived the following expression:

$$P/V(P_o - P) = 1/VmC + (C-1)/VmC.(P/P_o)$$

Where V = volume of gas adsorbed at equilibrium pressure P,
Vm = volume required to form one monolayer : Po = saturated vapour pressure of the adsorbent gas at the temperature of measurement and C is a constant.

For suitable adsorbents, plotting P/V(Po-P) against P/Po gives a linear plot in the range ca, $0.05 < P/Po < 0.30$, the slope given by (C-1)/ VmC and the intercept by 1/ VmC.

Sample preparation for BET analysis

Samples were initially outgassed at 150°C and pressure of ca 5 x 10^{-2} bar to remove weakly adsorbed contaminants such as water. Measurements were performed using a purpose built automatic instrument, where helium is the calibrant and nitrogen the adsorbate at –196°C. Surface areas are calculated via the BET program assuming a cross sectional area of 0.162 nm^2 for the nitrogen molecule.

2.2 Quantachrome measurements

In addition to BET analysis, surface areas were also measured using the quantachrome set-up, which finds utility for limited amounts of sample.
Here the material is exposed to varying nitrogen and helium ratios at –196°C. Usually the BET range of P/Po 0.05 to 0.30 is used but full isotherms can also be performed but with limited accuracy for low P/Po values (< 0.05).
Instead of interpreting pressure changes as with the BET set-up, the quantachrome measures the amount of nitrogen directly that has physisorbed on the surface. After approximately 10 minutes of equilibration the sample is rapidly warmed and any nitrogen that desorbs is registered as a count. An adapted thermal conductivity detector is employed for this purpose. After each P/Po point (usually five) a known amount of nitrogen is injected and the sample counts are compared to these calibrated values. Relative partial pressures for nitrogen, (P/Po), are controlled by manipulating the flow of nitrogen and helium gas over the sample to achieve the desired value. For example, a relative partial pressure of 0.1 is achieved by flowing nitrogen at 2 cm^3 / min with helium at 18 cm^3 / min.

2.3 Full Isotherms on the Vacuum microbalance

Samples can also have their full isotherms measured on the vacuum microbalance. This technique has the advantage over the quantachrome and the purpose built BET set-up, of increased accuracy at low P/Po values. Here the sample is simply exposed to given amounts of nitrogen at –196°C and vacuum. Any nitrogen uptake is measured by a micro-balance as a gain in weight of the sample.
In addition to adsorption isotherms, desorption isotherms can also be performed in which the nitrogen pressure is reduced and the loss in adsorbed nitrogen is followed as a decrease in sample weight.

2.4 SEM

Figure 2.4.1: The model of SEM that was used in sample characterisation: JSM 840-A

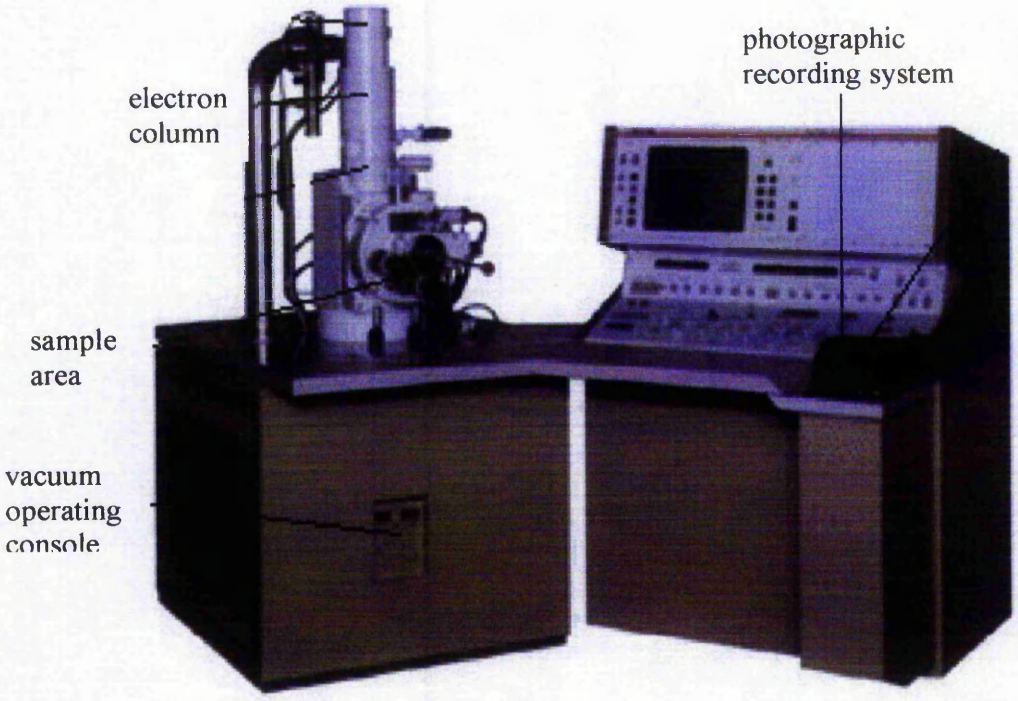

Figure 2.4.1 is a picture of the model of SEM that was used for some of the samples. The SEM that was used at Jeol ltd was the JSM 5610-LV series, which is very similar to the above SEM. Both machines had an operating voltage of 4keV for the samples under investigation. Samples were loaded on a 12.5 mm aluminium stub with carbon adhesive. Samples were then coated with carbon. This has the advantage of reducing sample charging but unfortunately cannot withstand the higher operating voltages required for superior resolution. However, for the samples under investigation some important detail can be resolved with the lower voltage of 4keV. In order to get visual information on the effect of preparation method and gold loading on the support / gold particles for both support types, scanning electron microscopy (SEM) was employed. It was found that samples were not successfully imaged using the departmental transmission electron microscope (TEM) and consequently a

decision was made to use an outside SEM (Jeol ltd) for some samples and later on the departmental SEM for the remaining samples. Also, EDX was performed on some samples to establish the existence of gold particles when assumed present from SEM images. EDX measures the X-rays emitted as electrons are knocked out of their orbitals (by the electron beam) to inner orbitals. Each element possesses a characteristic X-ray wavelength or signature.

2.5 TPR

The extent and temperature range in which bulk and surface reduction of a supported catalyst can be measured reaches up to 1000°C using temperature programmed reduction (TPR). In the set-up, a flow of hydrogen (5% in argon) is passed over the catalyst and any hydrogen uptake is measured by a thermal conductivity detector. A difference in pre and post reactor hydrogen concentration constitutes the TPR signal.

As H_2 / Ar is passed over the catalyst, the temperature of the reactor bed is increased at a given ramp-rate. The combined data; hydrogen uptake as a function of temperature, comprise the TPR profile.

Because experimental conditions can have marked influences on TPR profiles, it is important to establish optimum conditions that take into account important experimental variables. This is assisted by using the Monte Baiker[2] approach:

Monte Baiker equation: $K = S_o / (V.C_o)$

Where; K is a constant of calculation

S_o is the total amount of reducible species (μmol)

V is the total flow rate of the gas stream (ml s^{-1})

C_p is the initial concentration of the reducing gas (μmol ml^{-1})

It has been found that optimum reduction profiles are obtained when K is close to 100.This has been achieved in the current research.

2.6 Powder X-Ray Diffraction (XRD)

X-ray diffraction may be used to identify the crystalline phase present in a sample. Diffraction occurs when the angle of incidence of X-rays on a solid satisfies the Bragg equation:

Bragg equation: $n\lambda=2d\sin\theta$

Were: n = a low value integer

λ = wavelength of X-ray source

d = crystal plane separation

θ = angle of incidence of X-rays

Reflections from a diffraction pattern can be compared with tabulated values[3] therefore facilitating compound identification.

Measurements were performed using a Hiltonbrooks modified diffractometer with a Cu Kα source possessing a wavelength of 1.542Å. Typically a scan range of 5 – 80° 2θ was employed as all the reflections of analysis fell within this range.

For both the MgO and Fe_2O_3 supported classes, a step size of 0.02° was used but with 0.5s dwell time for MgO compared to 8s dwell time for Fe_2O_3. This disparity is accounted for by the much greater degree of crystallinity for MgO than Fe_2O_3.

2.6.1 Determination of crystal size:

Application of the Scherrer equation gives crystal sizes associated with particular reflections in an X-ray diffraction:

Scherrer equation: $d = k\lambda / B\cos\theta$

Where: d = average particle size diameter in Å

K = constant (57.296°)

λ = wavelength of X-ray source / 1.5418Å

B = FWHM / degrees

θ = Angle of incident X-ray / degrees

2.7 X-ray Photoelectron Spectroscopy (XPS)

XPS is one of the most versatile techniques for investigating surfaces. The basis of XPS is founded on the photoelectric effect, whereby photons of a suitable, fixed energy (hv) induce emission of electrons from both valence and core orbitals of an atom. Valence electron energy distributions are influenced by their immediate environment but core electron binding energies are principally determined by the atomic number and hence can be used as signatures of atom type.

The conservation equation: $KE = h\nu - (BE + \phi)$

Can be used to estimate kinetic energies of electron given a known photon energy;

Where: h = planck's constant
I = binding energy of electron
Ekin = kinetic energy of electron
ϕ = work function

Magnesium Kα radiation was used, giving $h\nu$ = 1256 eV incident to the sample. Binding energies were calibrated using adventitious carbon, and assuming a binding energy of 284.6 eV. All peaks were identified according to the handbook of photoelectron spectroscopy[4].
In order to calculate the relative contribution from individual species in the samples, the following expression was used:

$$N_A/N_B = I_A/I_B \times \delta_A/\delta_B[E_A/E_B]^{0.6}$$

Where: A,B: elements A and B
I: peak area (corrected for number of scans)
N_A/N_B: surface ratio of species A to B
δ: photoionisation cross sectional area
0.6: instrument specific

Samples were attached to the probe using double-sided sticky tape. During measurement, the pressure in the analysis chamber was typically 5 x 10^{-8} mbar.

2.8 Isotopic Oxygen Exchange Measurements

Usually 20 –100 mg of material were loaded into the micro-reactor (depending on surface area) so as to expose approximately equal surface areas to the gas phase, (around 1 – 3 m^2). The material is placed in between silica wool plugs. The integrity of the rig is tested to ensure leak tightness and then the sample is heated under static conditions at 465°C for approx 12 hours to remove any hydroxyl groups from the surface. The temperature is lowered to the exchange temperature of 435°C and evacuated as much as possible by opening the leak valve to the mass spec (which is off). Once the system is evacuated, oxygen 36 is carefully dosed into the micro reactor so that the number of gas phase molecules is in excess of the number of surface exchangeable sites. The leak valve to the mass spec is then opened and the products of exchange are monitored using a quadrupole mass spec.
It is of interest to compare moles of oxygen in the sample to that of the gas phase. If bulk exchange were occurring instead of surface monolayer exchange, then these calculations would show how much gas phase oxygen would be required for this to happen.
For a 100 mg sample of magnesia exposed to 25 mbar of oxygen:

Oxygen molarity in sample: 0.1g / 40 g = 0.0025 moles (1.5 E21 atoms of oxygen)
Oxygen molarity of gas phase: n = PV / RT
P = 25 / 1000 * 101325 nm^3 = 2533.1 nm^3
V = 50cc / 10E6 = 5.0E-5 m^3
R = 8.314 J^{-1} K^{-1} mol^{-1}
T = 298 K
N = (2533.1 * 5.0E-5 m^3) / (8.314 * 298) = 5.11 E-5 moles of O_2 (6.2 E19 atoms of oxygen). Therefore there are 24 times as many oxygen atoms in the sample than in the gas phase. This result illustrates the importance of only exchanging the surface by setting a low enough exchange temperature, (as was done in this research).

2.9 The experimental set-up.

All samples undergo oxygen exchange in the micro-reactor as shown below:

Figure 2.9.1: the micro-reactor set-up

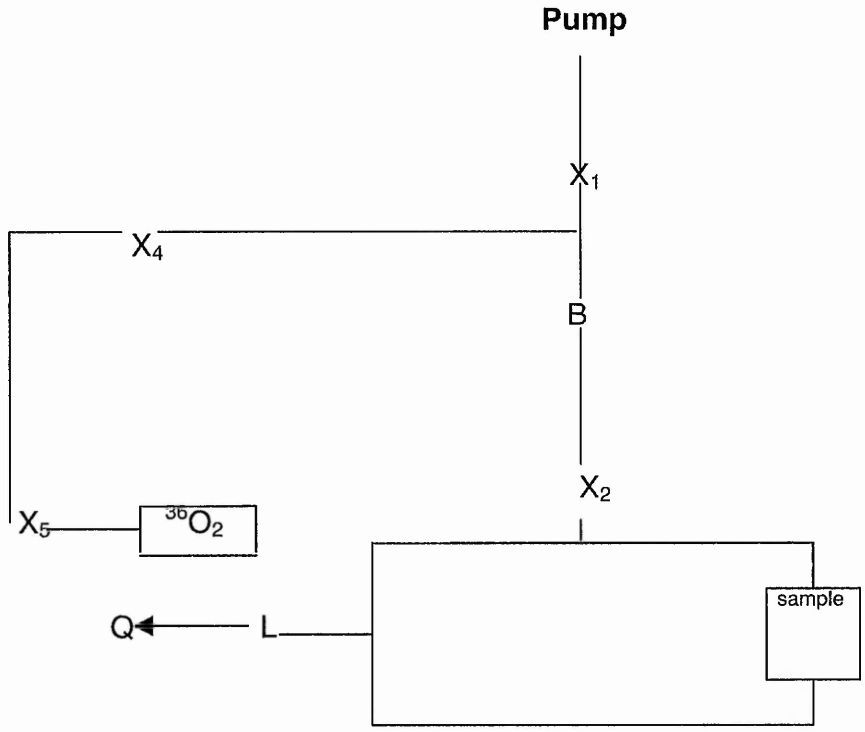

L = leak valve

X = valve

B = barocell

Q=quadrupole

2.10 The Quadrupole Mass Spectrometer

The main components of a mass spectrometer are the ionising chamber, the analysis components and the detector. In a quadrupole mass spectrometer the ionising electrons are produced by a hot filament, and the analyser consists of two pairs of conducting rods, one pair at a positive DC potential with respect to the other pair, which is at a negative DC potential with respect to earth. Superimposed on the DC potential is a radiofrequency (RF) potential, which cycles between the pairs of rods at around 10^8 Hertz. Therefore even though the DC potentials are constant, at any given time one pair of rods is at an RF potential that is positive with respect to the other pair, which has a negative RF potential. The next RF cycle produces a reversal of this situation.

Figure 2.10.1:

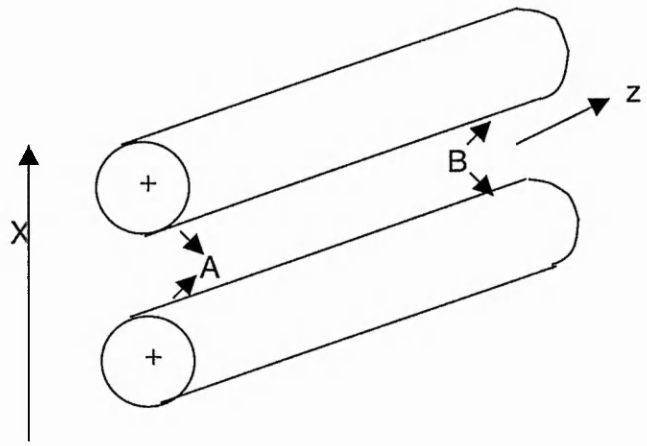

Figure 2.10.1 shows the effect of an RF potential on the behaviour of ions in the absence of a DC potential for a pair of positive rods in the x-z plane. During the positive half of an RF cycle the ions (which also have a positive charge) are repelled from the rods into the quadrupolar space as represented by A. During the negative half the ions are attracted and collide with the rods and thus are carried off as uncharged species, as represented by B.

With the addition of the positive DC potential a competition emerges between the negative excursion of the RF potential and the DC potential on the behaviour of the ion and the result depends upon a) the amplitude of the RF voltage and b) the mass of the ion. Heavy ions will require greater amplitude than lighter ions to develop unstable oscillations that will carry them to the rods and thus escape detection and are less affected by the RF potential and more under the influence of the DC potential. Lighter ions will be affected more by the RF potential than heavier ions and will require smaller amplitudes to develop unstable oscillations. The influence of the DC potential is correspondingly reduced for lighter ions. Hence lighter ions are more likely to collide with the rods and escape detection in the above system. Therefore positive rods in the x-z plane can be viewed as filters *against* low mass ions.

For negative rods in the y-z plane the situation is reversed. Here positive ions would always be attracted to the negative rods and become neutralised thus escaping detection, if it were not for the positive excursion of the RF potential. Here lighter ions are influenced more by the RF field than heavier ions and are repelled into the quadrupolar space whilst heavier ions, more under the influence of the DC potential, are more likely to collide with the rods and escape detection.
In effect it is the sum of the fixed DC potential and the instantaneous RF potential that determines if a given species will be detected or not. The mass of a species and the amplitude of the RF potential influence this sum.

The combined effect from both pairs of rods is illustrated in figure 2.10.2.

Figure 2.10.2:

Here diagram a) represents a filter against low mass ions, such as the positive rods in the x-z plane. Diagram b) represents a filter against high mass ions, such as the negative rods in the y-z plane. The shaded area refers to ions that are transmitted to the detector.

Combining the 2 diagrams gives figure 2.10.3:

Figure 2.10.3:

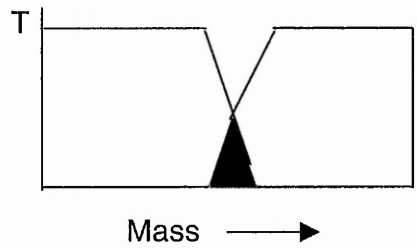

Here the ions that are neither too light nor too heavy (in black) have stable oscillations and are detected. Ions that are too light or too heavy develop unstable oscillations, collide with the rods, and so are not detected. It can be seen that only a small proportion of ions get through to the detector. These are the ions of a *particular* mass that we are interested in during a part of the scan cycle. Adjusting the ac and dc potentials can alter the size of the shaded area.
Once the ions are transmitted through the rods they are detected either by a Faraday cup or an electron multiplier. The electron multiplier is sensitive to 10^{-12} bar whilst the faraday cup operates to 10^{-9} bar. All the studies reported here have been carried out in Faraday cup mode.

2.11 CO oxidation

For measurements of the rate of carbon monoxide oxidation, samples are secured between two glass wool plugs in a glass lined stainless steel reactor vessel (ID 12 mm). Reactant gases (40% oxygen 5% carbon monoxide, balance helium) are fed at controlled flows using a set of mass flow controllers across the material and at a range of temperatures. Online gas chromatography (GC) follows the products of oxidation. The amount of material depends on the type of catalyst, with impregnated materials generally denser than co-precipitated materials. Consequently a variable amount of material (dependent on preparation class) is used so as to achieve a gas hourly space velocity (GHSV) of around 30,000 - 40,000 ml/h^{-1}. In practice this means usually a 100 mg of impregnated material and 30 – 40 mg of co-precipitated material is added to the reactor set-up.

2.11.1 Gas chromatographic analysis

Products are separated according to their mass flow characteristics and column interactions. In order to achieve better separation of oxygen and carbon monoxide, the column used (porapak QS) comprises an inner and outer column. The inner column elutes oxygen and CO_2 while the outer column elutes CO and also oxygen. Once the carrier gas has eluted through the column, the components are detected by a thermal conductivity detector (tcd). The individual components are now discussed.

2.11.2 The column

The components of the gas stream are separated according to their affinity for the material of the column. The material of the column consists of a mixture of porous polymers that separate the constituents of a gas according to shape, size and functionality.

2.11.3 Thermal Conductivity Detector (TCD)

The principle underlying the operation of a TCD is that a hot object loses heat at a rate that is dependent on its gaseous environment. This thermal conductivity of a gas mixture is determined by its composition. In the TCD set-up two heated filaments of high resistance (eg, platinum) are located in separate channels in a metal block. Pure helium flows through one channel and the effluent from the column the other. The rate of heat loss from a filament determines its temperature and hence its resistance. Differences in gas composition between the two filaments show up as a signal and this represents the different components of the effluent gas stream. A typical TCD is shown in figure 2.11.3.

Figure 2.11.3

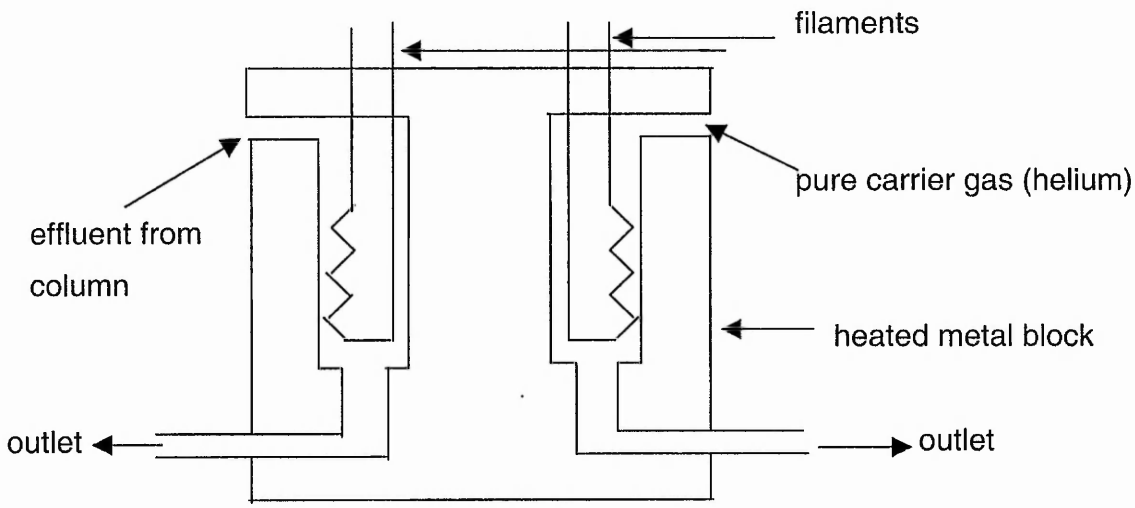

2.12 Materials

Eight classes of materials have been chosen for the investigation, prepared by co-precipitation or impregnation, and calcined at 435°C or 800°C, employing either iron oxide or magnesium oxide as support.

2.13 Material preparation

2.14 Impregnation

A solution of chloroauric acid (Johnson Matthey 49.46% gold) is added dropwise to an amount of magnesium oxide or iron oxide (Aldrich 99.99%) in powdered form until the mixture *just* becomes tacky (incipient wetness). The material is then heated in an oven at 110°C for approx 20 hours, ground up with a pestle and mortar, and then calcined for 3 hours at either 435°C or 800°C in a ceramic crucible in static air. For both supports the gold loading is manipulated to achieve a range of loadings based on the amount of support material used.

2.15 Co-precipitation

A solution of chloroauric acid (amount dissolved in 10-15 cm^3 water varied according to the doping level required, Johnson Matthey, 49.46% gold) was added to a solution of magnesium nitrate hexahydrate (1-2 grams dissolved in 15-20 cm^3 water , Aldrich 99.99+%) or iron nitrate nonahydrate (1-2 grams dissolved in 15-20 cm^3 water, Aldrich 99.99+%) and the resulting mixture was heated on a magnetic heater-stirrer with additions of ammonium carbonate (Aldrich reagent grade) to raise the pH to neutral and co-precipitate the mixture. This was then filtered and washed with a wash bottle of distilled water and heated in an oven for approx 20 hours at 110°C (or in the case of iron oxide, dried under vacuum at 75°C for 20 hours), ground with a pestle and mortar and then calcined for 3 hours at either 435°C or 800°C in a ceramic crucible with a static air flow.

For both classes of support the gold loading was manipulated to achieve a range of different gold loadings from 0.1% to 10% by weight of precursor for magnesium oxide and as a ratio of gold to iron for iron oxide support, (referred to as WW_{at}% in this report). Hence there is correspondingly more gold in magnesia based samples than iron oxide based samples when prepared by co-precipitation. Impregnated materials have comparable gold loadings for both types of support.

For a sub-class of iron oxide materials, the acid mixture was prepared initially and then added drop-wise to heated ammonium carbonate.

2.16 References:

1: Gregg.S.S, Sing.K.W.S, Adsorption Surface Area and Porosity. Academic Press, 2nd Edition, (1982).

2: Monti.D.A.M, Baker.A, Journal of Catalysis, **83**, 323-335 (1983)

3: JCPDS international center for diffraction data- search manual and data cards (1988).

4: Wagner, C.D, Davis.W.M, Moulder.J.F, Muilenburg.G.E. Handbook of Photoelectron Spectroscopy, (1978)

Chapter three

Our scientific power has outrun our spiritual power. We have guided missiles and misguided men.

Martin Luther King, Jr

Chapter 3: Characterisation

3.0 Introduction:

In order to gain greater insight into the catalysis and exchange performance across sample classes, several different methods have been employed to enable characterisation of the samples used.

Because it is essential to normalize isotopic oxygen exchange and CO oxidation performance relative to the surface area used, the samples have all had their surface areas measured either by the digisorb BET, quantachrome BET or under nitrogen adsorption by weight. As well as providing data that can be used in conjunction with reactor data, the variation of surface area across sample classes is of interest in itself, as described later on.

It was also of concern to ascertain the influence of gold on the reduction of support. In order to achieve this, TPR was performed on iron oxide supported materials.

In order to get visual information on the influence of preparation on support / gold morphology, Scanning Electron Microscopy (SEM) was employed. These images and their interpretations are discussed later on.

X-Ray Diffraction (XRD) analyses were performed in order to establish that gold was successfully incorporated into the support and to what extent this influenced the various support crystallite sizes across different classes of prepared material.

X-Ray Photoelectron Spectroscopy (XPS) was used in order to probe the surface chemistry of the samples and so gain information on the presence of chlorine and gold on the surface of the samples. Also the binding energy (B.E) value is used to establish the chemical environment of the species under study, ie, metallic or oxidized gold.

3.1 Surface area measurements

As described earlier, three different approaches have been employed to measure sample surface areas; The digisorb BET, Quantachrome and nitrogen adsorption by weight of nitrogen. [1] Adsorption isotherms have been classified into five main types by Brunauer, Demming, Demming and Teller (BDDT).[1] Figure 1 shows adsorption and desorption isotherms that are typical for the materials studied here. There shape conforms to (for the most part) type II of the BDDT classification, and indicates the absence of microporosity (pore diameter, d < 20 Å) and mesoporosity (20 Å < d < 500 Å).

Figures 2 and 3 detail the effect of gold loading on surface area across all classes. These data were gathered using either of the first two approaches. In order to get more insight into nitrogen adsorption above the usual BET range of P/P_o : 0.05 – 0.30, full isotherms were performed on all sample classes.

Figure 3.1.1.1: The five adsorption isotherms.

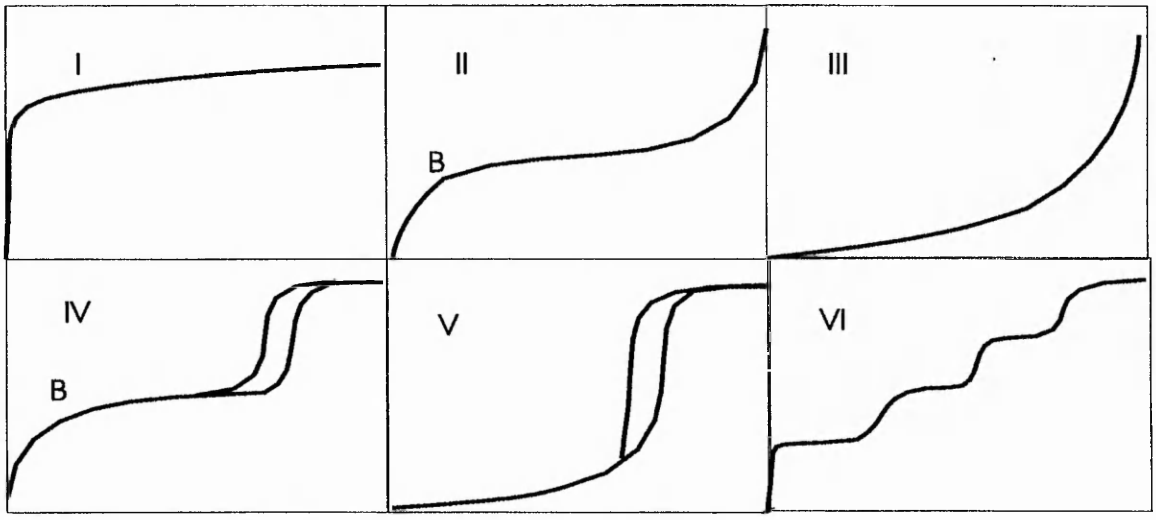

Where I is typically found for micro-porous materials, II is found for non-porous materials, III is also found for non-porous materials but with weak initial adsorption, IV is found for meso-porous materials, V is also found for meso-porous materials but with weak initial adsorption. VI is a stepped isotherm.

As mentioned earlier, all samples have been characterised by either BET or quantachrome methods. The agreement between the two techniques is good at between 2-5%. Most of the quoted MgO sample surface areas are from the BET set-up. Most of the Fe_2O_3 samples are taken from the quantachrome.

Figures 3.1.1.2 and 3.1.1.3 show the way in which the surface areas of the samples studied depend on preparation method and gold loading, for MgO and Fe_2O_3 supported catalysts respectively.

Figure 3.1.1.2: The influence of gold loading on material surface area for MgO

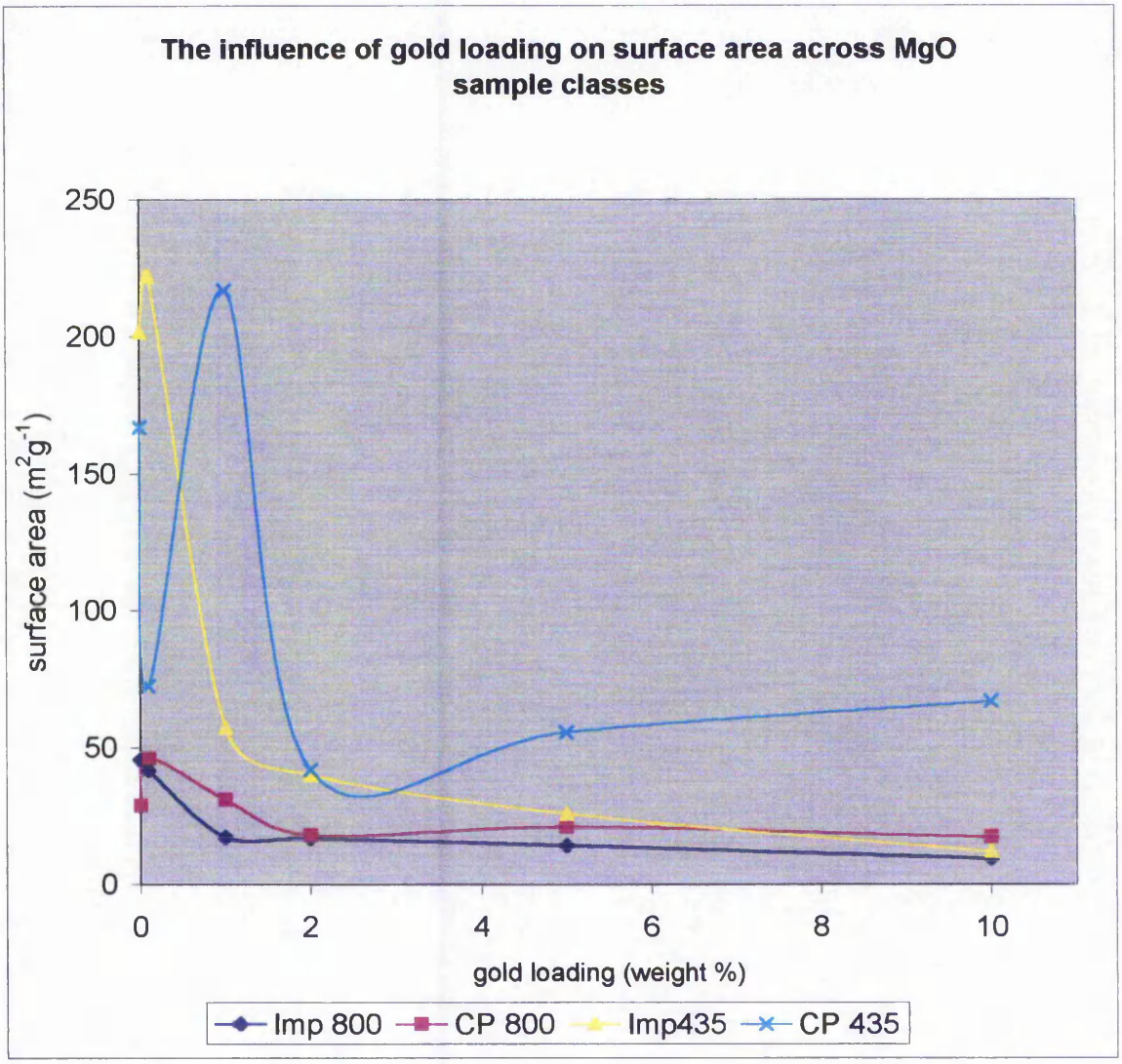

Figure 3.1.1.3: The influence of gold loading on material surface area for Fe_2O_3

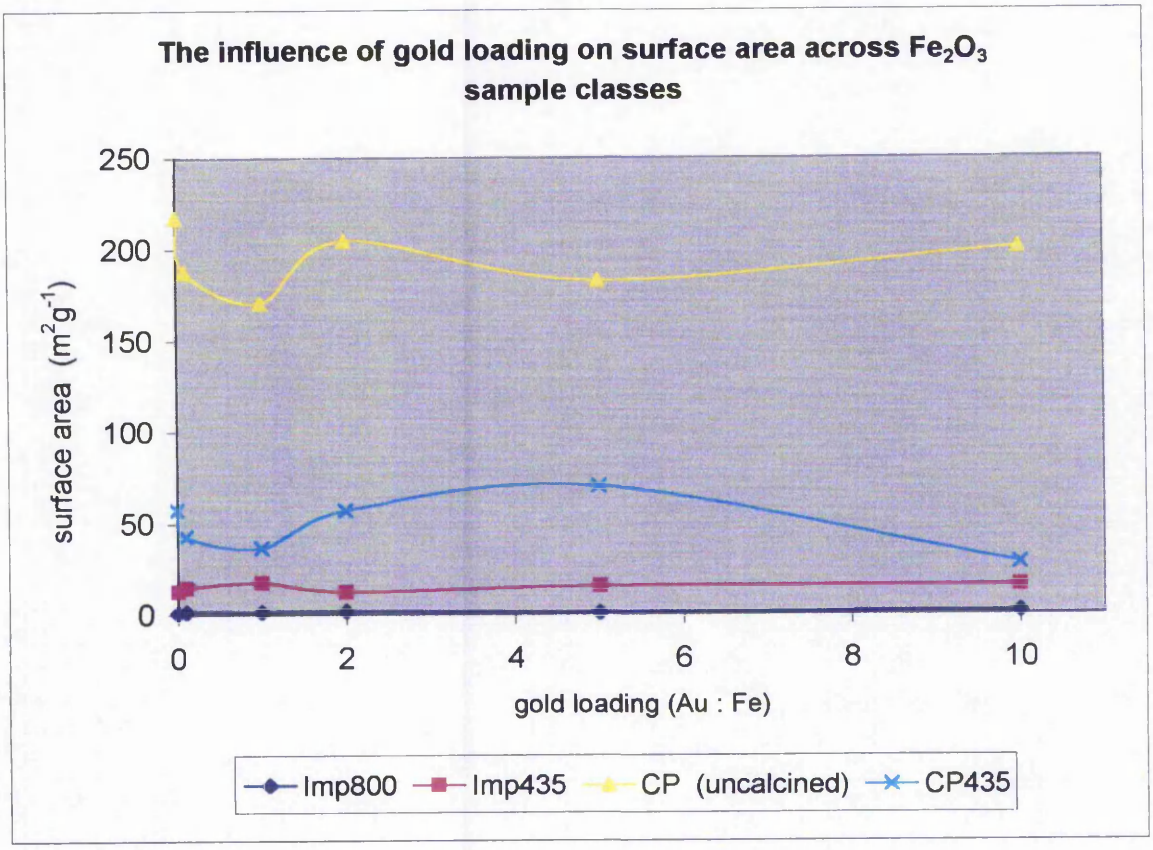

Figures 3.1.1.2 and 3.1.1.3 show that the surface areas of the materials may be strongly influenced by the way in which gold is introduced and the calcination temperature. Increasing the gold content appears significantly to reduce the surface area of the MgO based materials, although it has less influence on the surface area of the iron oxide supported catalysts. Why this is so can only be speculated on but gold (III) substitution into the support has been postulated.[2] Gold may cause an increase in the number of defects leading sintering.

If this is the mechanism underlying the loss of surface area with gold loading then it can be speculated that Fe_2O_3 is not amenable to lattice substitution with gold.

For MgO supported catalysts there is a greater dependence of surface area variations on calcination temperature than for Fe_2O_3, which displays greater surface area variation with preparation method. The observation that uncalcined co-precipitated Fe_2O_3 catalysts display high (200 m^2g^{-1}) surface areas may go some way to explaining their high catalytic ability as shown in this research.

3.1.2 Full Isotherms on all sample classes

As mentioned earlier, all classes have had one of their samples full isotherm measured in order to categorize the adsorption / desorption profile according to one of the 5 different classes. Figures 4-11 give these profiles. In each case a nominal 5% gold loaded sample was chosen.

Figure 3.1.2.1: Adsorption / desorption isotherm for 5%Imp800 (MgO)

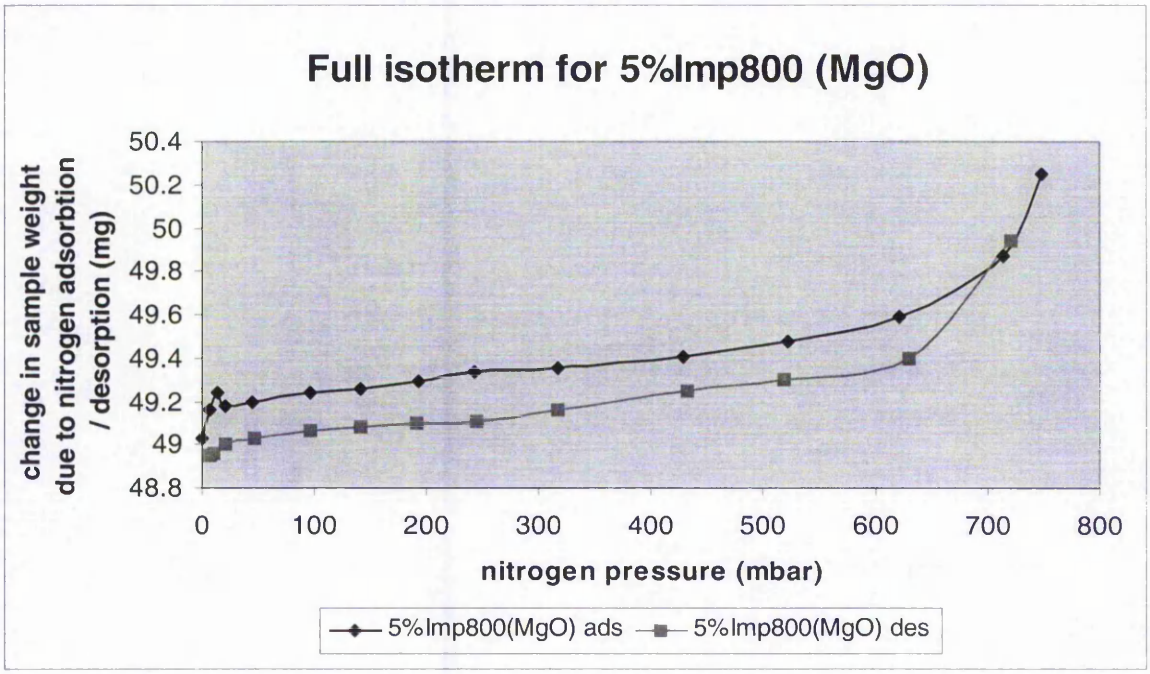

Figure 3.1.2.2: Adsorption / desorption isotherm for 5%CP800 (MgO)

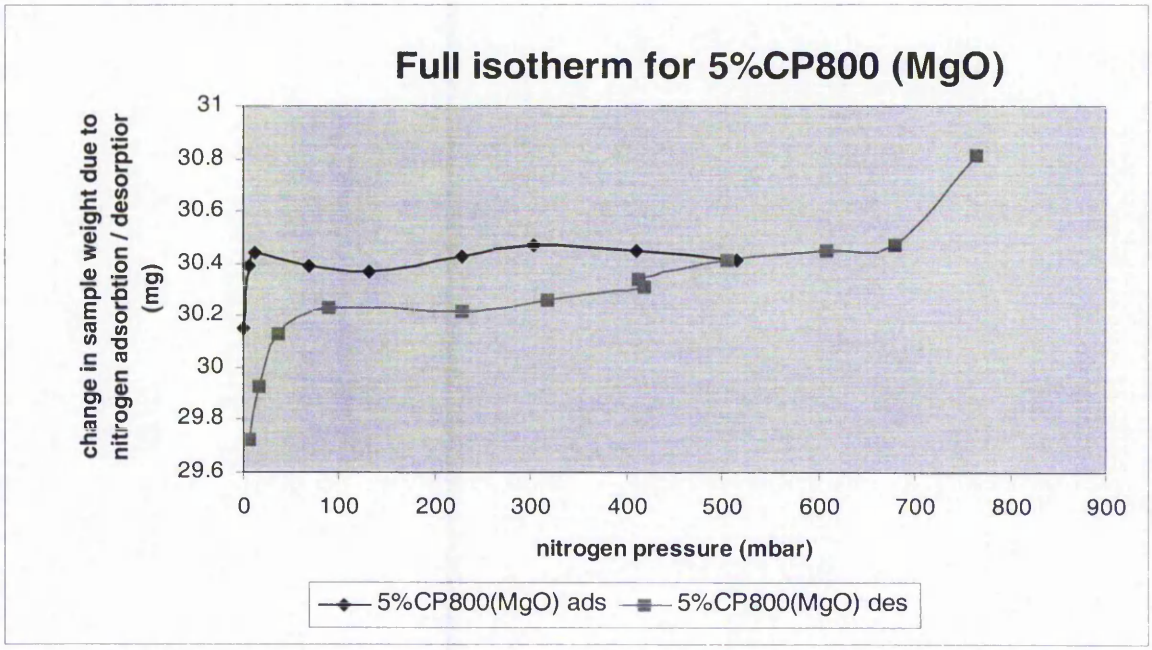

Figure 3.1.2.3: Adsorption / desorption isotherm for 5%CP435 (MgO)

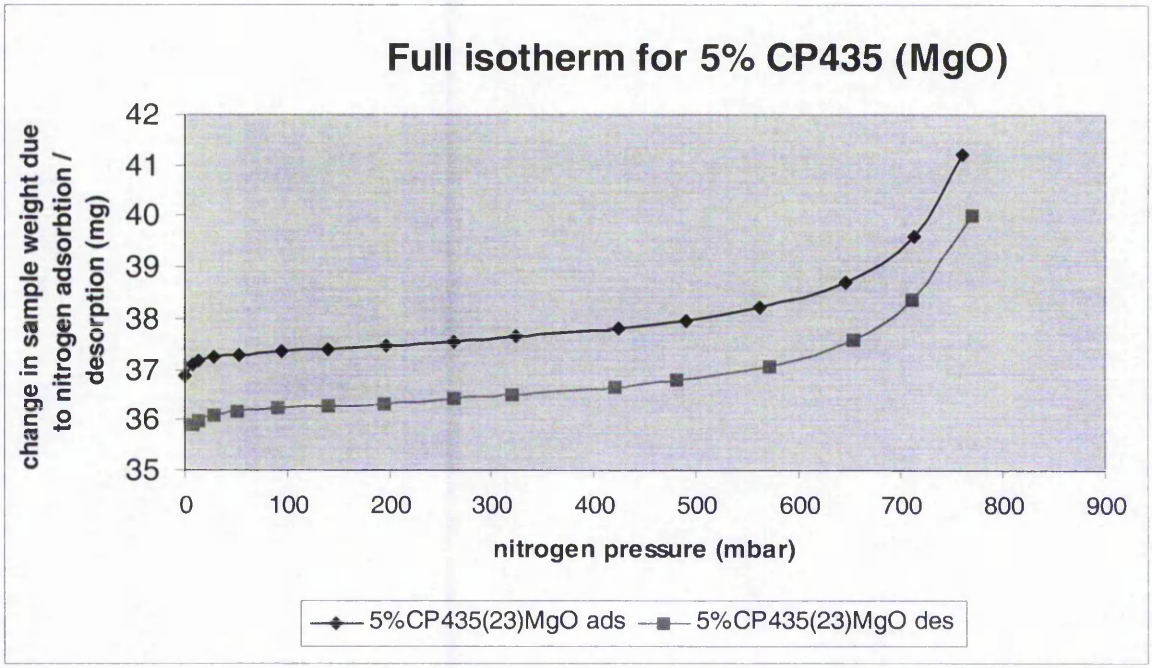

Figure 3.1.2.4: Adsorption / desorption isotherm for 5%Imp435 (MgO)

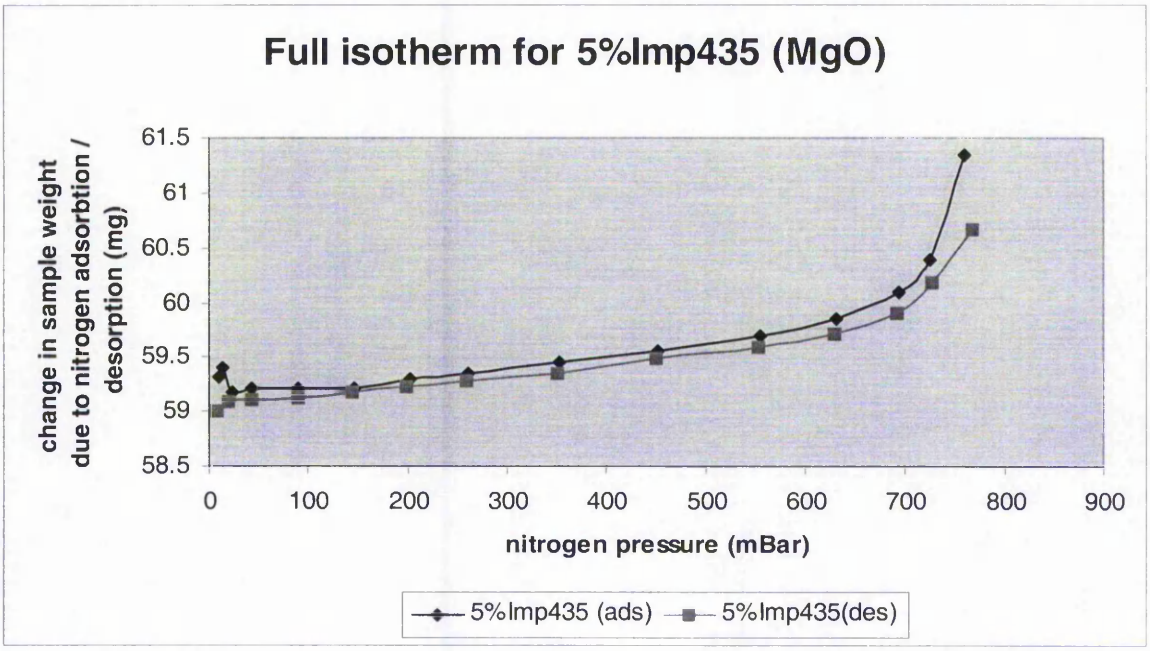

Figure 3.1.2.5: Adsorption / desorption isotherm for 5%Imp800 (Fe_2O_3)

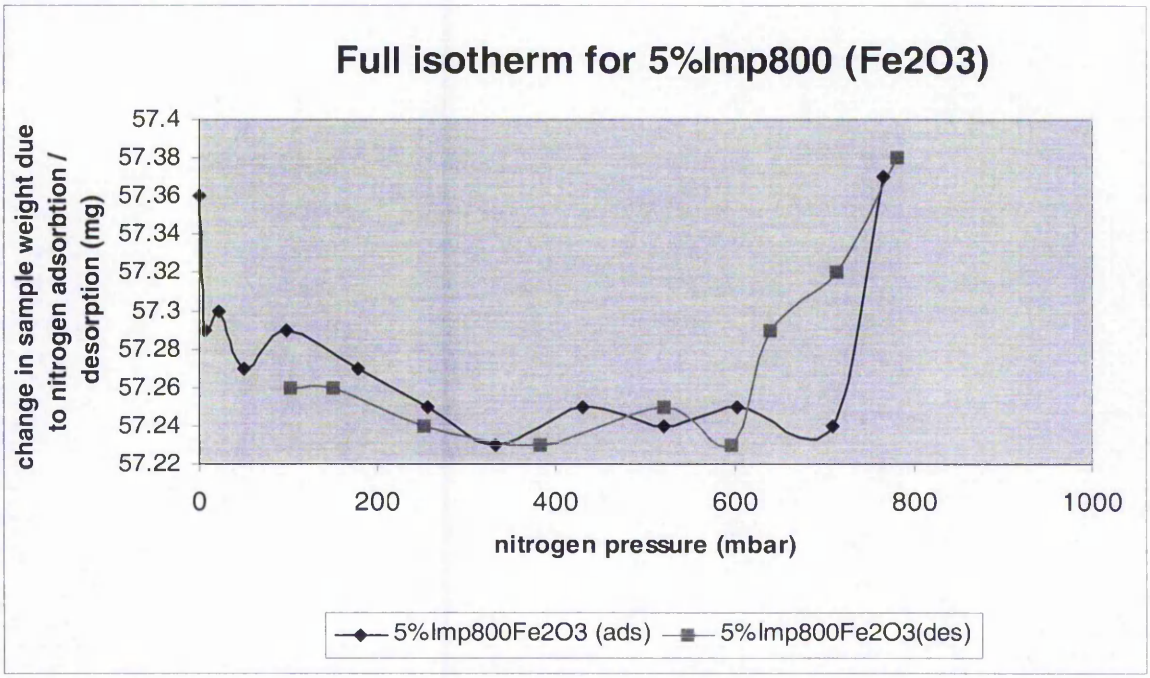

Figure 3.1.2.6: Adsorption / desorption isotherm for 5%Imp435 (Fe_2O_3)

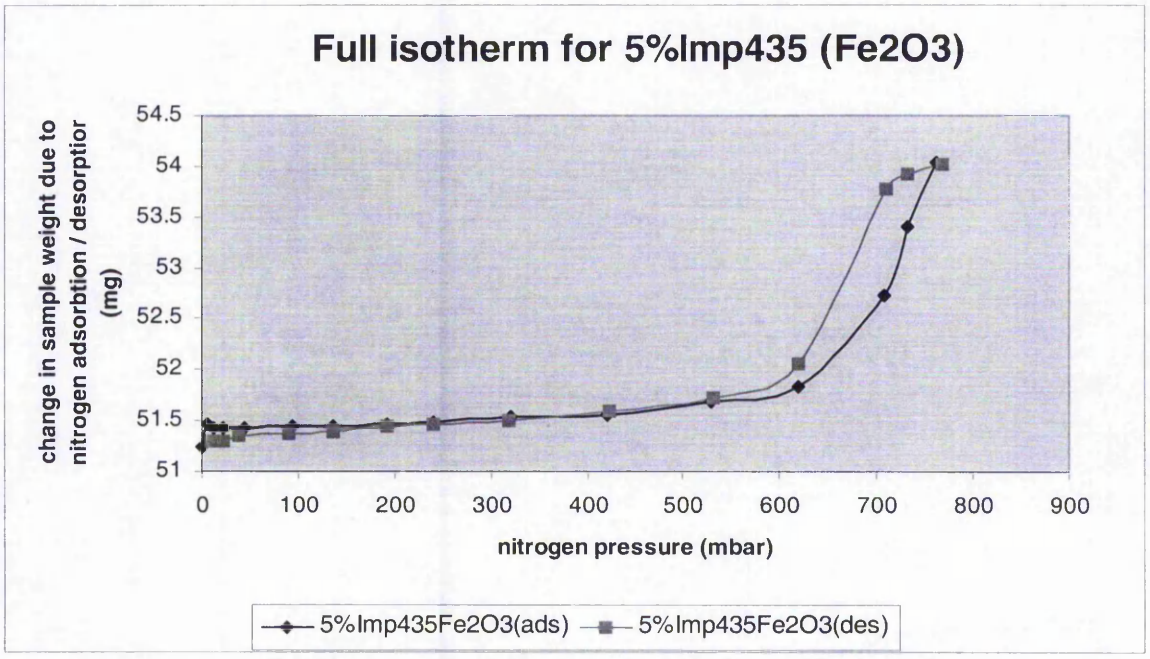

Figure 3.1.2.7: Adsorption / desorption isotherm for 5_{at}%CP (Fe_2O_3)

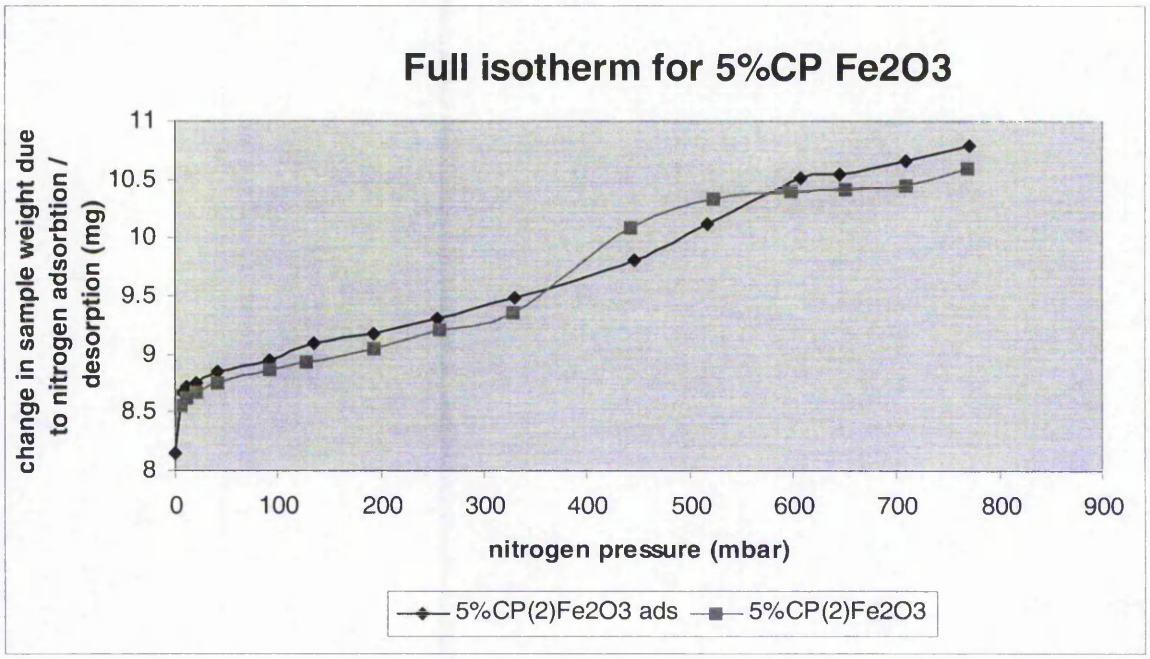

Figure 3.1.2.8: Adsorption / desorption isotherm for 5_{at}%CP435 (Fe_2O_3)

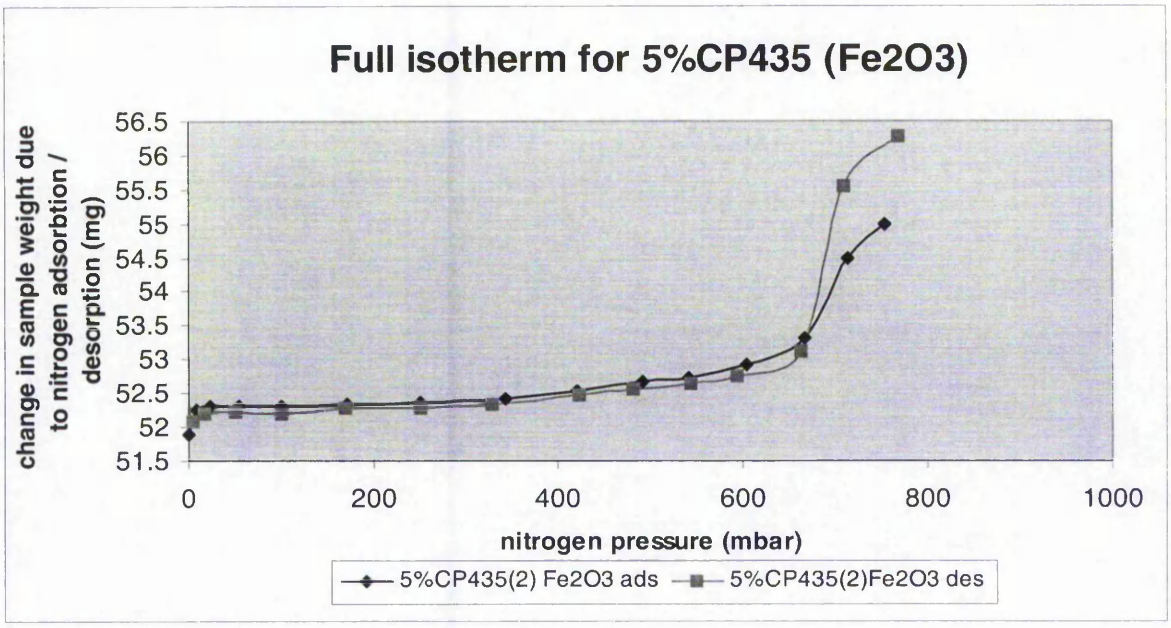

3.1.3 BET discussion

As can be seen, all of the sample classes conform generally to a type 2 isotherm but with the additional observation of a very sharp point of inflexion which suggests a degree of microporosity in these materials. Also, for some isotherms there is evidence of hysteresis, suggesting mesoporosity. Because the BET surface area calculations are most suited to a type 2 or 4 isotherm (because of the sharp point of inflection), the BET surface areas quoted can be relied upon with a high degree of confidence.

Other researchers using different supports and reaction / preparation conditions have arrived at different isotherms and surface areas. Shastri et al[3] Investigating the influence of pre-treatment conditions on BET surface area found that up to 300°C there was a slight increase in BET surface area from 118 m^2g^{-1} to 135 m^2g^{-1} followed by a total collapse to 2.7 m^2g^{-1}. This was interpreted to be attributable to conversion of anatase to the rutile form of TiO_2. Unlike the samples in this research (that were based on MgO and Fe_2O_3 as supports), gold appeared to have a retardant effect on

thermally induced surface area collapse. The reason for this is not completely understood, especially as metal ions can sometimes promote low surface area phase transformation by the encouragement of vacancy formation. The investigators introduced the idea of gold atoms or ions occupying interstitial lattice sites and therefore inhibiting any phase transformation that would otherwise occur.
Baiker[4] et al investigating CO oxidation over amorphous gold-silver-zirconium and gold-iron-zirconium alloys and found distinctive type 1 isotherms, indicating the presence of micro-porosity. These samples showed no evidence of meso-porosity as suggested by an absence of hysteresis. This is important as it shows that alloying of gold so that gold particles are present on the support surface (in this case, zirconium) with highly dispersed iron or silver promotes the formation of micropores which might be responsible for the high activity over time with little deactivation (40 hours).
Wagner[5] et al found that the method of preparation had a significant influence on the surface area of iron oxide supported gold, with impregnated samples giving lower surface areas than co-precipitation. Also the influence of gold loading had different effects depending on the method of preparation. For impregnated materials there was a loss of surface area with gold doping. For co-precipitated materials there was a loss of surface area with gold loading for those samples prepared by co-precipitation and left (before any other treatment) for 20 hours. For those samples left for 8 hours there was no relationship with gold loading. Intriguingly, co-precipitation (addition of acid to base) produced larger surface areas than inverse co-precipitation (addition of base to acid). This is in direct contradiction to the results that have been found in this research where inverse co-precipitation (base to acid) produced samples with around 200 m^2g^{-1} and co-precipitation resulted in surface areas of around 50 m^2g^1 (these data are not shown as the samples were not extensively tested for CO oxidation due to low conversion.) The reason for this large disparity is not known but is most likely the result of the accumulation of small preparation differences that can have marked effects on surface areas.

3.2 TPR Characterisation

Because it is of interest to investigate whether ease of reduction of iron oxide supported materials is influenced by gold loading and other experimental manipulations, all iron oxide samples have been characterised using TPR (temperature programmed reduction).

Brown[6] studied the TPR of bulk iron oxide and found that the reducibility of Fe_2O_3 differed markedly from the reduction of Fe_3O_4. In addition to distinct reduction profiles it was also found that the reduction step Fe_2O_3 to Fe_3O_4 occurred at a lower temperature than subsequent reduction steps. This observation is utilised in the current research by following the change in Tmax of several reduction steps with gold loading for iron oxide support. Others[9,10] have reported significant effects of gold on TPR profiles for iron oxide as support.

Also of interest and not really investigated by others is the influence gold might have on the amount of iron oxide that is reduced at each reduction step. In order to quantify any reduction it is necessary to use a calibrant. The most commonly used is CuO.

3.2.1 TPR calibration

CuO is used as a calibrant in TPR studies because it possesses a sharp reduction peak attributable to the single reduction step: $CuO + H_2 \longrightarrow Cu + H_2O$.[2] This is a highly repeatable result and occurs at a relatively low temperature (300 to 360°C). Calibration of a Fe_2O_3 reduction peak using CuO calibration data will be shown.

Figure 3.2.1.1 shows a typical TPR profile from the reduction of CuO.

Figure 3.2.1.1: Calibration of CuO reduction

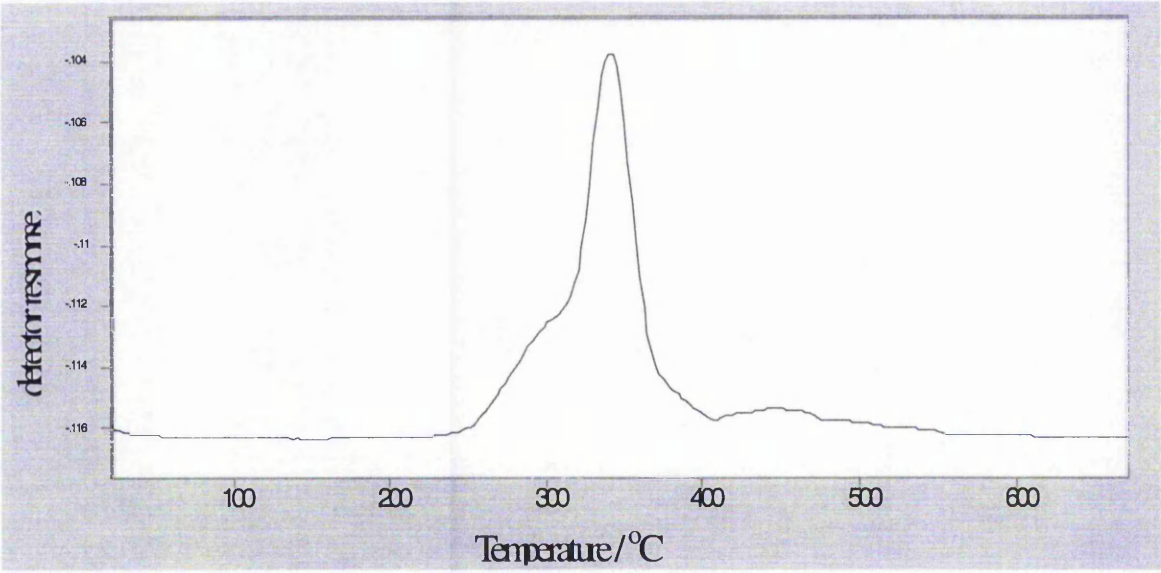

The area of this peak (baselined) is 0.6974 (arbitrary units).

The amount of CuO used: 0.0100g.

This equates to: 0.0100 / 79.55 = 1.257 E-4 moles reduced and also (because of the stoichiometry of the reduction step) 1.257 E-4 moles of H_2.

Because *exactly* the same conditions (flow rate, ramp rate etc) were used in the calibration, the peak integration can be used with confidence to estimate moles of H_2 needed to reduce Fe_2O_3 to Fe_3O_4 and eventually Fe_3O_4 to FeO, (and at high enough temperatures >900°C, FeO to Fe). Therefore there are assumed to be 3 steps in the overall reduction of Fe_2O_3 to Fe.

3.2.2 Quantification of Fe_2O_3 reduction: An example:

To illustrate how to measure the H_2 molarity associated with a particular peak, 10% CP435 Fe_2O_3 will be used.

Figure 3.2.2.1: Reduction profile for 10_{at}%CP435 (Fe_2O_3)

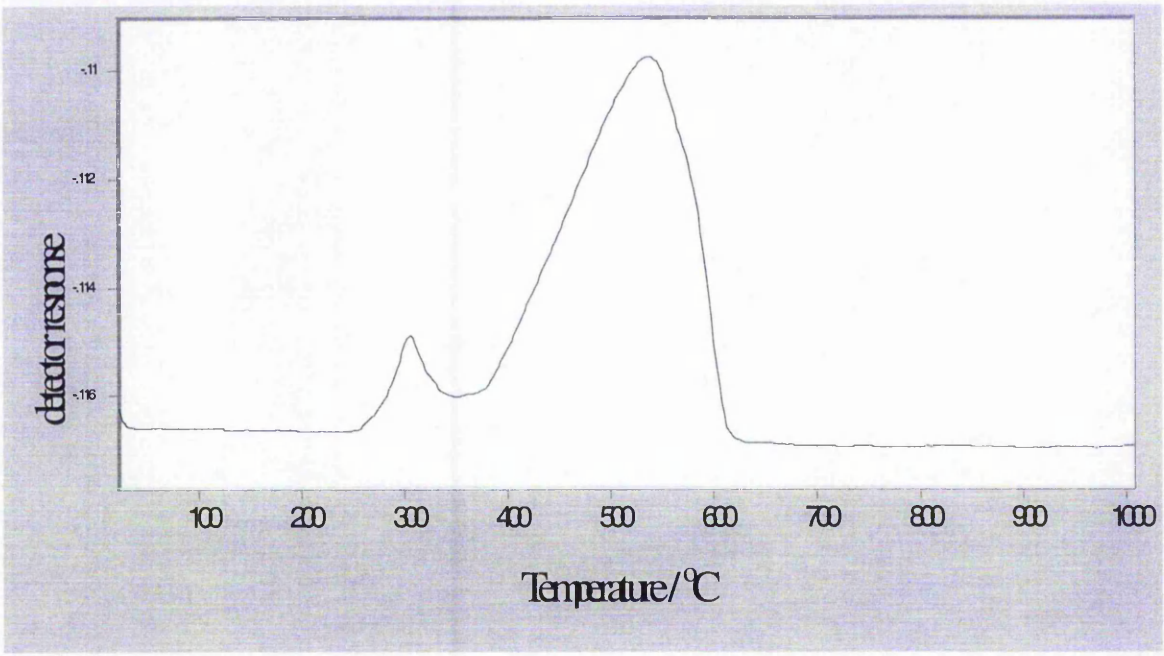

In figure 3.2.2.1 above, integration of the first peak (by forcing the integration point onto the baseline) gives a value of 0.094, integration of the main peak gives: 1.004 (arbitrary units for both). This corresponds to 1.695 E-5 moles of H_2 (minor peak) and 1.811 E-4 moles of H_2 (major peak). Ratio of minor to major peak = 1:10.7, this is in reasonable agreement with the predicted ratio of 1:9. This result supports the hypothesis of initial reduction of Fe_2O_3 to Fe_3O_4 (first peak) and subsequent total reduction to Fe, (second major peak).

To establish the reliability of the above calibration approach, the moles of Fe_2O_3 reduced (calibration calculated) can be compared to the maximum number of moles of Fe_2O_3 that can be reduced: 0.0122g of 10_{at}%CP435 Fe_2O_3 = 0.0096g Fe. 0.0096 g / 159.6 = 6.02E-5 moles of Fe_2O_3 * 3 = 1.805 E-4 moles of H_2.

This compares very favourably to the calibrated value of 1.981 E-4 moles of H_2 for the overall reduction of Fe_2O_3 to Fe. *It can therefore be concluded that both peaks can be associated with the complete reduction of iron oxide below* 700°C. This is lower than that seen by others, in which reduction of FeO to Fe occurs at 900°C.[9,10]

3.2.3 The influence of gold loading

It is of interest to examine whether gold loading has an effect on the reducibility of the support. Ease of reduction is indicated by a decrease in the Tmax of a reduction peak. Other researchers have found that the presence of a dopant (i.e., Pt on CuO) can significantly reduce reduction temperatures. It is speculated that dissociative adsorption of H_2 occurs on the metal with spillover onto the support, thus facilitating reduction at lower temperatures.[8] However, gold is not considered active in hydrogen dissociation.

Figure 3.2.3.1: Influence of gold loading on initial reduction step for Fe_2O_3

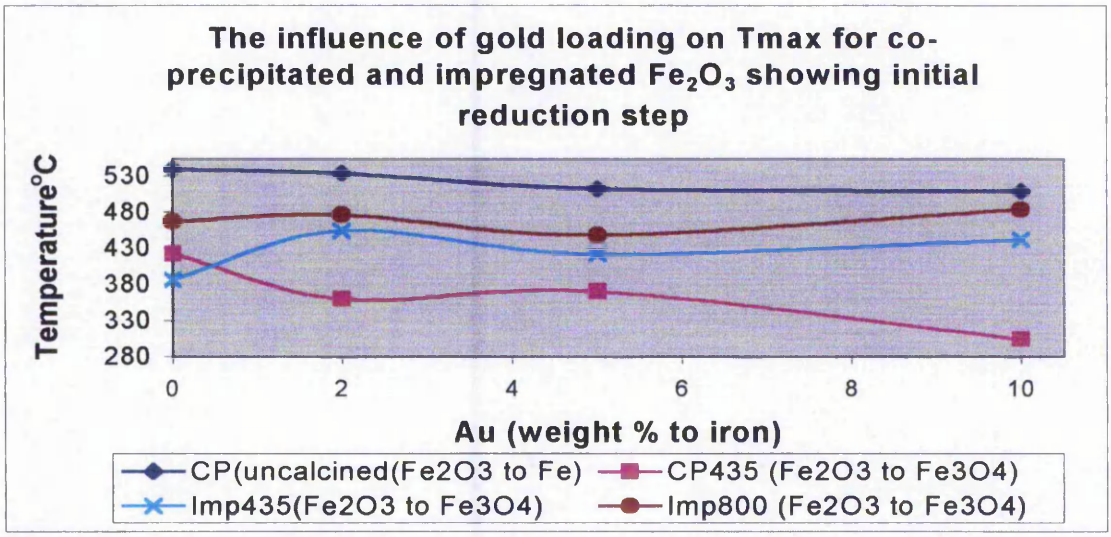

Figure 3.2.3.2: Influence of gold loading on second reduction step for Fe_2O_3

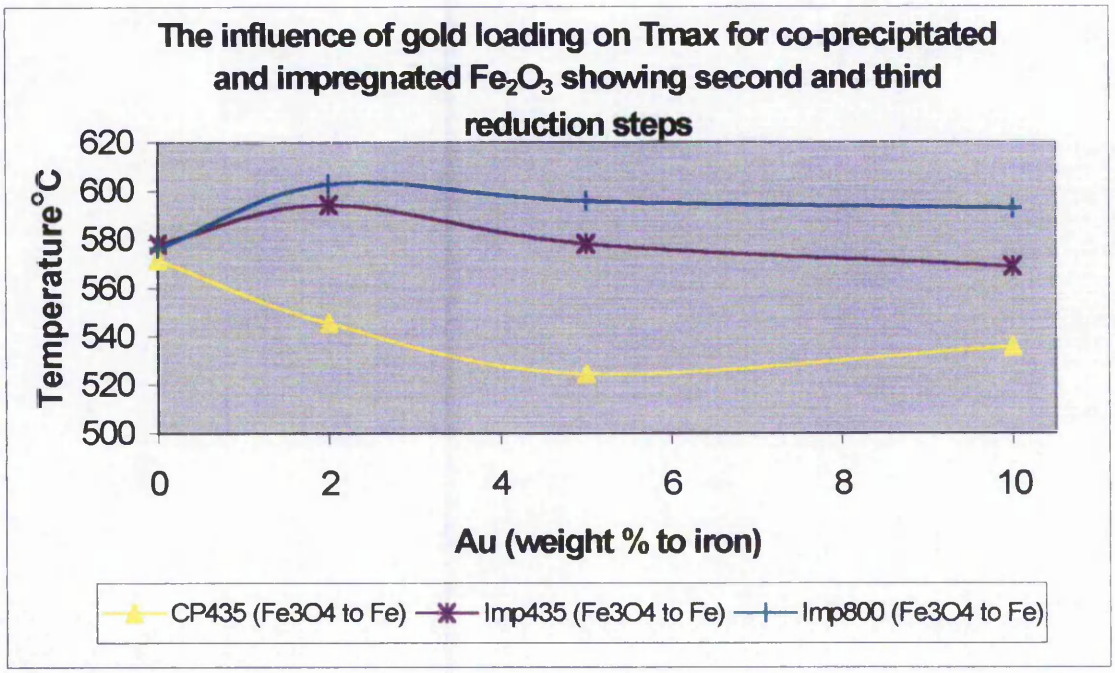

Figures 3.2.3.1 and 3.2.3.2 display the variation of Tmax for several reduction steps with gold loading for impregnated and co-precipitated materials. It is evident that co-precipitated materials display a general downward trend in Tmax with gold loading. This finding is in good agreement with Neri[9] et al, who found that the temperature of reduction of the first step was reduced by up to 140°C for the maximum gold loaded samples with respect to controls, however, the most apparent drop in Tmax is the first reduction step in *calcined* co-precipitated materials. This is contrary to the findings of Neri[9] et al who found calcination at 550°C increased Tmax for co-precipitated supported gold Fe_2O_3. Not all investigators have found that ease of reduction occurs with gold loading. Andreeva et al,[11] failed to find any influence on bulk ceria reduction that suggests gold related effects on reduction are support sensitive (even though ceria is a good supplier of lattice oxygen like iron oxide.)

Analysis of the impregnated data shows a flat relationship with gold loading. If anything, there is a slight upward trend.

It has been postulated that an increase in gold loading causes an increase of the ferrihydrite (highly hydroxylated) phase of iron oxide. These hydroxyl species are thought to be responsible for the decrease in Tmax with gold loading.

Other groups that are reduced during TPR include Au_2O_3. This is the oxidised form of gold that is reduced at relatively low temperatures (200°C – 300°C).

It is highly apparent in uncalcined co-precipitated materials but not their calcined equivalents. Also, impregnated samples show no evidence of Au_2O_3, as figure 3.2.3.3 demonstrates.

Figure 3.2.3.3: Reduction of Au_2O_3 for uncalcined co-precipitated Fe_2O_3

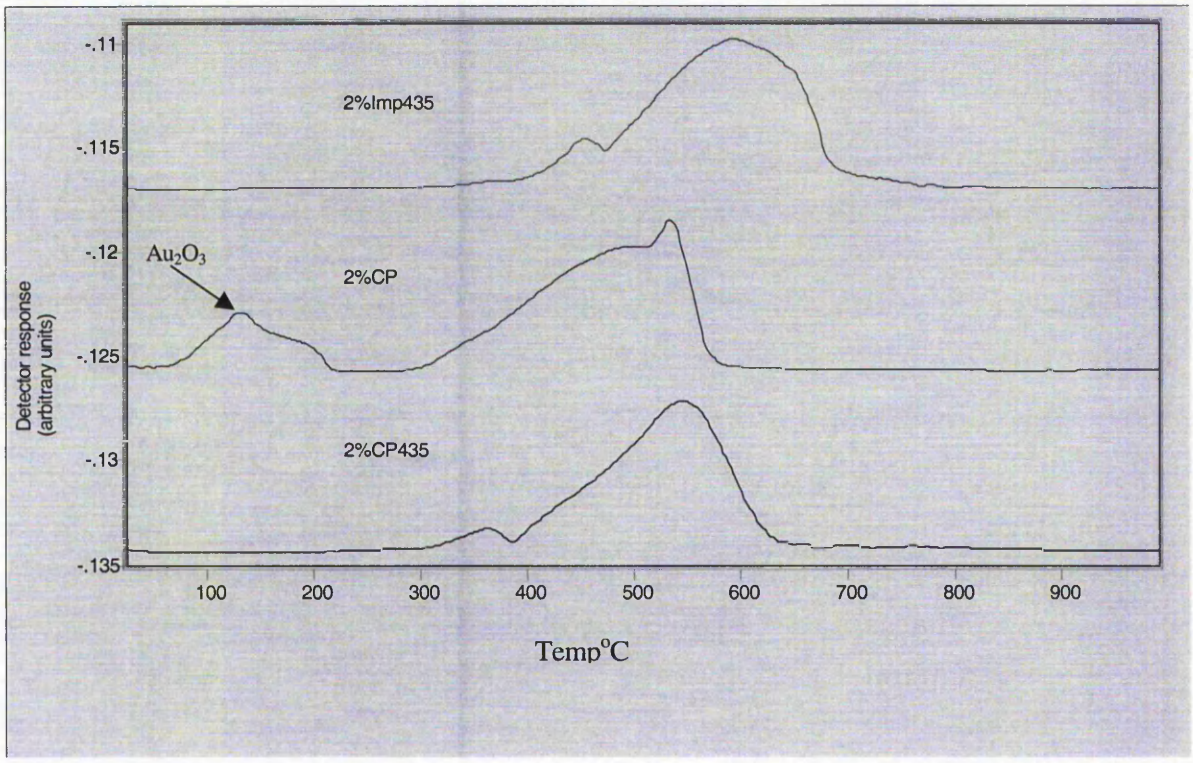

Others[12] have witnessed an absence of Au_2O_3 species for materials pre-treated for several hours at 400°C in air, oxygen and 300°C in H_2, and the presence of Au_2O_3 for samples pre-treated for only 30 minutes at temperature. Here, the Au_2O_3 integration areas increased with the oxidation state of gold (as determined by XPS).

The first set of results are not surprising as Au_2O_3 will decompose at relatively low temperatures as this oxide is not thermodynamically stable.

3.2.4 Integration of peaks

It is also of interest to compare the degree of reduction across the sample classes for each reduction step. As mentioned earlier, the first integration peak can be ascribed to initial reduction of Fe_2O_3 to Fe_3O_4 (although initial surface reduction cannot be ruled out) and the subsequent main peak is probably two reduction steps coalesced into one major peak, ie, Fe_3O_4 to FeO and FeO to Fe. It is important to note that integration units are arbitrary but have been obtained by applying trace limits from 10%Imp800 reduction profile to every other profile as a means of standardisation.

Figure 3.2.4.1: TPR peak areas for uncalcined Fe_2O_3

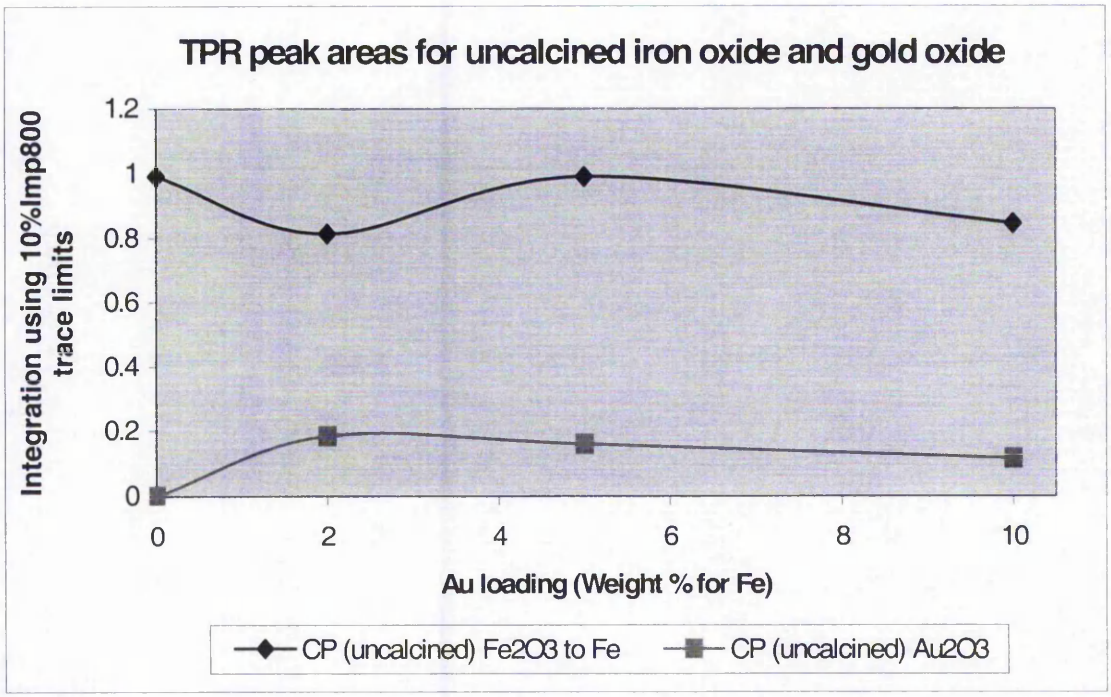

Figure 3.2.4.1 shows integration values for uncalcined co-precipitated (base to acid) iron oxide, including the Au_2O_3 peak. There doesn't appear to be much of a correlation between gold loading and peak integration for either the two reduction peaks although a positive relationship would be expected with Au_2O_3. This result suggests an upper limit to surface Au_2O_3 concentration at which point increasing gold loading has no impact.

Figure 3.2.4.2 gives reduction integration areas for the first integration: Fe_2O_3 to Fe_3O_4 as a function of gold loading. As can be seen, with the exception of the impregnated 800 class, there are increases in integration values at intermediate values and a drop at the highest gold loading. These values should not be over-interpreted as the first integration is only small and hard to separate from the second much larger integration peak. However, it does suggest that there is no clear-cut relationship between gold loading and degree of initial reduction. Integration values for uncalcined co-precipitated samples are included in figure 3.2.4.1 as these only give one clear reduction peak associated with Fe_2O_3 reduction.

Figure 3.2.4.2: first integration values for iron oxide reduction

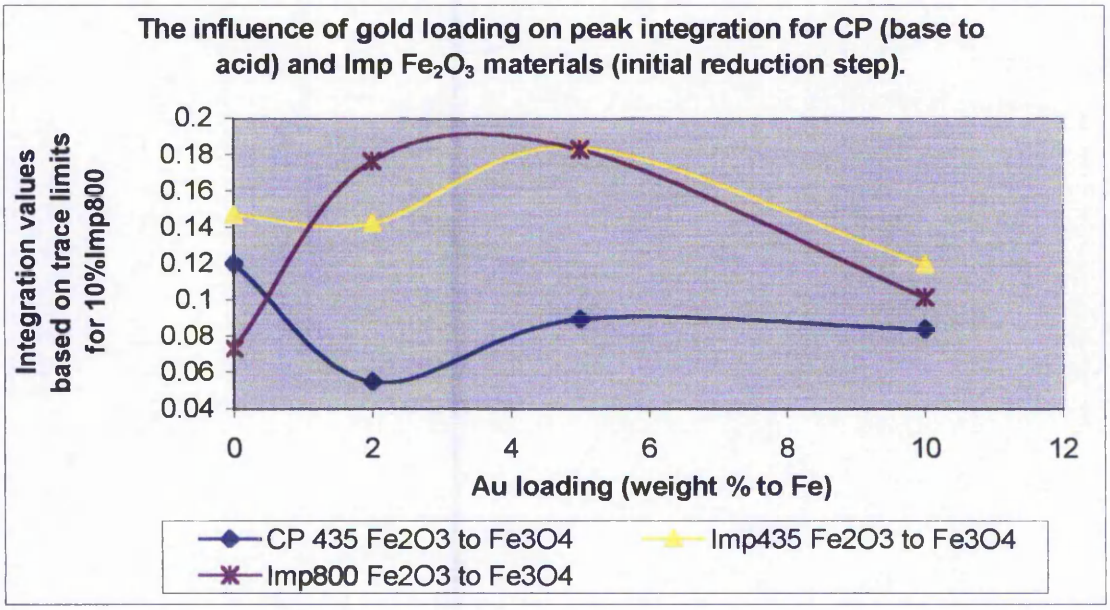

Figure 3.2.4.3: second and third integration values for iron oxide reduction

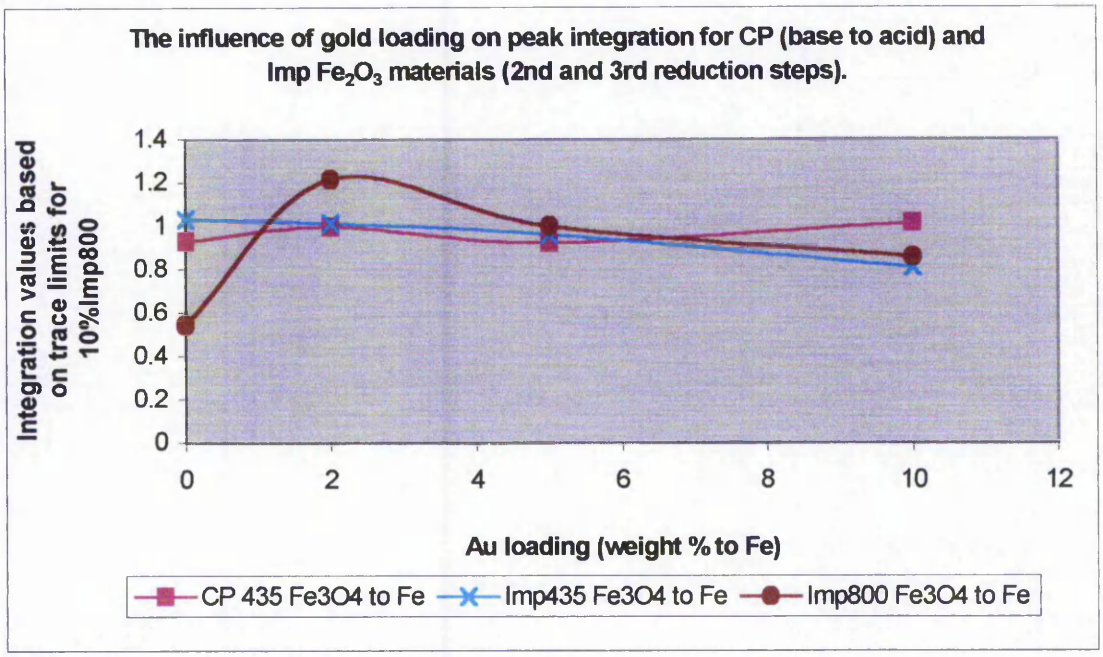

Figure 3.2.4.3 reveals the influence of gold loading on second and third integration values (Fe_3O_4 to Fe). There appears to be a general upward trend in the amount of reduced Fe_3O_4 species with gold loading for all sample classes, the effect being most marked for the impregnated 800 class. If this effect is genuine it suggests that gold not only lowers the temperature of reduction for iron oxide support but also encourages *more* iron oxide to undergo reduction at the lower temperature by a mechanism as yet unknown but could involve increased mobility of surface and bulk iron oxide species through gold transfer into the bulk and increased defect formation on the surface. Of course, all iron oxide will undergo reduction eventually as the temperature is ever increased but gold might encourage reduction in that percentage of iron oxide located in the tails of reduction peaks. Indeed the peaks become much sharper with gold loading.

Figure 3.2.4.4: Ratio of first and second / third integration values.

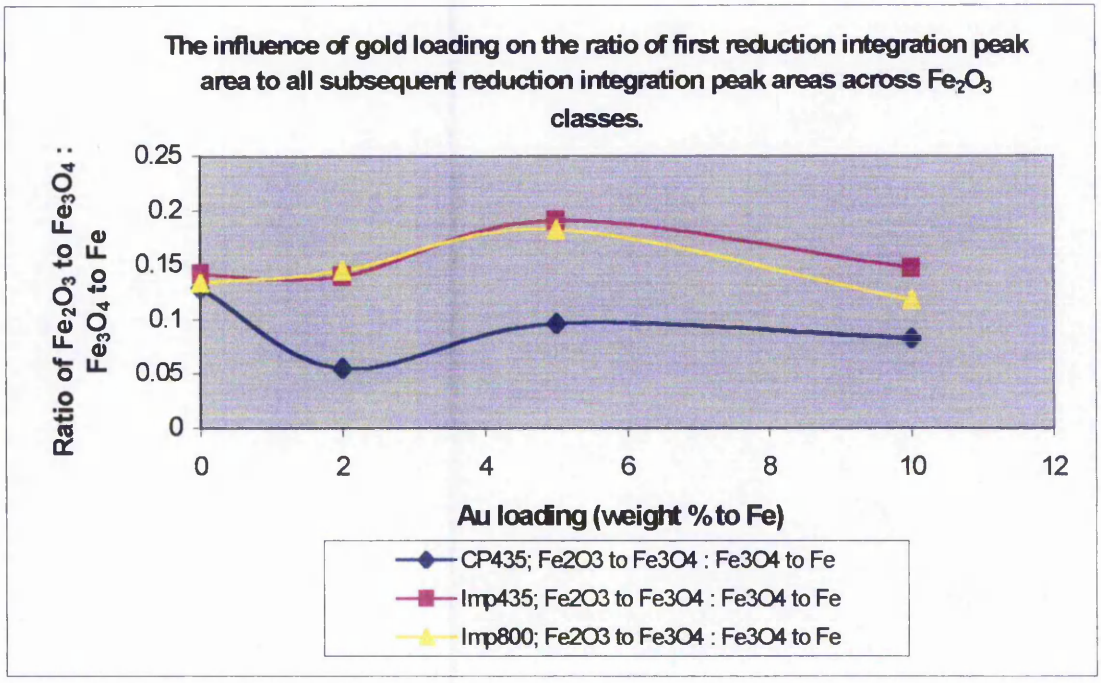

Figure 3.2.4.4 gives the ratio of integration values between reduction steps. This is done to see if gold loading has a disproportionate influence on either reduction step. As can be seen there is little influence of gold on the ratio for any sample class with the exception of the co-precipitated samples calcined at 435°C. These show a sharp decrease in the initial reduction peak relative to all subsequent reduction with 2_{at}% gold loading and a slight increase in the ratio for 10_{at}% loading. The other two classes show a maximum ratio at intermediate gold loadings for reasons that are not understood. Also the reliability of this approach can be seen in the very close control (0% gold) integration values for all sample classes.

3.2.5 Summary of reduction data

Table 3.2.5.1: The influence of gold loading on the first reduction step: Fe_2O_3 to Fe_3O_4

Au loading %	CP Uncalcined* Temp / °C	CP435 Temp / °C	Imp435 Temp / °C	Imp800 Temp / °C
0	540.1	423	387	468
2	535	360	454	477
5	513	371	422	448
10	509	304	442	484

Table 3.2.5.2: The influence of gold loading on the second reduction step: Fe_3O_4 to Fe

Au loading %	CP Uncalcined* Temp / °C	CP435 Temp / °C	Imp435 Temp / °C	Imp800 Temp / °C
0	540	572	578	577
2	535	546	594	603
5	513	525	578	596
10	509	536	569	593

* same values in both columns due to the appearance of only one reduction peak.

3.2.6 TPR conclusions

There are several points that are brought out from TPR research on Fe_2O_3 supported gold.

1: Three distinct reduction peaks are typically observed for samples prepared by co-precipitation. The first, at 100–200°C, is ascribed to the reduction of gold (III) oxide or its hydrated form. The other two, at 300-400°C and 500-580°C, are respectively attributed to the reduction of Fe_2O_3 to Fe_3O_4, and of Fe_3O_4 directly to metallic iron.

2: For samples prepared by other methods, only the two peaks due to the reduction of the iron oxide are observed.

3: The ease of reduction appears to be related to gold loading for materials prepared by co-precipitation, and this effect is enhanced by calcination. For catalysts prepared by impregnation, the presence of gold does not influence the reduction temperature.

4: There is no clear-cut relationship of gold loading with initial reduction step, but a suggestive upward trend for the second reduction step. Also, there is no differential influence of gold on either reduction step as evidenced by a constant hydrogen uptake ratio between reduction steps with gold loading.

3.3 SEM Characterisation of Fe_2O_3 and MgO supported gold.

As mentioned before, both iron oxide and magnesium oxide supported materials have been examined using SEM. Some samples (marked with *) have been performed on the departmental SEM and others on an outside (Jeol ltd) SEM.

3.3.1 Magnesium oxide supported gold

Figure 3.3.1.1: control Imp800 (MgO)

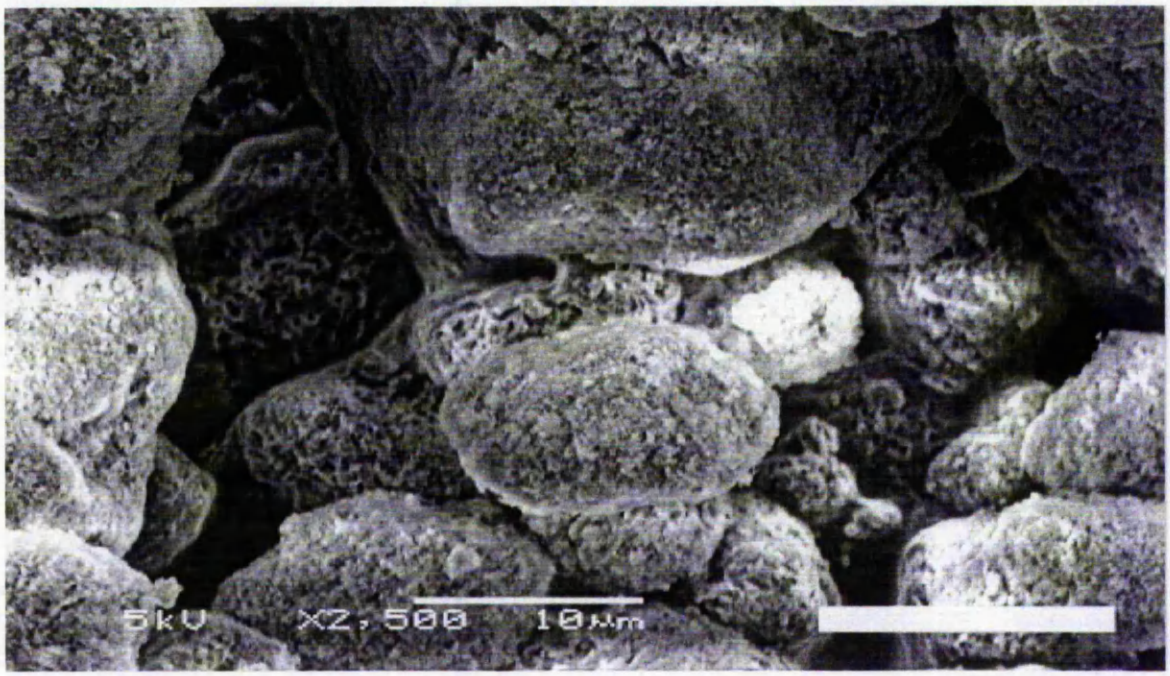

Figure 3.3.1.1 shows a SEM of undoped magnesium oxide. The material displays a typical blocky morphology that has been seen elsewhere[13] although there is more than a magnitude increase in size (10μm) of surface crystallites compared to those reported, probably due to the high temperature of calcination (800°C) for the materials studied. Also the agreement with the corresponding XRD reflections of 200 Å to 321 Å is very poor.

3.3.2 **Figure 3.3.2.1**: * 10%Imp800(MgO)*

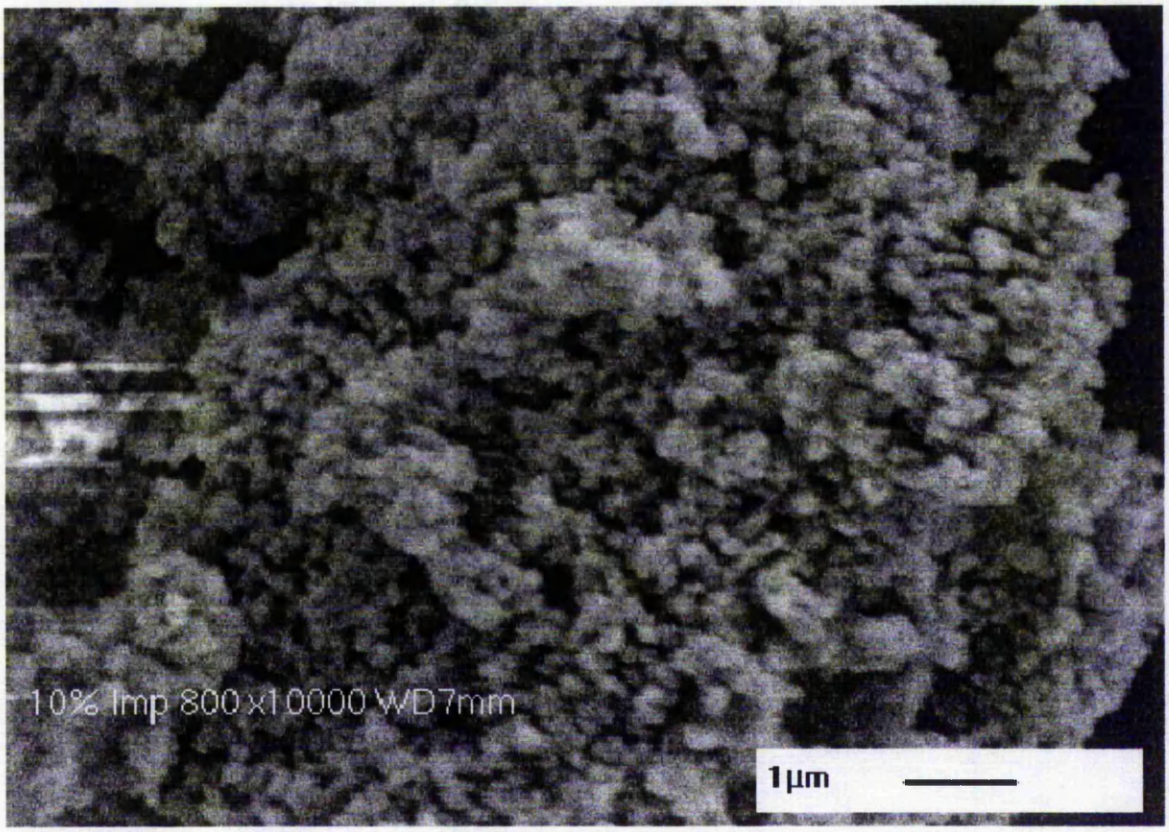

Figure 3.3.2.1 shows a SEM of 10% gold MgO. There appears to be a proliferation of smaller particles arranged on much larger clumps. These are interpreted to be gold particles with a diameter range 100-200 nm. This is of the same magnitude (but still larger) than reported elsewhere.[14] The large gold particle sizes measured are in keeping with typical values for impregnated materials.[15] Although the corresponding XRD reflection gives 38.7 nm.

3.3.3 **Figure 3.3.3.1**: 2%CP435 (MgO)

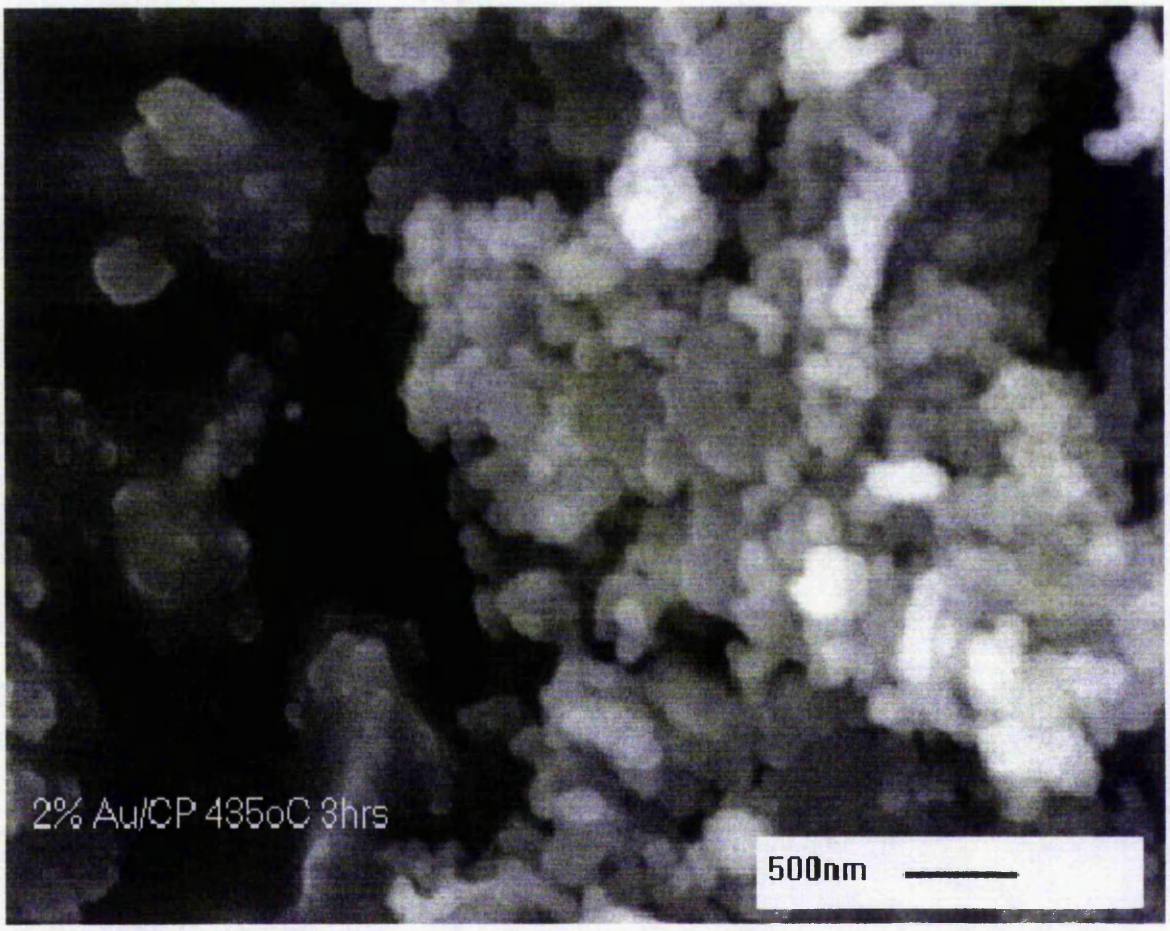

Figure 3.3.3.1 reveals the effect of calcination of intermediate loaded sample (co-precipitated, 2%) at 435°C. It is quite hard to make out the gold particles from the support particles but they appear to be in the 100 – 200 nm range. This is similar in range to those particles on impregnated MgO materials and suggests that for MgO, preparation technique has insignificant influence on gold particle dimensions.

3.3.4 **Figure 3.3.4.1**: 2%CP800 (MgO)

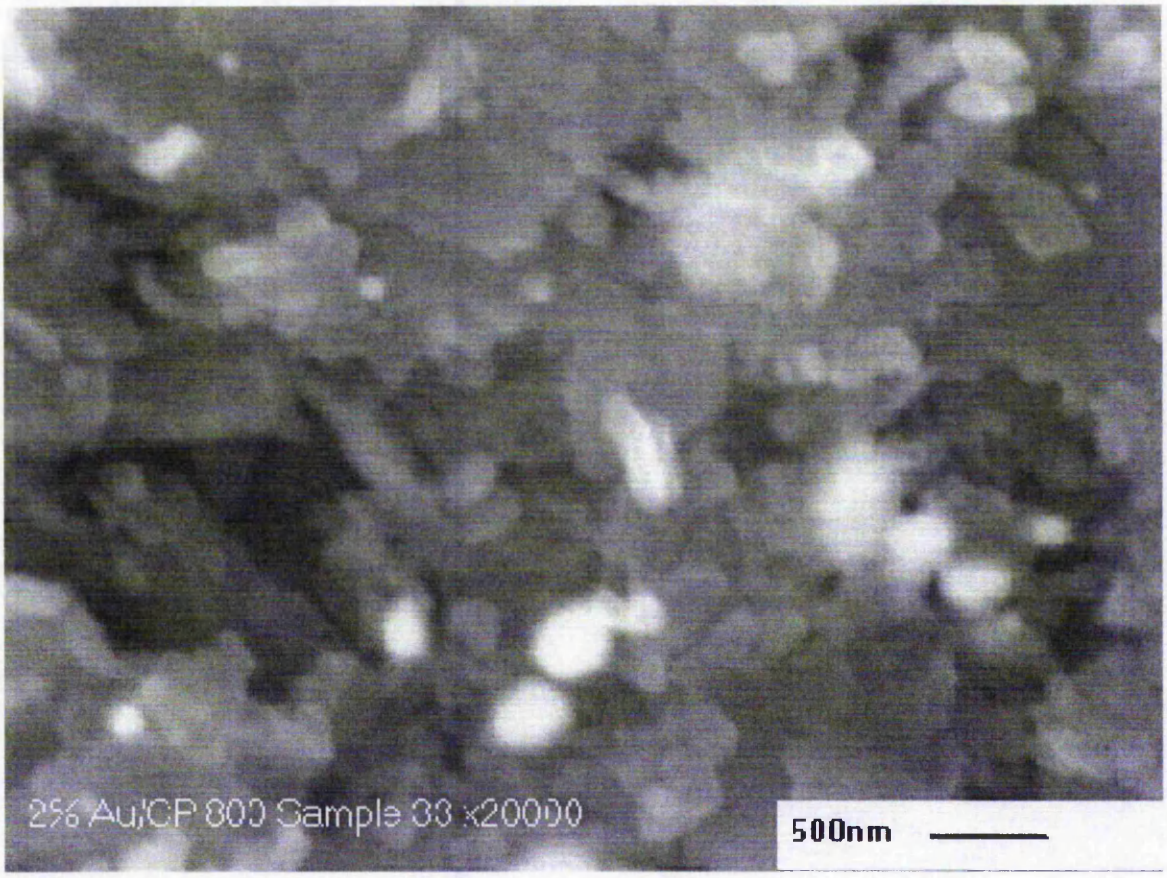

Figure 3.3.4.1 reveals the effect of high temperature calcination on gold particle size. Comparing figures 3.3.3.1 and 3.3.4.1 illustrates the sintering effect on gold of increasing calcination temperature. Here, gold particles are in the range 300 – 400 nm in diameter, more than double the size of the low temperature impregnated samples. Comparing SEM images from samples with different gold loadings reveals a preponderance of gold particles for high loaded samples and a paucity for samples with lower gold loadings although the dimensions are roughly comparable.

3.3.5 **Figure 3.3.5.1**: 10%CP435 (MgO)

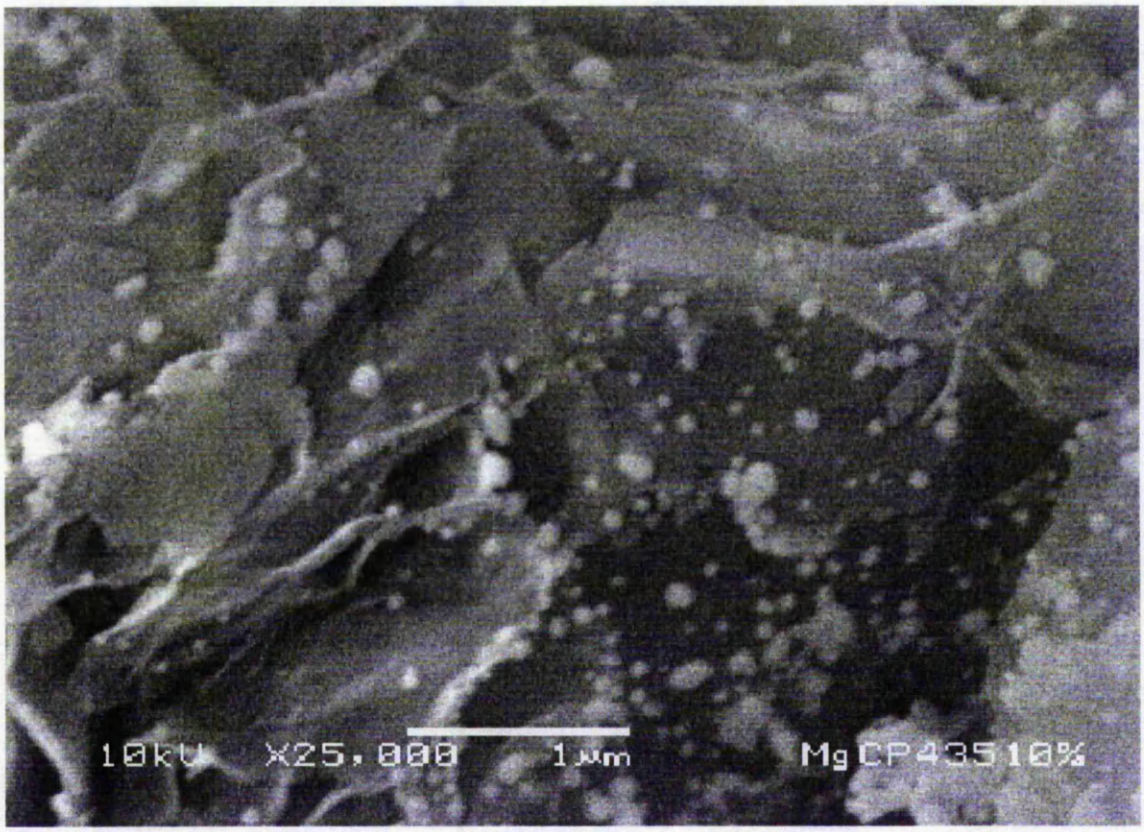

Figure 3.3.5.1 which is a SEM of 10% gold loaded co-precipitated magnesium oxide clearly shows the presence of discrete well separated gold particles on flake like support crystallites. The measured diameter of the gold particles at approximately 50 nm which is not that dissimilar from the XRD value of 39.3 nm is far higher than normal for co-precipitated materials where a value of 2-5 nm is more common.[16] Also there appears to be a large variation of particle size. These particles are not monodispersed in size variation. Monodispersion of particles has been associated with high catalytic activity and this sample is quite inactive for CO oxidation, even at high temperatures.

3.3.6 **Figure 3.3.6.1**: 10%CP800 (MgO)*

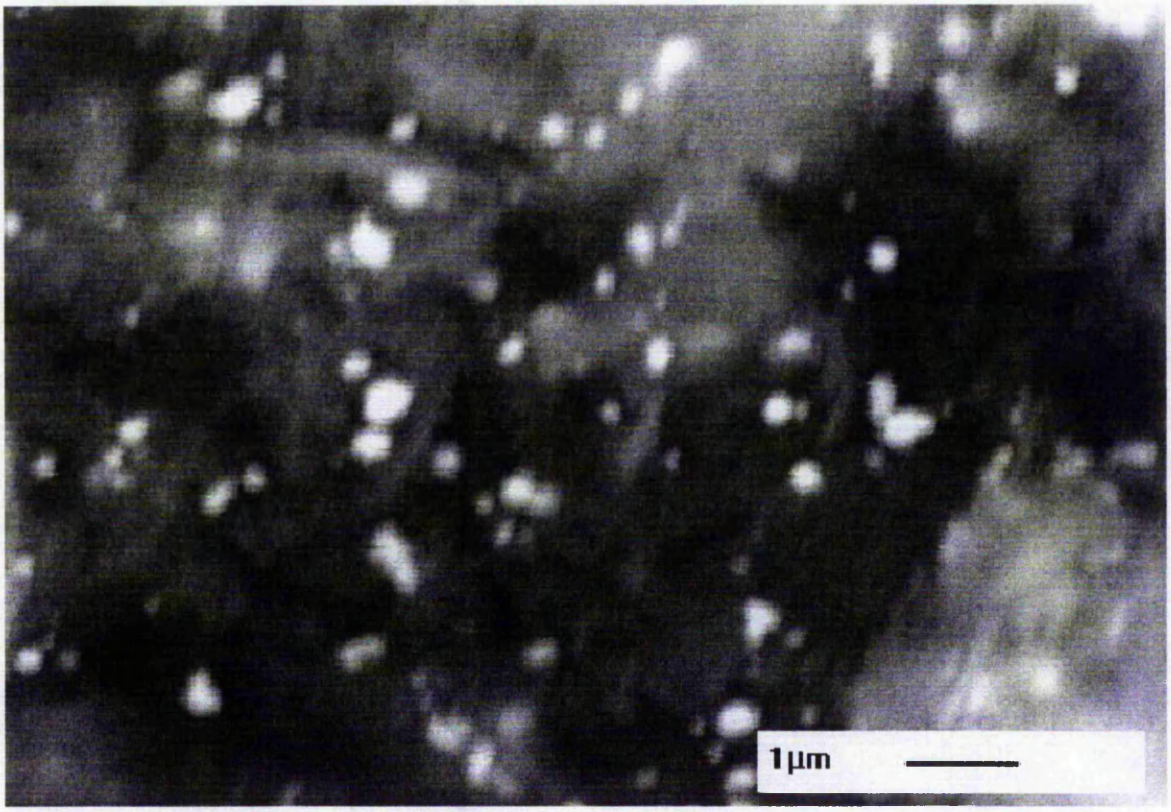

Figure 3.3.6.1 reveals the effect of high temperature calcination on high gold loaded magnesia sample. Has can be seen there is a clear increase in the size of the gold particles due to sintering from around 50 nm to 200 – 300 nm in diameter for samples calcined at 435°C and 800°C respectively. Also EDX reveals significant gold levels (relative to Mg signal) on the surface and so the existence of much smaller and less visible gold particles cannot be ruled out. The effect of increasing particle size in gold catalysis has been mentioned before (section 1.15). However the deleterious effect on catalysis or exchange is not repeated in this research. This is explained later.

3.3.7 Iron oxide supported gold

Figure 3.3.7.1: Control CP

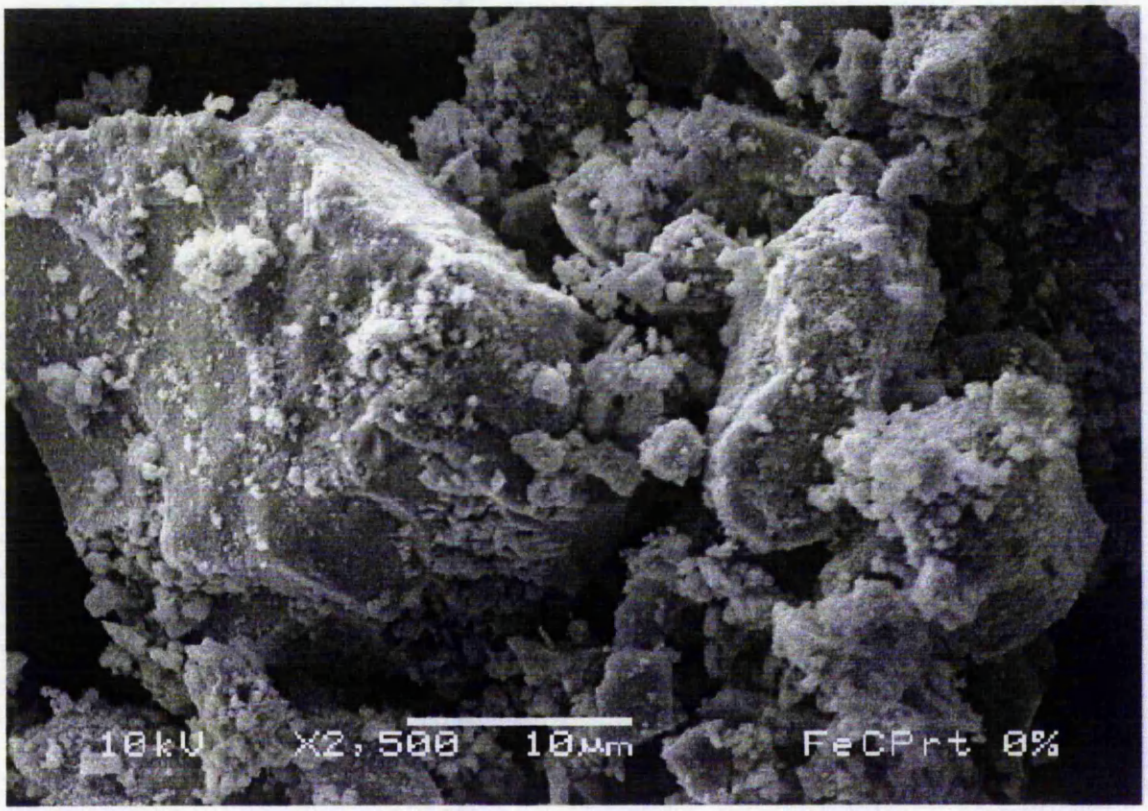

Figure 3.3.7.1 shows a SEM of co-precipitated Fe_2O_3 (Finch method) undoped material. The presence of bulky crystallites with a far larger number of "satellite" crystallites is apparent and therefore a caveat not to misinterpret small support particles as gold particles is warranted. In this research, however, usually elemental analysis (EDX) was performed to establish the reality of gold particles when assumed to be present.

3.3.8 Figure 3.3.8.1: 10_{at}%CP

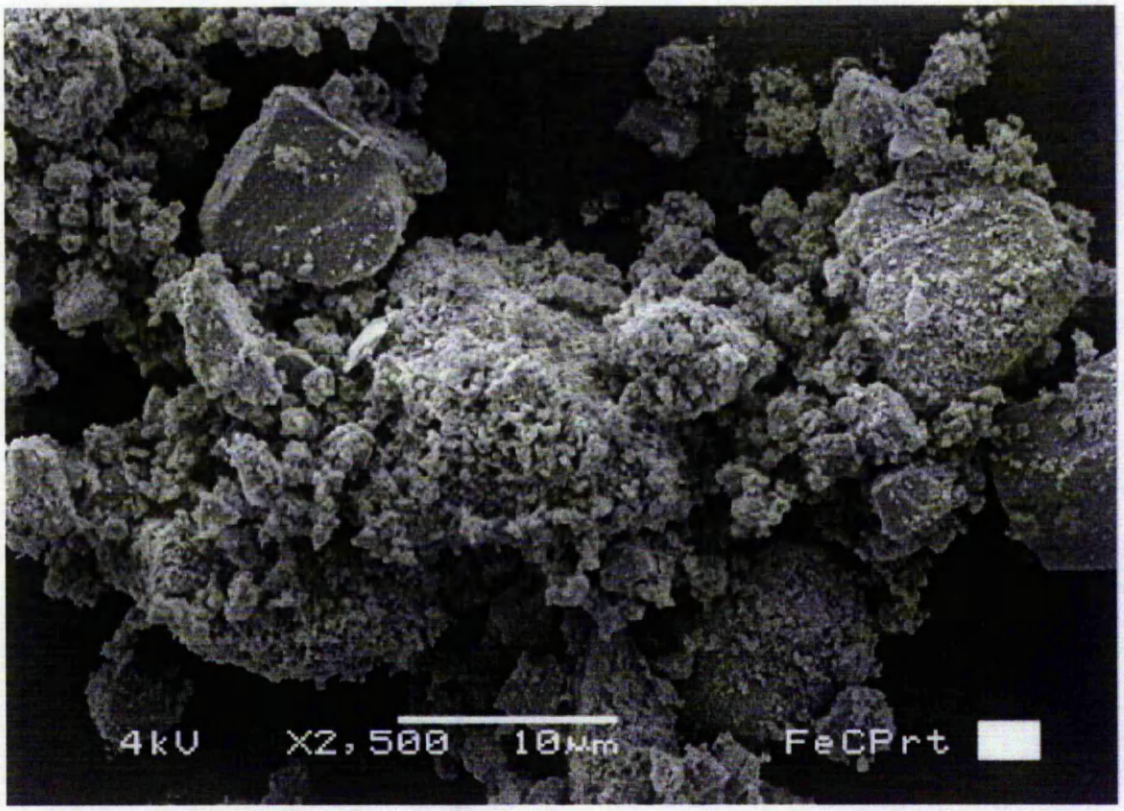

In figure 3.3.8.1 the existence of gold particles is not readily apparent from the SEM and both figures 3.3.7.1 and 3.3.8.1 look quite similar. It is possible that there are definable gold particles on the surface that are camouflaged by smaller support particles, but it should be remembered that both XPS and XRD analyses failed to detect any gold present and so the gold must be in a highly dispersed (and therefore catalytically active) state. Most researchers have found that co-precipitated Fe_2O_3 supported gold produces particles at around 2-3 nm in diameter.[17]

3.3.9 Figure 3.3.9.1: 10_{at}%CP435

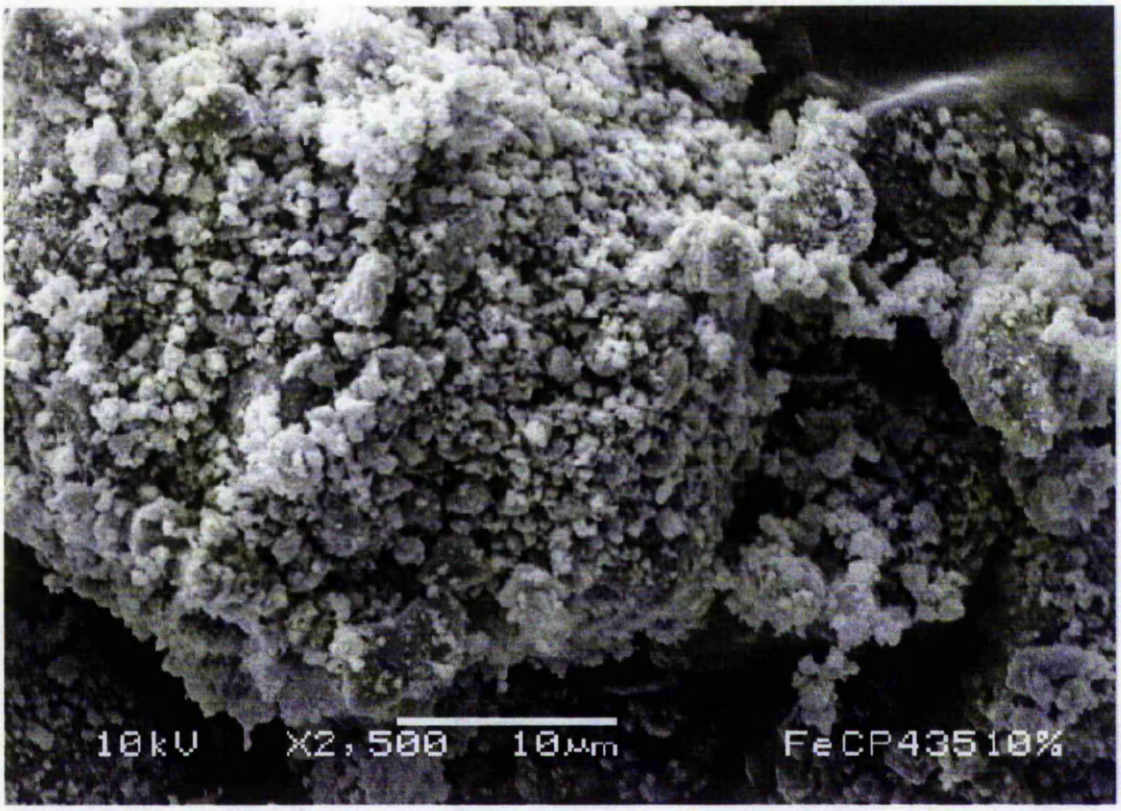

Figure 3.3.9.1 clearly shows the effect of calcination at 435°C for Fe_2O_3 co-precipitated materials. Comparing figures 3.3.8.1 and 3.3.9.1 reveals a significant degree of sintering and particle agglomeration on calcination. Unfortunately it is even harder to visually detect any gold (which should also undergo sintering) now that there are more clumps of support particles.

3.3.10 **Figure 3.3.10.1**: Control Imp800 (Fe_2O_3)*

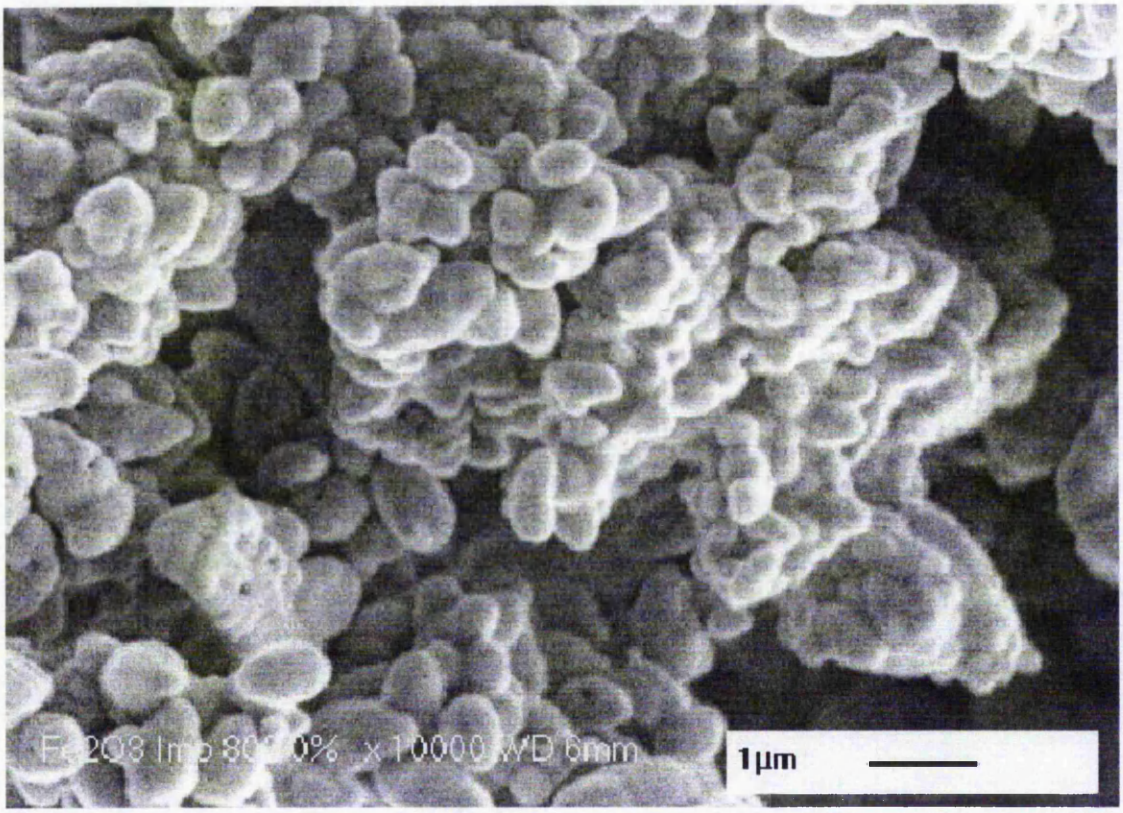

Figure 3.3.10.1 shows impregnated Fe_2O_3 crystallites with a diameter of around 500 nm that is an order of magnitude greater than that suggested by XRD.

3.3.11 **Figure 3.3.11.1**: 10% Imp800 (Fe_2O_3)*

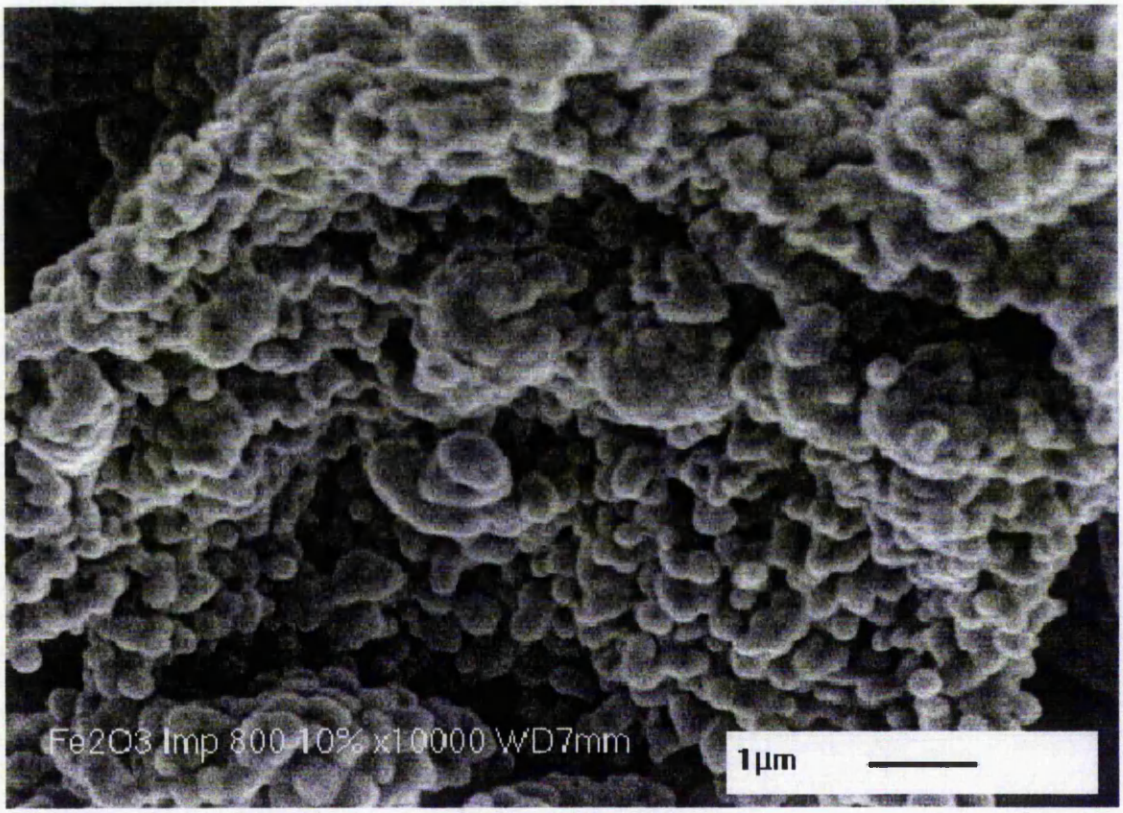

Here the effect of loading with 10% gold is explored. There appears to be sintered Fe_2O_3 crystallites with smaller gold particles associated with the surface.
Estimation of the size of the gold particles gives 250 nm, which is significantly higher than the XRD value of 44.5 nm. However, the higher value is in keeping with impregnated preparation giving much larger gold particle sizes.
Figures 3.3.10.1 and 3.3.11.1 bear a strong similarity to Fe_2O_3 SEM's by Kozlova[18] in which an impregnation technique was employed. However those crystallites were an order of magnitude smaller than the ones presented in this research.

3.3.12 SEM discussion

Most researchers employing TEM or SEM to investigate supported gold materials have often reported gold particle sizes significantly lower than obtained in this research. This is especially true for co-precipitated materials but not so for their impregnated equivalents. The fact that gold is hard to visually detect on co-precipitated Fe_2O_3 samples further complicates any comparison to the literature, but the co-precipitated Au / MgO sample (10%) does clearly reveal large gold particles. It is probable that the relatively high temperature of calcination (435°C) is responsible for surface gold sintering and larger particles. Comparison of these findings with the literature reveals further differences and similarities.

Haruta[17] obtained TEM evidence from co-precipitated Au / Fe_2O_3 that revealed supported small gold particles of 3.6 nm in diameter. Subsequent tests showed that the gold particles have their 111 planes in contact with the support and that epitaxial contact between support and particle is apparent. It was also established that impregnated materials again showed large gold particle sizes of 10 – 30 nm in diameter.

Hodge et al,[19] also investigating a Au / Fe_2O_3 system (2.1% gold) could not observe any gold particles during TEM measurements for dried samples which is similar to findings described in the authors research. However, after calcination at 400°C gold particles of size 3-5 nm were readily apparent, supported on Fe_2O_3 crystallites of 20 nm in size. This finding is contrary to the SEM in this report that reveals no discernable gold at 435°C calcination temperature, (although sintering of Fe_2O_3 crystallites might camouflage such particles). This is not that surprising as the resolving power of SEM is far less than that of a TEM.

Concerning the use of pre-treatments, it was found[20] that neither reductive or oxidative pre-treatment had any effect on the size of the gold particles which in this instance fell between 7.5 and 12.5 nm in diameter. It was found in this research that low gold loading lead to thinly dispersed gold particles, however this explanation does not hold for the research by the author as gold loadings as high as 10_{at}% were used and yet it was hard to distinguish any gold particles for Fe_2O_3 support.

Investigation by HRTEM of the influence of gold loading as shown[14] that morphology changes can be dependent on gold loading. Blick et al found that for MgO supported samples with gold loading less than 1.5% HRTEM suggested the presence of 2-dimensional rafts and for greater loaded samples the appearance of discrete particles was apparent. This effect wasn't investigated in this research as only the presence / absence of gold, calcination temperature, support and preparation technique on particle / support morphology were investigated. It is also important to remember that most researchers have not found morphological type dependence on gold loading as Blick et al have. Indeed the most notable influence of gold loading is to regulate gold particle dispersion. This is brought out by research by Grunwaldt[21] who found that a tenfold increase in gold loading on TiO_2 and ZrO_2 supports had only a marginal effect on particle size (2.0 to 2.5nm for TiO_2) but the higher loaded samples did give rise to localized bunching of larger particles. This phenomenon can have skewing effects on the data (i.e., an underestimation or over estimation of particle sizes) depending on where the catalyst is sampled by TEM. Therefore it should be remembered that low gold loaded samples tend to give more accurate measurements of particle size due to more uniform gold particle dispersion. In the authors research though, high gold loaded samples tend to be used for analysis and so the particle size values might not be that reliable.

Further evidence regarding the influence of calcination on temperature was produced by Bocuzzi et al,[22] who investigated this effect on Au / TiO_2 and found that increasing calcination temperature from 200°C to 300°C had no influence on the mean gold particle diameter but there was a reduction in the number of particles that fell between 1 – 2 nm. This suggested that particle agglomeration was occurring during calcination. An effect that could apply to the high temperature calcined materials of the author's research.

3.3.13 EDX characterisation of samples

In order to confirm that certain SEM images were indeed revealing gold particles, EDX was performed on suspect gold particles and compared to that of the support. As an example, EDX analyses performed on a 10%CP800 (MgO) sample will be shown.

Figure 3.3.14: EDX of 10%CP800 (MgO) support

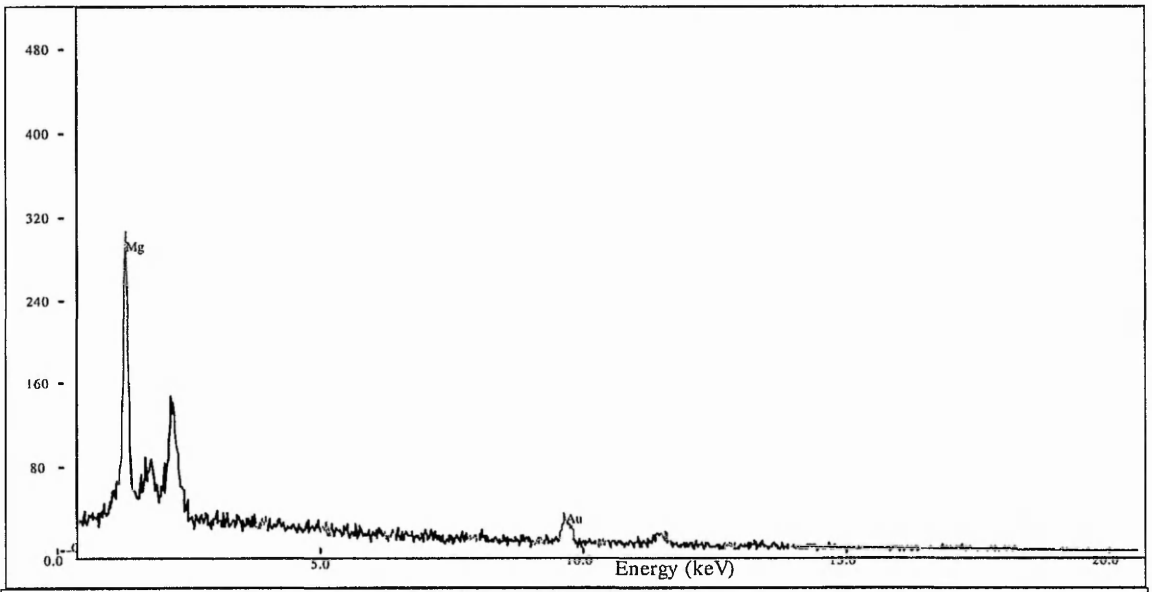

Z Element Line	K-Ratio	Concentration		
	wt%	at%	Cmpd	wt%
79 Au LA1	0.2358	31.724	5.420	31.724
12 Mg KA1	0.5907	68.276	94.580	68.276
	Total	100.000	100.000	100.000

Figure 3.3.14 reveals that there is a high concentration of gold (31.7%) on the support, even though this EDX was performed on an area of the support with no visible particles. This implies gold exists in a highly dispersed state as well as in particle form for this sample.

When gold particles are presumed to be present, EDX can be performed on them as figure 3.3.15 reveals.

Figure 3.3.15: EDX of suspect gold particle

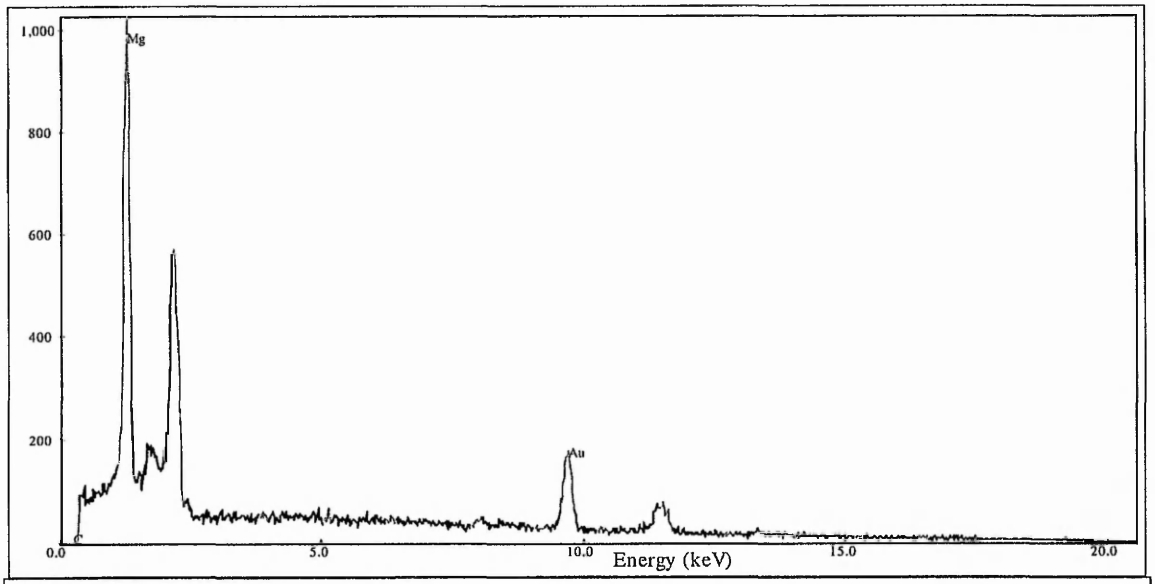

Z	Element	Line	K-Ratio	Concentration		
			wt%	at%	Cmpd	wt%
79	Au	LA1	0.3569	45.831	9.448	45.831
12	Mg	KA1	0.4542	54.169	90.552	54.169
			Total	100.000	100.000	100.000

Figure 3.3.15 reveals a significantly higher gold reading (45.8%) for EDX performed on a suspect particle. This supports the assertion that those images that look like gold particles actually are. In interesting to note the significant magnesium signal. This is because the probe electrons have high energy (20 KeV) and are able to penetrate the support by several microns as well as detect surface features.

More evidence for the existence of gold particles is found by mapping the gold counts and comparing these to suspect gold particles on the parent SEM image.

This comparison is shown in figures 3.3.16 and 3.3.17.

Figure 3.3.16: SEM image of suspect gold particles on 10%CP800 (MgO)

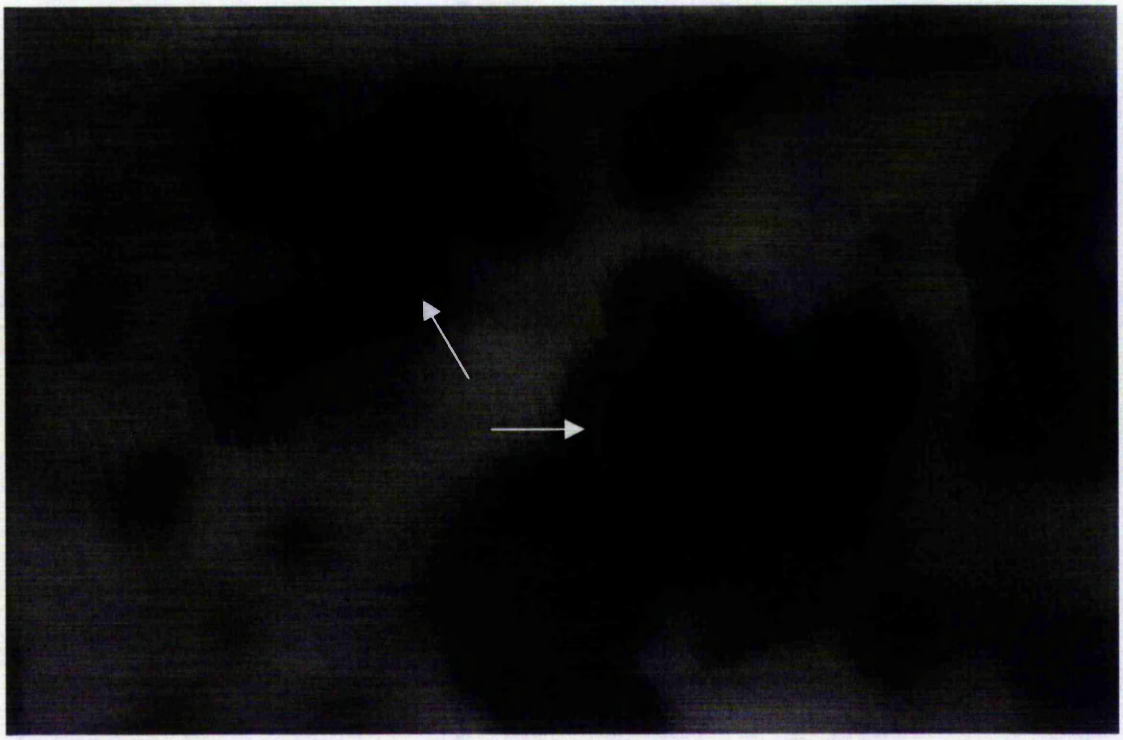

Figure 3.3.16 reveals the existence of assumed gold particles (arrowed) on 10%CP800(MgO) sample. The image is darkened due to lengthy scanning (10 minutes). This image is then compared to an equivalent mapped version as shown in figure 3.3.17.

Figure 3.3.17: Gold mapped version of the SEM image in figure 3.3.16

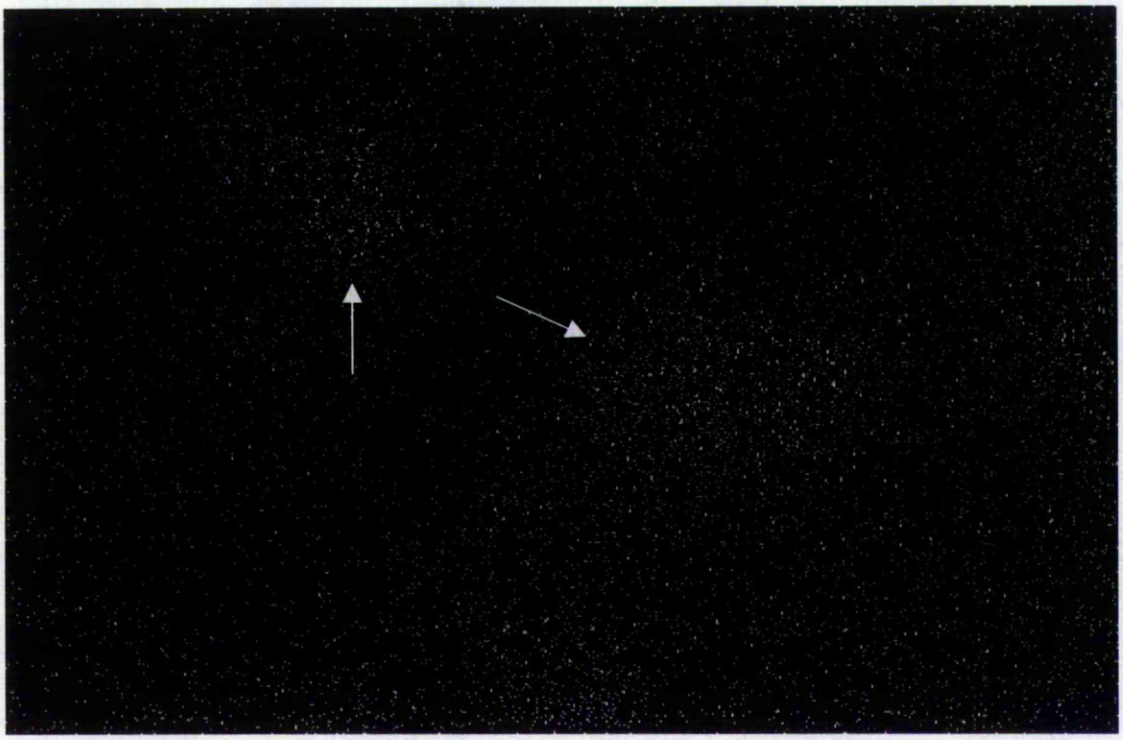

Close comparison of figures 3.3.16 and 3.3.17 does show an apparent correlation between suspect gold particles in figure 3.3.16 and high concentration of gold counts that form clusters of dots (arrowed) in figure 3.3.17. This relationship is further evidence for SEM detection of gold particles on support.

Some co-precipitated iron oxide samples have failed to register XRD, XPS or SEM evidence of gold and yet are catalytically active (chapter 7). It is therefore of interest to examine these samples using EDX. This is done in figure 3.3.18.

Figure 3.3.18: EDX of 5_{wt}%CP (Fe_2O_3)

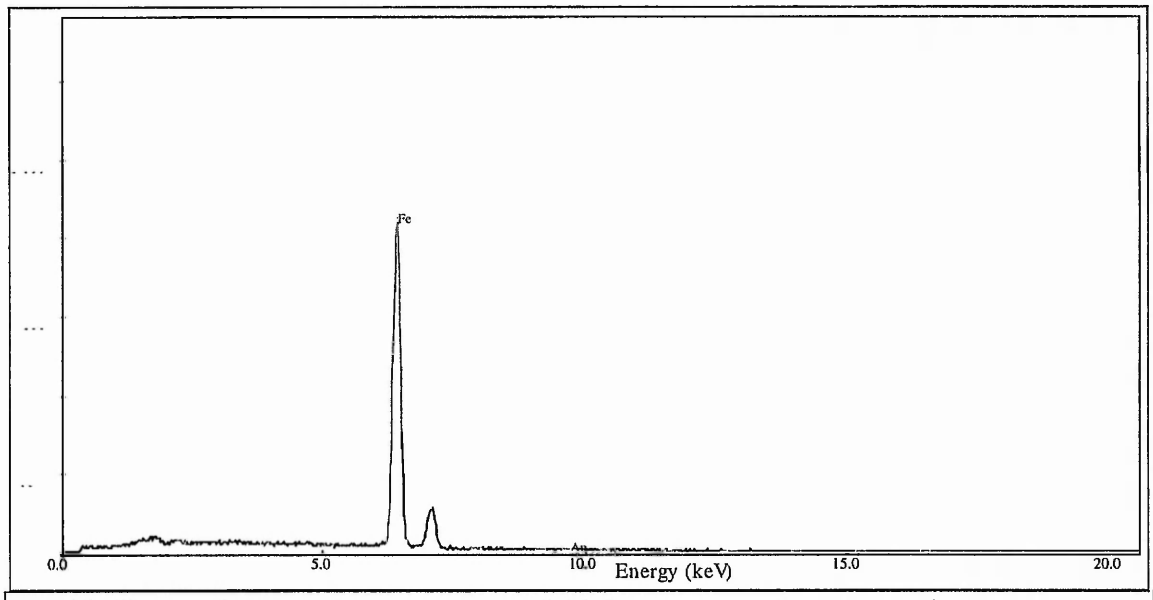

Z	Element	Line	K-Ratio	Concentration		
			wt%	at%	Cmpd	wt%
79	Au	LA1	0.0021	0.274	0.078	0.274
26	Fe	KA1	0.9975	99.726	99.922	99.726
			Total	100.000	100.000	100.000

Figure 3.3.18 confirms previous characterisation of this sample (and other co-precipitated iron oxide samples) by revealing a very small amount of gold (0.27%) on the surface. What is especially interesting is the observation that sub-surface (up to several microns) of material is probed and yet there is only trace gold detected, despite relatively high gold loadings (5_{at}%). This implies that gold is concealed deep down in the support during co-precipitation. Although these samples have only trace amounts of gold on the surface they are extremely active for catalysis.

3.4 Powder X-Ray Diffraction (XRD) investigations

3.4.1 XRD of MgO support classes:

As described earlier there are 4 different classes of sample based on MgO support. Characterisation using XRD was performed on all of them. They are presented in a stacked format (increasing gold loading) for each class below:

Figure 3.4.1.1: Impregnated MgO class calcined at 800°C

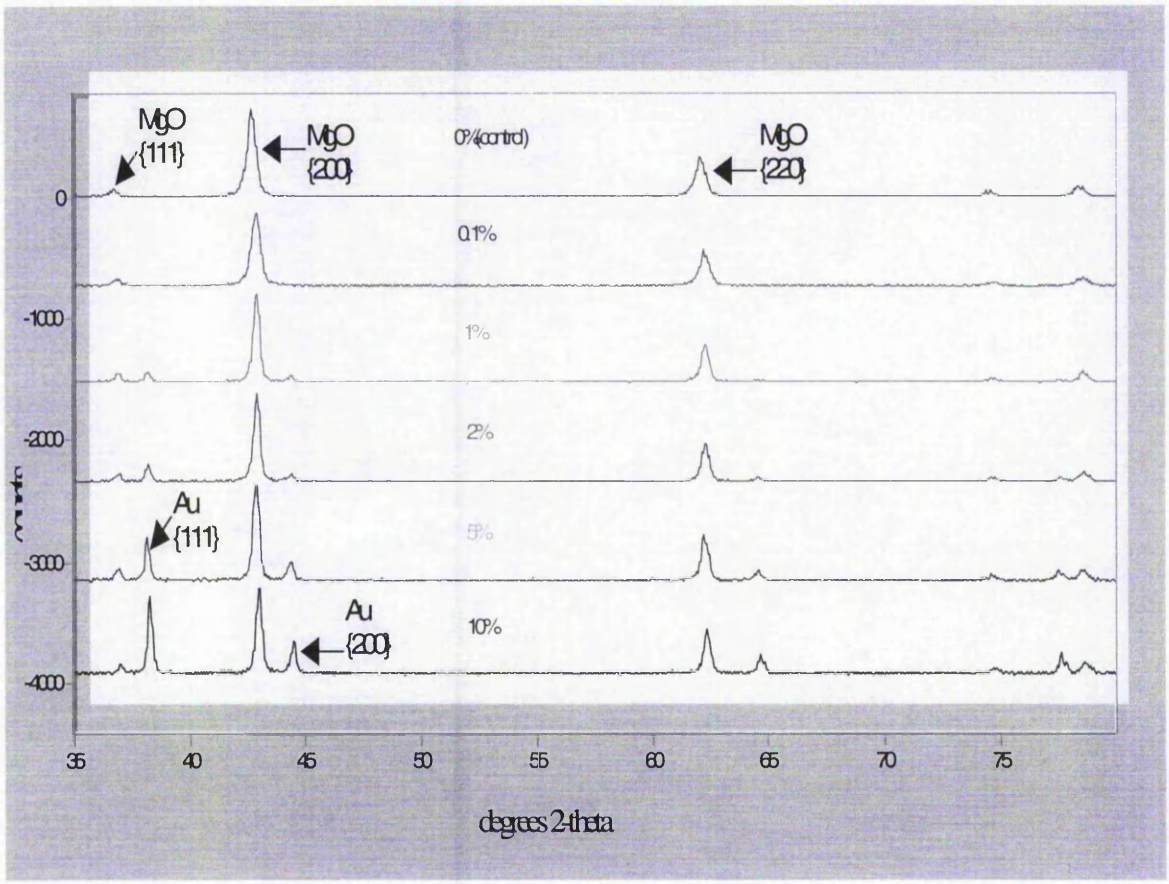

Figure 3.4.1.2: Impregnated MgO class calcined at 435°C

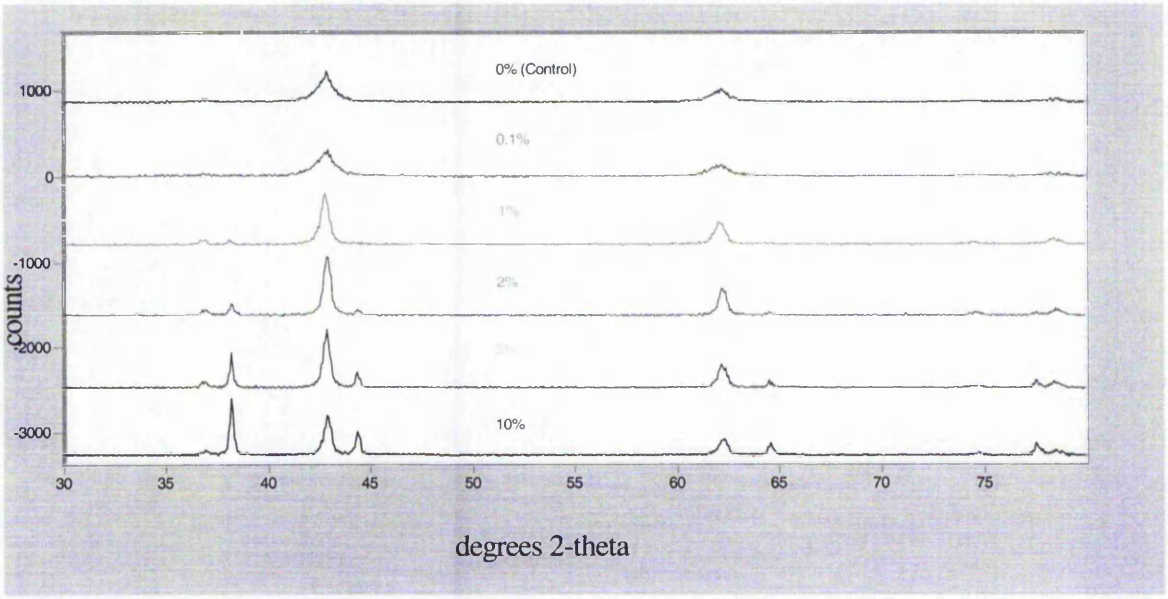

Figure 3.4.1.3: Co-precipitated MgO class calcined at 800°C

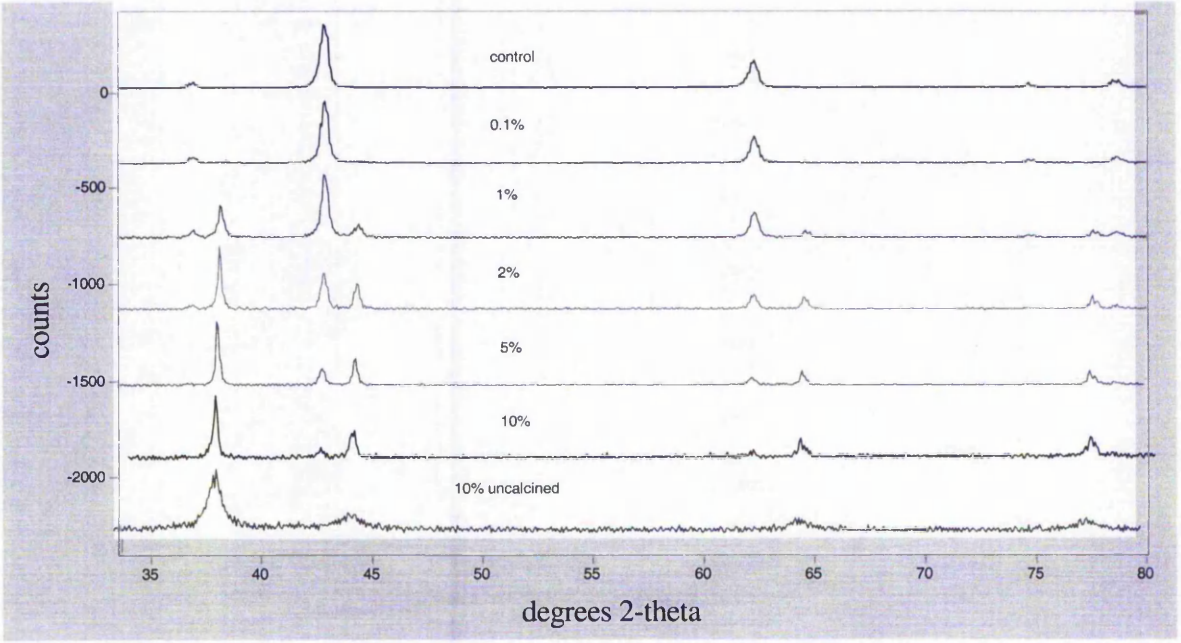

Figure 3.4.1.4: Co-precipitated MgO class calcined at 435°C

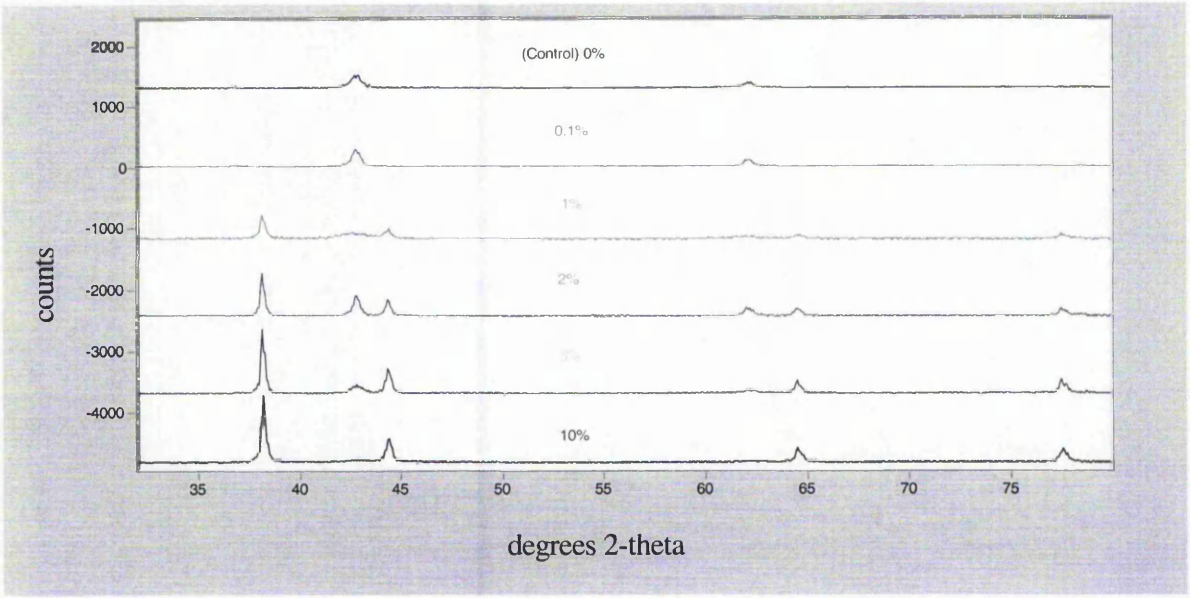

As can be seen, for all classes, with increasing gold loading there are more prominent gold reflections, as expected. Interestingly, however, there appears to be a decrease in the MgO reflection width (FWHM) with increasing gold loading suggesting larger MgO support particles. For impregnated materials no such effect exists. (See figure 3.4.1.1 for MgO and Au reflections). There is also no support for an evolution of gold morphology from 2-dimensional rafts to discrete hemispheres with increasing gold loading, as found elsewhere.[23] Any change of this magnitude would clearly show as very noticeable change in the width of gold reflections from very broad to quite narrow. No such changes occur.

It is also apparent that low temperature calcined co-precipitated materials give well defined gold reflections but ill defined MgO reflections suggesting a high degree of amorphous nature for the support. At higher calcination temperature the support reflections become much more well defined suggesting a return to a high degree of crystallinity for these materials.

3.4.2 XRD of Fe_2O_3 supported materials:

In addition to characterisation of MgO supported gold materials, Fe_2O_3 supported gold samples have also been investigated using XRD.
The results for Fe_2O_3 are presented in the same format as with MgO for the 4 different classes.

Figure 3.4.2.1: Impregnated Fe_2O_3 materials calcined at 800°C

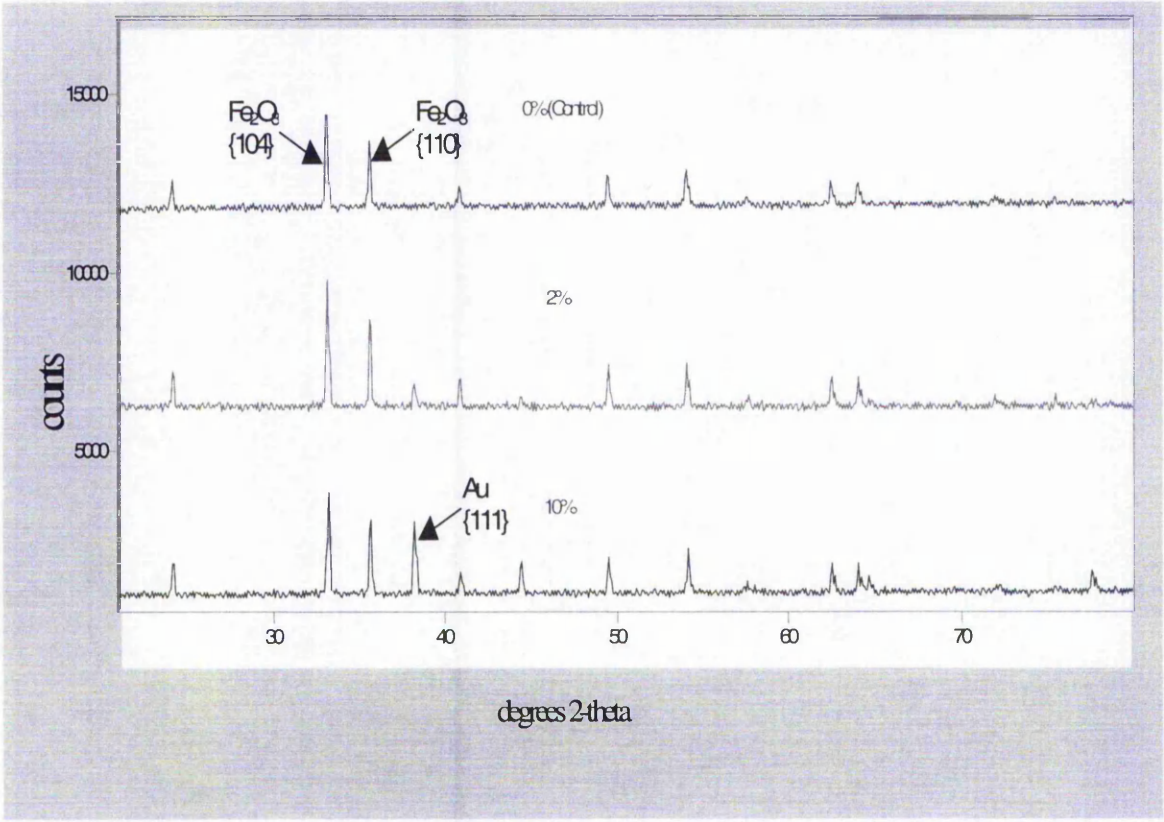

Figure 3.4.2.2: Impregnated Fe_2O_3 calcined at 435°C

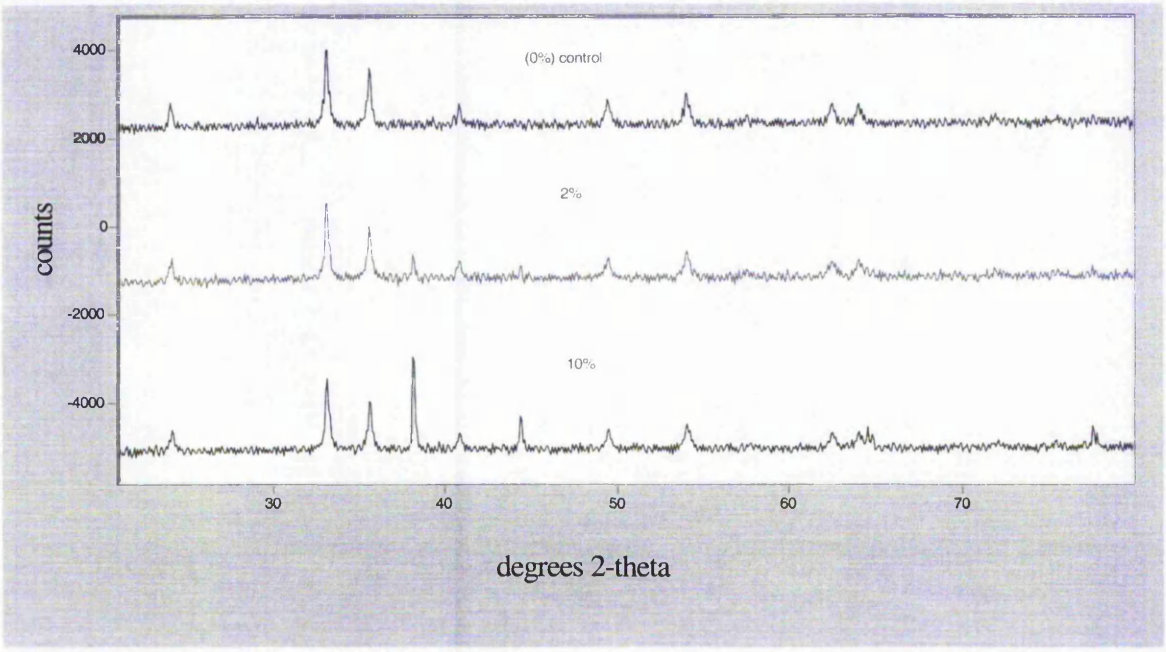

Figure 3.4.2.3: uncalcined co-precipitated Fe_2O_3

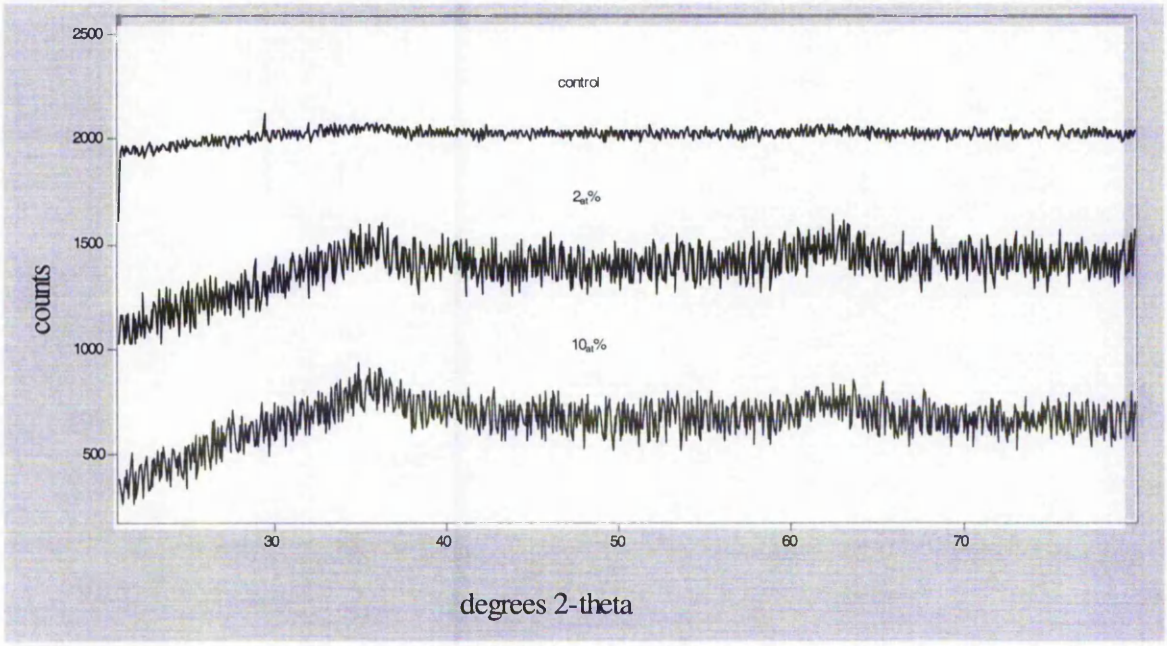

Figure 3.4.2.4: Co-precipitated Fe_2O_3 calcined at 435°C

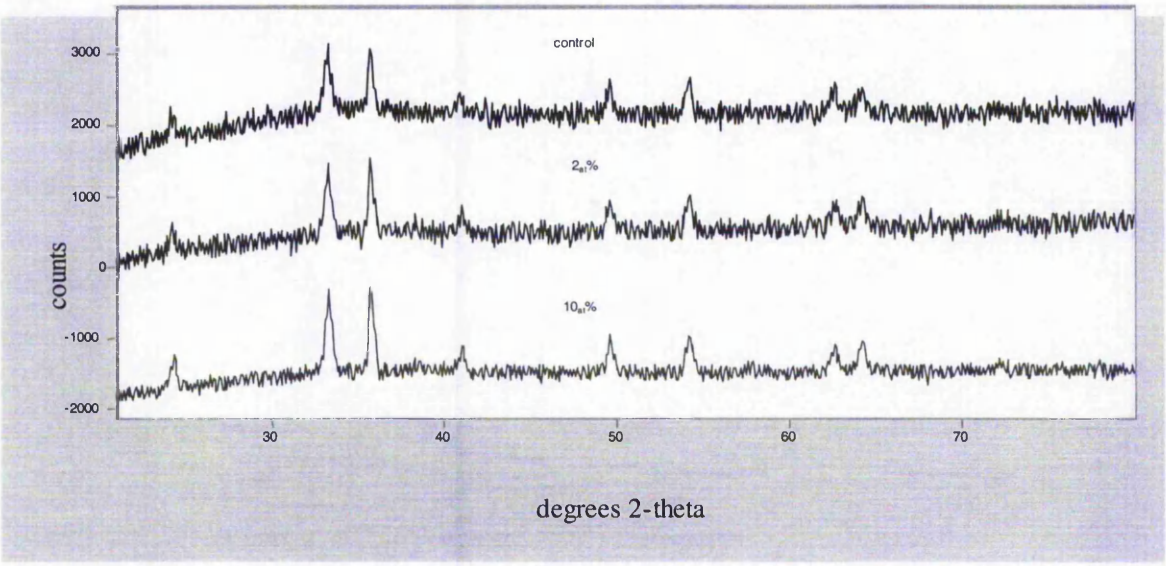

3.4.3 XRD Discussion

XRD analysis of Fe_2O_3 supported materials reveals a considerable difference in the degree of crystallinity between co-precipitated and impregnated samples with sharp reflections for impregnated materials and broad reflections for co-precipitated materials. For impregnated materials there is evidence of sintering, once again, with increasing gold loading. Also, as expected, samples calcined at the higher temperature of 800°C show evidence of larger (sintered) crystallites than lower temperature (*435°C*) calcined samples.

Uncalcined co-precipitated materials prepared by co-precipitation (base to acid) display the characteristic 2 broad reflections, otherwise referred to as '2-line ferrihydrite,'[24] indicative of the initial chemical state of co-precipitated iron oxide and prepared by rapid hydrolysis at neutral or above pH : $Fe_5(OH)_8 : 4\ H_2O$. This pre-cursor has been found by others[24,25] but not all cases for co-precipitated Au / Fe_2O_3, because of differences in experimental variables such as the temperature at which base is added and terminal pH.[26] Research suggests this is the most catalytically active pre-cursor of iron oxide.[24] Upon calcination at 435°C a greater degree of crystallinity is observed although there is no evidence of gold loading, suggesting

that the gold is in a highly dispersed form upon the surface of co-precipitated iron oxide. Others have followed the change in crystallinity following calcination at a range of temperatures. Kozlova et al,[27] revealed an increase in crystallinity following calcination of as precipitated wet $Fe(OH)_3$. Samples were calcined at 200°C, 300°C, 400°C and 500°C. Samples calcined at 473 K revealed an absence of reflections demonstrating the amorphous nature of low temperature calcined Au / $Fe(OH)_3$. Samples calcined at the higher temperatures revealed progressively stronger reflections associated with an ever-increasing degree of crystallinity. Both α-Fe_2O_3 and γ-Fe_2O_3 were observed as low as 100°C calcination temperature. Both these forms of iron oxide are clearly present in the XRD data displayed above with reflections resulting from α-Fe_2O_3 and γ-Fe_2O_3 positioned at $2\theta = 33^\circ$ and 36°, respectively. The investigators also observed gold reflections for samples calcined at temperatures at and above 100°C, again, very similar to the research described previously by others and the author.

XRD characterization has been used to follow the influence of gold on the reduction of Fe_2O_3 under a flow of hydrogen.[28] Here, investigators maintained a flow of hydrogen over Fe_2O_3 catalyst at a range of temperatures from 23°C to 427°C and found evidence that gold lowered the temperature of the reduction step: Fe_2O_3 to Fe_3O_4 by 80°C from 177°C to 97°C. This research is an XRD analogue of the TPR data in this report that details the same ease of reduction effect for gold (section 3.2.3). Similarly there wasn't an identifiable reduction to FeO suggesting a single combined reduction step from Fe_3O_4 to Fe. The authors make no attempt to explain this effect but it is possible that gold causes an increase of the highly hydroxylated ferrihydrite phase that is associated with an ease of reduction of Fe_2O_3 to Fe_3O_4. Horvath et al,[26] found that pre-treatment affected the phase of iron oxide that was detected by XRD. Reductive pre-treatments gave a maghemite phase while oxidative pre-treatments produced only haematite with a reduced intensity to the as-prepared samples due to a higher amorphous component. There was also an absence of gold

reflections despite TEM observations of particles with diameters 7.5 – 12.5 nm. The authors concluded that the loading of gold used (0.94%) was too low to be detected by XRD although TEM was sensitive to clusters of gold particles. In the author's research, Au reflections have been seen as low as 0.5% loading for MgO and 2% loading for Fe_2O_3. Further effects of gold have been examined by Knell et al,[29] who examined the influence of gold loading on Au / ZrO_2 system and found far broader zirconia reflections for 10% mol weight of gold sample than a 1% sample. This result suggests that gold has a stabilizing influence on zirconia crystallites during calcinations and protects them from sintering. However the stabilizing effect of gold has not really been observed in the author's research. In fact the opposite effect is apparent with sharper reflections accompanying increasing gold loading, consistent with a crystallite sintering effect as described above. These conflicting results point to the complex role played by support / gold interactions during calcination.

Figure 3.4.4: XRD summary for iron oxide materials

Material	Support or gold	Position of reflection (degrees 2θ)	{hkl}	FWHM	Crystallite size (Å) (Scherrer method)*
Control CP 435	Fe_2O_3	33.28	104	0.46	201
Control CP 435	Fe_2O_3	35.66	110	0.33	281
10_{at}%CP 435	Fe_2O_3	33.28	104	0.42	220
10_{at}%CP 435	Fe_2O_3	35.74	110	0.34	273
10% Imp 435	Fe_2O_3	32.96	104	0.27	341
10% Imp 435	Fe_2O_3	35.70	110	0.27	344
10%Imp800	Fe_2O_3	33.33	104	0.22	419
10%Imp800	Fe_2O_3	35.68	110	0.16	580
10%Imp800	Au	38.31	111	0.21	445
Control Imp800	Fe_2O_3	33.11	104	0.18	512
Control Imp800	Fe_2O_3	35.74	110	0.20	464

Figure 3.4.4: XRD summary for magnesia materials

Material	Support or gold	Position of reflection (degrees 2θ)	{hkl}	FWHM	Crystallite size (Å) (Scherrer method)*
Control Imp800	MgO	36.76	111	0.29	321
Control Imp800	MgO	42.68	200	0.44	216
Control Imp800	MgO	62.07	220	0.50	206
Control Imp800	MgO	74.60	311	0.33	337
Control Imp800	MgO	78.40	222	0.57	200
10%Imp800	MgO	36.94	111	0.23	405
10%Imp800	MgO	42.97	200	0.33	288
10%Imp800	Au	38.26	111	0.24	387
10%Imp800	Au	44.43	200	0.25	382
Control CP800	MgO	36.99	111	0.42	222
Control CP800	MgO	42.84	200	0.45	211
5%CP800	MgO	36.92	111	0.33	282
5%CP800	Mg	42.92	200	0.34	279
5%CP800	Au	38.18	111	0.22	425
5%CP800	Au	44.41	200	0.25	382
5%CP435	MgO	42.78	200	0.57	166
5%CP435	Au	38.18	111	0.24	390

Figure 3.4.4 is a summary of most XRD sample characterization. Conclusions derived from these data are given below

3.4.5: XRD conclusions

1: Not surprisingly, higher temperature of calcination causes sintering of both gold and support crystallites leading to larger crystals and consequently sharper XRD reflections. However the influence of calcination is especially marked for MgO as a support relative to Fe_2O_3 at the same temperatures.

2: Increasing gold loading across all MgO sample classes results in an increase in MgO crystallite size, possibly mediated by a gold facilitated increase in MgO defect formation leading to MgO crystallite sintering.[1]

3: Increasing gold loading for Fe_2O_3 supported catalysts doesn't have a consistent effect on support particle size as it does with MgO as support.

4: Co-precipitation appears to result in smaller support crystallites than impregnation, especially for Fe_2O_3 supported gold catalysts. This may have implications when considering the individual catalytic merits of each preparation technique across both support types.

5: There is no detectable gold for co-precipitated Fe_2O_3 catalysts. There is also no detectable influence on support crystallites from any gold that may be present (but XRD undetectable).

3.5 X-ray Photoelectron Spectroscopy (XPS)

3.5.1 XPS of MgO samples:

In order to investigate the surface chemistry of MgO samples, XPS was performed on several materials from a variety of different classes.

Figure 3.5.1.1: XPS of gold doped MgO

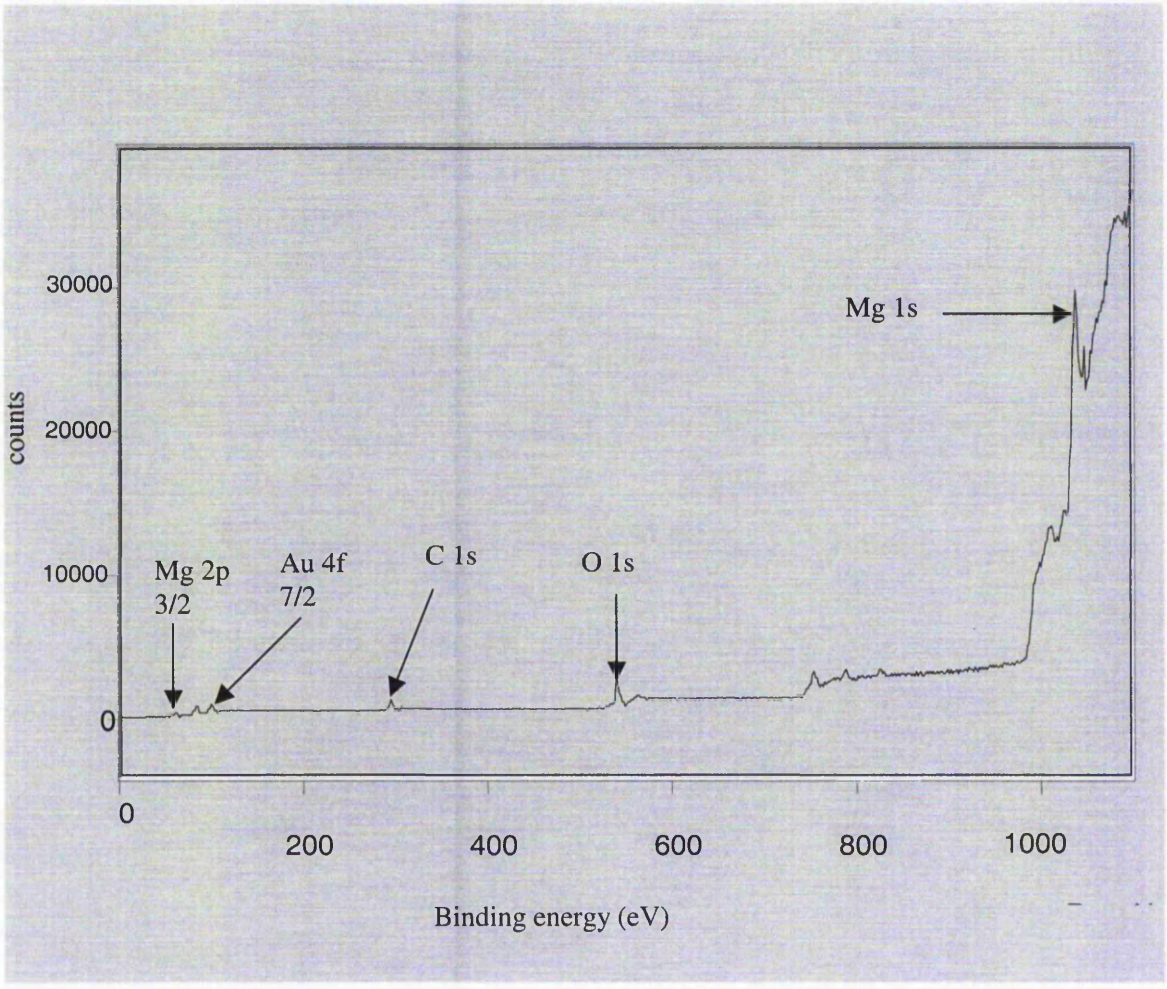

Figure 3.5.1.1 shows a typical MgO XPS profile (5% co-precipitated MgO). All the relevant peaks can be seen including the adventitious carbon (C 1s) peak that is used to as a reference in order correct for sample charging and the spectrometer

work function. This gives more reliable binding energies for peaks that are observed.

Figure 3.5.1.2: Break down summary of MgO XPS data

Sample	Calcination temperature °C	B.E., eV (FWHH)				atomic ratio		Content wt%	
		Au $4f_{7/2}$*	Au $4d_{5/2}$ **	Cl 2p ***	Au $4d_{5/2}$ /Mg 2p	Cl 2p/ Mg 2p	Cl/Au ****	Au	Cl
10%Au/MgO, impregnated	435	84.0	334.5 (3.18)	199.2 (3.38)	0.0059	0.0238	4.03	2.49	1.81
	800	84.0	334.0 (3.71)	no	0.0034	-	-	1.13	-
10%Au/MgO, co-precipitated	435	84.0	334.1 (4.25)	199.2 (2.31)	0.0282	0.0096	0.34	9.79	0.6
5%Au/MgO, co-precipitated	800	84.2	334.3 (3.66)	199.1 (1.95)	0.0103	0.0056	0.55	4.28	0.42

XPS data of Au/MgO catalysts (B.E. C 1s = 285.0 eV used as reference).
Figure 3.5.1.2 gives a summary of XPS data on all four different MgO sample classes.

There are several salient points to note; firstly that calcination at 800°C for impregnated materials completely removes any chlorine (which is a well known catalyst poison in which most researchers take steps to remove)[30] present but not at 435°C. This is clearly shown in figure 3.5.1.3.

Figure 3.5.1.3: the influence of calcination temperature on chlorine levels

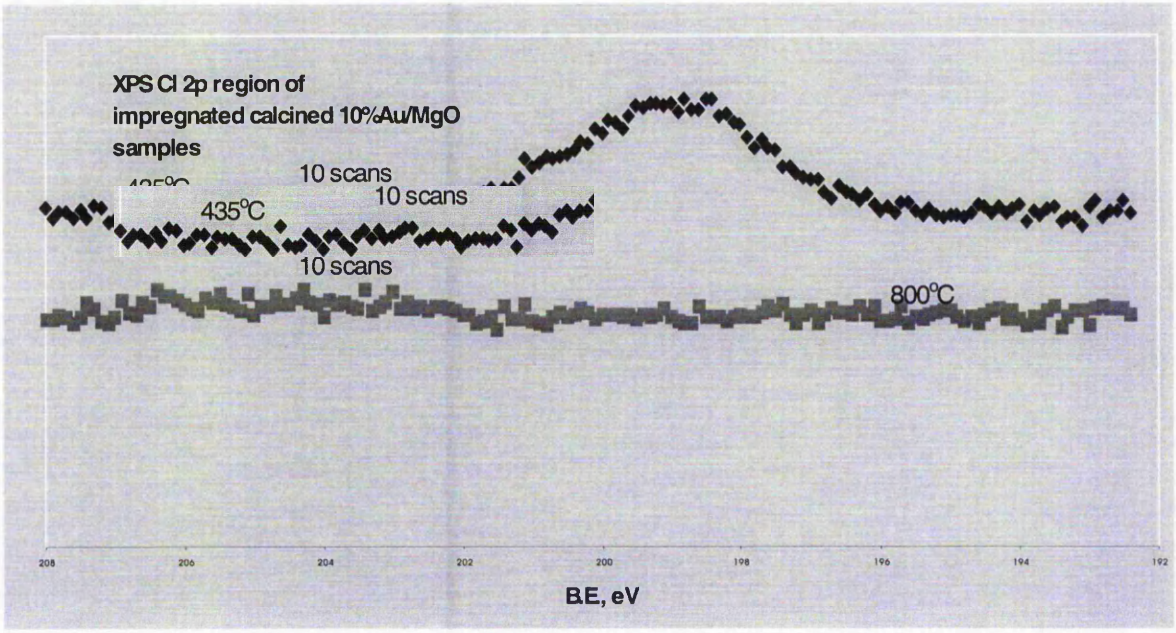

This result has implications for understanding the oxygen exchange profile for this sample class as described later on.

Increasing calcination temperature has less of an impact at removing chlorine for co-precipitated materials than impregnated materials in which all chlorine is removed at 800°C.

Also, it is apparent that at the higher calcination temperature for the impregnated class, there is apparently *less* gold than for the lower calcined sample. This could possibly be due to sintering of gold particles, as XPS is less sensitive to larger particles. This has the effect of increasing the gold peak area for a surface covered with many small particles as opposed to a surface covered with fewer larger particles. Such an effect would manifest as in figure 3.5.1.4.

Figure 3.5.1.4: The influnce of increasing calcination temperature on detected gold levels

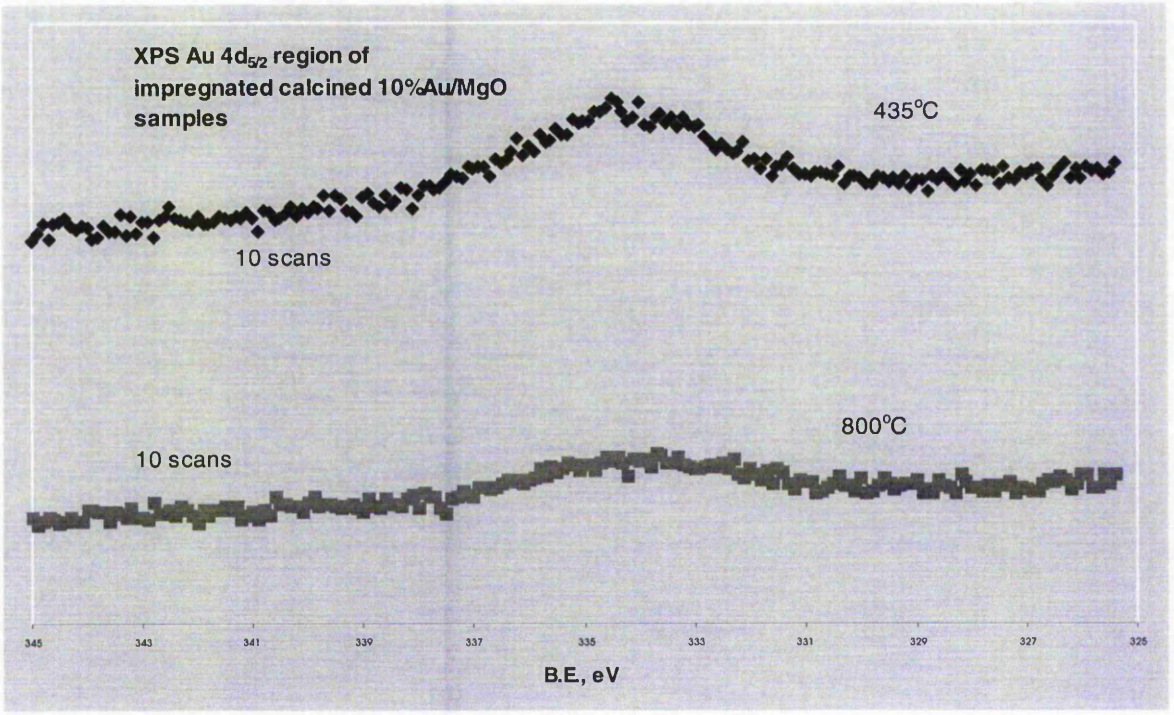

Figure 3.5.1.4 shows the effect of calcination on the Au signal for 10% loaded MgO. There is a significantly attenuated signal with higher calcination temperature, when in actual fact both samples have the same gold loading. An explanation is postulated above.

3.5.2 XPS of Fe_2O_3 samples:

Figure 3.5.2.1: XPS of gold doped Fe_2O_3

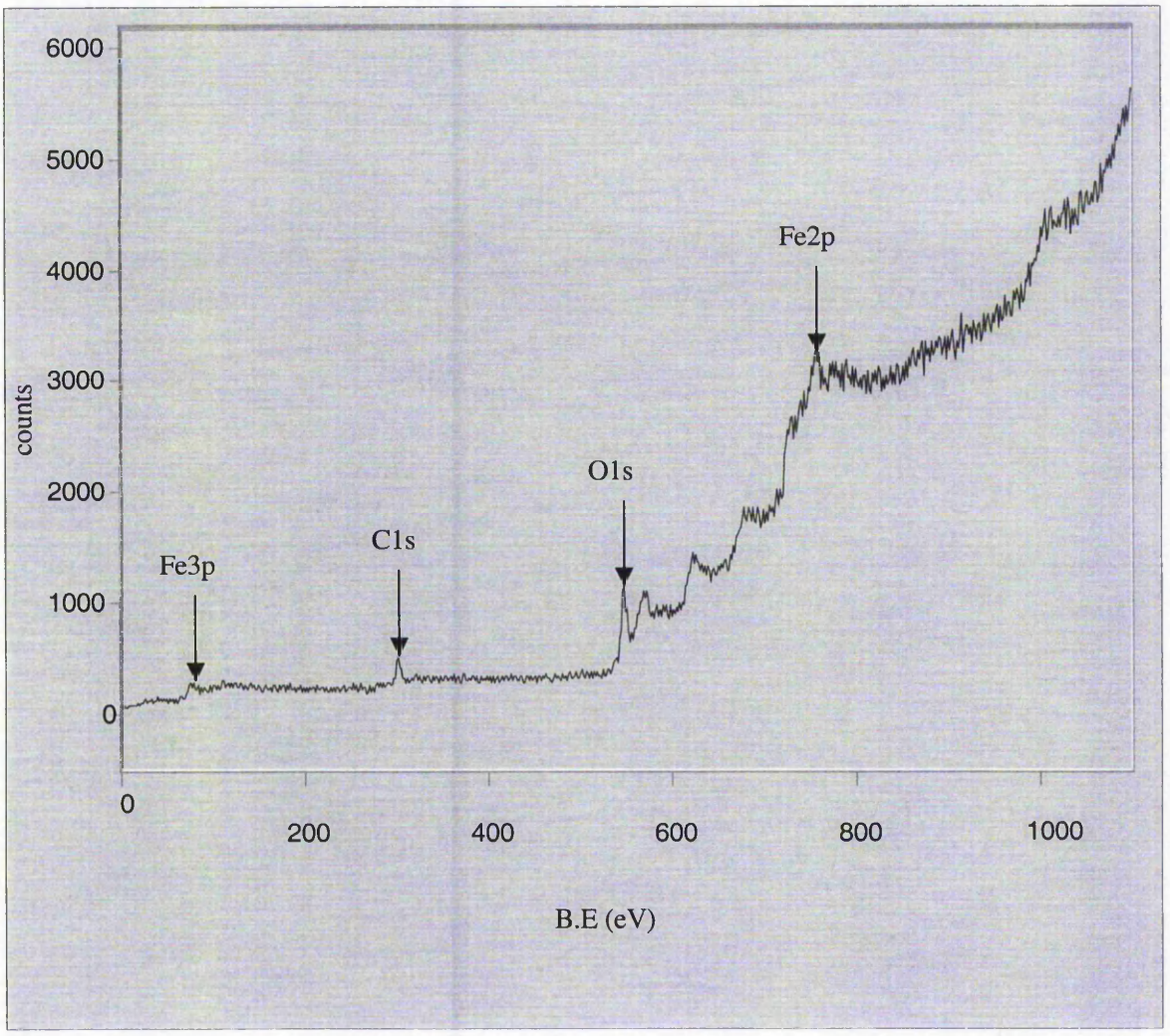

Figure 3.5.2.1 shows a spectrum taken of a 5_{at}% Au / Fe_2O_3 co-precipitated sample (base to acid). As can be seen most peaks are identified. The adventitious carbon peak at 300 eV being used as a reference (should be 285 eV). There is no gold detected on this material at either 85 eV (Au $4f_{7/2}$) or 335 eV (Au $4d_{5/2}$), even after 20 scans. Also absent is chlorine (2p) peak after 20 scans. This is surprising as others[37] have found the presence of gold as low as 1% wt for co-precipitated materials.

Figure *3.5.2.2* summarizes XPS investigations on Fe_2O_3 supported samples.

Figure 3.5.2.2: breakdown summary of Fe_2O_3 XPS data

Sample	Calcination temperature, °C	B.E., eV (FWHH)					atomic ratio		Content	wt%
		Fe $2p_{3/2}$	Au $4f_{7/2}$ *	Au $4d_{5/2}$ **	Cl 2p ***	Au $4d_{5/2}$ /Fe 2p	Cl 2p / Fe 2p	Cl/Au ****	Au	Cl
10%Au/ Fe_2O_3, impregnated	435	709.1 (4.79)	85.4 (2.58)	335.0 (4.09)	199.8 (3.45)	0.0191	0.113	5.92 ($4d_{5/2}$) 5.29 (4f)	3.69 ($4d_{5/2}$) 4.12 (4f)	3.92-3.94
	800	710.2 (4.82)	85.1 (1.83)	334.9 (3.57)	no	0.0339		-	6.03 ($4d_{5/2}$) 8.36 (4f)	-

	Calcination temperature, °C	B.E., eV (FWHH)				Atomic ratio		Content	wt%
		Fe $2p_{3/2}$	Au $4f_{7/2}$ *	Au $4d_{5/2}$ **	Cl 2p ***	Au $4d_{5/2}$ /Fe 2p	Cl 2p / Fe 2p	Cl/Au ****	Au
Control Impregnated	800	708.0 (4.78)	–	–	–	–	–	–	–
Control CP Finch	uncalcined	709.3 (4.46)	–	–	–	–	–	–	–
5_{at}%CP Finch	uncalcined	710.4 (7.14)	No detectable gold	No detectable gold	–	–	–	–	–
5_{at}%CP Finch	435	709.0 (4.303)	No detectable gold	No detectable gold	–	–	–	–	–

XPS data of Au/Fe_2O_3 catalysts (B.E. C 1s = 285.0 eV was used as reference).

3.5.3 XPS discussion

Impregnated samples again show no evidence of surface chlorine at the higher calcination temperature and detectable chlorine levels for samples calcined at the lower calcination temperature of 435°C. As opposed to the MgO sample classes there appears to be a protective effect of Fe_2O_3 on gold sintering at the higher calcination temperature as evidenced by a higher gold to iron ratio for samples calcined at the higher calcination temperature. However, it is possible that sub-surface gold could make its way to the surface more easily at 800°C rather than 435°C and this could more than offset any loss of a gold signal through enhanced sintering at 800°C. Comparing gold B.E reveals a typically metallic form (84.0 eV) for magnesium oxide and evidence of oxidized gold for iron oxide (>85.0 eV). This suggests greater interaction between iron oxide support and gold than for magnesium oxide materials and is corroborated by TPR of some iron oxide materials that show a clear effect of gold on the ease of reduction of co-precipitated iron oxide. Regarding the co-precipitated (base to acid) Finch[31] type materials, after repeated attempts no gold was detected unlike other investigations.[32] This is attributed to the fact that far less was used in co-precipitated sample manufacture as according to the published method by Finch in which gold to iron (not iron oxide) is used. Also, it has to be remembered that a relatively old and insensitive XPS was used in all these analyses, therefore reducing the detection response for low concentration of surface species. Hao et al,[37] characterising co-precipitated Au / Fe_2O_3 catalysts by XPS found that pre-treatment conditions affected the position of the Au 4f 7/2 peak thus providing information on the degree of oxidation of gold. It was found, predictably, that oxidative pre-treatment lead to the formation of partially oxidized gold and reductive pre-treatment lead to the formation of metallic gold. Most interestingly, however, high temperature oxidative pre-treatment *also* lead to the formation of metallic gold (as evidenced by a binding energy close to the expected 84.0 eV). The observation that this sample also gave low activity for CO oxidation (i.e., only active at much higher reaction temperatures than low temperature oxidized samples) suggests that investigators should be very careful in conducting pre-treatments at

temperature. It must said that this result is not supported in the present study in which high temperature calcined samples had the *same* binding energy for gold than low temperature calcined samples, although the gold ratio was less at the higher calcined temperature for reasons explained above. Further investigations of pre-treatment conditions on the state of gold were performed by Park et al,[33] who found that increasing the temperature of calcination from 100°C to 200°C and then to 300°C caused a shift in the Au 4f peak from 86.5 eV (highly oxidized gold: Au_2O_3) to 84.3 eV (metallic gold) at 300°C. At the intermediate temperature of 200°C there was evidence of co-existence of oxidized and metallic gold by the presence of 3 broad peaks around the binding energies of both Au_2O_3 and metallic gold. The samples were also investigated after the CO oxidation reaction and it was found that those samples that took part in dry runs (no moisture) were reduced (i.e., gold binding energies of 84 eV) and samples used in wet runs (moisture present) retained 40% oxidized gold. Thus it appears from the XPS evidence that moisture can protect against reduction from CO. Similarly, Kozlova et al,[34] found that calcination of Au / Fe_2O_3 caused the formation of metallic gold from oxidized gold as evidenced by a fall in the binding energy of gold from 84.9 to 84.1 eV. Also they found that higher calcination temperatures (400°C) decreased the gold to iron ratio as seen in this research. Others [35,36] have found the same reductive effect of calcination, this time using titania as a support. Also, low gold (<1%) loadings[35] gave no XPS signal whereas higher gold loadings produced detectable gold peaks. This indicates an association between low gold loading and low frequency of gold particles, resulting in reduced or absent gold peaks in XPS. Overall, XPS observations reveal two repeatable aspects of supported gold research; the reductive effect of calcination / high temperature oxidative and reductive pre-treatment and the loss of detectable gold at higher calcination temperature due to sintering. The latter of these observations has been seen in the author's research.

3.5.4 Characterisation: summary and conclusions

Extensive characterisation studies have been performed on both iron oxide and magnesia supported gold samples prepared by impregnation and co-precipitation. These provide important insight into the catalytic and isotopic exchange profiles that will be displayed later on, and for the most part are congruous with previous characterisation studies on gold catalysts.

Surface area measurements performed on these samples are necessary so that normalized rate constant values can be obtained, but these observations have also revealed interesting support, preparation and gold loading influences on surface area. Most notable is the collapse in surface area with gold loading for MgO samples, especially those calcined at the lower temperature of 435°C that show a precipitous fall with initial gold loading. Others have postulated[2] gold substitution to account for sintering effects and therefore loss of surface area. This however does not appear to occur for iron oxide samples in which there is no influence of gold on surface area. The observation that this effect is most apparent for magnesia low temperature calcined samples suggests that it is camouflaged by sintering influences for samples calcined at the higher temperature of 800°C. Support influences also manifest in the impact of preparation on surface area with co-precipitated samples revealing superior surface areas than impregnated materials for iron oxide but not for magnesia support in which no real differences were found. For both support types there was a general fall in surface area with higher temperature of calcination, as expected. Analysis of full isotherms demonstrates the general type 2 BET isotherm but with sharp points of inflexion for many samples which suggests a degree of microporosity. The presence of hysteresis for some samples, especially iron oxide as support, suggest the presence of mesoporosity as well.

TPR analyses were done to ascertain the effect of gold on the ease of reduction of iron oxide samples. Examination of hydrogen uptake by integration of TPR peaks revealed evidence to support the hypothesis of initial reduction of Fe_2O_3 to Fe_3O_4 and subsequent total reduction of Fe_3O_4 to Fe.

It was found that ease of reduction was significantly increased for co-precipitated samples with calcined samples showing an even greater fall in Tmax of reduction. Others[9,10] have postulated the gold facilitated production of hydroxyl groups in order to account for the ease of reduction observed with gold loading. However, the observation of a fall in Tmax upon calcination does not lend support to this argument as most hydroxyl groups will be removed at the temperature of calcination, 435°C. Therefore other modes of reduction are required, in particular it has been hypothesized that gold itself can reduce iron oxide support via oxidized (III) gold.[10] For impregnated materials there is no effect of gold on either reduction step and suggests impregnation is not a useful technique for creating strong support / gold interactions.

Examination of the integration data reveals no reliable impact of gold on either the first reduction step or the ratio of the first and second reduction peaks (and therefore no differential effect of gold on either reduction step). There is a moderate (although not very convincing) upward trend in second integration values with gold loading.

Observation of SEM images reveals very clear gold particles for magnesia based samples but less so for iron oxide samples, with no gold particles detected for co-precipitated (base to acid) iron oxide. Although these latter materials were good catalysts (chapter 7) in relation to their controls, SEM completely failed to detect any gold particles on the surface. This suggests the particles are nanometer in size, a finding further corroborated by XRD evidence that failed to detect any gold on them either. These catalytically active catalysts therefore support gold particles that are less than 3nm in diameter.

SEM examination of magnesia samples revealed very large gold particles of the order 100 – 200 nm in diameter. Preparation technique had little impact on gold particle size with impregnation and co-precipitation producing similar sized particles. Not surprisingly, increasing the temperature of calcination lead to larger gold particle diameters. Gold particles on iron oxide support were similarly sized at around 250 nm for impregnated samples. XRD evidence corroborates these particle size similarities but nearly an order of a magnitude smaller.

The reason for this could be due to the sampling error associated with SEM in which larger particles are more likely to be observed and recorded. This systematically overestimates particle sizes in SEM. One consistent finding was the strong relation between particle frequency and gold loading; the higher the loading the more particles were observed. However, there wasn't a noticeable increase in gold particle diameter with gold loading. XRD revealed consistent increases in crystallite size for magnesia with increasing gold loading but no increase in iron oxide crystallite size. These observations correspond very closely to sample surface areas for both supports and is, of course, expected as crystallite size determines surface area. Further corroboration between XRD and BET surface areas comes from analysis of the impact of preparation, with co-precipitation producing smaller support crystallites than impregnation, especially for iron oxide support. Remember that this support gave much higher BET surface areas for co-precipitated materials (base to acid) than impregnation. For magnesia, preparation also influenced the degree of crystallinity, with low temperature calcined co-precipitated materials revealing a high degree of amorphous nature as indicated by very small, undefined support reflections. All other samples gave well-defined sharp reflections indicative of highly crystalline materials. For XPS characterisation, this revealed important clues to explain the isotopic exchange profiles for magnesia supported gold samples. Here it was found that significant chlorine levels were present on the surface of low temperature calcined impregnated samples but at higher calcination temperatures this was removed. The impact of calcination was explored with higher temperatures giving smaller gold integration. A possible candidate for this could be sintering in which XPS is less sensitive to fewer larger gold particles than many smaller gold particles. Surprisingly, no gold was detected on the co-precipitated iron oxide samples despite repeated attempts, but confirms XRD and SEM evidence on the difficulty of detecting nanometer sized gold particles, that in this case are highly active for CO oxidation.

3.5.5 References for chapter 3

1: Gregg.S.S, Sing.K.W.S, Adsorption Surface Area and Porosity. Academic Press, 2nd Edition, (1982).

2: Blick.K, Mitrelias.T.D, Hargreaves.J.S.J, Hutchings.G.J, Joyner. R.W, Kiely. C.J, Wagner.F.E, Catalysis Letters, **50**, 211-218, (1998)

3. Shastri.A.G, Datye.A.K, Schwank.J
Journal of Catalysis, **87**, 265-275, (1984)

4. Baiker.A, Maciejewski.M, Tagliaferri.S, Hug.P
Journal of Catalysis, **185**, 407-419, (1995)

5. Wagner.F.E, Galvagno.S, Milone.C, Visco.A.M, Stievano.L, Calogero.S
J. Chem. Soc., Faraday Trans, **93**(18), 3403-3409, (1997)

6: Brown.R, Cooper.M.E, Whan.D.A,
Appl. Catal, **3**: 177, (1982)

7: Gentry.S.J, Hurst.N.W, Jones.A,
J.Chem.Soc, Faraday Trans, **77**, 603, (1981)

8: Jones. A, McNicol.B.D
Temperature Programmed Reduction for Solid Materials Characterisation
Chemical Industries, / **24** (Marcel Dekker, Inc. Publ)

9: Neri.G, Visco.A.M, Galvagno.S, Donato.A, Panzalorto.M,
Thermochimica Acta, **329**, 39-46, (1999)

10: Ilieva.A, Andreeva.D.H, Andreev.A.A,
Thermochimica Acta, **292**, 169-174, (1997)

11. Andreeva.D, Idakiev.V, Tabakova.T, Ilieva.L, Falaras.P, Bourlinos.A, Travlos.A
Catalysis Today, **72**, 51-57, (2002)

12. Hao. Z, An. L, Wang. H
Science in China, Series B. Vol. **44** No.6, (2001)

13: Hargreaves J.S.J, Joyner.R.W, Mellor.I.M
Journal of Molecular Catalysis A: Chemical, **141**, 171-176, (1999)

14: Blick. K, Mitrelias.T.D, Hargreaves.J.S.J, Hutchings.G.J, Joyner. R.W, Kiely.C.J, Wagner.F.E.
Catalysis letters, **50**, 211-218, (1998)

15: Haruta.M, Uphade.B.S, Tsubota.S, Miyamoto.A,
Res.Chem. Intermed, **24**, 329, (1998)

16: Horváth.D, Toth.L, Guczi.L,
Catalysis Letters, **67**, 117-128, (2000)

17: Haruta.M Tsubota.S, Kobayashi.T, Kageyama.H, Genet.M, Delmon.B
Journal of Catalysis **144**, 175-192, (1993)

18: Kozlova.A.P, Sugiyama.S, Kozlov.A.I, Asakura.K, Iwasawa.Y
Journal of Catalysis, **176**, 426-438, (1998)

19. Hodge.N.A, Kiely.C.J, Whyman.R, Siddiqui.M.R.H, Hutchings.G.J, Pankhurst.Q.A, Wagner.F.E, Rajaram.R.R, Golunski.S.E
Catalysis Today, **72**, 133-144, (2002)

20. Horvath. D, Toth.L, Guczi.L
Catalysis Letters, **67**, 117-128, (2002)

21. Grunwaldt.J.D, Kiener.C, Wögerbauer.C, Baiker.A
Journal of Catalysis, **181**, 223-232, (1999)

22. Boccuzzi.F, Chiorino.A, Manzoli.M, Lu.P, Akita.T, Ichikawa.S, Haruta.M
Journal of Catalysis, **202**, 256-267, (2001)

23: Blick.K, Mitrelias.T.D, Hargreaves.J.S.J, Hutchings.G.J, Joyner. R.W, Kiely. C.J, Wagner.F.E, Catalysis Letters, **50**, 211-218, (1998)

24: Finch.R.M, Hodge.N.A, Hutchings.G.J, Meagher.A, Pankhurst.Q.A, Siddiqui.M.R.H, Wagner.F.E, Whyman.R, PCCP, **1**, 485-489, (1999)

25: Neri. G, Visco. A.M, Galvagno.S, Donato.A, Panzalorto.M
Thermochimica Acta, **329**, 39-46, (1999)

26: Horvath.D, Toth.L, Guczi.L
Catalysis Letters, **67**, 117-128, (2000)

27. Kozlova.A.P, Kozlov.A.I, Sugiyama.S, Matsui.Y, Asakura.K, Iwasawa.Y
Journal of Catalysis, **181**, 37-48, (1999)

28. Gupta.N.M, Tripathi.A.K
Journal of Catalysis, **187**, 343-347, (1999)

29. Knell.A, Barnickel.P, Baiker.A, Wokaun.A
Journal of Catalysis, **137**, 306-321, (1992)

30: Cunningham. D.A.H, Vogel.W, Haruta,M.
Catalysis Letters, **63**, 43-47, (1999)

31: Finch.R.M, Hodge.N.A, Hutchings.G.J, Meagher.A, Pankhurst.Q.A,
Siddiqui.M.R.H, Wagner.F.E, Whyman.R, PCCP, **1**, 485-489, (1999)

32: Visco.A.M, Neri.G, Donato.A, Milone.C, Galvagno.S,
PCCP, **1**, 2869-2873, (1999)

33. Park.E.D, Jae.S.L
Journal of Catalysis, **186**, 1-11, (1999)

34. Kozlova.A.P, Kozlov.A.I, Sugiyama.S, Matsui.Y, Asakura.K, Iwasawa.Y
Journal of Catalysis, **181**, 37-48, (1999)

35. Stangland.E.E, Stavens.K.B, Andres.R.P, Delgass.W.N
Journal of Catalysis, **191**, 332-347, (2000)

36. Su.Y-S, Mei.Y.L, Lin.S.D
Catalysis Letters, **57**, 49-53, (1999)

37. Hao.Z, An.L, Wang.H, Hu.T,
React.Kinet.Catal.Lett Vol, **70**, No.1, 153-160, (2000)

Chapter four

Nothing is too wonderful to be true if it be consistent with the laws of nature.

Michael Faraday

Chapter 4: Isotopic Oxygen Exchange over Magnesia Supported Gold

4.0 Introduction

As discussed in the introduction, there have been quite extensive studies of isotopic oxygen exchange over magnesium oxide[1,2,3] in an attempt to understand the exchange process and the reactivity of surface oxygen species, the effect of the co-ordination environment on exchange, and the influence of experimental and preparation variables. So far these studies have furnished important information regarding many aspects of exchange, so that there is now evidence to show that, for instance, exchange over MgO is structure insensitive[4] and that co-ordination environment appears to have no impact on exchange kinetics. Studies have also shown a dependence on exchange related to the investigated metal oxide bond strength that also correlates well with CO oxidation ability.[5] These studies are important as some of them provide evidence for the Mars Van Krevelen mechanism for CO oxidation (section 1.27.1) in which oxygen activation is thought to be rate determining. In this study, exchange was carried out over Au / MgO catalyst***s*** in an attempt to follow the influence of preparation and gold loading. This was done because MgO is a well-studied material in exchange studies[6,7] and previous tests in the same lab had given reproducible rates of exchange results.[4] Essentially MgO is a simple oxide in which it should be relatively straightforward to observe any an effect of gold loading or other variables on exchange. Should the data reveal correlations between exchange and gold loading / preparation variables, this may help in understanding the mechanism of CO oxidation, as some supported gold catalysts are highly effective CO oxidizers.

This can be understood by examining figures 1 and 2.

Figure 4.1: Exchange on naked support

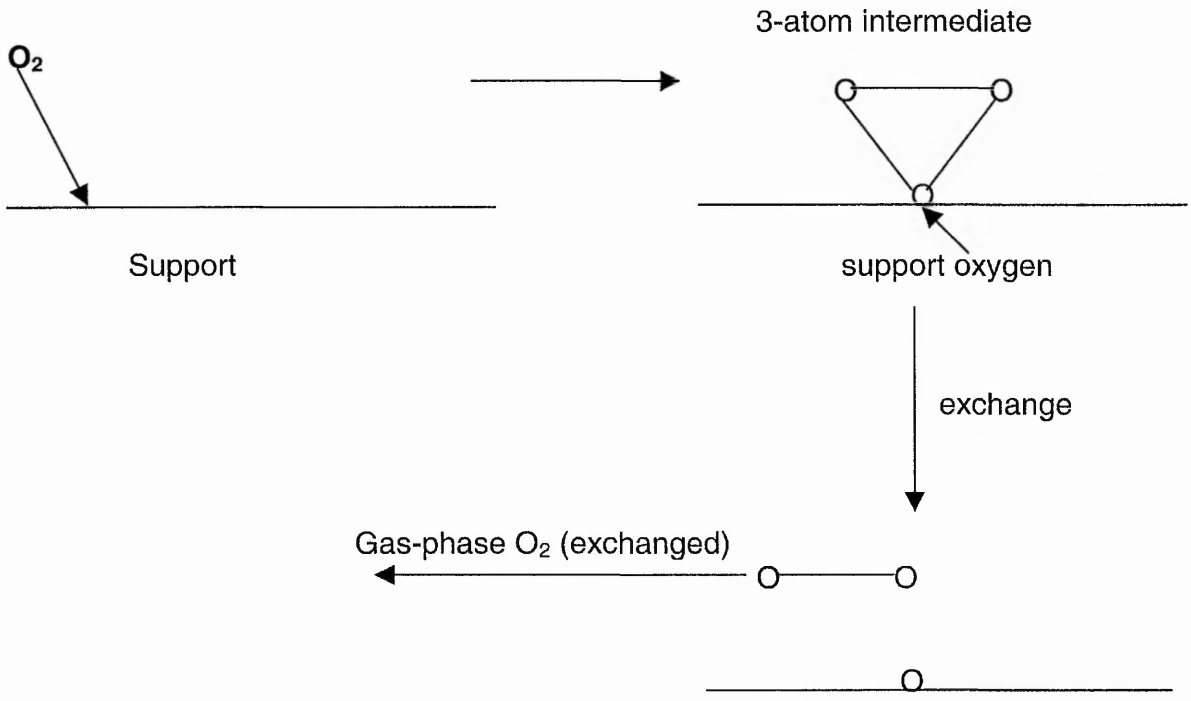

Figure 4.1 shows the exchange process on a support alone. As mentioned earlier (section 1.3) both R1 and R2 processes can occur (and have done in this research) but only R1 exchange is shown for clarity.

Gas phase oxygen adsorbs molecularly on the support surface and participates in a 3-atom intermediate stage with a support oxygen. During this stage exchange with the support oxygen occurs followed by desorption of exchanged O_2 (one gas phase oxygen, one support oxygen). The support now contains an oxygen atom from the gas phase.

Figure 4.2: Exchange on supported gold

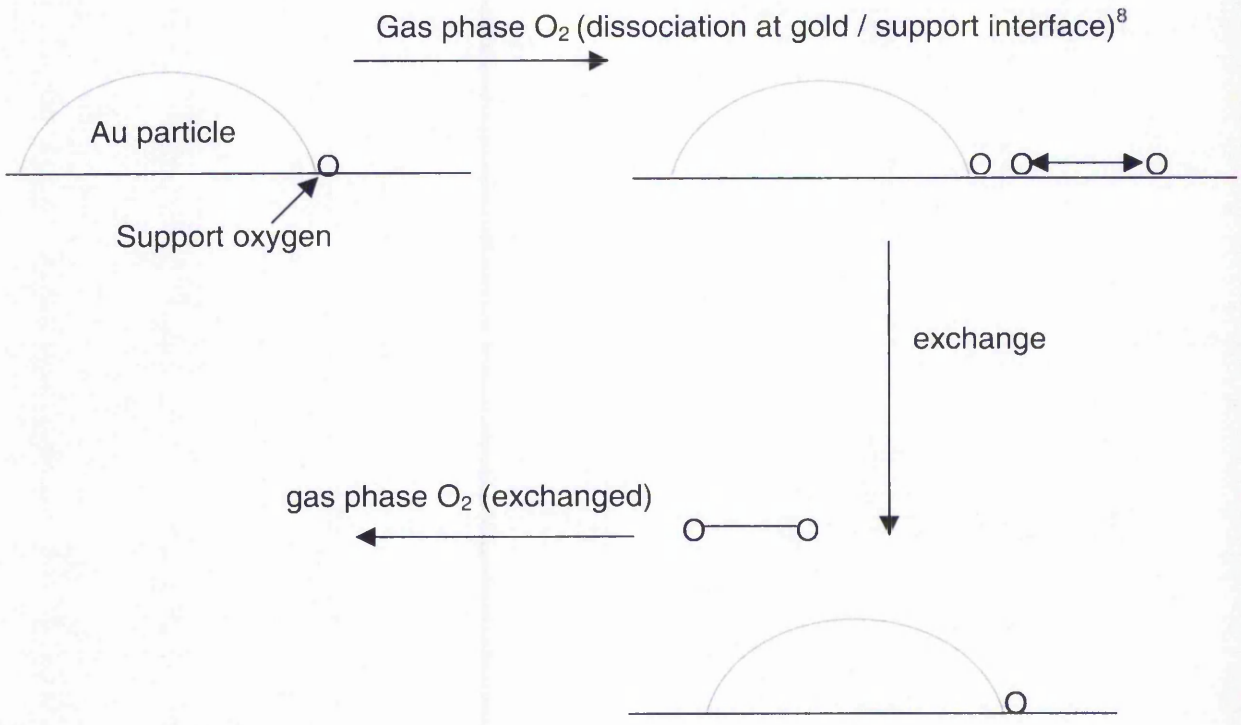

Figure 4.2 shows R1 exchange occurring on a supported gold surface. In this mechanism it is thought (by some investigators[8]) that oxygen dissociatively adsorbs at the gold / support interface. In exchange studies this means that an adsorbed oxygen atom can exchange with one in the lattice. The product of exchange (one gas phase oxygen, one support oxygen) then desorbs, leaving a substituted oxygen in the support. It can now be seen why exchange is so important in understanding CO oxidation as exchange and one of the principal mechanisms for CO oxidation both require dissociation of oxygen.

4.3 Kinetics underlying exchange:

Exchange of oxygen with the support involves adsorption of oxygen on the surface and exchange with lattice oxygen of the material. The fall in gas phase oxygen is dependent on the fraction of lattice sites that have *yet* to exchange at a given time, as given by the following expression:

Equation 4.1: $-dp / dt = k P_{O2} (1-\theta_t)$

Where: $-dp / dt$ is the fall in pressure of oxygen with time.

k = rate constant for exchange

P_{O2} = pressure of oxygen

$1-\theta_t$ = fraction of sites yet to undergo exchange at time t.

The pressure of gas phase oxygen (P_{O2}) is first order in equation 4.1, however, because oxygen is dosed far in excess of the number of exchangeable sites, the above equation is actually pseudo-zero order with respect to gas phase oxygen. This is done to isolate the first order influence of exchangeable sites on the rate of exchange.

4.4 Results

Treatment of data and kinetics of oxygen exchange

The partial pressure data points from a reactor run are converted into mole fractions according to equation 4.2. This is done so that fluctuations in the sensitivity of the mass spectrometer are corrected, and also to ensure that the data is insensitive to the fall in pressure that occurs as a result of leakage into the mass spectrometer.

Equation 4.2: mole fraction (X) = P_x / (P_{32} + P_{34} + P_{36})

Where X = oxygen isotope that is analysed.

P = partial pressure of the oxygen isotope that is analysed

Figure 3 displays mole fraction results from a typical experiment given by equation 4.2.

Figure 4.3: a typical mole fraction data plot for an exchange run

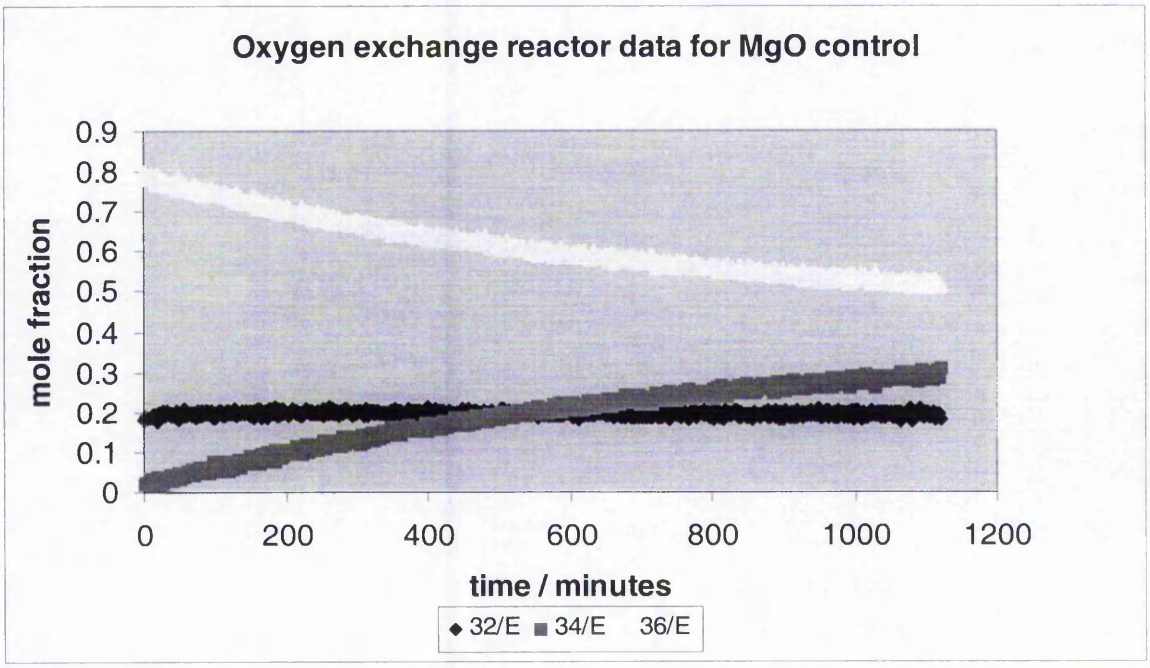

Figure 4.3 shows a typical exchange profile in which $^{36}O_2$ is allowed to exchange with the surface of undoped magnesium oxide at 435°C. As exchange proceeds there is a gradual disappearance of oxygen 36 and a corresponding increase in oxygen 34, indicating that only one oxygen atom per molecule has exchanged. This finding supports earlier research by Winter[6] and has been continually observed in this research to date. The blue line represents oxygen 32 that is steady as background, although R2 exchange in which both oxygens exchange with the lattice has also been observed. This results in an increase in signal 32.

It has been shown by Hargreaves[4] et al, that the exchange of molecular oxygen with magnesium oxide is pseudo-zero order in excess oxygen pressure (as used in these experiments), and first order in the number of exchangeable surface sites.

It follows from equation 4.1 that extent of exchange at time t, follows equation 4.3.
Equation 4.3: $\theta_t = P_i - P_t / P_i - P_f$ and equation 4.4: $1-\theta_t = P_t - P_f / P_i - P_f$

Where: θ_t = fraction of surface that has exchanged at time t

$1-\theta_t$ = fraction of surface yet to exchange at time t

P_i is the initial pressure of $^{18}O_2$

P_t is the drop in $^{18}O_2$ until time t

P_f is the final pressure of $^{18}O_2$

We can now define a new expression in terms of pressure changes:

Equation 4.5: $\mathbf{-dP/dt = k (P_t - P_f) / (P_i - P_f).}$

Integration of the above expression gives equation 4.6.

Equation 4.6: $\mathbf{k't = (P_i - P_f) \ln (P_i - P_f)/(P_t - P_f)}$.

Plotting $(P_i - P_f) \ln (P_i - P_f) / (P_t - P_f)$ against time for the above mole fraction data should give a straight line as shown in figure 4.4. Thus the model is obeyed.

Figure 4.4: A typical first order exchange plot

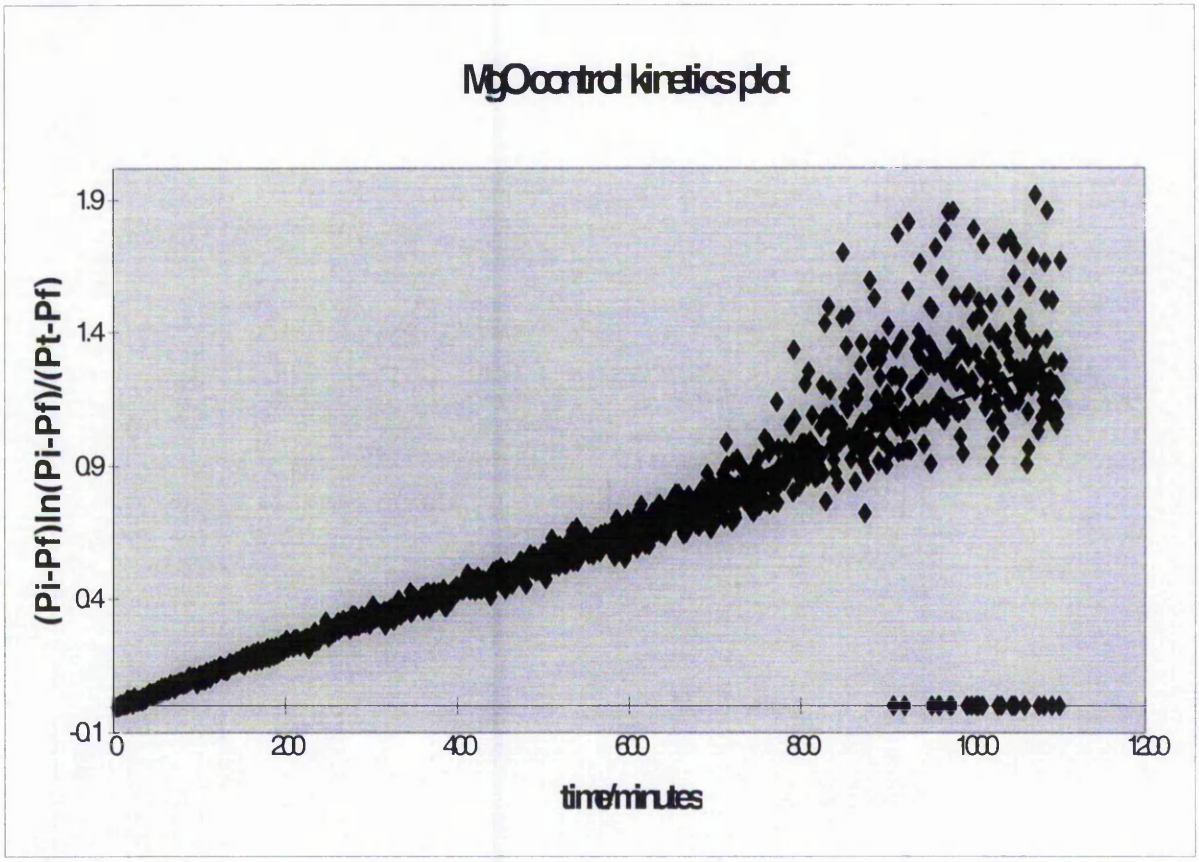

The slope of the first order plot allows the calculation of the rate constant for exchange on that sample. This value is then normalised with respect to the surface area in the exchange reactor (i.e., the product of the sample mass and sample surface area). This is important, as different samples have widely divergent surface areas, (section 3.1). It is important to note that exchange over magnesia based samples in this study occur with less than one monolayer participation. This is significant as it shows the temperature of exchange is not too high and means only surface processes are involved in exchange, enabling a comparison with oxidation data.

Note also, that because in exchange experiments complete exchange never occurs, (i.e.,occurs at $t = \infty$), P_f is treated as a disposable parameter and can be altered to achieve a better R^2 value for the above kinetic plot. A strong relationship, as in figure 4.4, implies that the data fits equation 4.3 well and confirms that exchange follows first order kinetics. In practice, it was found that lowering P_f by a small amount, around 0.04 – 0.05 mole fraction for signal 36, resulted in a drastic improvement in the R^2 values, typically to the 0.95 to 0.99 range. Consequently, a decision was made to standardise this approach by lowering P_f by 0.05 mole fraction (36 signal) for *all* samples plots. All exchange data to be presented has been modified in this way.

4.5 Relative activity

To facilitate comparison between different samples, all rate constants have been normalised to unit surface area (referred to as the specific rate constant), and compared to that for undoped magnesia, calcined at 800°C, which has arbitrarily been set to unity. Comparison of exchange with this sample gives the *relative activity*, as shown in figure 4.5.

Figure 4.5: Influence of gold loading on exchange performance for MgO class

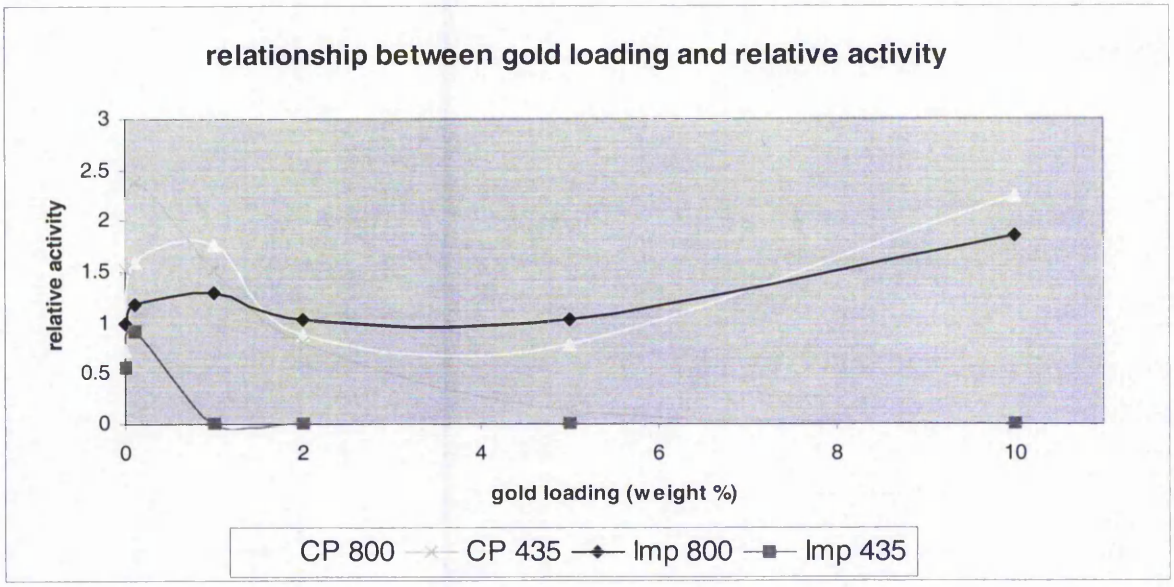

For a good proportion of these samples repetitions were performed in order to ascertain reproducibility. While findings varied, overall, reasonably good replication was achieved. For example, specific rate constants for 10% loaded sample calcined at 800°C lie between 2.87 E-4 ± 0.22 E-4 s^{-1}/m^2 and 0.1% loaded sample at 1.84 E-4 ± 0.17 E-4 s^{-1}/m^2 These are typical uncertainty values associated with exchange, around ± 10%.
Figure 4.5 reveals the strong influence of both preparation methods and gold loading on the exchange performance of the magnesia supported materials. What is most noticeable is the interplay between temperature of calcination and gold loading. Samples calcined at high temperature (800°C) demonstrate a recovery in exchange at high gold loadings whilst low temperature calcined (435°C) materials lose all exchange ability at intermediate gold loadings. XPS investigations mentioned earlier (section 3.5) suggest that chlorine (which is removed at high temperature but not at low temperatures) might be responsible for this behaviour. It is well known[9] that chlorine is an effective catalyst poison and evidence exists that it inhibits exchange also.[10] Also apparent is the general sharp increase in exchange performance with minimal gold loading (0.1%). This suggests that there is something special about very low gold loaded samples, for example smaller gold particle diameters,[11] that is lost upon subsequent loading. The increase in exchange ability for co-precipitated materials with calcination temperature cannot be explained by reference to their morphology. As SEM revealed (section 3.3.3 - 3.3.6) there is an increase in gold particle size diameter upon calcination at a higher temperature by about 2-4 times with regard to both the
2% and 10% loaded samples. Despite these unfavourable changes, exchange ability is enhanced from no activity to relatively high activity for 10% loaded samples, also there appears to be a negligible effect of calcination temperature on 2% loaded samples. High temperature calcined impregnated materials also show significant exchange activity despite relatively large gold particles (100 – 200 nm). These results suggest exchange is not influenced by gold particle size.

An exchange process that is not occurring at the support / particle interface appears more likely. Combining both the XPS evidence and SEM images with the exchange data tentatively suggest that exchange occurs independent of gold morphology and is influenced more by surface chlorine concentration. However the recovery of exchange with high gold loading (for high temperature calcined materials) suggests that once the chlorine is removed, the positive effect of gold manifests itself. There is also a clear effect of preparation method on exchange, with impregnated materials having lower rates of exchange than co-precipitated materials for low to intermediate gold loadings. A general trend in exchange activity can be identified: CP435 > CP800 > Imp800 > Imp435. It is therefore apparent that low temperature calcined co-precipitated materials are the most active for exchange with low temperature calcined impregnated materials the least active. It is interesting that preparation heavily influences exchange in the same way it does CO oxidation activity.[12,13] This will be discussed in chapters 5 and 7. To examine the influence of gold loading on exchange performance in more detail it is of interest to probe the variations that occur using extent of exchange measurements, in comparison to relative activity calculations that are based on rates.

4.6 Extent of exchange

In this section the percentage monolayer that has undergone exchange is calculated from the reactor results, that gives the number of gas molecules that have exchanged, together with a calculation (from the material reactor surface area) of the number of oxygen atoms in the surface monolayer that are available to exchange. Dividing the first by the second gives the proportion of monolayer that has exchanged. It is important to distinguish this approach from the kinetic approach, which attempts to calculate rate of exchange. In terms of reproducibility, calculation of relative activity has a clear advantage over extent of exchange, with a 10% margin of error versus a 20% margin of error, (as calculated by repeating the reactor run at least twice and measuring the degree of variation from the average value.) This is understandable as far more data goes into a relative activity calculation and extent of exchange calculations depend much more on the initial output of the mass spectrometer, which can have variable sensitivity. These differences should be remembered when analysing the two kinds of results.

Figure 4.6: extent of exchange calculations for MgO class.

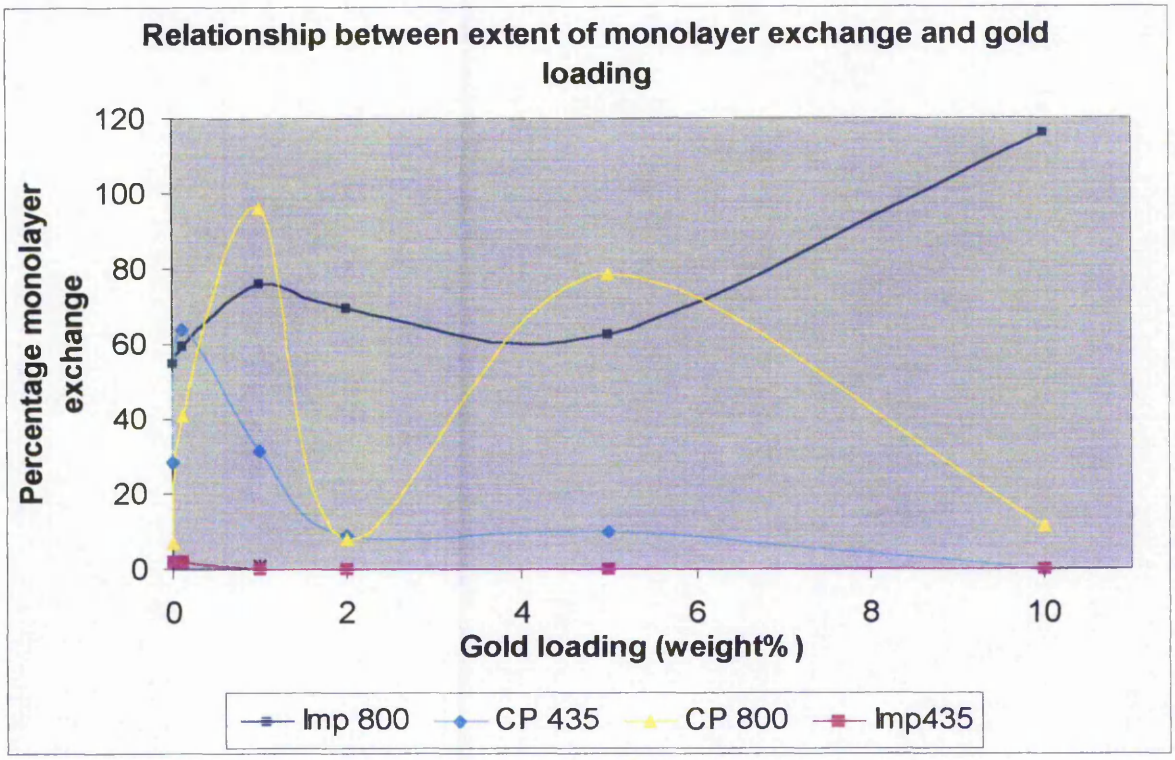

Figure 4.6 shows the influence of gold loading on extent of exchange for magnesia supported materials. In general the same trends observed with the rate data (figure 4.4) are repeated here with the exception of the co-precipitated 800 class which has an undulating profile. There appears to be marked decline of extent of exchange with gold loading save for the impregnated 800 class. Why these data appear to (in the main) reproduce the earlier rate calculations is unknown as they should be independent. It is possible that chlorine occupation of exchange sites could reduce extent of monolayer exchange. This would explain the above profiles in the same way as it explains the relative activity profiles with regard to the influence of calcination temperature. The impact of preparation appears more intense on the extent of exchange profiles than for relative activity (rates) calculations. This is especially evident when considering the low temperature impregnated data that show very little activity even at low gold loadings where rate calculations gave appreciable activity.

It is apparent that many samples have very significant degrees of exchange, approaching 100% monolayer exchange in some cases (and exceeding 100% for one sample). Others[14,15] have only observed of the order 10-30% monolayer exchange for undoped magnesia, which suggests gold might have a promotional effect on the degree of lattice exchange. This finding is undermined, however, by up to 60% monolayer exchange for some control (undoped) magnesia samples in this study.

4.7 The influence of preparation on R1 and R2 exchange

One interesting observation is the influence of preparation on the appearance of R2 exchange. Impregnation (with the exception of a few low temperature calcined samples) appears to give only R1 exchange, that is where only one oxygen of a gas phase oxygen molecule undergoes exchange with the oxide. However co-precipitation gives both R1 and R2 exchange in which both oxygens undergo exchange with the surface of the oxide, as figure 4.7 demonstrates.

Figure 4.7: The occurrence of both R1 and R2 exchange for co-precipitated material

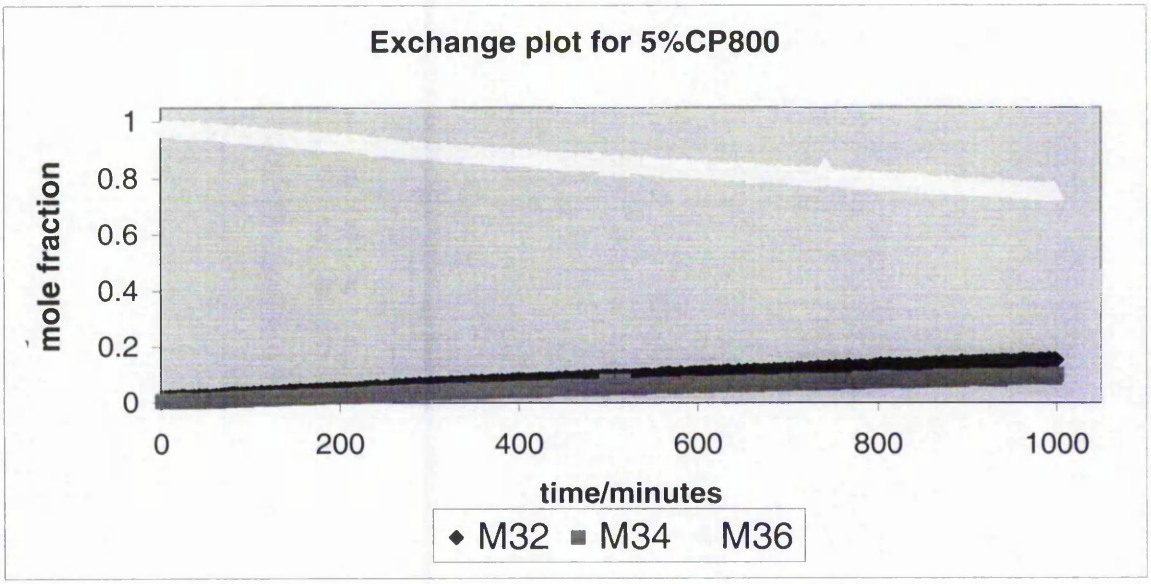

4.8 The relationship between surface area and exchange

Although exchange rate constants are normalised to surface area, it is of interest to examine whether any additional relationships between exchange and surface area extend beyond normalisation. In particular, it is known that high surface area materials are effective at stabilising small gold particles and reducing sintering during calcination. If such an effect of surface area exists on exchange, it should manifest itself in figure 4.8.

Figure 4.8: the relationship between surface area and relative activity.

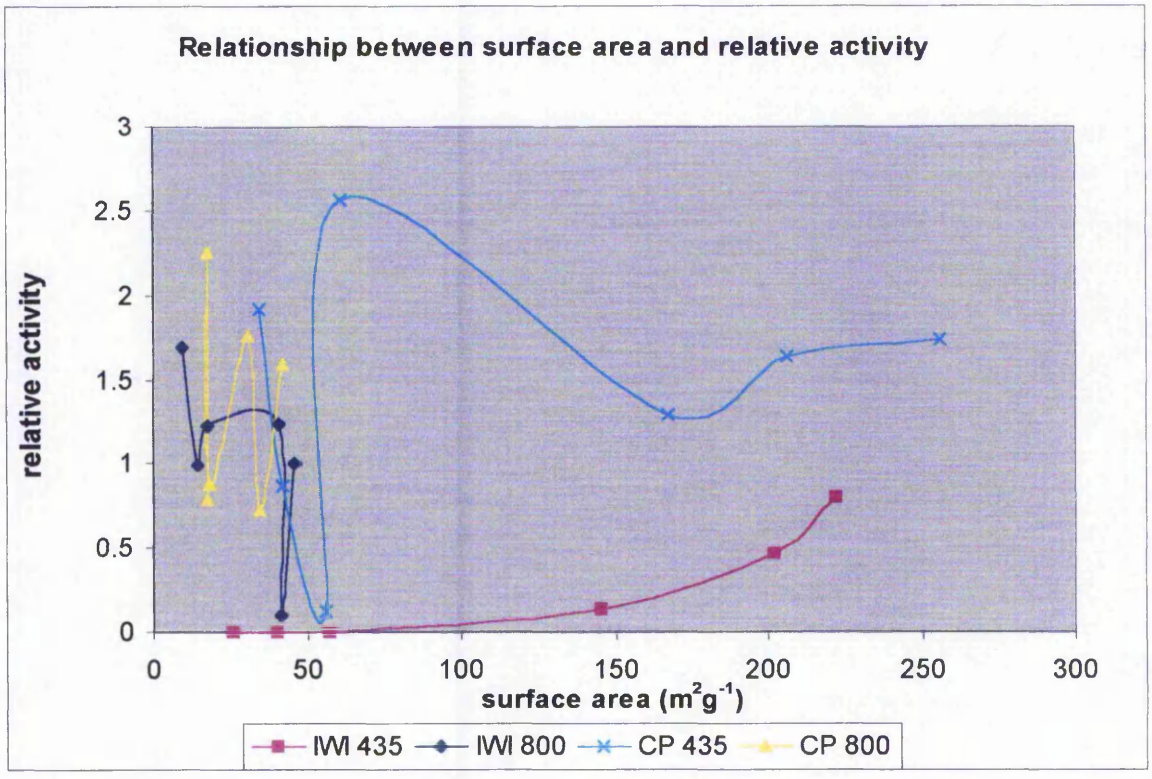

As can be appreciated, there is no relationship between exchange (relative activity) and material surface area, save for a suggestive positive relationship for low temperature calcined impregnated materials. Overall this suggests that once exchange data are normalized to surface area there is no additional influence from increasing surface area.

4.9 The effect of increasing sample mass on exchange

Figure 4.9: The influence of low sample weight: 0.0604 g

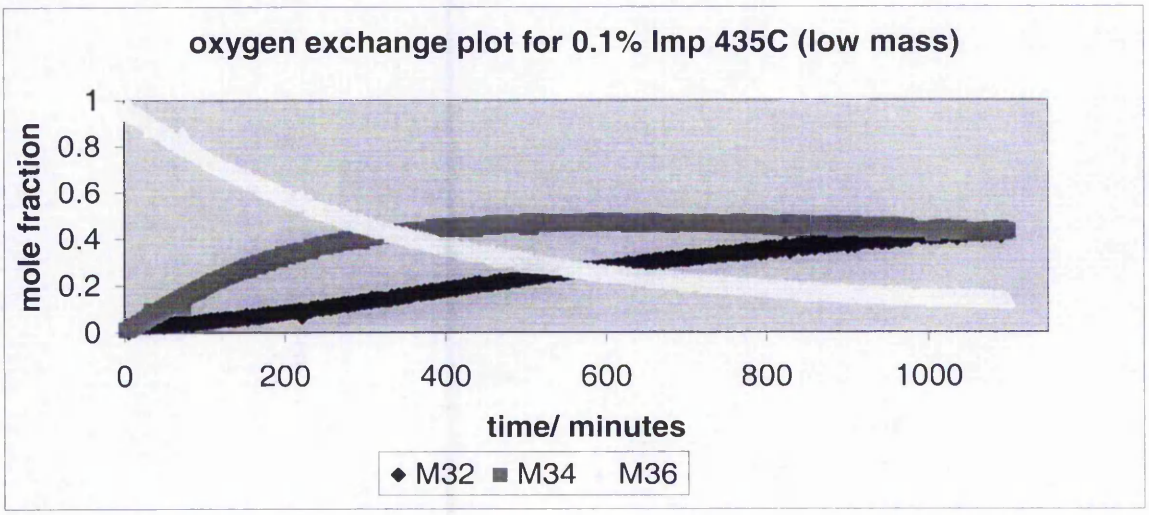

Figure 4.10: The influence of high sample weight: 0.1509 g

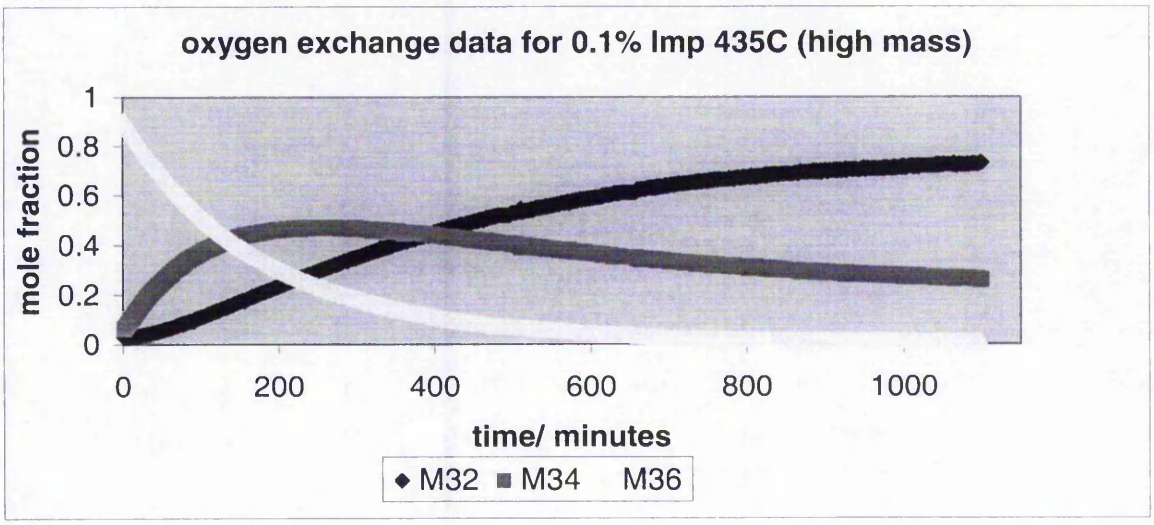

Because during most MgO exchange runs there are more gas phase oxygen molecules than exchangeable sites on the oxide surface, it is of interest to compare the effects of increasing the number of exchangeable sites considerably. This is illustrated in figures 4.9 and 4.10 in which low temperature calcined impregnated material with a low gold loading of 0.1% is used.

In figure 4.9, 0.0604 g is used and a much higher amount; 0.1509 g for figure 4.10. As can be seen, increasing the amount of material causes a rapid reduction in the 36 oxygen signal. After 200 minutes there is still a considerable 36 signal for the low mass sample but 80% of this has gone for the high mass sample at the same time. Also, because there are so many exchangeable sites with high mass, the product of R1 exchange, (signal 34) starts to exchange again via another R1 mechanism giving oxygen 32. This doesn't happen with the low mass sample that gives a typical exchange profile.

4.10 Discussion and conclusions

Examination of exchange data both from the perspective of rate calculations and extent of monolayer exchange reveal patterns highly dependent on preparation technique and gold loading. Explanations based on gold morphology cannot explain these variations as SEM images reveal larger gold particles that are associated, in this research, with high exchange activity. This finding is contrary to findings elsewhere[16] and is indeed hard to reconcile with any model that involves the support / particle interface or particle surface for exchange, as larger particles provide less surface atoms (overall) and less perimeter species (overall). As touched on earlier, XPS (section 3.5) characterization suggests the presence of chlorine in low temperature calcined materials that is removed at higher calcination temperature. This evidence in conjunction with SEM characterisations (section 3.3) when applied to the exchange profiles suggests an effect of gold that cannot be explained by resorting to simple morphological arguments. Instead other explanations are needed. There are two that appear most plausible: an effect of gold on the support itself and much smaller gold particles that are not detected by the resolving power of the SEM. The first suggestion would encompass exchange on the support alone but facilitated by the presence of gold by a mechanism not presently understood but could involve an increase in the number of support vacancies through gold substitution in the bulk, as others have hypothesized,[14] and which is supported by surface area measurements (section 3.1) that reveal consistent decreases in value as gold loading

increases. (Bulk substituted gold induced vacancies encourage support particle sintering and therefore loss of surface area). The second hypothesis envisions exchange catalysed by the presence of gold particles, the preponderance of which are nanometer in size[17,18] and not really resolvable by SEM. The negative effect of chlorine can be witnessed in both scenarios as exchange on support occurs in both and chlorine[10] is thought to occupy these sites and therefore inhibit exchange.
In conclusion it can be stated that exchange over magnesia supported gold is heavily influenced by preparation conditions and gold loading. XPS characterisation goes some way to explaining these variations based on chlorine content but explanations that appeal to gold particle differences are not really supported by SEM images.
In was also found that co-precipitated materials gave R2 exchange that supplemented R1 exchange whilst impregnated materials gave (for the most part) R1 exchange only. Why this is so it not understood but suggests that co-precipitation provides a different environment for exchange than impregnation, possibly by increasing the number of hydroxyl sites that might be involved in exchange.[4] Parallel hydroxyl sites could provide an opportunity for R2 exchange to occur. Also of importance is the validation of the model of exchange-as occurring over a finite number of exchangeable sites-by the manipulation of the weight of material in the reactor. This had the effect of greatly increasing the number of sites and therefore creating a dependence of exchange on gas phase oxygen concentration with the effect of lowering the rate constant value (which is based on first order exchange over exhaustible surface sites) and producing the exchange profiles that were seen earlier.

4.11 References for Chapter 4

1: Martin.D, Duprez.D.
J. Phys. Chem, **100**, 9429-9438, (1996)

2: Klier.K, Nováková.J, Jiru.P
Journal of Catalysis, **2**, 479-484, (1963)

3: Boreskov.G.K,
Adv Catalysis, **15**, 285-339 (1964)

4: Hargreaves. J.S.J, Joyner.R.W, Mellor.I.M
Journal of Molecular Catalysis A: Chemical, **141**, 171-176, (1999)

5. Boreskov. G.K.
Discussions Faraday Soc, **41**, 263-276 (1966)

6. Winter, E.R.S
Adv Catalysis, **10**, 196-241 (1958)

7. Karasuda.I, Aika.K
Journal of Catalysis, **171**, 439-448, (1997)

8. Schubert.M.M, Hackenburg.S
Journal of Catalysis, **197**, 113-122, (2001)

9. Lin.S, Bollinger.M, Vannice.M.A
Catalysis letters, **17**, 245-262, (1993)

10. Taha.R, Martin.D, Kacimi.S, Duprez.D
Catalysis Today, **29**, 89-92, (1996)

11. Hayashi.T, Tanaka.K, Haruta.M
Journal of Catalysis, **178**, 566-575, (1998)

12. Seker.E, Cavataio.J, Gulari.E, Lorpongpaiboon.P, Osuwan.S
Applied Catalysis A: General, **183**, 121-134, (1999)

13. Haruta.M, Kobayashi.T, Sano.H, Yamada.N
Chemistry Letters, 405-508, (1987)

14. Blick. K, Mitrelias.T.D, Hargreaves.J.S.J, Hutchings.G.J, Joyner. R.W, Kiely.C.J, Wagner.F.E.
Catalysis letters, **50**, 211-218, (1998)

15. Houghton.G, Winter.E.R.S,
Nature, **164**, 1130-1131, (1949)

16. Yuan.Y, Kozlova.A.P, Asakura.K, Wan.H, Tsai.K, Iwasawa.Y\
Journal of Catalysis, **170**, 191-199, (1997)

17. Haruta.M, Yamada.N, Kobayashi.T, Ijima.S
Journal of Catalysis, **115**, 301-309, (1989)

18. Hodge.N.A, Kiely.C.J, Whyman.R, Siddiqui.M.R.H, Hutchings.G.J, Pankhurst.Q.A, Wagner.F.E, Rajaram.R.R, Golunski.S.E
Catalysis Today, **72**, 133-144, (2002)

Chapter five

There are grounds for cautious optimism that we may be near the end of the search for the ultimate laws of nature.

Stephen W. Hawking

Chapter 5: Carbon Monoxide Oxidation over Magnesia Supported Gold.

5.0 Introduction

Although magnesium oxide supported gold is not ordinarily associated with catalytic CO oxidation, the few studies that have been done[1,2,3] do show moderate activity. As mentioned in chapter 4, the main reason CO oxidation studies were performed on Au / MgO materials was to enable a comparison to be made between their exchange and oxidation ability, in the hope of gaining insight into the CO oxidation mechanism. To this end, correlation data will be presented displaying any relationships that exist between oxidation and exchange across all MgO classes. Results that will be presented also include the influence of calcination on CO oxidation activity for some samples as well as all oxidation profiles across the MgO class.
An oxidation run is shown below.

Figure 5.1: GC trace for a typical CO oxidation run.

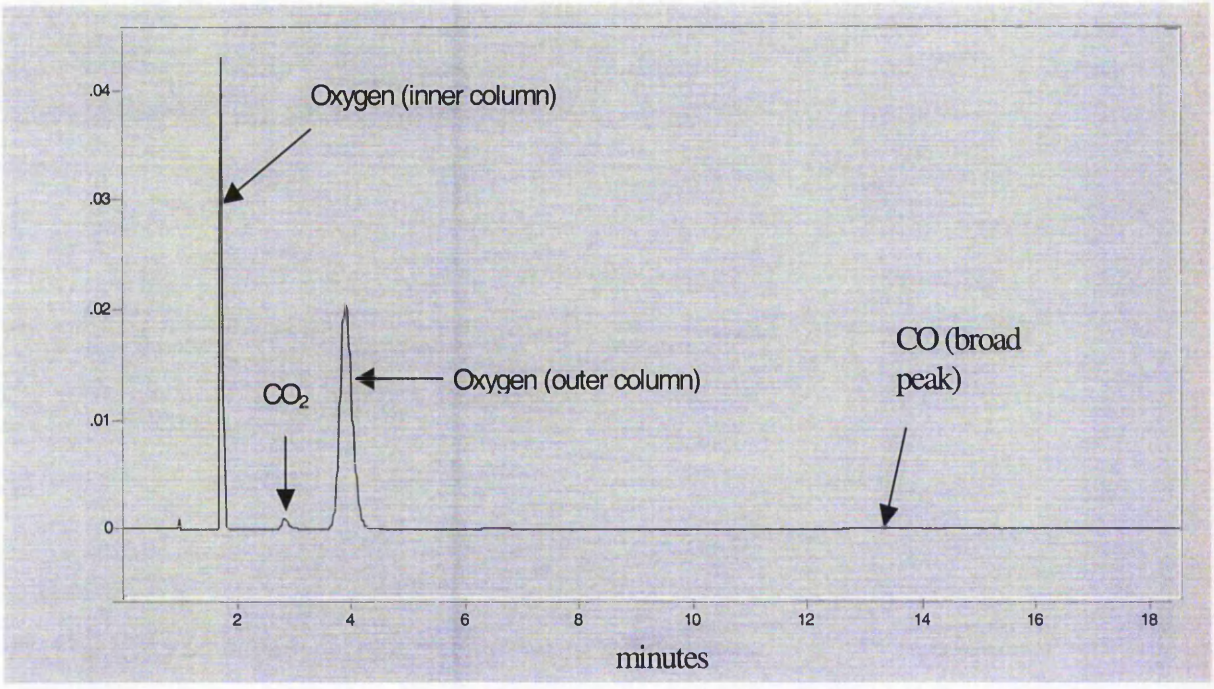

note that CO is a very broad peak and doesn't show up well in Grams (galactic software).

5.1 Kinetics underlying CO oxidation:

Oxidation of CO is a bimolecular reaction in which Langmuir-Hinshelwood kinetics are followed.
For oxidation of CO on a surface, both O_2 and CO have to adsorb according to equations 5.1 and 5.2.

Equation 5.1: $CO_{(g)} + X \rightleftharpoons CO_{(a)}$
Equation 5.2: $O_{2\,(g)} + X \rightleftharpoons O_{2\,(a)}$

Both CO and O_2 adsorb on specific sites (X). Notice that adsorption is a reversible process and an equilibrium exists between adsorption and desorption. The equilibrium constant K is given by: k_a / k_d, the ratio of the adsorption and desorption rate constants. Adsorption of gas phase molecules follows Langmuiran kinetics in which Equation 5.3 is followed:

Equation 5.3: $-d[A] / dt = P_A(1-\theta) = k_a (1-\theta) P_A$

Where: $-d[A] / dt$ is the fall of gas phase concentration of A with time
P_A = Pressure of A
k_a = rate constant for adsorption of A
$1-\theta$ = fraction of surface not covered with adsorbate

Coverage is related to pressure as follows: Equation 5.4: $\theta = aP / 1+aP$ where:
θ = coverage
a = equilibrium constant for adsorption / desorption of A.

Because in Langmuir-Hinshelwood kinetics, *both* CO and O_2 are adsorbed on the surface, a new expression to accommodate competetive bimolecular adsorption is conceived.

Equation 5.5: $\theta_A = aP_A / 1+aP_A + bP_B$

Where θ_A = coverage in A
b = equilibrium constant for adsorption and desorption of B
P_B = pressure of B.

Alternatively, coverage of B follows equation 5.6:
$\theta_B = bP_B / 1+aP_A + bP_B$
Where θ_B = coverage of surface in B.

It follows that both A and B (i.e., CO and O_2) have to adsorb in approximately equal quantities for maximium conversion to product (CO_2). Adsorption of one reactant in preference to the other, (or if one reactant is weakly adsorbed, i.e., high k_d, low k_a, low K), will also result in a lowered conversion rate.
Once the reactants have adsorbed, they can react on the surface and the products of reaction desorb to the gas phase according to equations 5.7 and 5.8.

Equation 5.7: $A_a + B_a \longrightarrow C_a$

Where: A_a is adsorption of A
B_a is adsorption of B
C_a is adsorption of product

Equation 5.8: $C_a \longrightarrow C_g + \times$

Where: C_g is desorption of adsorbed C to the gas phase
$\times$ is the newly vacated site.

These freshly vacated sites can participate in subsequent gas phase adsorption.

5.2 Results

Data conversion

CO conversions are calculated on a carbon-balance basis in which the GC integration value for CO_2 is divided by the sum of both CO and CO_2 integration values. In this research, detector sensitivities (as calculated by comparing integration values for CO, CO_2, and O_2 with actual measured individual flow rates using a flow meter) are different for CO and CO_2 with greater sensitivity (33%) for CO. Therefore the integration for CO_2 is corrected accordingly before a CO conversion is calculated. This approach has the advantage of being relatively simple but is susceptible to under estimation of conversion if bypass of reactant gas occurs between sample and holding tube. For this reason the samples were prepared (in clear tubes) so that no collapse in sample bed could be observed. Also some samples gave 100% conversion that could not occur with bypass.

5.3 Profiles:

Figure 5.2: CO oxidation across MgO classes.

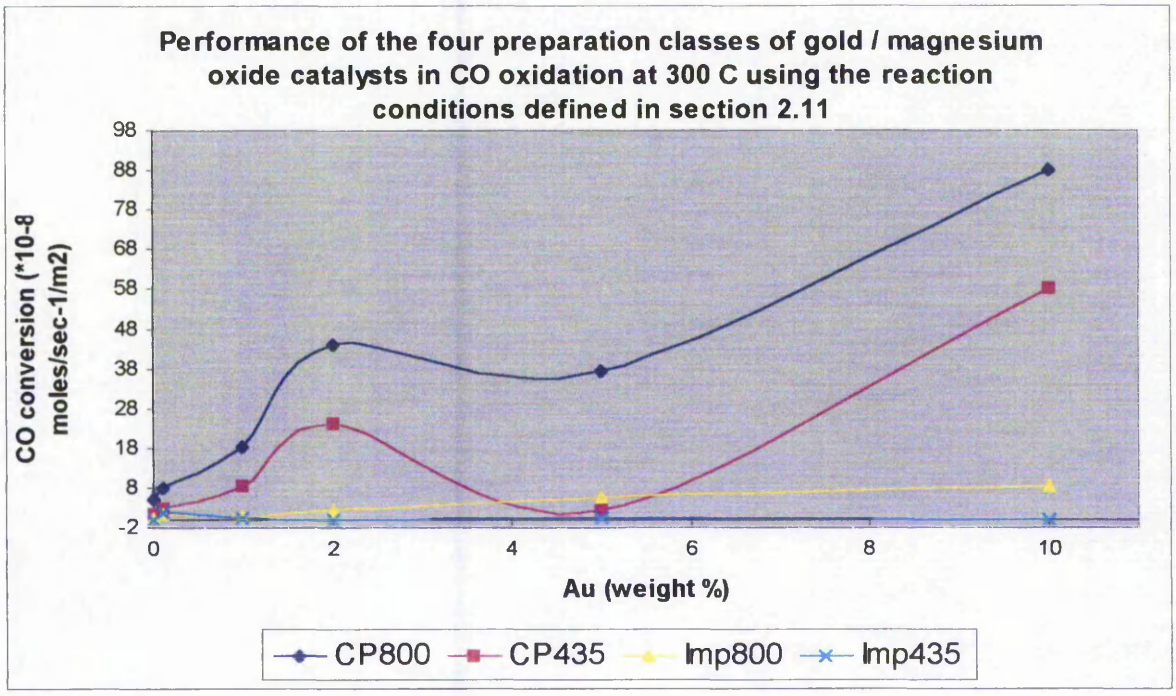

Figure 5.2 reveals the strong influence of preparation method on CO oxidation activity across magnesia supported gold. Here, molar CO conversions at 300°C are used. This temperature was chosen as a reference because appreciable conversion for most classes of material only starts to occur at this point. Of course, if a higher temperature was used, then the curves might look quite different, especially if the activation energies for the different classes were a lot different. There are several noticeable observations related to preparation and gold loading variables. As can be seen, co-precipitation imbues highly significant advantages over impregnation for CO oxidation, as others have consistently observed.[4] Intriguingly, both co-precipitation classes follow similar profiles, suggesting that different gold loadings have an influence on CO oxidation that is not lost on increasing the calcination temperature. In accord with most other observations,[5,6] impregnated materials performed very badly with respect to their co-precipitated counterparts, but like co-precipitated materials, there was a general upward trend in oxidation performance with increasing gold loading, again suggesting that high gold loaded samples are especially active for CO oxidation (as others have seen[7,8]) although for the co-precipitated classes there is a surprising dip in oxidation at 5% loading. Across all sample classes, an order in reactivity can be established thus: CP800 > CP435 > Imp800 > Imp435, therefore high calcination temperature imparts superior activity for both impregnated and co-precipitated materials, perhaps because of the same reason as outlined in chapter 4, i.e., an absence of chlorine for high temperature calcined materials as supported by XPS studies, (although the increase in oxidation for 10% loaded *low* temperature calcined material points to a more complex argument than chlorine loss at *high* temperature calcination). Most interestingly, however, is the similarity between sample class orders of reactivity for *both* exchange and oxidation, suggesting a general correlation between the two. Finally, the best MgO performers give a CO oxidation level comparable to that seen with more established supports.[9,18] such as Au / TiO_2 and Au / Fe_2O_3. Although CO oxidation studies are usually performed at ambient temperature for these supports and not the elevated temperatures for Au / MgO.

Individual class profiles:

5.4 **Figure 5.3**: oxidation across Imp 435 samples.

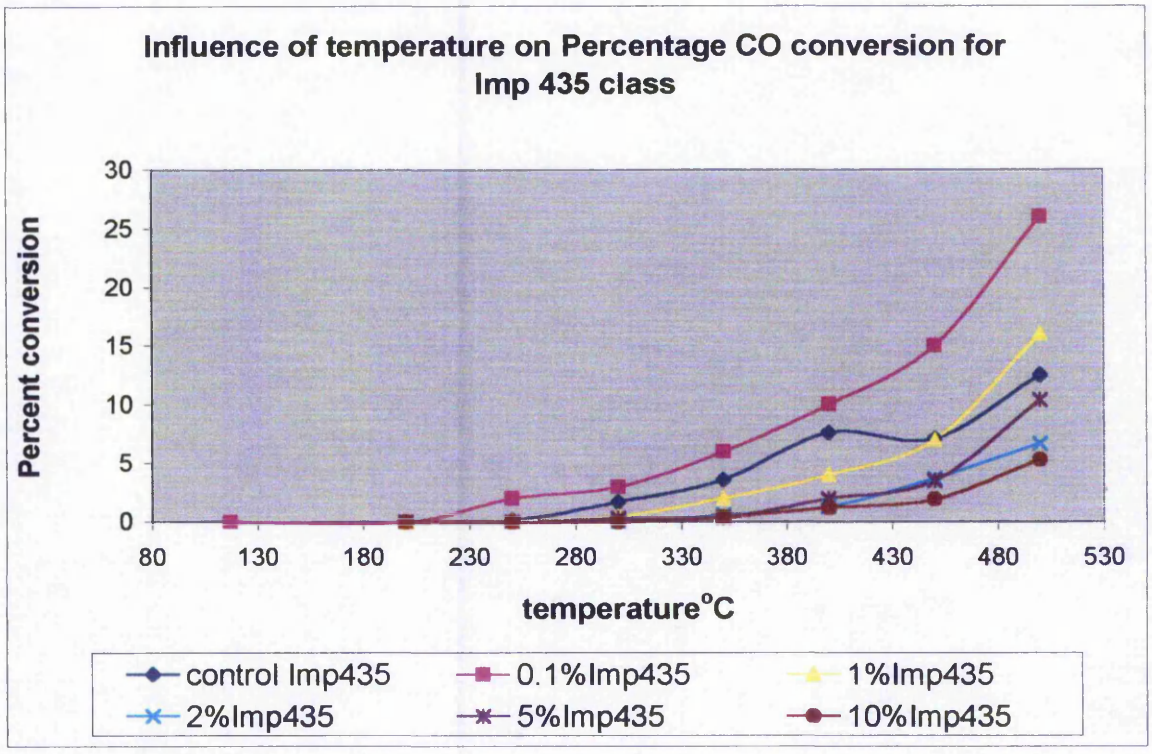

Figure 5.3 gives the CO oxidation performance for all low temperature calcined impregnated samples across the full temperature range. As with all these classes there is a general increase in CO oxidation with increasing temperature. There is therefore no immediate evidence of a negative activation energy as others have reported for CO oxidation over MgO supported gold catalysts.[12]

It can be seen that there is a significant trend towards lower overall activity with increasing gold loading. This profile can be explained by resorting to the XPS evidence (section 3.5) in which low temperature calcined materials contained significant chlorine at high gold loadings.

5.5 Figure 5.4: oxidation across Imp 800 class

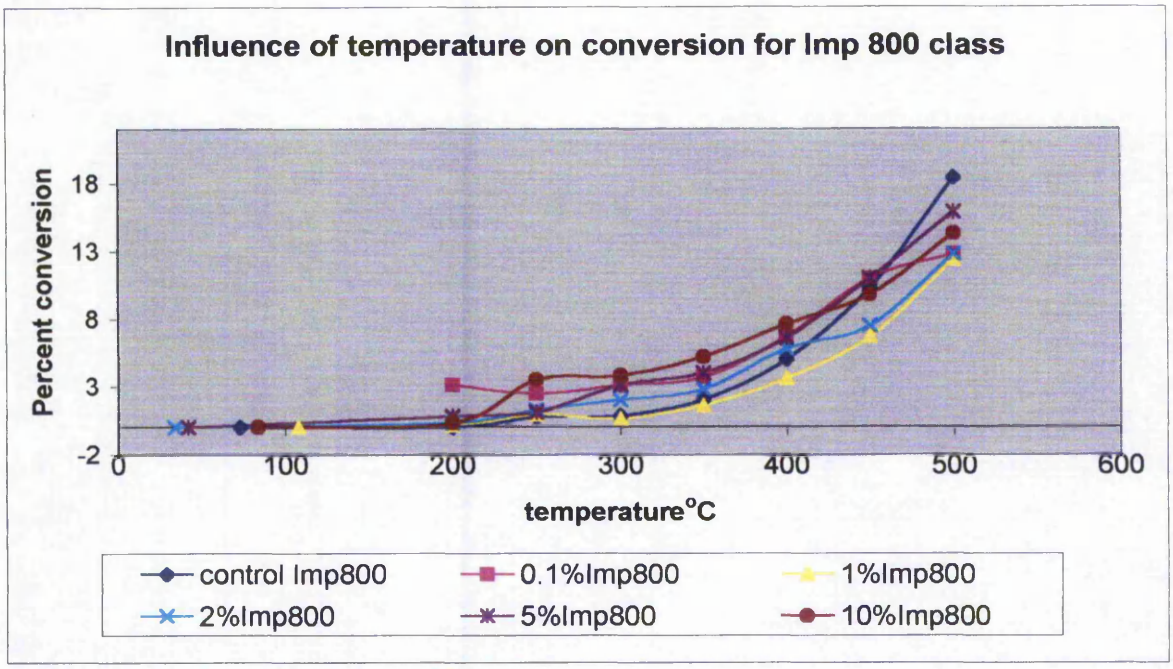

Figure 5.4 gives oxidation across high temperature calcined impregnated samples for the whole temperature range. There doesn't appear to be a noticeable influence of calcination temperature on either of the two sets of profiles across the whole temperature range. There also doesn't appear to be an identifiable trend with gold loading at any temperature, as the profiles are too closely packed.

5.6 **Figure 5.5**: oxidation across CP 435 class

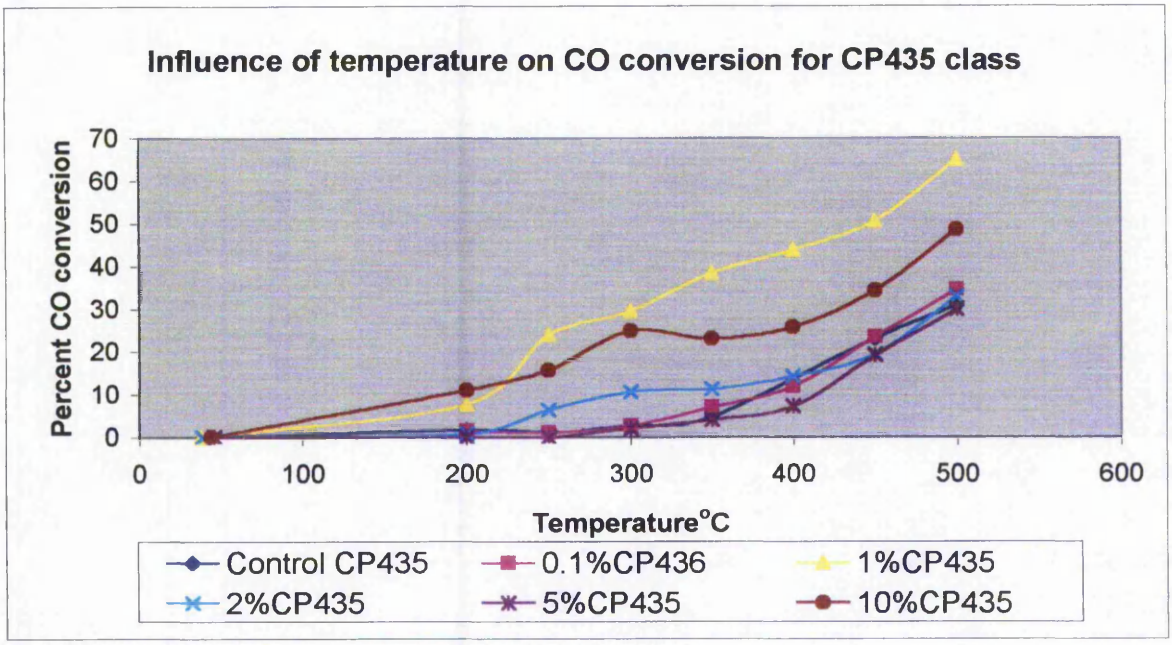

Figure 5.5 gives oxidation across low temperature calcined co-precipitated samples. Rates of oxidation are much higher for this co-precipitated class than for the impregnated classes, especially at intermediate temperatures.

Again there is a clear increase in oxidation with increasing temperature with a sharper incline at higher temperatures (as with all these sample classes) but most noticeable is the division of profiles, with 1% and 10% loaded samples giving superior oxidation performance across all temperature ranges than the other loaded samples. Why these two samples should be especially active is not understood but intermediate loaded materials have performed well in other aspects of the research described. Thermal stability of these samples with respect to the others could be a possibility, but is hard to explain as all samples were calcined under identical conditions and should all be thermally stable.

5.7 **Figure 5.6**: oxidation across CP 800 class

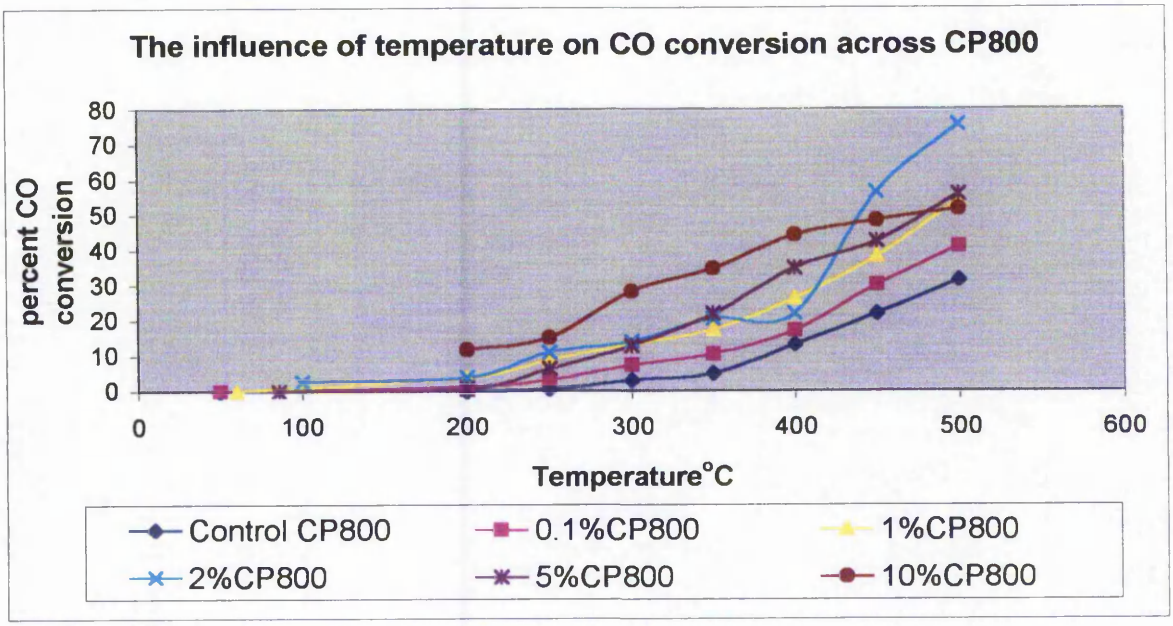

Figure 5.6 gives oxidation results for the high temperature calcined co-precipitated samples. This class gives the highest oxidation performance of all the MgO classes. More than any other class there is a strong trend of increasing CO oxidation with increasing gold loading across the whole temperature range (starting at intermediate temperatures). However, the most active sample is 2% loaded and produces nearly 80% conversion at maximum temperature. It is of interest that SEM imaging reveals that this sample produces quite large gold particles (300 – 400 nm) even though only a few were detected. This is a counter-intuitive observation as most researchers[13] have found that a proliferation of very small gold particles (2 – 5 nm) is associated with high catalytic ability.

5.8 The effect of calcination on CO oxidation

The role of calcination is still controversial in CO oxidation catalysis, with researchers often producing conflicting results.[14,15,16] It is therefore of extreme interest to examine the impact of calcination on catalysis for several MgO materials.

Figure 5.7: The role of calcination for control MgO materials

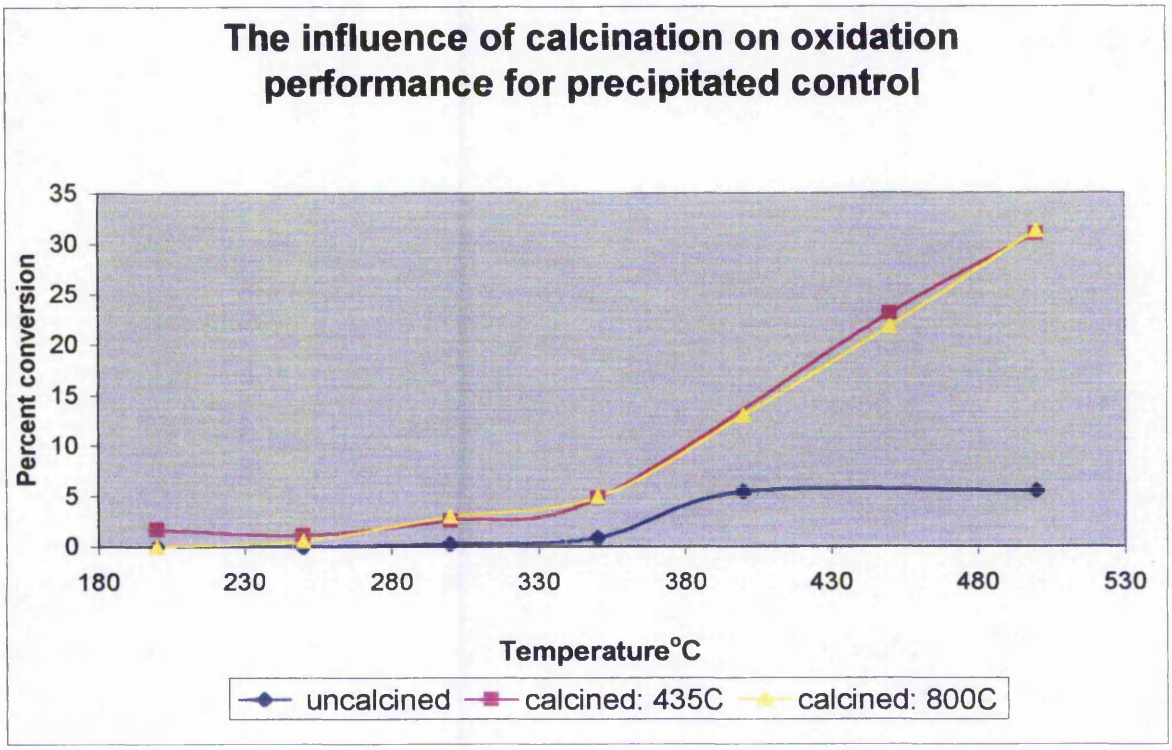

Figure 5.7 reveals the effect of calcination on CO oxidation activity across the full temperature range for control materials. This is important as a comparison can be made with loaded samples. As can be seen, calcination imparts superior catalytic performance on samples, however there appears to be no marked impact from calcination temperature with both calcined samples having very similar profiles.

5.9 **Figure 5.8**: The role of calcination for gold loaded MgO samples

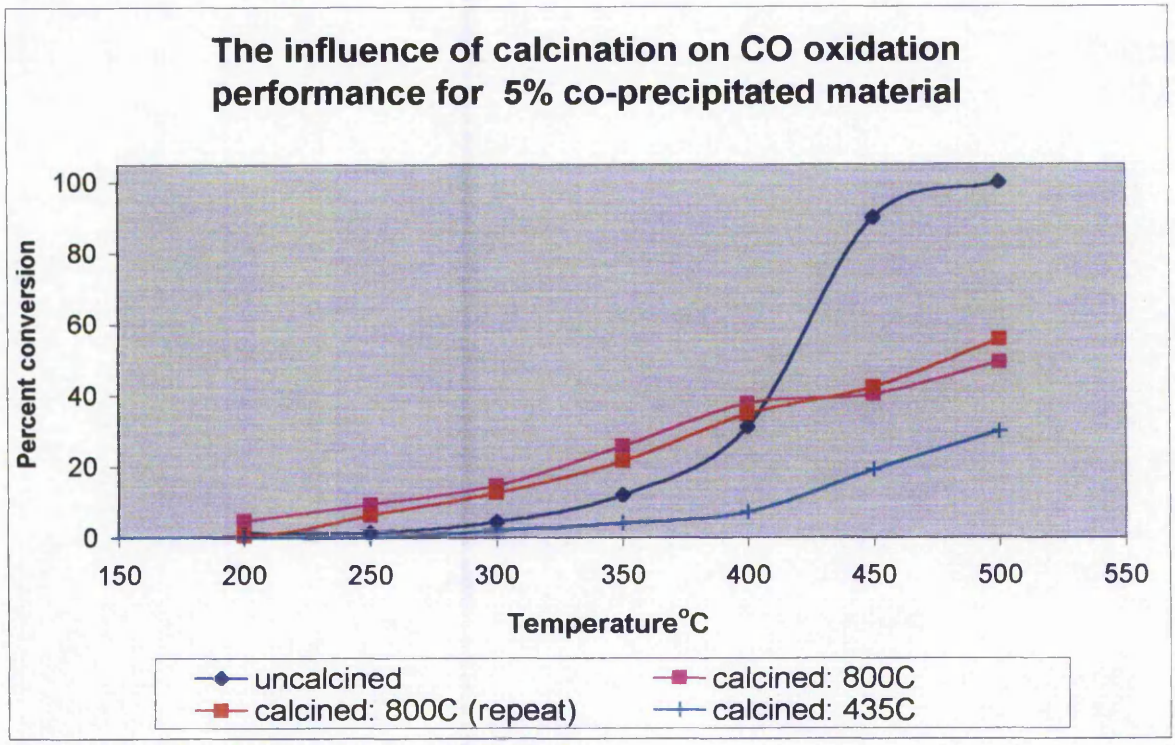

Results in figure 5.8 contrast sharply with those in figure ***5.7***, with a reversal of the calcination effect upon loading with gold. As can be seen uncalcined 5% loaded MgO performs best, giving a typical oxidation S shaped profile. Samples calcined at 800°C perform less well at high temperature (although there is some evidence of superior performance at intermediate temperatures) while samples calcined at 435°C give the lowest oxidation performance. These results reveal an overall retardant effect of calcination that is in keeping with most investigators, although the increase of activity associated with increasing the calcination temperature from 435°C to 800°C is not.[14] It is highly probable that has the reaction temperature is increased, calcination of the uncalcined sample is occurring thus leading to superior performance at higher reaction temperatures. However, because these oxidation runs are fairly rapid (60 – 80 minutes to reach 350°C) this suggests that any calcination is best performed only for a relatively short duration and not the standard 3 hours that is part of this research.

Unfortunately this 'short duration' hypothesis has not been tested in this research. As can be seen a repetition run is included for 5%CP800 sample, which illustrates the high reproducibility encountered in the authors CO oxidation research.

5.10 Correlating exchange and oxidation data.

Because CO oxidation might involve lattice oxygen as part of the Mars van Krevellen mechanism (section 1.27.1) it is important to see if a positive correlation exists between isotopic exchange and oxidation data. Oxygen activation or bond weakening is thought to play a major part in both exchange and oxidation reactions and is thought to be rate determining for both these reactions.[17] Clearly, comparison of the data is an initial step in trying to understand this process. When comparing exchange and oxidation data a standard measure is taken for both, that is moles of gas exchanged or oxidized per second per m^2 of catalyst. It must be remembered that the molarity data for exchange is taken from extent of exchange (rates) calculations and so the caveat concerning variable mass spectrometer sensitivities has to be applied here also. More confidence is associated with the values for CO oxidation.

Figure 5.9: The strongest correlation for a MgO class

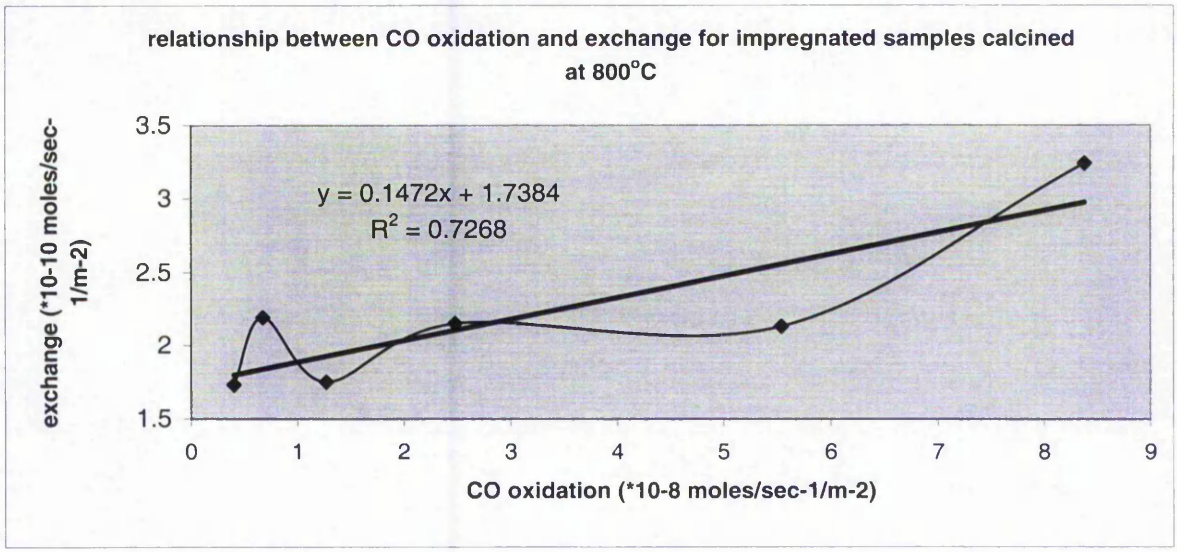

Figure 5.9 gives the strongest relationship found for a class of MgO materials. The observed correlation coefficient of 0.73 is suggestive of a relationship between exchange and oxidation but is largely due to the last data point and is also undermined by an absence of a relationship for any other class of MgO material. This indicates the above correlation should be regarded with scepticism and not representative of any process occurring on the MgO surface. Assuming there is no relationship between exchange and oxidation, this suggests that lattice oxygen is not really involved in the oxidation process and instead CO oxidation consists simply of gas phase adsorption of reactants on the MgO surface and subsequent reaction.
It is interesting to note that wide disparity in performance between oxidation and exchange with the former up to 2 orders of magnitude greater than exchange. This fact alone suggests the two are different processes altogether.

5.11 Discussion and Conclusions.

This research has demonstrated encouraging indications of CO oxidation ability by MgO supported gold at intermediate and high temperatures, (from 200°C onward). However there is an absence of oxidation at low temperatures below 200°C, which is disappointing as this is the central interest of present research. Analysis of reactivity data performed at 300°C reveals a highly significant influence of preparation on CO oxidation with co-precipitated materials far outperforming their impregnated counterparts. This is in keeping with the generality of observations from researchers[4,5,6] and suggests that any further attempts to improve magnesia supported gold catalysis should not be concerned with impregnation as a preparation option. Further, it is apparent that increasing the calcination temperature positively influences catalysis. This is contrary to most findings[14,19] that tend to show a retardant effect of high calcination temperature. As mentioned earlier, the most likely explanation for this is the removal of chlorine by the higher calcination temperature. This is supported by XPS characterisation (section 3.5) in which samples calcined at higher temperature had lower or a complete absence of chlorine.
Interestingly, however, is the observation that samples with no gold or very little (i.e., control and 0.1% loaded) and therefore little or no chlorine, still perform better when

calcined at higher temperature. This suggests there are other factors responsible for superior activity at high calcination temperatures in this research.

Analysis of individual class profiles reveals no obvious influence of gold on CO oxidation, except for a fairly clear retardant effect through the whole temperature range for low temperature calcined impregnated materials (Imp435), most likely a function of chlorine doping. Inspection of the high temperature calcined co-precipitated profile (CP800) reveals a moderate positive trend with gold loading and suggests that once chlorine is removed the catalytic influence of gold manifests itself. Essentially these individual class profile data reflect the molarity data (figure 2) but at the whole temperature range.

As mentioned in the General Introduction, calcination is a controversial topic in gold catalysis, with researchers split as regarding its efficacy. The findings outlined suggest a negative effect of calcination for gold loaded magnesium oxide samples. Intriguingly, this effect is reversed for undoped samples. Here, calcination improves CO oxidation performance. For the doped uncalcined sample (5%) as the reaction proceeds, calcination is actually occurring. Because CO conversion increases above the 'other' calcined samples at higher reaction temperatures, this supports the assertion that limited calcination times using a gradual ramp rate is most effective. This observation actually has support from others.[20]

At the beginning of this chapter it was reported that the main impetus for CO oxidation studies on magnesia supported gold was to enable a comparison with isotopic exchange data to be made in the hope of gaining insight into the CO oxidation mechanism. It has been found that there is no substantial correlation between exchange and oxidation for any class save for the high temperature calcined impregnated (Imp800) samples, and here the relationship is only modest. This weak result taken with the total absence of a relationship for any other sample class, suggests oxidation occurs by a *non-lattice* involved pathway. However, as mentioned before, there is a general relationship when comparing sample classes to each other. For instance the exchange data reveal the order: CP435 > CP800 > Imp800 > Imp435 which is similar to the oxidation order: CP800 > CP435 > Imp800 > Imp435. This suggests that there might be a *general* relationship between exchange and oxidation that is lost when comparing individual sample data points.

5.12 References for chapter 5

1. Cunningham, D.A.H, Vogel. W, Kageyama, H. Tsubota, S. Haruta. M,
Journal of Catalysis, **177**, 1-10, (1992)

2. Sanchez.R.M.T, Ueda.A, Tanaka.K, Haruta.M
Journal of Catalysis, **168**, 125-127, (1997) (research note)

3. Galvagno.S, Parravano.G.J
Journal of Catalysis, **55**, 178-190, (1978)

4. Haruta.M, Kobayashi.T, Sano.H, Yamada.N
Chemistry Letters, **17**, 405-408, (1987)

5. Visco.A.M, Neri.F, Donato.A, Milone.C, Galvagno.S
Phys.Chem.Chem.Phys,**1**, 2691-2873, (1999)

6. Bond.G.C, Thompson.D.T
Catalysis Reviews-SCI.ENG, **41**(3&4), 319-388, (1999)

7. Uphade .B.S, Yamada.Y, Akita.T, Nakamura.T, Haruta.M
Applied Catalysis A: General, **215**, 137-148, (2001)

8. Bailie.J.E, Abdullah.H.A, Anderson.J.A, Rochester.C.H, Richardson.N.V, Hodge.N, Zhang.J.G, Burrows.A, Kiely.C.J, Hutchings.G.J
Phys. Chem. Chem. Phys, **3**, 1-9, (2001)

9. Schubert.M.M, Plzak.V, Garche.J, Jürgen Behm.R
Catalysis Letters, **76**, 143-150, (2001)

10. Hutchings.G.J, Rafiq.M, Siddiiqui. M, Whyman. R, Burrows.A, Kiely C.J
J.Chem.Soc., Faraday Transactions, **93**(1), 187-188, (1997)

11. Haruta.M, Genet.M.J, Delmon.B
Journal of Catalysis, **144**, 175-192, (1993)

12. Cunnigham.D.A.H, Vogel.W, Haruta.M
Catalysis Letters, **63**, 43-47, (1999)

13. Kozlova.A.P, Kozlov.A.I, Sugiyama.S, Matsui.Y, Asakura.K, Iwasawa.Y
Journal of Catalysis, **181**, 37-48, (1999)

14. Hodge.N.A, Kiely.C.J, Whyman.R, Siddiqui.M.R.H, Hutchings.G.J, Pankhurst.Q.A, Wagner.F.E, Rajaram.R.R, Golunski.S.E
Catalysis Today, **72**, 133-144, (2002)

15. Haruta.M Tsubota.S, Kobayashi.T, Kageyama.H, Genet.M, Delmon.B
Journal of Catalysis, **144**, 175-192, (1993)

16. Park.E.D, Lee.S.J
Journal of Catalysis, **186**, 1-11, (1999)

17. Borezkov.G.K,
Diss. Faraday. Soc, **41**,263-276, (1966)

18. Kahlich.M.J, Gasteiger.H.A, Behm.R.J
Journal of Catalysis, **182**, 430-440, (1999)

19. Tripathi.A.K, Kamble.V.S, Gupta.N.M
Journal of Catalysis, **187**, 332-342, (1999)

20. Grisel.R.J.H, Nieuwenhuys
Journal of Catalysis, **199**, 48-59, (2001)

Chapter six

I think there is a world market for about five computers.

Thomas Watson (founder of IBM)

Chapter 6: Isotopic Oxygen Exchange over Iron Oxide Supported Gold

6.0 Introduction:

Because previous research[1,2,3] has shown that iron oxide supported gold is especially active for CO oxidation, it is of interest to investigate the exchange process over these materials so that greater insight into the CO oxidation mechanism can be achieved. To this end, several classes of iron oxide supported gold have been tested for their ability to exchange oxygen. In this chapter both impregnated and co-precipitated exchange results will be shown, including both base to acid (Finch method) and acid to base co-precipitated samples.

As mentioned in the introduction, there have been some studies investigating isotopic oxygen exchange over iron oxide supported gold samples[4,5,6] but these have employed this technique in combination with CO oxidation in order to shed light on the CO oxidation process. This approach has also been employed in the author's research and is described in chapter 7, however, there is utility in researching exchange only, as this gives a data base in order to quantify the impact of preparation and gold loading on ease of exchange and which can be compared with CO oxidation data. Throughout this chapter, reference to previous work detailing characterisations used, will be employed in order to gain insight into the exchange profiles presented.

6.1 **Figure 6.1**: exchange over impregnated iron oxide

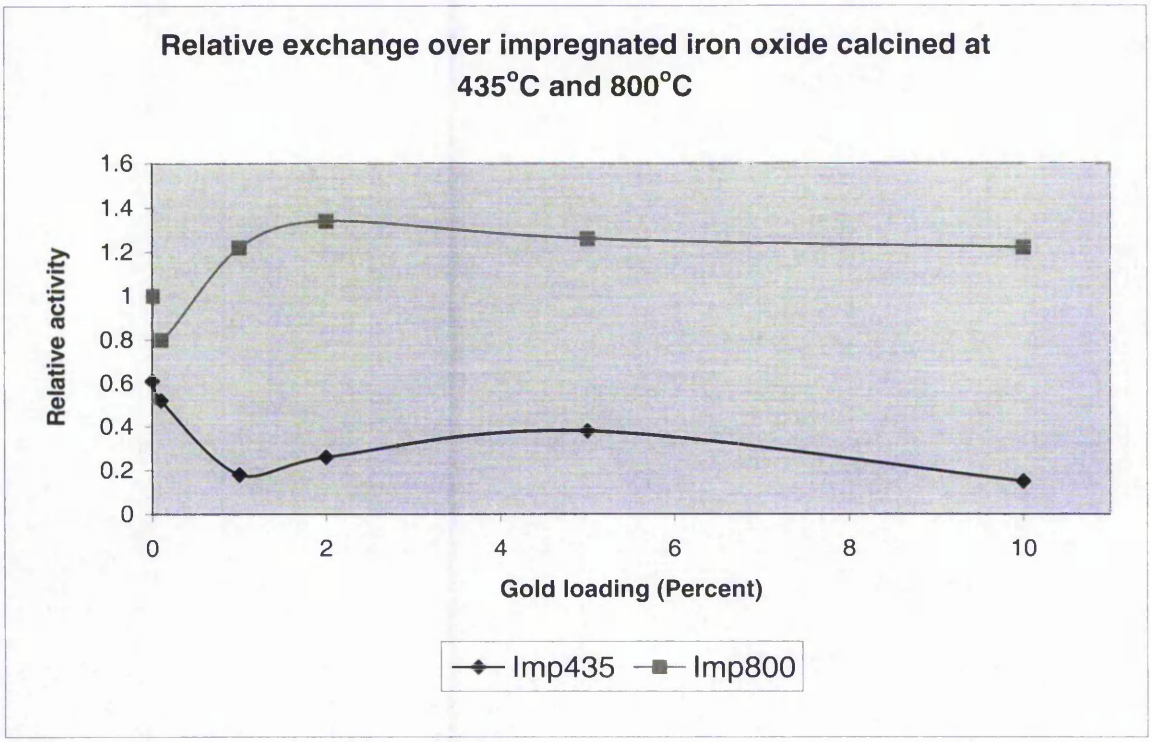

Figure 6.1 reveals the significant effect of calcination temperature on exchange at 435°C and 10 – 20 torr, across impregnated iron oxide samples. There is a 3-fold gain in exchange for samples calcined at the higher temperature for reasons that are not completely understood. There is a magnitude reduction in surface area with higher temperature calcined samples that could explain this difference (low surface area means a greater activity per m^2, from which the above data are distilled), however, these data are normalized to sample surface area. The simplest explanation is that high temperature calcination engenders positive influence on exchange through changes in surface morphology. SEM images (section 3.3.10 – 3.3.11) suggest large gold and support particles on the surface of both control and 10% loaded high temperature calcined materials of around 250 nm. It would appear that sintering of both support and gold is advantageous to exchange. This finding is counter-intuitive, in that most researchers[7,8,9] have found catalytic activity (that might possess similar surface processes to isotopic exchange) to be inversely related to particle size.

This relationship between particle size and exchange activity was hinted at for exchange on MgO (chapter 4) and appears to be a general feature of exchange on supported gold in the author's research. Analysis of individual profiles reveals no detectable influence of gold on exchange performance for high temperature calcined samples (unlike the equivalent MgO samples) but there is a decline in exchange performance with increasing gold loading for low temperature calcined materials. As with equivalent MgO samples, chlorine poisoning is the most likely explanation as low temperature calcination fails to remove this by-product of preparation. XPS analysis (section 3.5) of 10% loaded impregnated samples confirms this reasoning with the high temperature calcined sample having zero chlorine and the low temperature calcined sample revealing detectable chlorine levels. The absence of an effect through gold for high temperature calcined samples suggests that the support plays more of a role in the exchange process for gold supported on iron oxide than for MgO samples. It is also worthy of note that most iron oxide samples gave R2 and R1 exchange in equal measure as shown by equally increasing 32 and 34 signals, typified in figure 6.2.

6.2 **Figure 6.2**: R1 and R2 exchange over iron oxide sample at 435°C

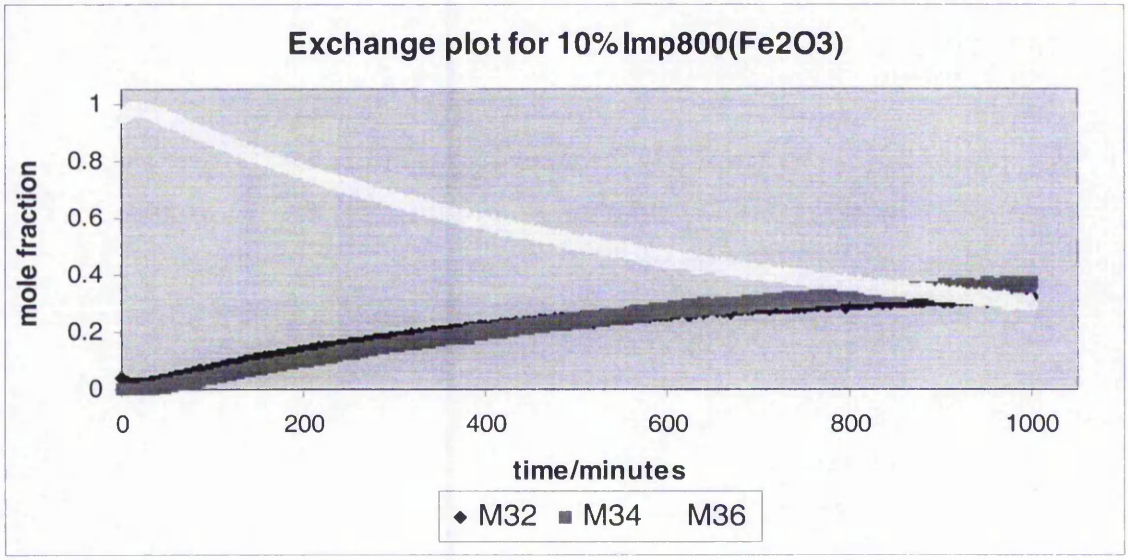

It is hypothesized[10] that R1 and R2 exchange occur by a three and four atom intermediate, respectively. Because of greater oxygen reactivity for iron oxide as compared to magnesium oxide, it is not surprising that impregnated iron oxide samples give significant R2 exchange (as revealed by a rising 32 signal) that is absent in the equivalent MgO sample class.
Exchange was also performed on co-precipitated materials as figure 6.3 shows.

6.3 Figure 6.3: Exchange over co-precipitated (base to acid) iron oxide.

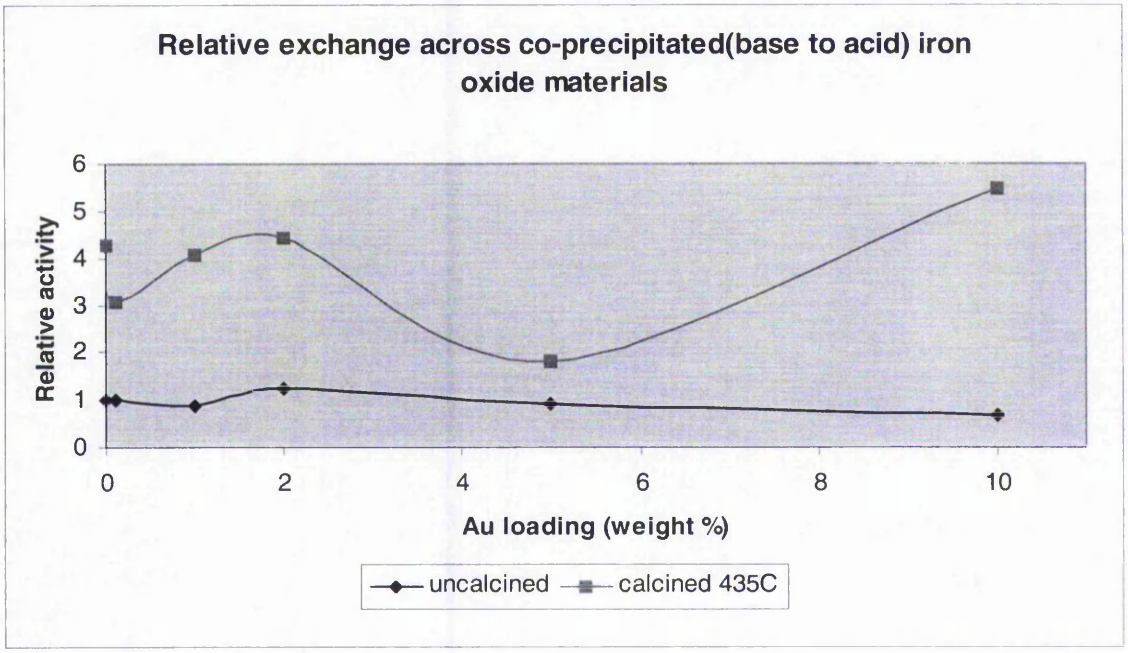

These data are standardized to the exchange performance of the control uncalcined co-precipitated sample. Again, calcination appears to be beneficial to exchange with the calcined samples outperforming the uncalcined samples. Data normalization to sample surface area eliminates surface area differences (which again are considerable, section 3.1) as explanations for the above profile differences. SEM imaging (section 3.3.7 – 3.3.9) reveals the expected sintering effect of calcination on surface support crystallites but this only appears to enhance exchange, as with the impregnated samples. For the calcined samples the influence of gold is unclear as the profile has an undulating appearance. For uncalcined samples there appears to be a moderate negative influence of gold loading on exchange performance.

It should be pointed out that exchange was performed at different temperatures regarding sample preparation with impregnated samples exchanged at 435°C and co-precipitated (base to acid) samples exchanged at 350°C. This was because earlier exchange studies on co-precipitated (acid to base) samples at 435°C resulted in bulk exchange, with, for example, the equivalent of 652 monolayers (or 77% of the bulk!) undergoing exchange for control co-precipitated (acid to base) calcined sample.

6.4 **Figure 6.4**: exchange over co-precipitated (acid to base) uncalcined iron oxide samples

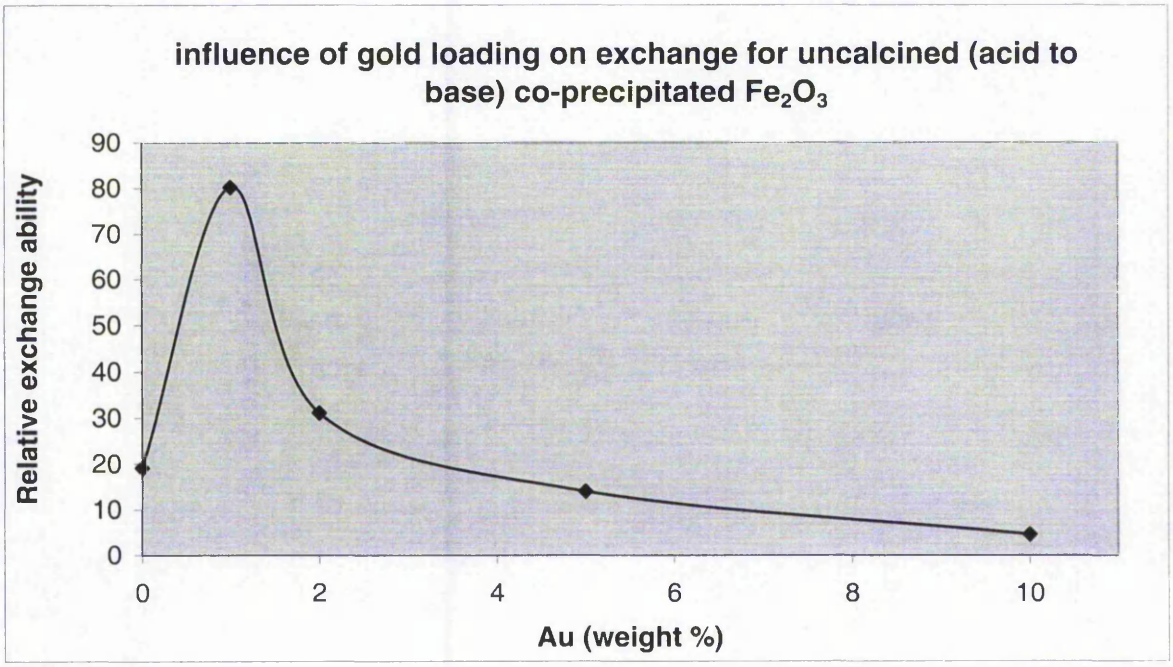

Here, exchange (still using uncalcined control co-precipitated (base to acid) sample as standard; equals 1 on scale) over uncalcined co-precipitated materials at 435°C is revealed. As bulk exchange is occurring at this temperature it is not surprising that relative exchange is up to 2 magnitudes greater than with co-precipitated (base to acid) materials exchanged at 350°C. Most interestingly however, is that there still appears to be an effect of gold on this type of exchange with increasing gold loading imparting a negative influence on bulk exchange.

This result is repeated for calcined co-precipitated (acid to base) materials.

6.5 **Figure 6.5**: exchange over co-precipitated (acid to base) calcined iron oxide samples

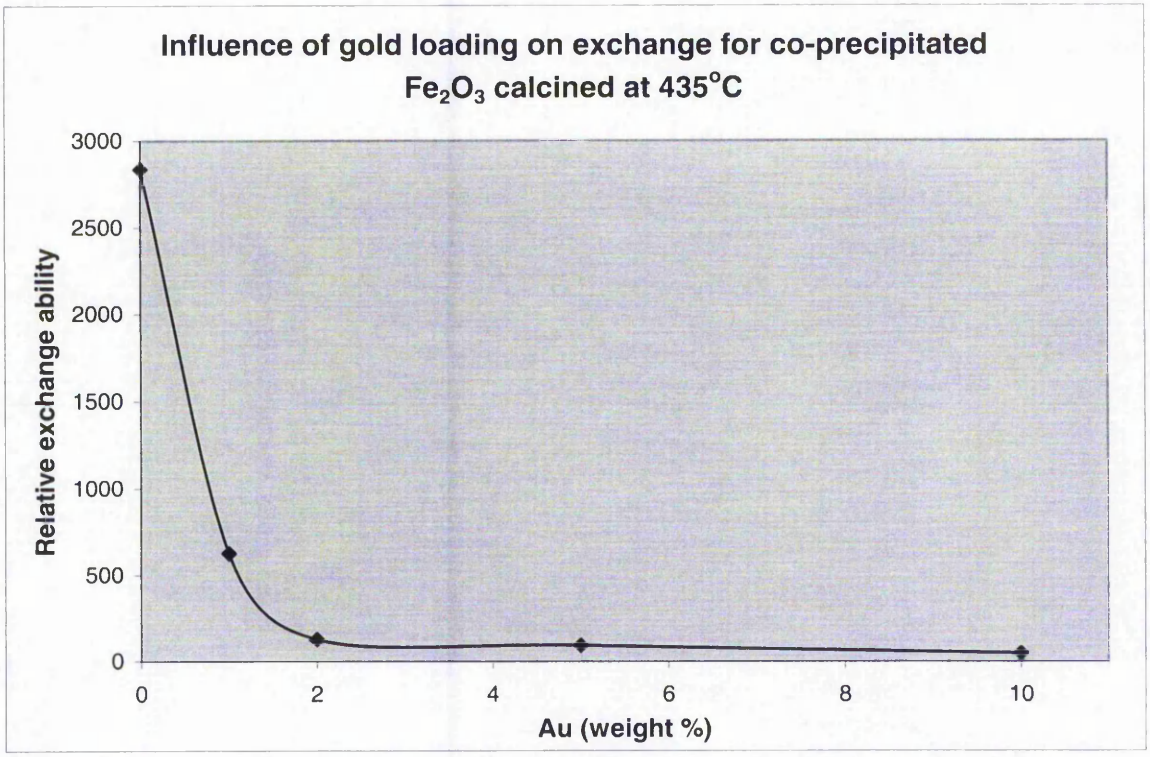

Figure 6.5 reveals the dramatic effect of gold loading for calcined co-precipitated (acid to base) materials. There is an immediate fall in bulk exchange. Again this result demonstrates gold can influence (negatively) exchange of bulk oxygen. A possible explanation is most likely centered on a blocking / poisoning effect of chlorine or even gold on support exchange in which exchange is inhibited by gold dispersed on the surface. SEM images (section 3.3.8 – 3.3.9) of co-precipitated iron oxide (base to acid) has failed to reveal the presence of any discrete gold particles and this strengthens the hypothesis that gold over co-precipitated (acid to base) iron oxide samples is similarly highly dispersed (no SEM's were performed on this class). So far relative activity calculations have been used to compare different sample classes but comparisons can also be made based on extent of exchange.

6.6 Figure 6.6: Extent of exchange on iron oxide samples

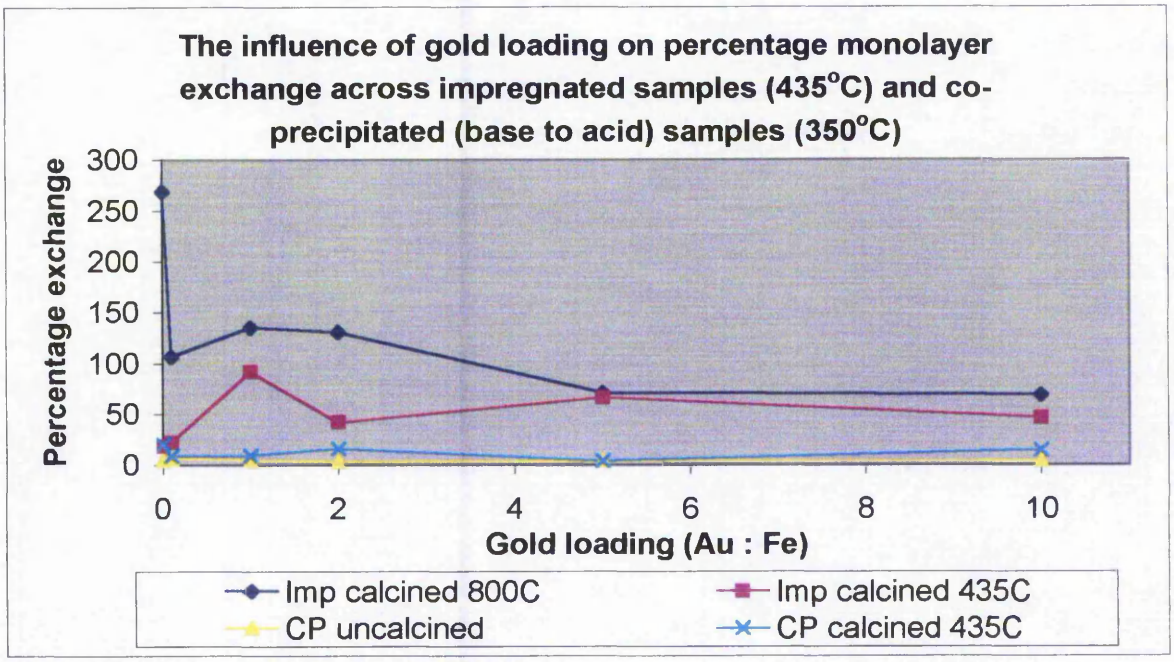

Figure 6.6 reveals the influence of preparation and gold loading on extent of exchange across all iron oxide sample classes. What is most apparent is the greater extent of exchange for impregnated as compared to co-precipitated (base to acid) samples. This divergence might be ascribed to large variations in surface area between impregnated and co-precipitated samples with the former a magnitude less than the latter. However there are also large differences in surface area between both classes of impregnated samples, but these give comparable extents of exchange and so the extent of exchange profiles probably go deeper than simple surface area differences. Taken prima facie, these data suggest impregnated iron oxide materials are able to exchange more of their monolayer than co-precipitated (base to acid) iron oxide materials. It must be stressed that co-precipitated materials (base to acid) were run at 350°C as earlier samples, co-precipitated (acid to base) iron oxide, gave extreme values of exchange that were interpreted as involving the bulk. Exchange over impregnated samples was conducted at 435°C as this was found to give very reasonable exchange values. This difference in temperature makes it hard to directly compare exchange on co-precipitated (base to acid)

and impregnated samples, but it does suggest that preparation technique influences the mobility of the bulk support as a function of temperature.

Analysis of individual profiles reveals no noticeable effect of gold on extent of exchange for any class. This contrasts with the MgO (chapter 4) exchange profiles that are markedly influenced by preparation technique and gold loading.

In order to gain a greater insight into the role of preparation for each support type, it is instructive to have all classes represented at a given gold loading, in this case 0.1%. Figure ***6.7*** reveals the influence of preparation on relative activity calculations for exchange across MgO samples.

6.7 **Figure 6.7**: The impact of preparation on exchange for MgO.

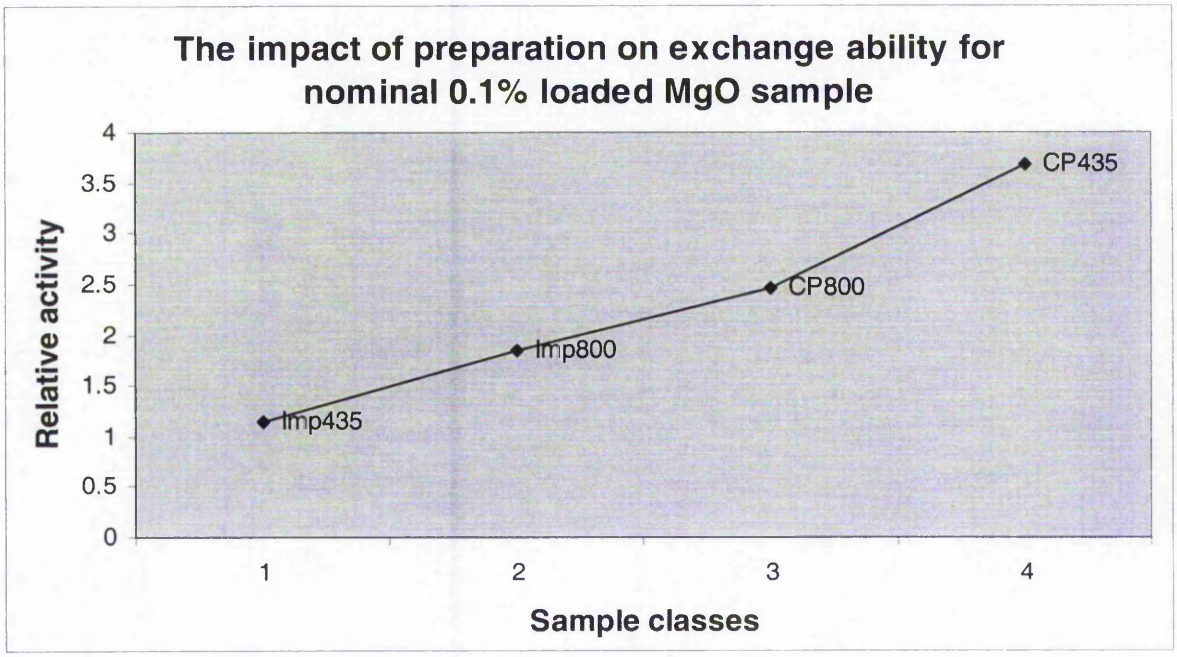

Figure 6.7 reveals the impact of preparation on exchange across MgO samples for a nominal loaded sample, 0.1%. There appears to be a linear progression from low to high temperature calcined impregnated samples through to high temperature calcined co-precipitated and finally low temperature calcined co-precipitated samples. This profile contrasts sharply with exchange over iron oxide samples as figure 6.8 reveals.

6.8 **Figure 6.8**: The impact of preparation on exchange for Fe_2O_3.

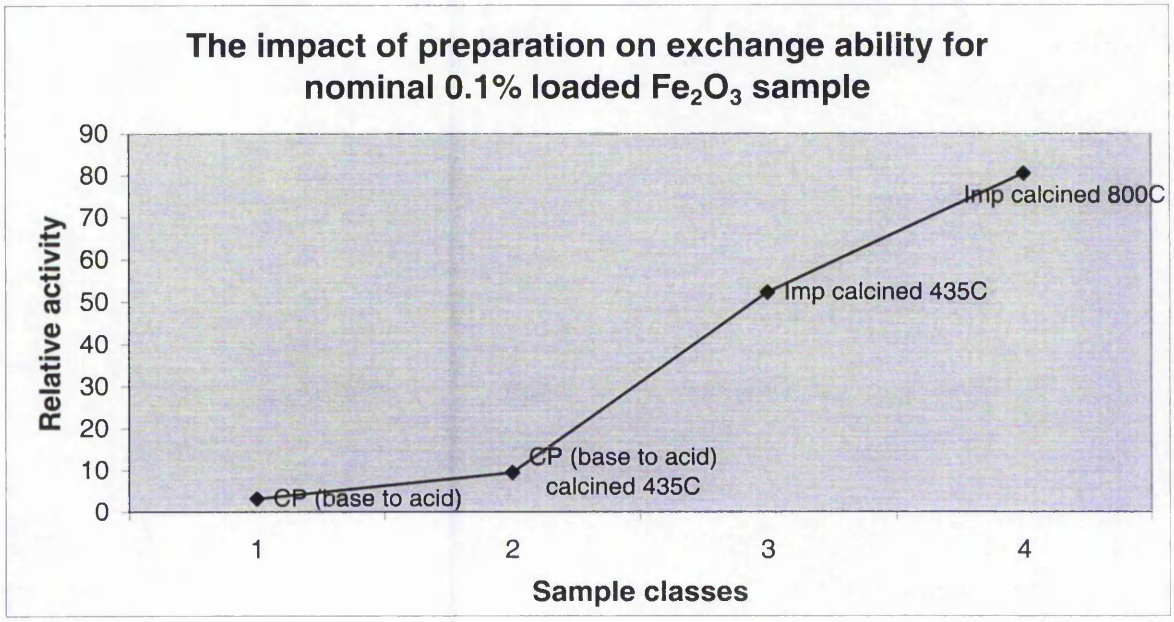

Figure 6.8 reveals the impact of preparation for nominal 0.1% loaded iron oxide samples. There is nearly a reversal in class performance when comparing this profile with the MgO (figure 6.7) profile. For iron oxide it appears that impregnated samples are superior for exchange than co-precipitated samples and calcination, especially at high temperature, beneficially influences exchange. The relative activity calculations are comparable across supports. Comparing figure's 6.7 and 6.8 reveals how adept iron oxide is at exchange relative to magnesia as support. This observation is most likely related to the higher oxygen concentration on iron oxide as opposed to magnesia.[3]

6.9 Discussion and conclusions

Analysis of the various iron oxide class profiles reveals two consistent characteristics, namely the invariance of exchange with gold loading and the profound effect of preparation variables such as calcination temperature and whether co-precipitation (acid to base, base to acid) or impregnation was used. As mentioned before, calcination, especially at high temperature imparts even superior exchange performance. This is surprising as calcination is associated by many researchers[13,14] with unfavourable morphological changes such as support and particle sintering and also loss of oxidized gold species that are thought to be catalytically active. Now, if exchange is similar to aspects of CO oxidation (and several models suggest it is) then these positive influences on exchange activity should not be witnessed, but they are. These results suggest exchange on iron oxide occurs by a mechanism not associated with the presence of gold but more with the support itself. SEM imaging of co-precipitated samples fails to reveal the presence of discrete gold particles although there is evidence of them on impregnated iron oxide. XPS characterisation (section 3.5) does reveal the presence of chlorine on low temperature calcined impregnated iron oxide but not high temperature calcined impregnated iron oxide. This is the same for MgO supported gold, but here there are noticeable influences of gold loading (and chlorine loading) on exchange but intriguingly not for iron oxide. It is also of interest to examine the TPR evidence that did reveal a consistent ease of reduction with gold loading for iron oxide samples. Neri et al[15] explained this effect as gold encouragement of hydroxyl group formation during preparation. Now, If hydroxyl groups are involved in exchange, as others have postulated,[12,16] then a positive relationship between exchange and gold loading would be observed, however, this is not the case. This suggests either an alternative explanation for the ease of reduction effect observed in TPR studies or that exchange does not occur with the involvement of surface hydroxyl groups.

The influence of gold was observed, however, in co-precipitated (acid to base) exchange profiles. Unfortunately these exchange runs were conducted at 435°C and

therefore involved bulk exchange. This makes the results harder to interpret but do suggest an effect of gold on bulk mobility.

It is also of interest to compare the exchange ability of MgO and Fe_2O_3 as supports. Comparison of figures 6.7 and 6.8 reveal that iron oxide is far superior to MgO as a support for exchange. As mentioned earlier, the impact of preparation variables is reversed between supports, with MgO exchange profiles revealing the benefit of co-precipitation and iron oxide profiles demonstrating the positive influence of impregnation. This is further evidence for the role of support on exchange performance and suggests (with supporting characterisation evidence) an influence of gold for MgO exchange but not Fe_2O_3 exchange.

6.10 References for chapter 6

1. Bond.G.C, Thompson.D.T
Gold Bulletin, **33**(2), (2000)

2. Liu.H, Kozlov.K.I, Kozlova.A.P, Shido.T, Iwasawa.Y
Phys.Chem.Chem.Phys, **1**, 2851-2860, (1999)

3. Schubert.M.M, Plzak.V, Andre.C.V.V, Behm.J.R, Muhler.M, Hackenburg.S
Journal of Catalysis, **197**, 113-122, (2001)

4. Boccuzzi.F, Chiorino.A, Manzoli.M, Lu.P, Akita.T, Ichikawa.S, Haruta.M
Journal of Catalysis, **202**, 256-267, (2001)

5. Boccuzzi.F, Chiorino. Tsubota.S, Haruta.M
J. Phys. Chem, **100**, 3625-3631, (1996).

6. Naito. S, Tanimoto.M
J. Chem. Soc., Chem. Commun, **12**, 832-834, (1988)

7. Cunningham, D.A.H, Vogel. W, Kageyama, H. Tsubota, S. Haruta. M,
Journal of Catalysis, **177**, 1-10, (1992)

8. Seker.E, Cavataio.J, Gulari.E, Lorpongpaiboon.P, Osuwan.S
Applied Catalysis A: General, **183**, 121-134, (1999)

9. Haruta.M, Yamada.N, Kobayashi.T, Iijima.S
Journal of Catalysis, **115**, 301-309, (1989)

10. Borezkov.G.K,
Diss. Faraday. Soc, **41**, 263-276, (1966)

11. Tripathi.A.K, Kamble.V.S, Gupta.N.M
Journal of Catalysis, **187**, 332-342, (1999)

12. Hargreaves J.S.J, Joyner.R.W, Mellor.I.M
Journal of Molecular Catalysis A: Chemical, **141**,171-176, (1999)

13. Kozlova.A.P, Kozlov.A.I, Sugiyama.S, Matsui.Y, Asakura.K, Iwasawa.Y
Journal of Catalysis, **181**, 37-48, (1999)

14. Hodge.N.A, Kiely.C.J, Whyman.R, Siddiqui.M.R.H, Hutchings.G.J, Pankhurst.Q.A, Wagner.F.E, Rajaram.R.R, Golunski.S.E
Catalysis Today, **72**, 133-144, (2002)

15. G. Neri, A.M. Visco, S. Galvagno, A. Donato, M. Panzalorto,
Thermochimica Acta, **329**, 39-46, (1999)

16. Cunningham. J, Healy. C.P
JCS Faraday Trans, **I**, 83, 2973-2984, (1987)

Chapter seven

A bank is a place that will lend you money if you can prove that you don't need it.

Bob Hope

Chapter 7: Carbon Monoxide Oxidation over Iron Oxide Supported Gold.

7.0 Introduction

Iron oxide was chosen as one of the supports in this research as it has been extensively used for CO oxidation, often with very promising results.[1]
Although most studies have demonstrated low temperature oxidation of carbon monoxide using iron oxide as a support, it is important to remember that preparation and treatment of the catalyst is critical in achieving the desired ambient oxidation of CO. This should be borne in mind when analysing the reaction data that is highly dependent on mode of preparation, and whether calcination was employed or not. In this chapter, all CO oxidation profiles will be presented together with associated Arrhenius data. To gain insight into the mechanism behind iron oxide supported gold CO oxidation, correlations will be sought between exchange and oxidation data gained from research on iron oxide. In addition to these, there will be a presentation of a 3-way catalyst exchange experiment in which an effective ambient CO oxidation catalyst was run in a static atmosphere of CO, and $^{36}O_2$ / $^{32}O_2$. The results from this experiment provide interesting clues as to what is occurring on the surface of a catalyst during CO oxidation. Also to be presented will be experiments performed in the absence of gas-phase oxygen in which oxidation of CO can only occur via the lattice of iron oxide. Throughout all these discussions, reference will be made to characterisation performed on these materials that, in combination with the reactor data, shed further light on the CO oxidation process.
The first series of profiles to be examined relate to percentage CO oxidation over low temperature calcined impregnated materials. Initially however, there will be an overview of how the catalysts perform at a set temperature, using moles of CO oxidized per m^2 of catalyst. This enables a comparison of the influence of gold loading on CO oxidation within a class and an overall impression of the influence of preparation technique and calcination temperature.

7.1 **Figure 7.1**: CO conversions (moles) across all sample classes

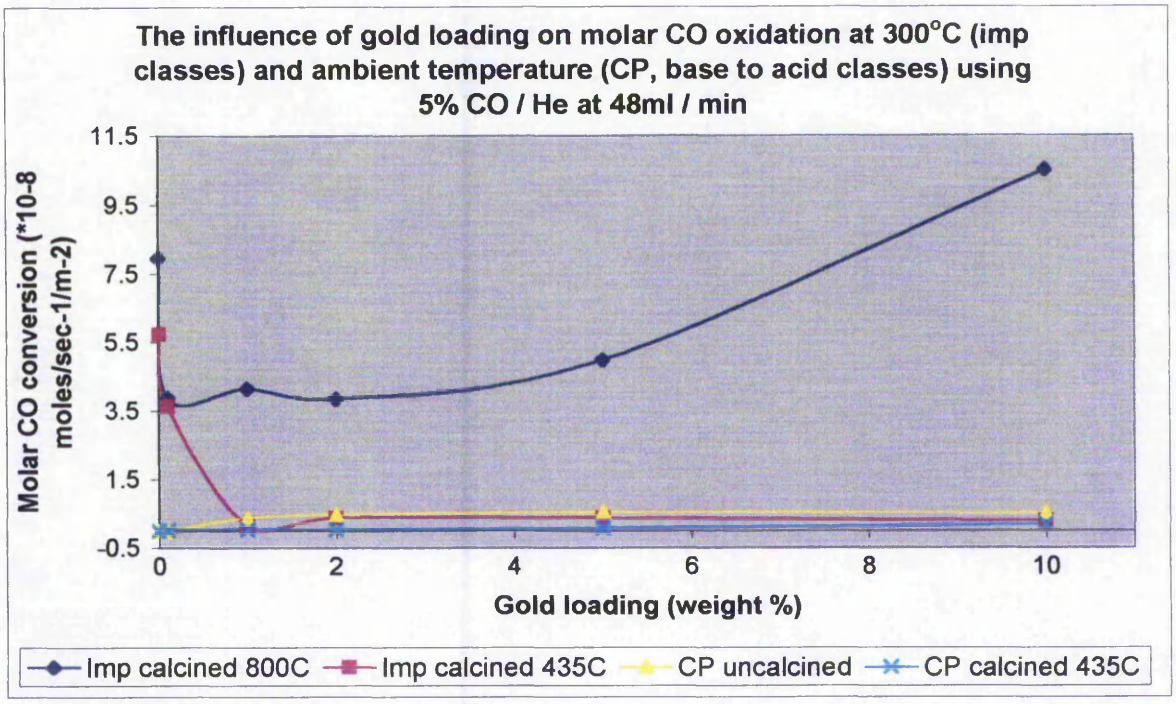

Figure 7.1 reveals the effect of both preparation and gold loading on CO conversion. It is apparent that high temperature calcined materials are active only at high temperature (300°C, this temperature being chosen because it was the lowest that gave appreciable CO oxidation for all classes) are more active than any other sample class. However, this is misleading as uncalcined co-precipitated samples (base to acid) give near 100% conversion at room temperature. A possible reason for these results is the 2 magnitude difference in surface area between low temperature calcined impregnated materials (1-2 m^2g^1) and co-precipitated materials (180-200 m^2g^1). There are trends with gold loading for the impregnated class with a positive trend seen for high temperature calcined materials and a collapse in oxidation with gold loading of low temperature calcined materials. This same trend has been seen with exchange (and to a lesser extent, oxidation) performed on equivalent MgO samples (chapters 4, 5). The most probable explanation is based on surface chlorine

concentration that is removed by high temperature calcination but not low temperature calcination, as revealed by XPS measurements (section 3.5) of chlorine levels on these respective samples. There is also a positive effect of gold loading on CO oxidation for both co-precipitated classes. This effect is explored in more detail later on. Figures 7.2 and 7.3 detail oxidation over impregnated materials

7.2 **Figure 7.2**: CO Oxidation over imp calcined 435°C class

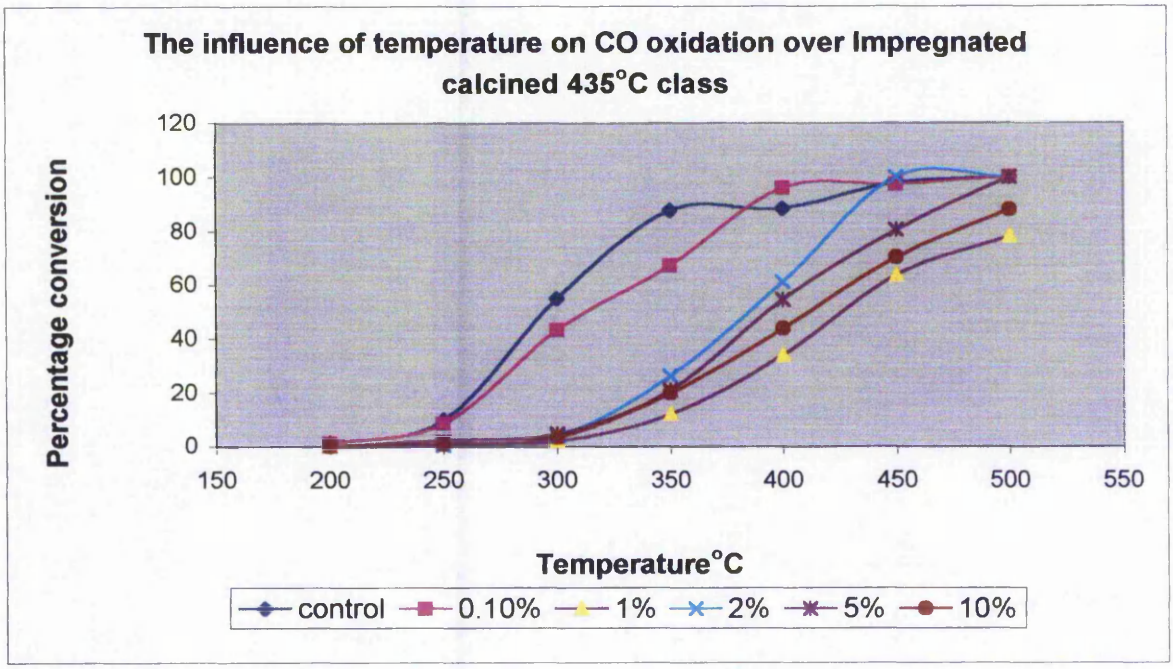

Figure 7.2 reveals what appears to be two separate groups of profiles, with low and zero gold loaded samples performing considerably better than higher loaded samples. All samples eventually reach 100% conversion at high temperature, but this achieved at much low temperatures for the control and 0.1% sample. Inspection of the other samples reveals a clear trend (with the exception of the 1% loaded sample) of decreasing activity with increasing gold loading. This observation was repeated for the equivalent MgO class for both exchange and oxidation but not for exchange over this class.

XPS investigations (section 3.5) do reveal significant surface chlorine levels on these materials and the explanation that with higher gold loading comes concomitant doping with chlorine looks very tenable. Investigators have found chlorine poisons both exchange[2] and CO oxidation.[3]

7.3 Figure 7.3: CO oxidation over Imp800 class

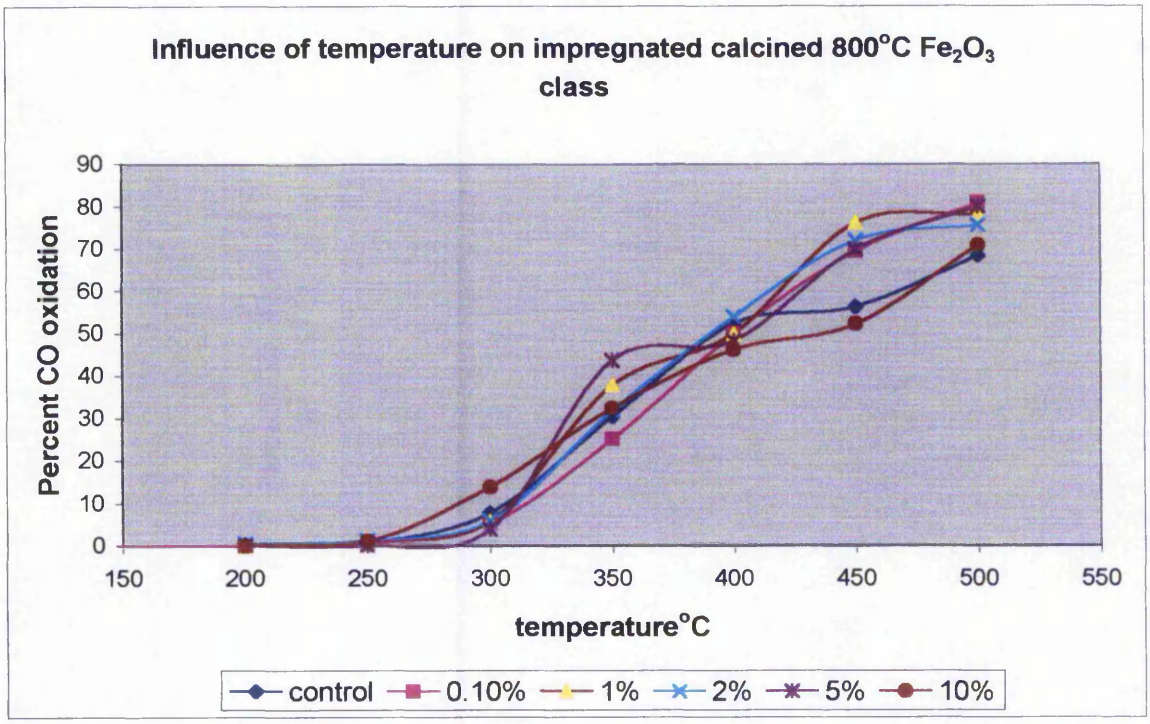

Figure 7.3 reveals the effect of gold loading for high temperature calcined impregnated iron oxide. Because the profiles are so closely packed together it is hard to discern any influence of gold loading. In any event it is weak at all temperatures. When examining exchange over this class, there was also an absence of any relationship to gold loading. Oxidation over the equivalent MgO samples also failed to show any relationship with gold loading. Comparing figures 7.2 and 7.3 suggests superior CO oxidation by low temperature calcined samples in which nearly 100% conversion is reached in nearly all samples. High temperature calcined samples reach a maximum of 80% conversion.

The most successful catalysts studied in the author's research were the uncalcined co-precipitated Au / Fe_2O_3 samples. These provided near complete oxidation of CO at ambient conditions, similar to other effective catalysts[5] and is reassuring in that regard. Figure 7.4 gives the results of this promising class.

7.4 **Figure 7.4**: ambient CO oxidation over co-precipitated materials (base to acid)

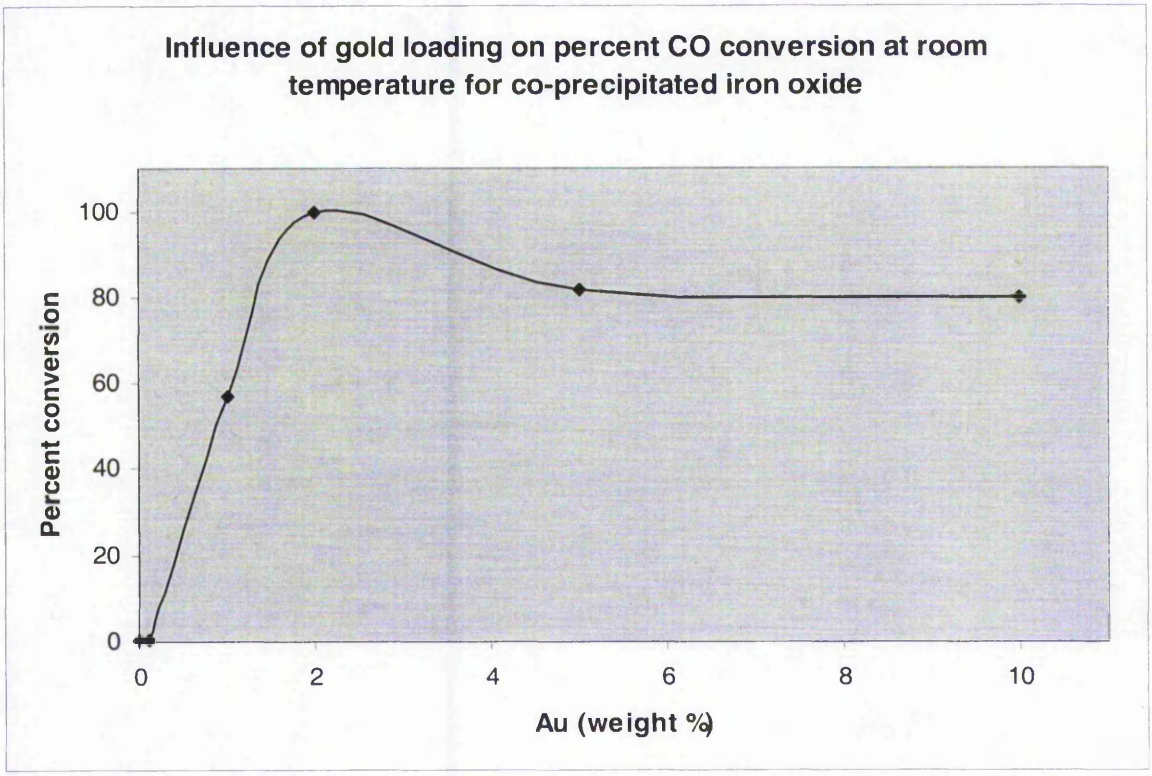

As figure 7.4 shows, these catalysts are the most successful out of all the classes tested so far, with the intermediate 2_{at}% loaded sample the most successful. There is a clear-cut effect from gold loading with the control and 0.1_{at}% loaded samples performing at close to zero conversion. There appears to be a plateau at 5_{at}% and 10_{at}% loaded samples. This suggests that maximum CO oxidation performance can be achieved with relatively low gold loadings, a finding that has obvious commercial implications.

Unfortunately the nature of the gold morphology responsible for this high activity is unclear as no discrete particles were detected by SEM imaging (section 3.3) and even XPS (section 3.5) failed to detect the presence of gold, even after many scans. There was also an invariance of surface area (section 3.1) with gold loading (which is also the case with impregnated samples) but TPR (section 3.2) did strongly suggest the influence of gold through an ease of reduction. This was seen for co-precipitated materials but not impregnated materials. This suggests that an ease of reduction with gold loading could be seen as a signature for high catalytic activity at ambient temperature. Investigators have postulated the existence of hydroxyl groups[6] responsible for lowering reduction temperature and which are facilitated by gold loading. Hydroxyl groups have also been implicated in CO oxidation[7] and several models of CO oxidation include them.

As mentioned before, the role of calcination is still controversial, with investigators providing conflicting evidence as to any benefits associated with calcining iron oxide supported gold. However as figure 7.5 demonstrates, there is a clear disadvantage in calcining co-precipitated iron oxide.

7.5 Figure 7.5: results for catalysts prepared by the method of Finch et al, (base to acid) followed by calcination at 435°C: note that the maximum conversion observed is ca 3%, compared to ca 100% for the best uncalcined materials.

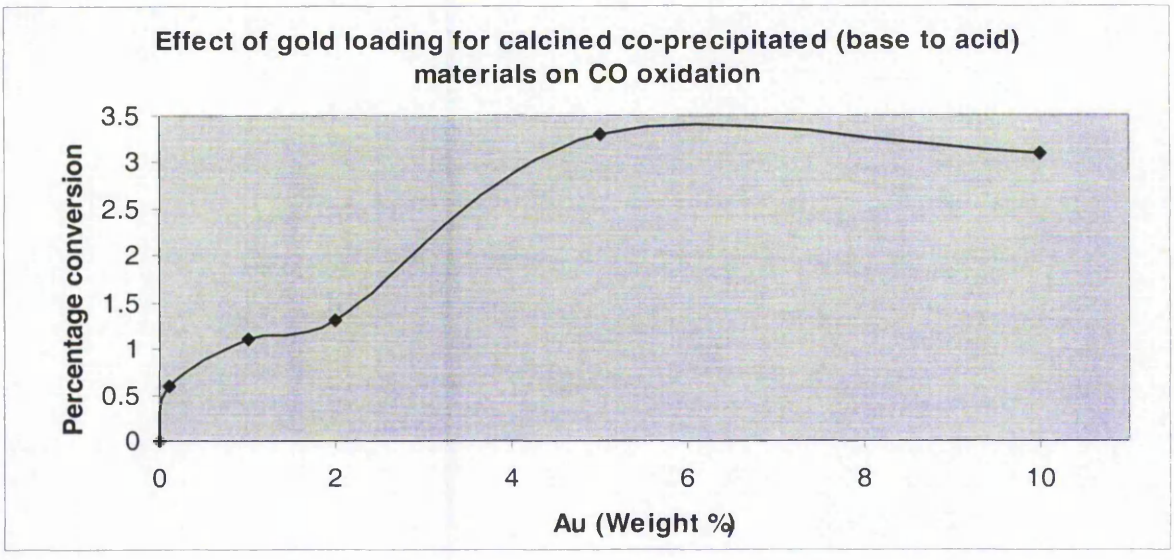

Although figure 7.5 reveals a collapse in CO oxidation upon calcination (to a maximum of 3% conversion) there is still a prominent positive effect of gold loading on CO oxidation activity that plateaus at 5_{at}% loading. This finding is in keeping with the majority of investigators[8,9] who have found the same negative influence of calcination. It is in strong contrast to the findings of Haruta[10] who tends to find strong benefits through calcination.

To investigate the effect of calcination further it is instructive to examine its influence on impregnated materials.

7.6 **Figure 7.6**: The effect of calcination for undoped impregnated iron oxide

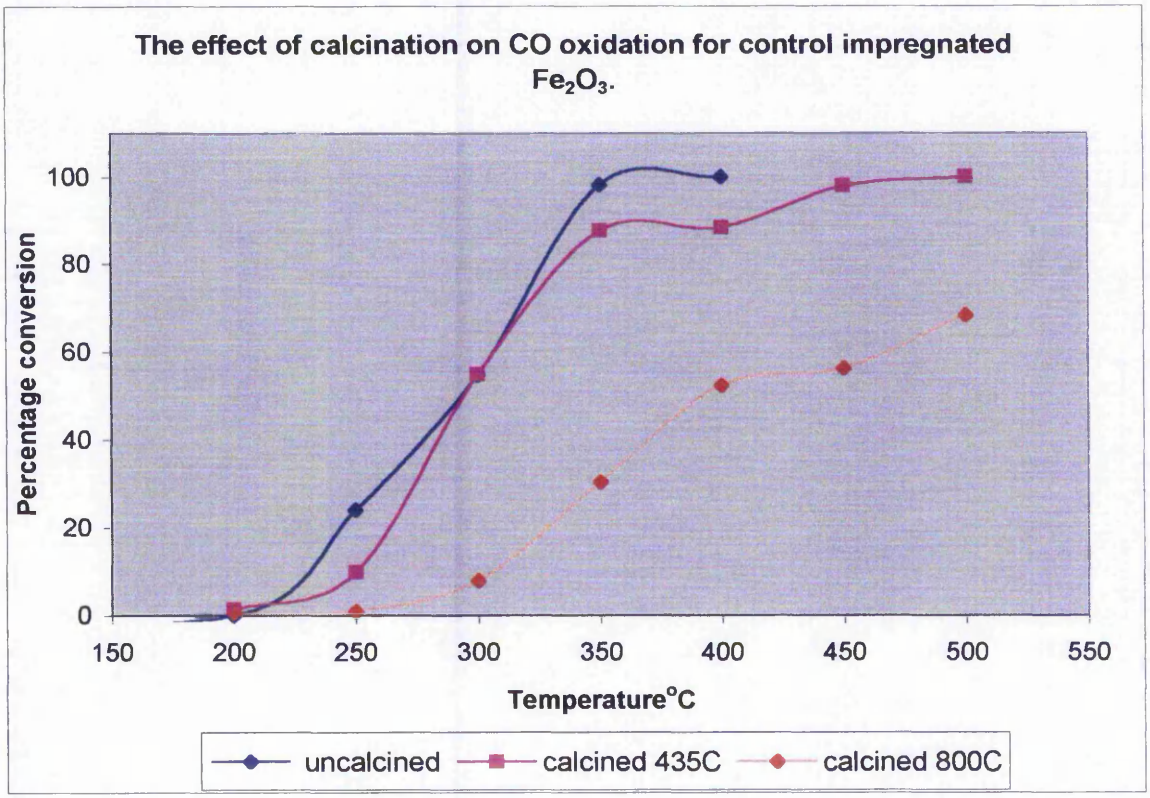

Figure 7.6 shows that only very high temperature calcination (800°C) is detrimental to catalyst performance.

7.7 **Figure 7.7**: The effect of calcination for 2% loaded impregnated iron oxide

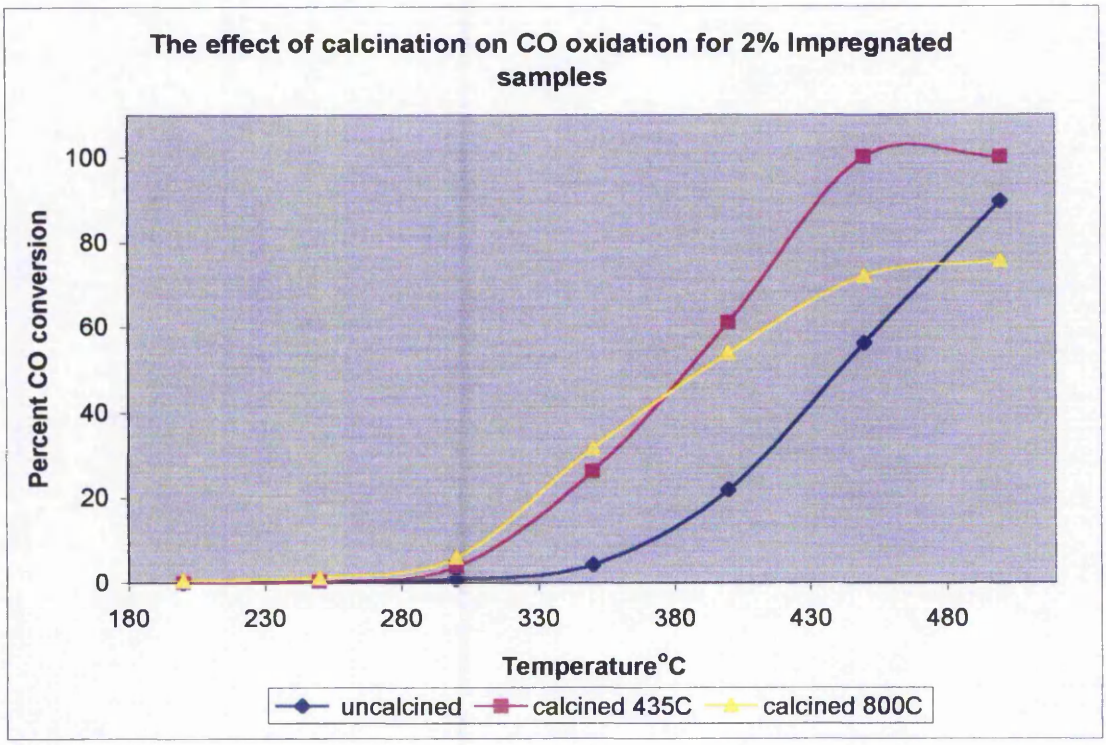

With this gold loading, there appears to be a reversal of the effect of calcination, with higher oxidation activity bestowed by calcination. However the effect is lost or even reversed slightly upon calcination at a higher temperature. This is in contrast to the effect of calcination for equivalent MgO sample classes, that revealed a calcination benefit for control samples and calcination induced loss of activity for loaded (5%) sample. This indicates that the support influences the catalyst response to calcination.

One very important aspect of this research is to follow CO oxidation on stream over time, to ascertain the extent of any deactivation of catalyst. As figure 10 reveals, there is a definite deactivation profile for the best performer: 2_{at}% loaded co-precipitated sample.

7.8 **Figure 7.8**: Deactivation of catalyst

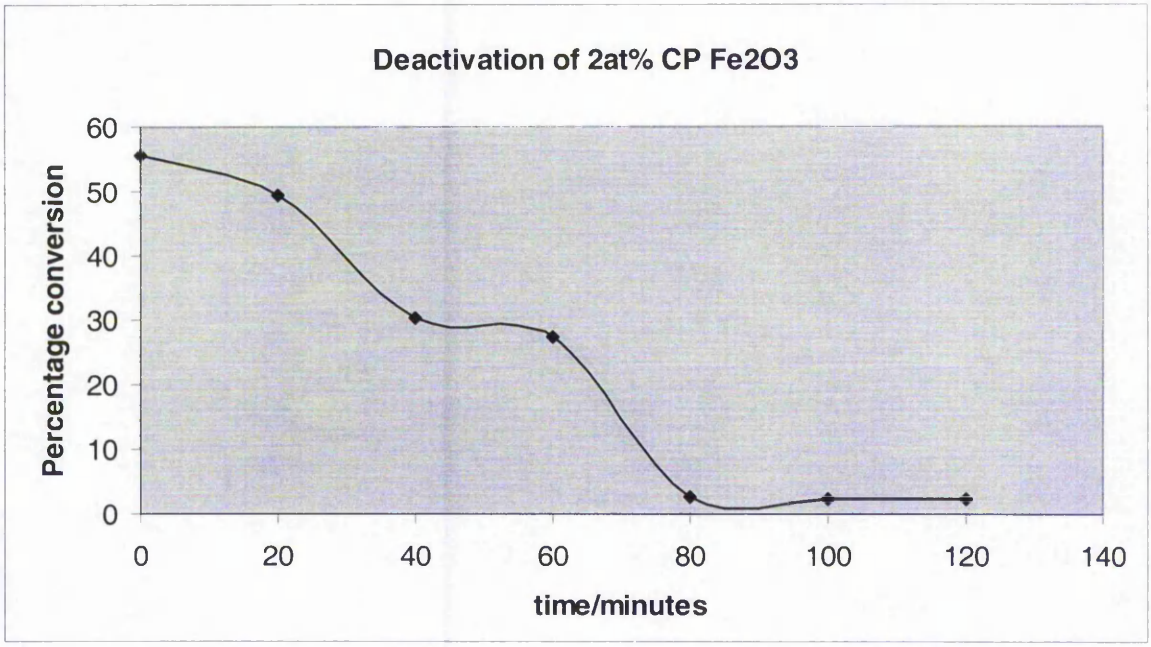

There is a definite fall over time in the performance of the 2_{at}% loaded sample. After 80 minutes a near total absence of activity appears evident. Others have witnessed the same level of deactivation over similar times.[11]

In order to probe the ability of lattice oxygen to oxidize CO, several experiments were performed on co-precipitated iron oxide (uncalcined) samples at range of gold loadings in which oxygen was absent from the passing gas, (and was exhaustibly removed with helium prior to admission of CO). Any CO oxidation can only occur via lattice oxygen or any oxygen reservoirs on the surface of the catalyst. This experiment is very important because it is relevant to any mechanism behind CO oxidation as lattice oxygen is implicated in the Mars-van Krevelen mechanism. In fact, several researchers have found evidence for lattice oxidation of CO using iron oxide supported gold as catalyst.[12] Figure 7.9 gives the result of these experiments.

Figure 7.9: CO oxidation by the lattice of co-precipitated iron oxide

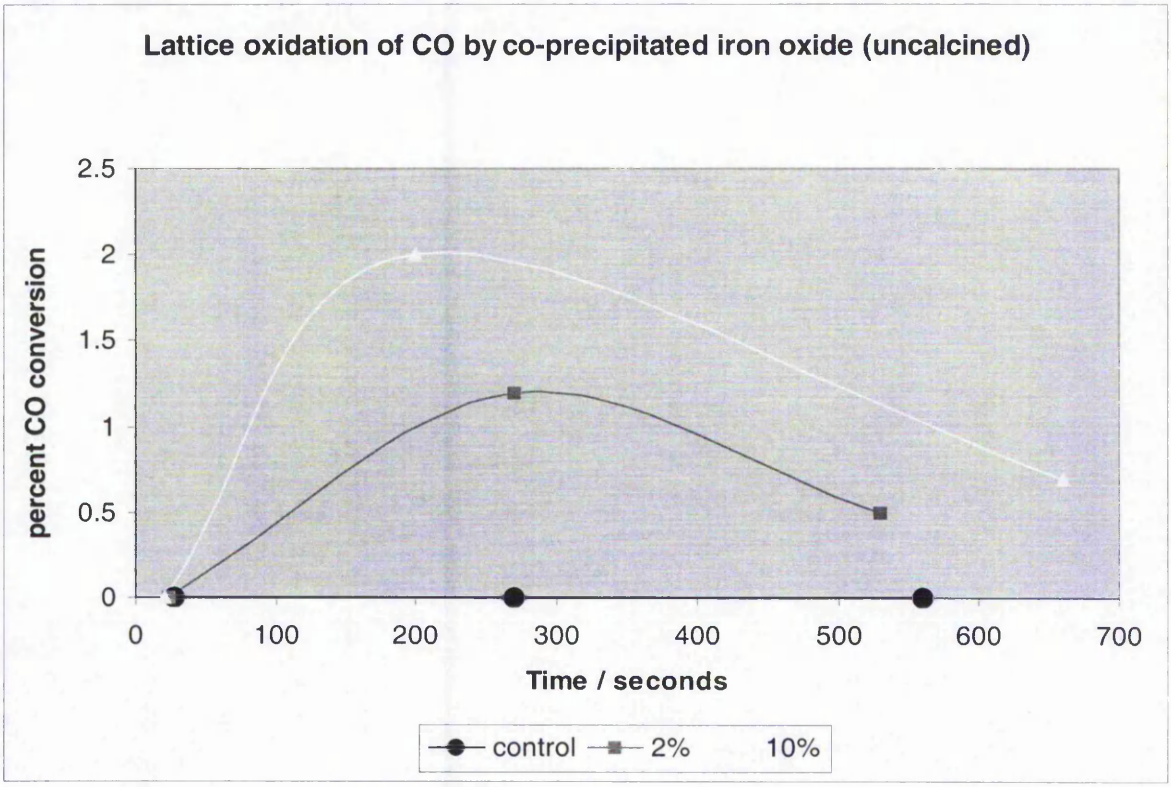

Figure 7.9 reveals that indeed these samples undergo lattice oxidation. The conversions represent only a fraction of the lattice that is undergoing oxidation at a given time. In the case of 2% CO oxidation (that is the maximum achieved) this corresponds to 0.1% of the iron oxide monolayer. One can visualize a fraction of a percent of the monolayer that is oxidizing CO at a given moment, which is then undergoing replenishment from gas phase oxygen. Calculations based on the assumption of significant bulk oxide participation give a much lower degree of lattice oxygen involvement, of the order 10^{-5}. Indeed, when gas phase oxygen was admitted, CO conversion returned to values comparable to those seen before. These results support a Mars-van Krevelen mechanism for CO oxidation in which gas phase oxygen replenishes lattice oxygen lost during oxidation of CO. Analysis of the above profiles reveals a common trend with time, with both samples reaching a peak at 200 – 300 seconds and then tailing off. This is to be expected, given the finite

supply of lattice oxygen available for oxidation. There appears to be a positive relationship of lattice CO conversion with gold loading. However this is illusory as figure 7.10 reveals. Unlike figure 11, that gives percentage CO conversion, figure 7.10 gives molar CO conversions that reveal hardly any difference between 2_{at}% and 10_{at}% loaded samples.

7.10 **Figure 7.10**: molar lattice CO conversions.

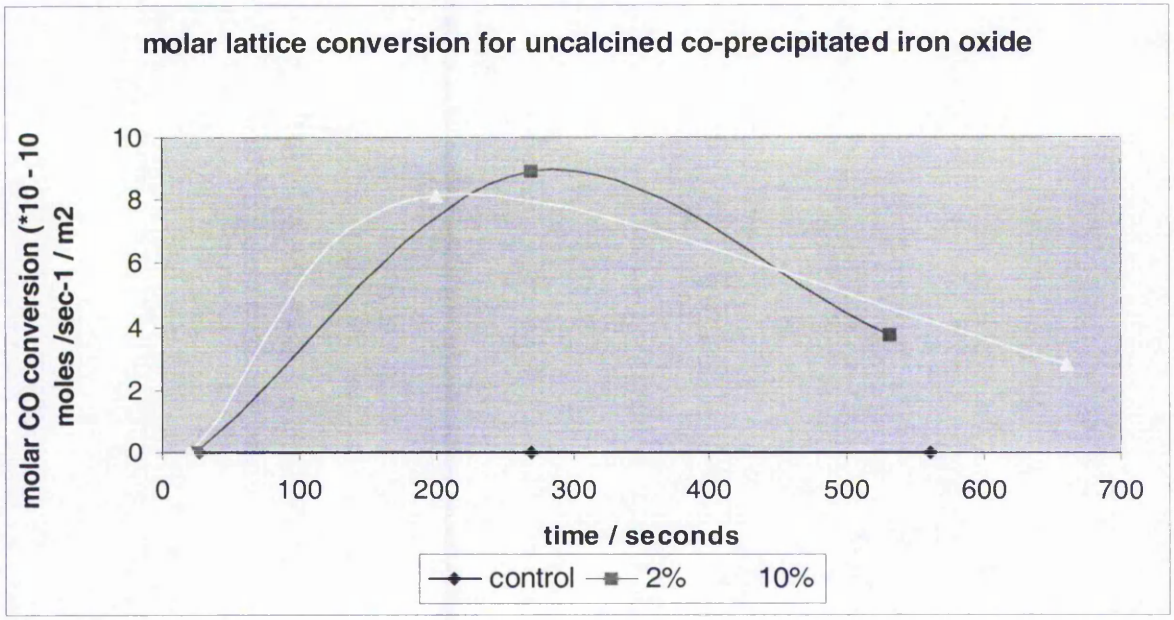

As figure 7.10 reveals, there is no obvious influence of gold loading on the lattice oxidation performance of co-precipitated iron oxide supported gold. Although gold clearly catalyses CO oxidation for this class of material, its impact in the absence of gas-phase oxygen is less apparent, even though there is no oxidation from undoped catalyst. This result suggests an upper limit of 2_{at}% gold loading for lattice oxidation that is not enhanced upon greater loading, a result similar to oxidation in the presence of oxygen.

7.11 Catalysis Exchange Experiment:

The results reported in this chapter and by many others show that iron oxide catalysts are very effective in CO oxidation near to room temperature. However, has been shown in chapter 6, no exchange of gas phase oxygen with the catalyst occurs in this temperature range. The possibility of homophase oxygen equilibration in which the simple exchange: $^{18}O^{18}O + {}^{16}O^{16}O \longrightarrow 2(^{18}O^{16}O)$ occurring over iron oxide at room temperature has also been explored by having labeled oxygen $^{36}O_2$ and unlabelled $^{32}O_2$ released over a 5_{at}% loaded co-precipitated sample (that had given 80% CO conversion before) and the products of equilibration followed using mass spectrometry. The results suggested that no homophase equilibration had occurred. Lastly, experiments have also been conducted to see if any exchange occurs in parallel with CO oxidation, when the catalyst is exposed both to carbon monoxide and oxygen. It was speculated that maybe oxygen dissociation was occurring but that oxygen occupied specific sites leaving no sites available for homophase equilibration to occur. It therefore follows that if CO reacts with adsorbed oxygen this will release sites where homophase exchange can occur. To test this hypothesis both labelled and unlabelled oxygen were admitted to the sample with the addition of CO. The results of this experiment are presented in figures 7.11 and 7.12.

Figure 7.11: Catalysis / exchange experiment

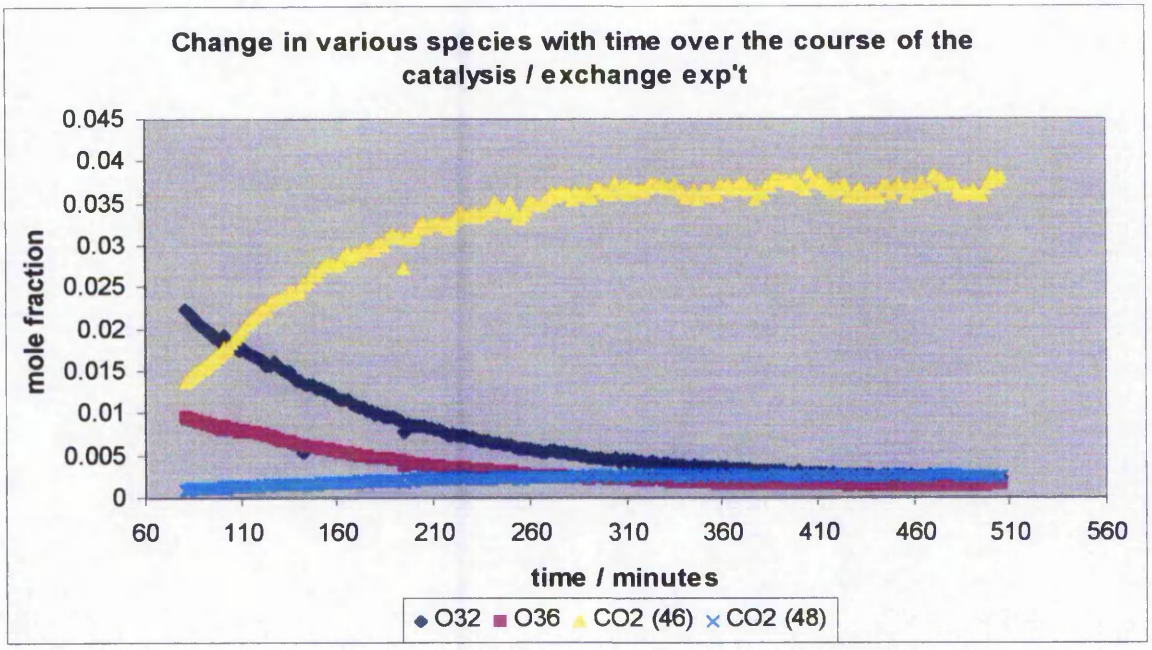

Figure 7.11 shows the main result of the catalysis exchange experiment. The initial data points are missing as the mass spec recorded rapid fluctuations in all species during this time and the data was deemed unreliable. However, after an initial period there is a definite series of profiles that makes sense when interpreting the data. Figure 7.11 reveals the effect of dosing of CO (which was dosed in excess so as to react with as many adsorbed oxygen atoms as possible). It can be observed that a steady decrease in oxygen both oxygen 32 and 36 occurs. This is because both are adsorbing on the surface of the catalyst. There is an increase in CO_2 44 (not shown for clarity), 46 and 48 as CO reacts with oxygen 16, 18 and 2(18) respectively. The increase in 48 signal is interesting and suggests the existence of a 3-atom intermediate in CO oxidation (so that $C^{18}O^{18}O$ can exist). The observation of a much greater 46 signal than 48 suggests that carbonate intermediate formation via molecular reacting O_2 plays a minor role in CO oxidation. The reason for this comes from a 2:1 ratio of 46 to 48 that would be observed if only a carbonate mechanism operated. The observed ratio is around 10:1.The second piece of supporting

evidence for the dissociation of oxygen on specific sites hypothesis comes from analysis the 34 signal as is revealed in figure 7.12.

Figure 7.12: Catalysis exchange experiment.

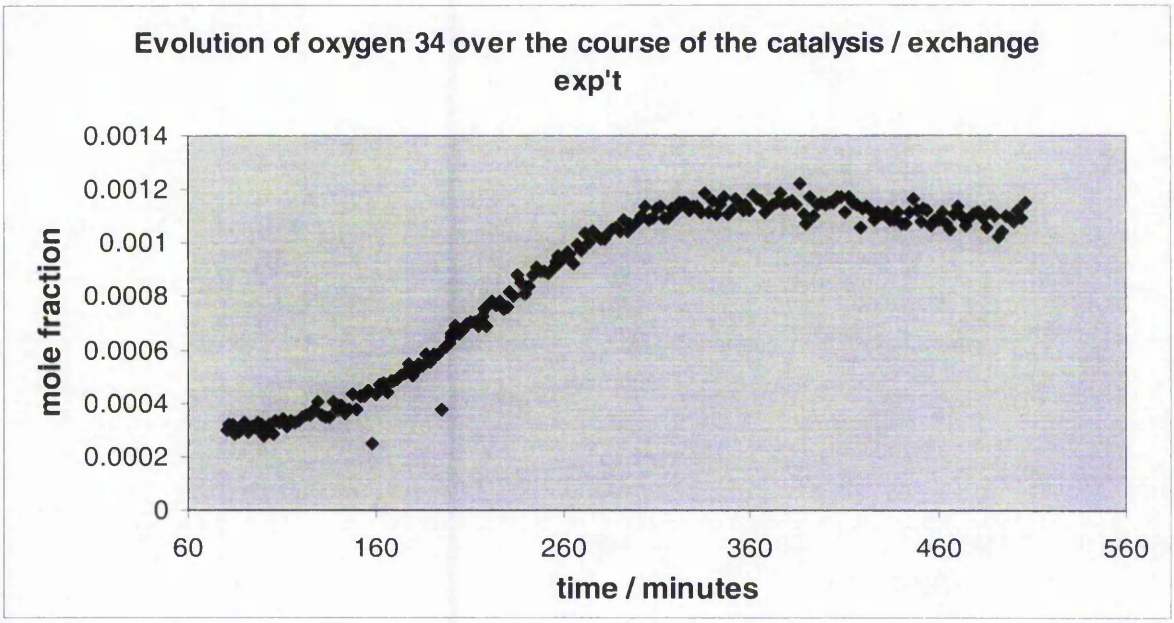

Figure 7.12 reveals an increase in 34 signal that is concordant with the view that once adsorbed oxygen sites are released, homophase exchange can then occur with the production of $^{18}O^{16}O$. However an alternative explanation is via reversible carbonate formation: $CO + {}^{18}O_2 \longrightarrow CO_3 \longrightarrow C^{18}O + {}^{18}O^{16}O$. This gives the scrambled product; $^{18}O^{16}O$ as seen earlier. The 34 signal is much weaker than that ordinarily seen in exchange experiments and suggests either that dissociated oxygens do not readily vacate their adsorbed positions and react, or that reversible carbonate formation is not a dominant process on the catalyst surface.

7.12 Correlating exchange and oxidation

Because previous research described has suggested the occurrence of both lattice oxygen in low temperature oxidation (but not exchange at low temperature) but also the dissociative adsorption of oxygen at room temperature over catalyst surface and subsequent reaction, it is instructive to clarify matters by searching for any correlations between oxidation and exchange data. These are shown in figure 7.13.

Figure 7.13: Correlation between molar exchange and molar oxidation.

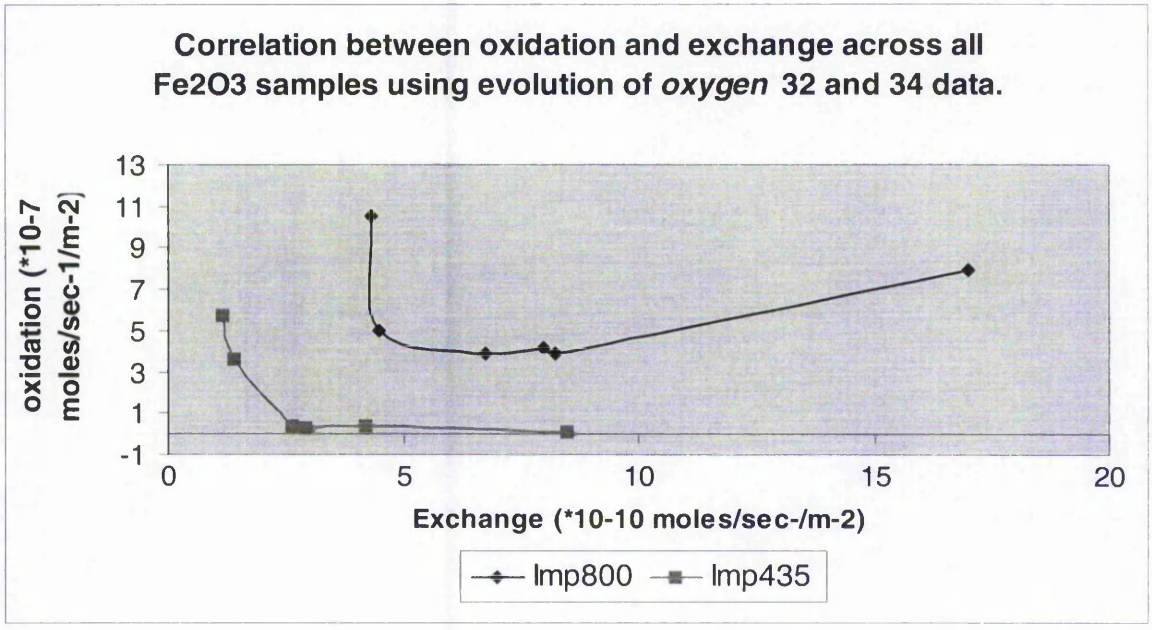

Figure 7.13 reveals a moderate negative correlation between molar exchange and molar CO oxidation for impregnated materials. This result is not impressive especially as there is no correlation using inverse co-precipitated data. Taken prima facie it suggests there are *opposing* mechanisms involved in exchange and catalysis. A finding that doesn't make sense given the above data and general observations from exchange and oxidation catalysis. However, the 3-fold magnitude superiority towards oxidation than exchange mirrors similar data on MgO and reveals that oxidation by

these materials is far more facile than for exchange. This supports the notion of separate reaction pathways for exchange and oxidation with oxidation primarily occurring by a non-lattice involved pathway and exchange involving the lattice. This is because if oxidation occurred substantially by the lattice, then a correlation would be expected with exchange data as exchange also involves participation of lattice oxygen during replacement of gas-phase oxygen for lattice oxygen.

7.13 Conclusions and discussion

Oxidation has been performed using iron oxide supported gold catalysts leading to the conclusion that preparation method, gold loading and reaction conditions all exert significant influences on CO oxidation performance. Principally it has been observed that uncalcined (base to acid) co-precipitated iron oxide supported gold is effective at room temperature for complete conversion of CO. This is the only class of catalysts in this work studied that are able to achieve full conversion even under varying CO and O_2 concentrations. Analysis of percentage conversion profiles as well as molarity data reveal trends with gold loading that are explicable in terms of chlorine content as revealed by XPS observations (section 3.5) for impregnated materials but not for co-precipitated materials, as these had no chlorine on their surfaces (XPS; section 3.5). The adverse effect of calcination is seen with co-precipitated catalysts that reveal a collapse of oxidation upon calcination. For both calcined and uncalcined catalysts there is a trend with gold loading (especially for calcined catalysts) that show very little activity for undoped and 0.1_{at}% loaded samples that immediately climbs with higher gold loading. This sharp influence of gold loading is not seen with impregnated materials and again reveals the importance of preparation on CO oxidation performance. The interplay of gold doping and calcination is clearly seen for impregnated materials. Here, high temperature calcined, undoped iron oxide performs badly relative to its uncalcined equivalent. For loaded iron oxide (2%) the effect is reversed, giving an advantage to calcination. These results show that the presence of gold influences the calcination process, increasing activity upon calcination. Intriguingly, this effect is reversed for MgO materials, illustrating the effect of support also.

Investigations performed to reveal more of the nature of oxidation revealed detectable lattice involvement in the absence of gas phase O_2. This result supports the Mars-van Krevelen mechanism behind CO oxidation in which lattice oxygen participates. Further experiments aimed at investigating the nature of CO oxidation by exposing the catalyst to unlabelled and labelled oxygen as well as CO (the catalysis / exchange experiment) suggest that oxygen dissociatively adsorbs on the catalyst surface and occupies specific sites. When these sites are freed during oxidation, combination of adsorbed oxygen can occur giving rise to the $^{18}O^{16}O$ (oxygen 34) species. These results taken in combination suggest two modes of CO oxidation, one occurring with the participation of lattice oxygen and the other occurring without. To clarify matters further, correlations were performed between exchange and oxidation but these revealed no correlations save for some moderate negative relationships using impregnated data. These are most likely (given the overall zero correlations in this research) artefactual and can be ignored. Although this approach has not revealed any interesting relationships between exchange and oxidation (therefore supporting the non-lattice involved pathway) they do show that oxidation is far more facile than exchange, most likely due to the higher activation energy associated with lattice participation than simple oxygen dissociation on the surface.

7.14 References for chapter 7

1. Hodge.N.A, Kiely.C.J, Whyman.R
Catalysis Today, **72**, 133-144, (2002)

2. Taha.R, Martin.D, Kacimi.S, Duprez.D
Catalysis Today, **29**, 89-92, (1996)

3. Lin.S, Bollinger.M, Vannice.M.A
Catalysis letters, **17**, 245-262, (1993)

4. Mellor. J.R, Palazov.A.N, Grigorova.B.S, Greyling.J.F, Reddy.K, Letsoalo.M.P, Marsh.J.H. Catalysis Today, **72**, 145-156, (2002),

5. Kozlova.A.P, Kozlov.A.I, Sugiyama.S, Matsui.Y, Asakura.K, Iwasawa.Y
Journal of Catalysis, **181**, 37-48, (1999)

6. Neri.G, Visco.A.M, Galvagno.S, Donato.A, Panzalorto.M,
Thermochimica Acta, **329**, 39-46, (1999)

7. Liu.H, Kozlov.K.I, Kozlova.A.P, Shido.T, Iwasawa.Y
Phys.Chem.Chem.Phys, **1**, 2851-2860, (1999)

8. Park.E.D, Lee.S.J
Journal of Catalysis, **186**, 1-11, (1999)

9. Hodge.N.A, Kiely.C.J, Whyman.R, Siddiqui.M.R.H, Hutchings.G.J, Pankhurst.Q.A, Wagner.F.E, Rajaram.R.R, Golunski.S.E
Catalysis Today, **72**, 133-144, (2002)

10. Haruta.M, Kobayashi.T, Sano.H, Yamada.N
Chemistry Letters, **2**, 405-408, (1987)

11. Lee.S.J, Gavriilidis.A
Journal of Catalysis, **206**, 303-313, (2002)

12. Boreskov.G.K
Adv Catal, **15**, 285-339, (1964)

13. Winter. E.R.S
Adv Catal, **10**,196-241, (1958)

14. Tripathi.A.K, Kamble.V.S, Gupta.N.M
Journal of Catalysis, **187**, 332-342, (1999)

Chapter eight

If one cannot enjoy reading a book over and over again, there is no use in reading it at all.

Oscar Wilde

Chapter 8: Conclusions and future work

8.1 Conclusions

Extensive CO oxidation and isotopic exchange studies have been performed on both iron oxide and magnesia supported gold, in addition to supports alone. The ways in which different preparation methods, changes of gold loading, variation in pretreatment procedures and choice of support influence both oxygen exchange and CO oxidation activity have all been examined.

Initially, isotopic exchange studies were performed on magnesia supported gold and it was found that calcination temperature appeared to dictate the exchange profiles observed, with little exchange activity for low temperature calcined samples with gold loading and an enhancement in exchange with gold loading for high temperature calcined samples. XPS measurements revealed significant chlorine levels on the surface of these low temperature calcined samples, suggesting that chlorine poisoning could be responsible for the difference in exchange profiles. Chlorine is thought to be a poison for isotopic exchange[1], perhaps by blocking sites of exchange. Interestingly, SEM images revealed large gold particles associated with some active exchange samples. An Increase in gold particle size is implicated in a reduction in catalysis and suggests that exchange on MgO is not moderated by gold morphology as much as other factors. By comparing exchange and oxidation performed on magnesia it was found that no correlation existed between the two, save for a moderate relationship with high temperature calcined impregnated samples. This result was taken to support a *non-lattice* involved pathway for oxidation on magnesia. However, this argument is undermined somewhat by a *general* relationship when comparing sample classes. For instance, impregnated samples perform relatively poorly for both exchange and oxidation whereas co-precipitated samples perform best. Why co-precipitated materials should be more effective at promoting exchange in the same way as oxidation is not understood, but SEM results suggest it is not a function of gold particle size and could be related to preparation influence on support. However, overall, these comparisons do support the non-lattice involved pathway for oxidation on magnesia supported gold. What was also revealed was the several magnitude difference between rate of exchange and oxidation, with oxidation the

faster. This again suggests that different processes are responsible for exchange and oxidation. Exchange and oxidation studies were also performed on iron oxide supported gold. Exchange on iron oxide materials occurred at a much faster rate than on magnesia, even when accounting for the higher oxygen concentration for iron oxide. This result could be due to the lower lattice bond strength for iron oxide as compared to magnesia which means oxygens in iron oxide are easier to exchange than in magnesia. Also, exchange over MgO occurred with participation of one monolayer or less whilst for co-precipitated (acid to base) iron oxide, bulk exchange was clearly evident at MgO exchange temperatures. This again could reflect the lower bond strength for iron oxide as compared to magnesia. Intriguingly, exchange over impregnated iron oxide occurred to a comparable extent with MgO, implying a strong influence of preparation on extent of exchange. Most notable for exchange on iron oxide samples was the invariance with gold loading. The main influence came from calcination temperature and preparation techniques. Again, high temperature calcination afforded the highest exchange activity, contrary to observations in general oxidation catalysis and providing further evidence of different processes governing exchange and oxidation. This observation is reinforced by examination of SEM (section 3.3) images that detail large gold particles that appear not to be disadvantageous to exchange as they are to oxidation.[2]

Examination of oxidation profiles reveals that co-precipitated (base to acid) samples achieved 100% conversion of CO at room temperature as previously observed by others.[3] Calcination of these samples resulted in a collapse in oxidation performance, again as generally observed.[4]

Comparison of exchange and oxidation data for impregnated materials, (this was not done for co-precipitated, base to acid, catalysts as oxidation on these materials was performed at room temperature only and exchange at much higher temperatures) again revealed an absence of any relationship between exchange and oxidation, further supporting the non-lattice oxidation pathway. Examination of MgO CO oxidation profiles reveals explicable trends with gold loading for impregnated samples. This is probably moderated by chlorine levels (XPS, section 3.5) and the effect of calcination temperature, as touched on earlier. For co-precipitated materials there is no chlorine present (XPS, section 3.5) and only the effect of gold is

manifested. This reveals a positive trend with gold loading for both calcined and uncalcined samples that plateaus at intermediate (2%) gold loadings. To examine the role (if any) of the lattice in oxidation, experiments on uncalcined co-precipitated materials were performed in the *absence of gas-phase oxygen*. Here, only lattice oxidation can occur. It was found that lattice oxidation did occur, but only to a small extent (maximum, 2% gas-phase CO) and rapidly declined over 10 minutes. Calculations revealed up to 0.1% of monolayer oxygen involvement at any one time and of the order 10 E-5 bulk oxygen involvement. This result gives limited support for the Mars-van Krevelen mechanism for CO oxidation. To investigate further the surface processes occurring during oxidation, a catalysis / exchange experiment was performed in which both oxygen-16 and oxygen-18, together with CO, were exposed on the surface of a successful room temperature catalyst. The results supported the hypothesis that oxygen dissociatively adsorbs on the surface of the catalyst and occupies specific sites. Once oxidation commences, these sites are released and combination of oxygen adatoms can occur. This resulted in a gradual increase in the mass spectrometer signal from $^{18}O^{16}O$.

An analysis and comparison of exchange and oxidation, performed on both magnesia and iron oxide supported gold, strongly supports the idea of a non-lattice involved pathway for CO oxidation. Experiments performed in the absence of oxygen give some evidence for an additional lattice route that augments the main non-lattice CO oxidation process.

8.2 Future Work

An interesting observation in this research was the apparent increase in isotopic exchange activation energy associated with increases in gold loading. This is contrary to what is expected and it would be interesting to see if the effect is repeated on other sample classes. This would also afford an opportunity to examine the influence of preparation and gold loading on activation energy for isotopic exchange. It is still not clear what role hydroxyl groups have in exchange and to what extent. Exchange is still apparent on samples calcined at 800°C where there shouldn't be

hydroxyl groups present but this does not preclude hydroxyl exchange for low temperature calcined and uncalcined samples. It would therefore be interesting to probe this by searching for characteristic OH stretching in infra-red spectroscopy on these suspect samples. Indeed one can go further by using labelled hydrogen (deuterium). Any isotopic hydrogen exchange will show up as an increase in m / z ratio of 3 (one hydrogen and one deuterium). By comparing the rate of isotopic hydrogen exchange with isotopic oxygen exchange, a measure of the overall influence of hydroxyl exchange on exchange can be measured and also the concentration of hydroxyl groups on the catalyst surface.

To examine the role of the lattice in CO oxidation, it would be of interest to test other sample classes and calculate the influence of different preparation techniques and gold loading on the ease of oxidation by the lattice.

To gain more insight into the mechanism of CO oxidation over supported gold catalysts a TAP study (temporal analysis of products) could be performed so that a step-by-step scenario behind CO oxidation could be visualized.

In order to probe CO oxidation and exchange correlations with particle morphology in greater depth it would be of interest to procure the use of a TEM so that careful measurement of gold particle size and distribution could be obtained. Any correlation of average particle size or degree of particle size monodispersion with CO or exchange activity would shed light on the role of gold and any mechanism underlying CO oxidation.

Finally, only two types of preparation technique have been explored; impregnation and co-precipitation (both acid to base and base to acid). It would therefore be instructive to examine the influence of different preparation procedures on exchange and oxidation performance. Other techniques that could be researched include deposition / precipitation (DP) and gas-phase grafting. The first approach has met with considerable success in CO oxidation by others.[5]

8.3 References for chapter 8

1. Taha.R, Martin.D, Kacimi.S, Duprez.D
Catalysis Today, **29** (1-4): 89-92 (1996)

2. Bond.G.C, Thompson.D.T
Catalysis Reviews- Science and Engineering, **41**, 319-388 (1999)

3. Kozlova.A.P, Sugiyama.S, Kozlov.A.I, Asakura.K, Iwasawa.Y
Journal of Catalysis, **176**, 426-438, (1998)

4. Park.E.D, Lee.S.J
Journal of Catalysis, **186**, 1-11, (1999)

5. Boccuzzi.F, Chiorino.A, Manzoli.M, Lu.P, Akita.T, Ichikawa.S, Haruta.M
Journal of Catalysis, **202**, 256-267, (2001)